SISSA - SCUOLA
INTERNAZIONALE
SUPERIORE
STUDI AVANZATI
TRIESTE
Strada Costiera 11

ISAS - INTERNATIONAL SCHOOL FOR ADVANCED STUDIES

A thesis submitted for the degree of

"DOCTOR PHILOSOPHIAE"

THE ECLIPSING COMPANION OF EPSILON AURIGAE

Candidate:

Steno Ferluga

Supervisor

Prof. M. Hack

Academic Year 1986/87

TRIESTE

T H E E C L I P S I N G C O M P A N I O N

O F E P S I L O N A U R I G A E

by

STENO FERLUGA

C O N T E N T S

(continued)

Part II - CONTRIBUTIONS

(continued)

APPENDIXES

F O R E W O R D

Subject

This book contains the second and conclusive part of an extensive study, devoted individually to the star Epsilon Aurigae. The first part of this study has been already published by the writer in an earlier volume: "The 1982-84 Eclipse of the Peculiar Binary Star Epsilon Aurigae" (Master Thesis, 1983).

In this new volume only the most updated literature is reviewed and only the latest original papers are reported, while the global content of the whole study (2 volumes) is the following:

- a general review of the literature on ε Aur, available before the 1982-84 eclipse (Master Th.) and after it (this work);
- a complete research report collecting the author's original work on ε Aur, also including excerpts of 9 published papers, from early results (Master Th.) to final interpretation (this work).

For each of the two volumes, Part 1 is devoted to review items, while Part 2 contains original contributions.

Observational Campaign

The present study on Epsilon Aurigae is based, as a whole, upon a considerable observational effort, carried out by the

author and occasionally by collaborators, during the last two-year-long eclipse of this star. Different instruments and techniques were employed, covering a wide spectral range from the ultraviolet to the infrared.

a) the IUE satellite, operated from VILSPA station (Spain);
b) the 152 cm telescope at the Obs. of Haute Provence (France), providing high-dispersion optical spectrograms;
c) the H_α narrow-band rapid photometer of the Trieste Observatory (Italy);
d) the 1.5 m infrared telescope T.IR.GO. (Switzerland);
e) the 70m – baseline Michelson interferometer at CERGA (France), operating in the IR mode.

Moreover some IUE spectra, taken by other observers, were obtained from the VILSPA data bank. Finally, extensive data analysis was performed at the ASTRONET pole of Trieste.

Real-time communication with other research groups was enshured by membership at the International Research Campaign on the 1982-84 Eclipse of Epsilon Aurigae . Then, collective discussion and coherent interpretation of the results were made possible, by personally taking part at the two workshops on ε Aur which were organized after the conclusion of the Campaign in 1985. The first one was held in Tucson (Arizona), in occasion of the 165th meeting of the American Astronomical Society. The second one was included in a "Joint Discussion" on Long-period Eclipsing Binaries, held in Delhi (India) during the XIX General Assembly of IAU.

Timely publication of the results was required in this kind of research. Hence, part of the contents of the present work have been anticipated in Papers I - IX by the author and collaborators.

Scientific Aim

Now, that also the 1982-84 eclipse of ε Aur is over, there are no other significant phenomena predicted for this star until the next eclipse, which will occur after 27 years. Hence a balance of the latest knowledge, acquired by observing the eclipse with modern astronomical tools, should remain a stable reference for future research, until the next "performance" on 2009-2011.

But there is another, deeper motivation, supporting such a study on ε Aur. A new feeling is arising among many researchers, who took active part in the recent Eclipse Campaign: in fact, with the latest eclipse data, there's no more space for the classical opposition of models of ε Aur, proliferating for long in the literature. Time should have come to unify into a coherent structure old different models, which now appear to be complementary rather than antithetic. Hence we shall try finally to outline such a new definite picture of Epsilon Aurigae, a star that has baffled astronomers for almost one century, showing an innocent naked-eye appearance but hiding one of the most bizzarre objects known in the sky.

--- o ---

Heard at the XIX General Assembly of IAU:

- Well, I think that the problem of Epsilon Aurigae is finally solved.
- Oh yes, but are you shure that cilyndrical stars...really exsist ?

PART I

REVIEW

1. - INTRODUCTION

The surprising peculiarities of Epsilon Aurigae, an apparently normal naked-eye star ($m_v \simeq 3.0$; Sp.FØ Ia), were first envisaged by the German astronomer H.Ludendorff (°) in 1903. Starting from all the (visual) observations then available, he realized that ε Aur was an eclipsing binary which underwent a long total eclipse in 1902. Later on, using spectroscopic measurements of radial velocities, Ludendorff confirmed that the motion of the visible primary component, rotating around an ideal barycenter, revealed the existence of another orbiting body which should have been responsible for the observed eclipse. Therefore, ε Aur had to be a single-spectrum binary system with a directly invisible secondary component, which could be observed only when eclipsing the primary.

Ludendorff also derived the first determination of the orbital elements of the system, founding a period of 27.1 years which at that time was the longest known. Moreover he noticed that during the whole eclipse, which lasted nearly two years, the brightness of the star was nearly constant and was reduced by 0.8 magnitudes.If normally interpreted, this flat minimum in the light curve should mean that the primary component was totally eclipsed by a larger secondary. In this case the luminosity during the minimum phase, corresponding to a fourth magnitude star, should come entirely from the secondary component. But then it seemed strange that such a bright star wasn't recognizable in any way outside the eclipse, by means of spectroscopic

---

(°) Astr. Nachr. 104, 81.

observations.

Another, much more sophisticated interpretation, was the one supposing that the eclipse was only pseudo-total in the following sense: the light which was observed on the minimum phase was still that of the primary, beeing somehow eclipsed by an obscure body. In this case, in order to explain the flat minimum, it would have been necessary to use particular hypotheses about the geometry of the system, and the nature of the secondary obscure component. Anyway, a complex picture of this type finally prevailed and was accepted: in fact the more superficial idea, that both components were ordinary stars, was destined to meet ever increasing difficulties. Such a simple assumption, for instance, implied that the primary's eclipse was to be followed by the secondary's one. Ludendorff predicted that the secondary eclipse was to occur about 18 years after the principal eclipse; but the event, surprisingly, didn't occur.

The mystery got deeper as soon as ε Aur became the object of more accurate observations, especially thank to new spectroscopic techniques, which were then introduced into astronomical research. The eclipse of 1929, which lasting two years had begun in 1928 and was over in 1930, was studied by Huffer (°) and others. He realized that during the total eclipse, but also outside the eclipse itself, the brightness was only approximately constant, due to slight aperiodical fluctuations of about 0.2 magnitudes Such nearly semiregular variability could be easily intrinsic in the primary component, considering the type of the star. In fact the supergiant stars commonly undergo such kind of phenomena, but anyway the general picture of the variability

---

(°) Ap.J. 76 , 1 (1932).

of the system became more complicated.

Furthermore Otto Struve and C.T. Elvey (°) had compared more than 250 spectra of Epsilon Aurigae, collected during the eclipse of 1929. They noticed that the spectral absorption lines, normally symmetric, had instead strange asymmetric profiles during the partial phases of the eclipse. In the total phase, though, the lines were once again symmetric and deeper. This fact could find an explanation in the Doppler effect, relative to the orbital velocities of the two components partially superimposed. But there were also, unexpectedly, some lines not participating in the phenomenon, which remained unchanged during the whole eclipse.

The most important problem, however, derived from the fact that the observations showed a grey eclipse, that is the depth of eclipse resulted independent from wavelength. Practically, during the eclipse phase the colour and the type of the spectrum remained unchanged, as if the eclipsing body was an opaque veil instead of a star. In fact, if it was a star it should have been identical to the eclipsed one, since the spectrum remained the same. Such hypothesis (primary and secondary supposed to be equal) didn't hold, since it was contradicted by observation : not only the secondary eclipse should have been visible, as foreseen by Ludendorff and never observed, but also the spectrum of the secondary out of eclipse should have been clearly visible, while it had never been observed.

Large incongruities became then evident, as soon as researchers tried to obtain mathematically from the observational data (by methods normally used for binary systems) the relationship between the radii of the two hypothetical components: the minimum of brightness, corresponding to the

---

(°) Ap.J. 71 , 136 (1930) .

total eclipse, was too deep for so long a period. Finally the two stars, forming the ε Aur system, seemed to be really enormous. To the primary component — being an early F supergiant — a mass equal to nearly 15 solar masses and a radius of about 50 solar radii could be reasonably assigned. From the parameters of the orbit, it resulted for the hypothetical secondary a mass of 10 to 20 solar masses, and dimensions which could be of hundreds of solar radii. How was it possible that such a gigantic body could remain invisible?

Something very strange should therefore be hidden inside the system of ε Aur; perhaps the secondary component, that is the eclipsing body, could be a unique type of a star, or the first one of a still unknown kind. From the time of these puzzling discoveries in the 1930's, to this day, remarkable theoretical efforts have been made in order to give an interpretation to the observed phenomena.

The 1956 eclipse (started in 1955 and finished in 1957), which at last was observed with modern methods, was supposed to give finally the answer to these problems. A large campaign of spectrographic and photometric observations was organized, in order to obtain a good "covering" of the phenomenon. The large amount of collected data helped to make up in detail the observational picture of ε Aur; even if the new data didn't add much to the matter already known (on the contrary they gave rise to new problems), they were to supply the material for different theoretical interpretations. A wide scientific discussion was to develop about a set of competing models, all of which could apparently explain the observations, but each one beeing based on a different picture of ε Aur (§ 4).

After the eclipse on 1956, ε Aur became the object of more and more sophisticated telescopic observations, in order to test the various models. In the meanwhile, spectroscopic studies (Morris, 1962) and astrometric measurements of great precision (van de Kamp, 1978a) had permitted to determine the orbit and the other parameters of the system in a better way. The following indicative values were reported by van de Kamp in an aged review article (1978b): Distance from the Earth 1,900 light-years, Separation between the components $3.93 \cdot 10^9$ km, Mass of the primary 15.5 solar masses, Mass of the dark companion 13.7 solar masses.

Decisive information about the nature of ε Aur were to be collected, however, by observations taken outside the traditional domain of visible light, particularly studying the infrared and ultraviolet. The results of infrared observations by Low and Mitchell (1965), and later by Woolf (1973), did not show any strong infrared excess; this ruled out finally the possibility for the secondary of beeing an hypothetical "Infrared Star", as originally proposed by Kuiper et al. in 1937. On the other hand Hack and Selvelli (1979) evidenced, by means of observations made by the satellite I.U.E., a remarkable ultraviolet excess; this was the sign of the presence of a hot star, which confirmed an hypothesis proposed by Hack herself 18 years before (Hack, 1961). As to the nature of the eclipsing body, anyway, it was still to decide upon its real structural parameters (dimensions, shape, and composition) and about its physical characteristics (temperature, density, and processes involved). Moreover it remained to clarify the position of this object, with respect to stellar evolution. Such was the situation, before the beginning of the last 1982-1984 eclipse.

2. - BASIC OBSERVATIONS

By briefly considering the basic observational data available for ε Aur before the last eclipse, let us notice that they will stay as an obvious reference frame for all the further research based on the 1982-84 Eclipse Campaign, including the present work.

2.1 The Astrometric Orbit

For almost fourty years (1939-77), using the Sproul 61-cm refractor, van de Kamp performed high precision astrometric measurements of the apparent orbit of the visible component. By fitting these data with a circular baricentric orbit, assumed as a first approximation (ignoring the eccentricity e = 0.2 given by spectroscopy), he found the geometric elements for the orbital plane (van de Kamp, 1978a):

(2.1) $i = 89^\circ \pm 3^\circ$

(2.2) $\Omega = 92^\circ \pm 3^\circ$,

where (as usual) i is the inclination of the orbital plane with respect to the plane of the sky, and Ω is the position-angle of the line of nodes (intersection between the two planes). The results obtained by van de Kamp are shown in Fig. 2.1. Moreover, his solution gives a value of 22.7 ± 1.0 milliarcsecs for the apparent orbital radius, which combined with the value of 13.2 AU for the corresponding

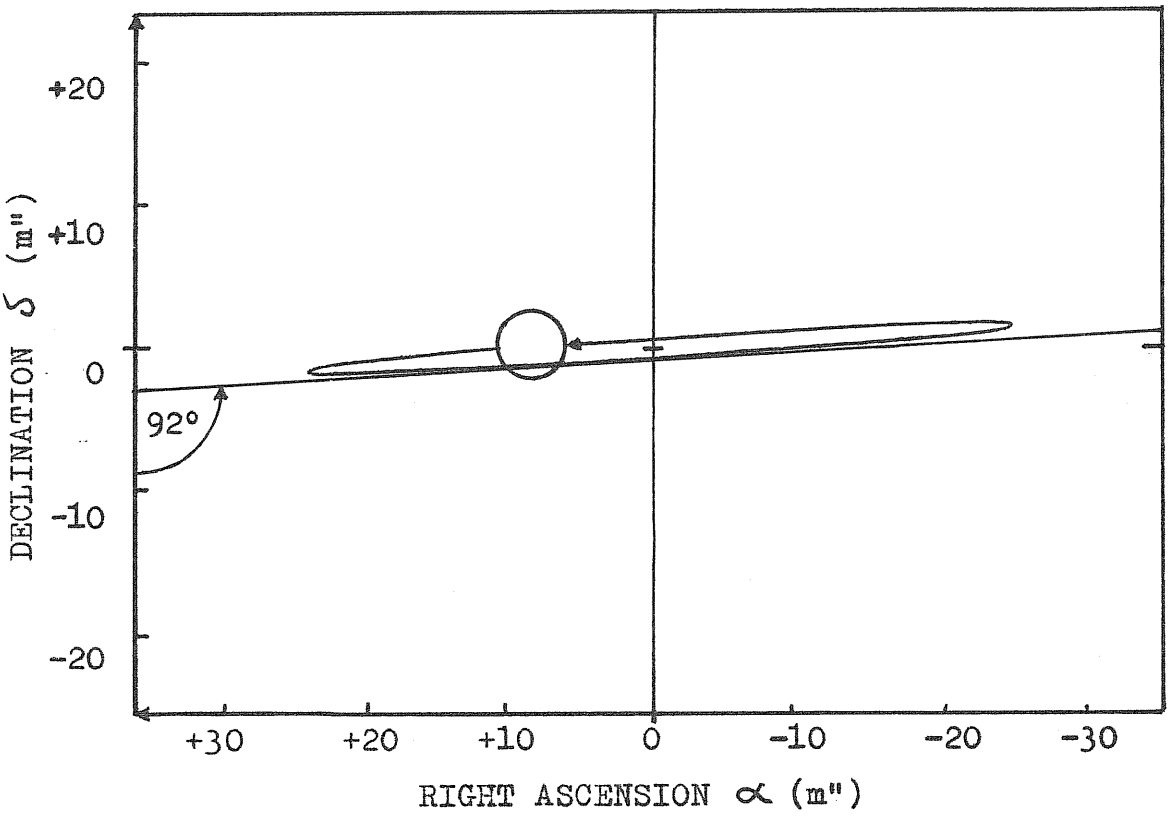

Fig. 2.1 – Orbital motion of ε Aur, as it is seen in the sky; note that α, δ are in milli-arcseconds (origin 0,0 at mid-eclipse). On the apparent orbit, by van de Kamp (1978a), it is placed the visible star at the position occupied in 1986, with its spectroscopical angular size of 4 m" (assuming a diameter of 277 $R_\odot$; Castelli, 1978). The obscure companion is not visible.

linear dimensions (Wright, 1970), provides the following result for the parallax of ε Aur:

(2.3) $\pi = 1.72\ (\pm.08)$ m" ,

where the error shown is only the astrometric one. Anyway, one has to remember that this result is based on some assumptions, regarding the linear dimensions and the circularity of the orbit.

The value (2.3), which has been found for the parallax, corresponds to the distance:

(2.4) $D = 581\ (\pm\ 27)$ pc .

Since m_V=3.0 ,the absolute V magnitude is -5.9 (±.1), affected by interstellar extinction. Adopting a visual interstellar correction of 0.8 mag (Morris, 1963), one then may obtain for ε Aur the absolute magnitude:

(2.5) $M_V = -6.7\ (\pm.1)$,

where error shown is only the astrometric one (not including a larger uncertainity due to the interstellar correction factor). Anyway, the astrometric result (2.5) can be usefully compared with other more indirect determinations of the absolute magnitude and related parameters, as radii and equivalent temperatures.

2.2 The Spectroscopic Orbit

The first spectroscopic measurements of radial velocities, providing orbital elements, were made by Ludendorff in 1924. Later Kuiper, Struve and Strömgren

(1937), covering more than one period, obtained the complete radial velocity curve (Fig. 2.2), and calculated a new orbit which changed slightly the period but leaved almost unchanged the other elements. Morris (1963) then combined these data with more recent ones, deriving an improved (°) radial velocity curve. Finally Wright (1970) revised Morris' solution by means of an iterative computer program, giving the orbital parameters listed in Tab. 2.2.

Problems arise, as soon as one considers the masses of the two components, which can be inferred from the observed spectroscopic orbit of the primary. Since we know that the secondary spectrum is not observable out of eclipse, only the primary mass function is available:

$$f(m) \equiv \frac{(m_2 \sin i)^3}{(m_1+m_2)^2} = 3.34\ M_\odot \ , \tag{2.6}$$

together with the primary's orbit semiaxis (projected along the line of sight):

$$a_1 \sin i = 13.3\ \text{AU} \ , \tag{2.7}$$

where the experimental values were derived by Kuiper et al. (1937). Such a high value of the mass function leads to a puzzling high value for the mass of the non-luminous secondary; this happens since the primary is supposed to be a normal F supergiant, having therefore not less than 10 solar masses.

Let us here examine closer the problem. Giving different values to the mass ratio (m_1/m_2), the observed value of the mass function (2.6) can be used for the computation of m_1 and m_2, assuming the astrometrical inclination angle (2.1) that is practically $i \simeq 90°$. Then, separation a is given by (2.7)

(°) Morris, 1983: Ph.D. Thesis, Univ. of Toronto

Table 2.1 - Possible masses

Mass Ratio m_1/m_2	Masses m_1	m_2	Separation a
1.5	31	21	33
1	13.4	13.4	26.5
1/2	3.8	7.5	20
1/4	1.3	5.2	16.5
1/10	0.4	4.0	14.5

Note to Tab. 2.1 : mass ratios are assumed; the corresponding possible values, for the masses (in $M_\odot$) and for the separation (in AU) of the two components, are derived from (2.6) and (2.7) with i=90°.

using the well-known relation: $a = a_1(m_1+m_2)/m_2$. In Table 2.1 the resulting values of masses and separation are listed, according to different assumed mass ratios.

The classical solution that has been usually adopted for ϵ Aur considers m_1/m_2 of the order of unity, implying (Tab. 2.1) a normally massive primary and a high mass for the non-luminous companion , difficult to be explained. But let us now hypotize a strongly undermassive primary (for its luminosity), because of mass loss in the post-main-sequence evolution . Let for instance the primary have a mass between 1 and 5 solar masses, which corresponds (Tab. 2.1) to a ratio m_1/m_2 of about 1/4 or 1/2. In this case one finds

that the mass of the secondary component lies between 5 and 8 solar masses, and such values could be consistent with the presence of a late B dwarf, suggested by the UV observations (§ 2.5).

Supposing the primary had an initial mass (on the m.s.) of about 10 ÷ 15 solar masses, the required final stage of less than 5 solar masses could have been reached after a post-main-sequence evolution during 10^6 years, with a mass loss of about 10^{-5} solar masses/year; these values are high, but still possible. In this case the origin of the extended eclipsing body, embedding the secondary, comes straightforward from the primary's mass loss. In fact the mass of the eclipsing object, estimated on the basis of its dimensions and of its electron density (deduced from opacity), appears to be not greater than 10^{-5} solar masses. Then, it is enough that only a very small part (10^{-6}) of the mass lost by the primary could have been captured by the companion, in order to provide the eclipsing body to be formed.

2.3 The Light Curve

The most complete investigation of the light curve of ε Aur may be considered the one of the 1955-57 eclipse, presented by Gyldenkerne (1970). These observations cover the various phases of the eclipse almost continously, except for two restricted gaps during totality and in the post-eclipse phase, due to the difficulty of observing this star in summer (when it undergoes lower culmination at night). Gyldenkerne's light curve for the V magnitude is shown in

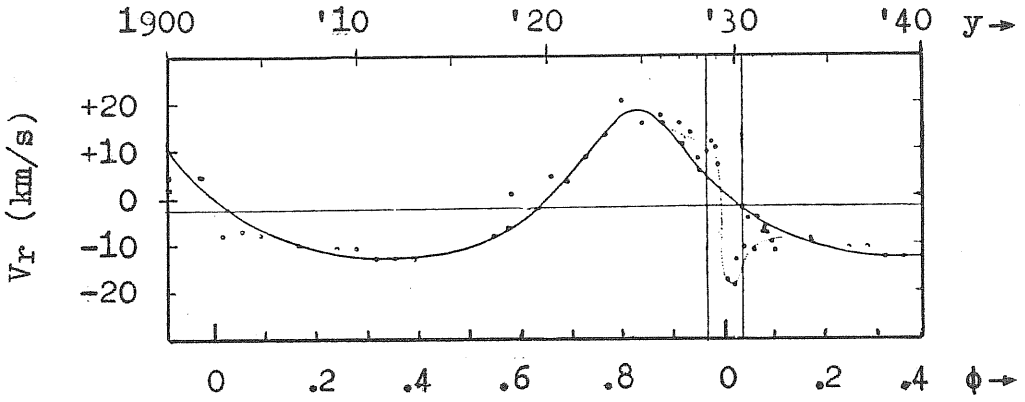

Fig. 2.2 - The radial-velocity curve of Epsilon Aurigae (Kuiper et al.,1937). The vertical lines show start and end of the 1928-30 eclipse. Dotted curve: effect of the presence of the shell-spectrum.

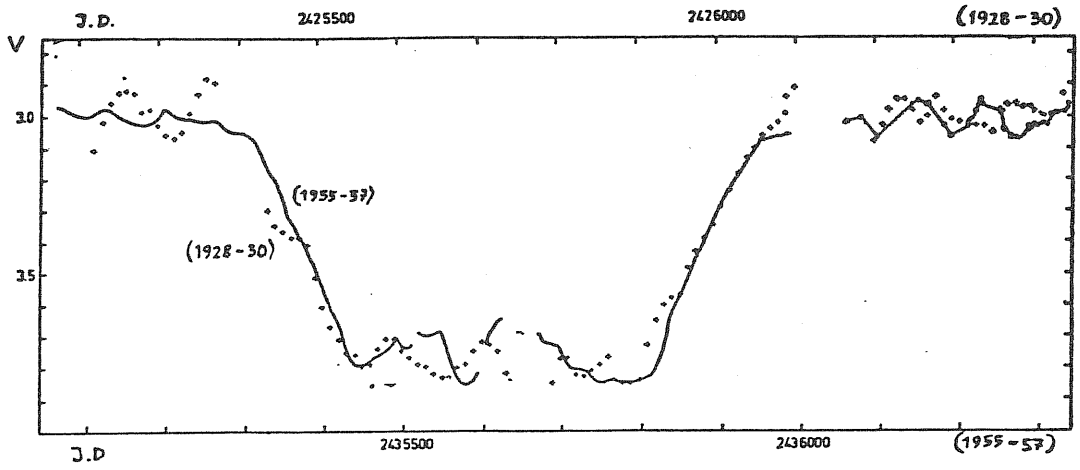

Fig. 2.3 - The 1955-57 light curve (solid line, lower abscissa) from Gyldenkerne (1970), together with the 1928-30 light-curve (dots, upper abscissa) by Güssow (1936); second-order variability appears superimposed in both cases.

Fig. 2.3, superimposed to the dotted light-curve of the preceding 1928-30 eclipse.

As a fundamental information, from the light curve it is possible to derive the radii of the two components, by measuring the duration of the eclipse phases (while assuming from the radial-velocity curve the orbital velocity and the orbital size). Table 2.2 lists the complete set of systemic parameters obtained for ε Aur, by combining astrometric data (apparent orbit), both with spectroscopic (radial velocities) and photometric ones (light curve).

Moreover, as one can see in Fig. 2.3 , on the light curve there are some second-order fluctuations which appear to be superimposed over the primary eclipse; this second-order variability has been analysed in detail. Notwithstanding the colour index is approximately constant during the eclipse, that is greyness is preserved over the phase , second-order fluctuations can be detected also on (B-V); those were related to the second-order fluctuations on V , by Gyldenkerne, obtaining

$$\Delta'(B-V) = -0.005 + 0.32 \cdot \Delta'V \ . \qquad (2.8)$$

The physical interpretation of this variability is still not clear. Since there is a similarity between this $\Delta'V/\Delta'(B-V)$ ratio and a corresponding one found for Cepheids (Larsson-Leander, 1958), it has been suggested that the second-order variability of ε Aur may be due to intrinsic cepheid-like pulsations of the primary component, a phenomenon which is common in supergiants. On the other hand it appears, also from data of 1928-30 eclipse, that the amplitude of fluctuations is larger during totality than out of eclipse. This should mean that second-order fluctuations are not intrinsic,

Table 2.2 - Basic data of the System

Parameter	Symbol	(Unit)	Value	Ref.
R.A. (Δy=year-1900)	α	(h)	$4^h58^m(+4^s\cdot\Delta y)$	(1)
Dec. (Δy=year-1900)	δ	(°)	$43°40'(+9'\cdot\Delta y)$	(1)
Apparent luminosity	U B V	(mag)	3.86 3.53 2.99	(2)
Eclipse depth	ΔV	"	0.75	(3)
Eclipse colour	Δ(B-V)	"	~ 0	(3)
Period	P	(days)	9885	(3)
1.Contact	t_1	(JD 2430000+)	5295	(3)
2.Contact	t_2	"	5430	(3)
Mideclipse	t_m	"	5624	(3)
3.Contact	t_3	"	5824	(3)
4.Contact	t_4	"	5965	(3)
Periastron passage	t_o	"	3346 ± 278	(4)
Periastron longitude	w_o	(°)	346 ± 11	(4)
Eccentricity	e		0.20 ± .03	(4)
Inclination	i	(°)	89 ± 3	(5)
Line of nodes	Ω	"	92 ± 3	(5)
Systemic velocity	v_o	(km s^{-1})	-1.4 ± .4	(4)
Velocity amplitude	K_1	"	15.0 ± .6	(4)
Semi-major axis	$a_1 \sin i$	(A U)	13.3	(6)
Mass function	f(m)	($M_\odot$)	3.34	(6)
Primary radius	r_1	($R_\odot$)	148	(4)
Secondary radius	r_2	"	$\sim$ 500	(4)
Distance from Earth	D	(pc)	581 ± 27	(5)

Note: Stellar radii are those obtained from eclipse data; data labelled (3) are referred to the 1955-57 eclipse.

Sources: (1) Batten et al.,1978; (2) Hoffleit,1982;
(3) Gyldenkerne,1970; (4) Wright,1970;
(5) van de Kamp,1978a; (6) Kuiper et al.,1937.

but somehow coupled with the primary variation. In this case an explanation could be found, for instance, on the basis of an hypotetical ring-like structure of the eclipsing body (Wilson, 1971). A possible solution of the problem could come by comparing the second-order photometric variability, with high-dispersion spectroscopic measurements of radial velocities; in case of cepheid-like nature of the pulsations, a characteristic correlation should come out.

2.4 The Infrared Excess

Apart from the first determination by Low and Mitchell (1965), the basic infrared observations of ε Aur out of eclipse are those by Woolf (1973), extending from 2 to 18 μm (Fig. 2.4). The shape of the spectral energy distribution, from the visual to 5 μm, is appropriate for a late A or early F star suffering about 1.3 mag of visual extinction. Longward of 5 μm an increasing IR excess is revealed, and after 10 μm the energy distribution is elevated of about a factor of 2; but still the observation at 18 μm sets a strong limit on the presence of any large cool star in the system.

The dimensions of the system imply anyway, because of heating by the F star, a temperature of several hundreds of degrees for any companion; such an object is then beeing predicted not to show up at wavelengths longer than 20 μm. In conclusion, it should be precisely the 5-18 μm excess to be interpreted as the very radiation from the companion of εAur, which could be also warmer than simply heated by the primary.

Substracting the expected contribution of the F star, one

finds that the radiation of this companion behaves as follows. The spectral flux F (ν) is approximately constant, at a level of about 10 flux units, between 5 and 10 μm. Then, at longer wavelengths it falls off like a blackbody, with a total radiation in this tail slightly larger than that produced by the F star.

By assuming that the object would become opaque to free-free radiation near 10 μm, a temperature $T \simeq 7000$ K and an electron density $N_e \simeq 10^{11}$ cm^{-3} were derived by Woolf, also predicting an optical depth $\tau \simeq 3$ from electron scattering; such values of T and N_e are in good agreement with those predicted by Hack's model (§ 4.2). On the other side the approximate equality of the 10-18 μm emission by the two components of the system is consistent with a model by Huang (§4.2), in which the projected area of the eclipsing object corresponds to an edge-on disk and is about equal to the surface area of the F star; in fact, having a temperature similar to that of the star and being optically thick longward 10 μm, the disk at such wavelengths would become almost as bright as the primary. Let us notice, however, that also a black-body emission at about 1 000 K can fit well the data, suggesting the possibility of a completely opaque object made of dust.

Woolf also predicts that near 10 μm there will be a long secondary eclipse, and its depth is expected to be of the order of 0.2 mag. But equally significant it is to study the IR behaviour during the 1982-84 primary eclipse: if the 15-18μm excess comes really from the eclipsing body, it should be enhanced during the eclipse, since the primary's contribution is attenuated.

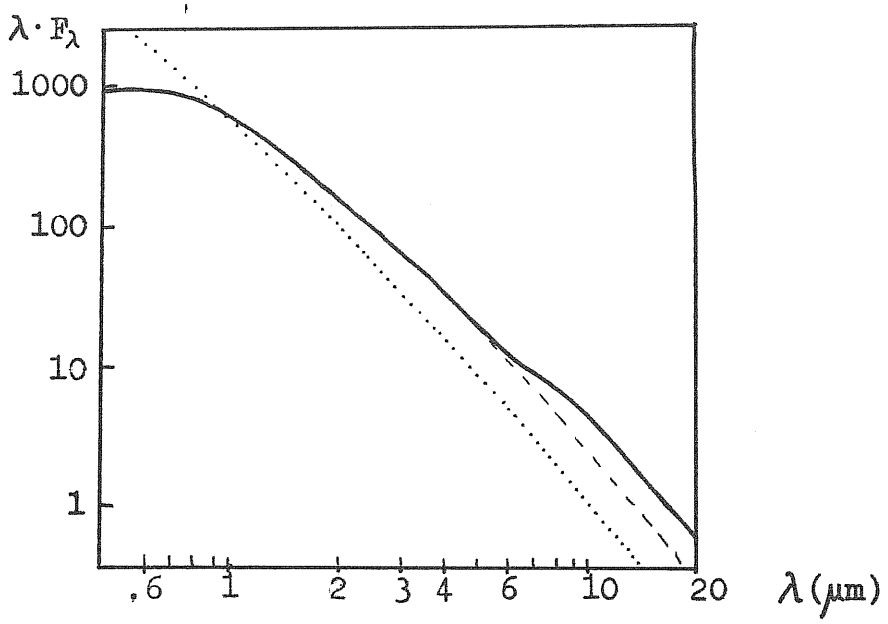

Fig. 2.4 - The IR Spectrum of ε Aur (Woolf, 1973), compared with the expected fluxes for an FØ star (dashed line) and for an AØ star (dotted line). The IR excess is evident longward 5 μm, and becomes rather constant over 10 μm.

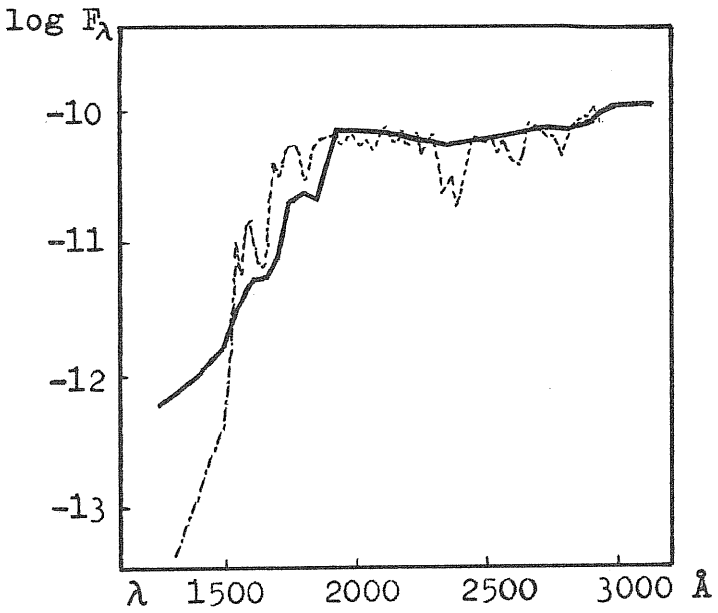

Fig. 2.5 - The UV spectrum of ε Aur (Hack, Selvelli, 1979), corrected for interstellar extinction (E_{B-V}= 0.30). The dashed line shows the theoretical flux (computed for an atmosphere with parameters T_e=7500 K and log g=1), which would be expected from a normal FØ Ia star. An UV excess is evident shortward 1500 Å (flux F_λ is in erg·cm^{-2}s^{-1}Å^{-1}).

2.5 The Ultraviolet Spectrum

The first ultraviolet observation of ε Aur was performed by Hack and Selvelli in 1978 with the "International Ultraviolet Explorer" satellite (IUE); an outstanding far-UV excess shortward 1650 Å was detected. The observed UV spectrum, corrected for interstellar extinction, is represented in Fig. 2.5 by the solid line; a comparison with the dashed line, representing the expected spectrum for the F star, shows the existence of an increasing UV excess towards the shorter wavelengths.

Interpreting the excess as due to the emission by a hot secondary component embedded in the eclipsing body, a radius and an effective temperature were derived for this secondary source, by a best-fit method assuming different radii and temperatures for the primary F star. Estimated values for the radius and the temperature of the secondary source were:

$$(2.9) \qquad r_B = (1.1 \pm .5)\cdot 10^{11} \text{ cm} \; ; \qquad T_B = 15\,000 \pm 3\,000 \text{ K} ,$$

while the radius and the temperature of the primary F star were consistent within the fitting range with those given by visible spetroscopy (§2.6). Assuming that the primary (FØ Ia) has absolute magnitudes $M(bol)_A = -7$ and $M(vis)_A = -7.1$ (°), values for the secondary's magnitudes can also be derived:

$$(2.10) \qquad M(bol)_B = -2.2 \; ; \quad M(vis)_B = -0.9 \; ; \; m(vis)_B = 9.2 .$$

Such a high value of $m(vis)_B$ could explain the difficulty of detecting the secondary in the visible.

Since the secondary is embedded in an extended envelope responsible for the primary's grey eclipse, the secondary itself should be permanently auto-eclipsed by such envelope.

(°) Note. These values for the primary are consistent with sp.cl. and U V data. But detailed model atmosphere (§2.6) provides fitting values 1.6 mag brighter : results (2.10) equally change.

Supposing this eclipse had the same grey depth (0.8 mag) as the primary's one, it was hypothized that secondary's "intrinsic" magnitude should be obtained by subtracting 0.8 mag from $M(vis)_B$ in (2.10), while the "intrinsic" radius should be about $\sqrt{2}$ times larger than r_B in (2.9). Such values lead, finally, to conclude that the secondary should be a late-B main-sequence star (°).

The mid-UV flux longward 1650 Å shows no appreciable excess; hence it should come almost entirely from the F star. A high-resolution analysis of the mid-UV spectrum was performed by Castelli et al. (1982), by fitting an LTE model atmosphere of the F star, previously used at visible wavelengths (§ 2.6). A complete line identification was given from about 2450 Å to 3230 Å; abundances were found to be almost solar, with a slight overabundance of iron-group elements but not of Fe itself. Several peculiarities were studied: (a) variability of some lines with time; (b) presence of emission components in the MgII λ 2800 Å resonance doublet and also in some other strong lines as FeII multiplets UV 1, 62 and 63; (c) presence in many lines of a blue-shifted variable absorption component.

These out-of-eclipse peculiar lines can be explained, supposing they are formed at various heights in an expanding region over the photosphere of the F star; expansion velocity of this "shell" is then found to be 37 ± 15 km/sec. The problem is where does this expanding medium extend in the system of ε Aur, since it could extend from the cromosphere to a circumstellar envelope or even to a surrounding interstellar region.

Ultraviolet observations have thus proved to be fundamental in unveiling the nature of the ε Aur system,

---

(°) Note. Let us remark that $M(bol)_B$ and $M(vis)_B$ could be also 1.6 mag brighter than in (2.10), if primary's assumed values are those of model atmosphere.

since : (i) the far-UV spectrum permits us to observe directly the secondary, and (ii) the mid-UV shows us the behaviour of primary's envelope. The study of the 1982-84 eclipse at ultraviolet wavelengths is then to provide otherwise inacessible informations, such as : (i) a possible discrimination of the two components' emission, and (ii) a test for the primary's envelope extension.

2.6 The Spectrum of the F Star

The spectrum of the visible star, that is the primary component usually classified as an F-type supergiant, has been studied out of eclipse first extensively by Hack (1959); identifications and equivalent widths were provided. Moreover it was evidenced spectroscopic intrinsic variability, as an effect of variable turbulence. In particular, slight variations in profiles and equivalent widths of the lines were found out of eclipse. Consequently certain close pairs of lines, such as the Fe I pairs at λ4250 and at λ4271, or the pair (Ti II + Sc II) at λ4400, sometimes are blended (broad-line spectrum) while at other times they are resolved (narrow-line spectrum); examples are shown in Fig. 2.6 .

Later the out-of-eclipse spectrum of ε Aur has been revisited by Castelli (1977), who measured radial velocities for all ions in different spectra. Analyzing intrinsic out-of-eclipse variability, she drived the following results: (i) a fast variation of equivalent widths and of profiles with time intervals even of 15 minutes, while there is no corresponding variation of radial velocity, and hence it

Table 2.3 - Basic data of the Components

Parameter	Symbol (Unit)	Primary Star	Secondary Star
Spectrum	Sp.Cl.	FØIa	B8:V
Absolute luminosity	M_{vis}(mag)	-8.7	-1.3 (b,c)
Bolometric corr.	B.C.(mag)	0.11	-1.3
Temperature	T_{eff} (K)	7800	15000
Radius (spectroscopic)	r ($R_\odot$)	277 (a)	1.8 (b,d)
Mass (spectroscopic)	m ($M_\odot$)	28	5: (e)
Surface gravity	log g (cgs)	1.0	4.5

Note. Data are best-fit values, for separate independent atmospheric models of the F star (Castelli, 1978) and of the B star (Hack and Selvelli, 1979).

Remarks: (a) differing from the value r_1 on Tab. 2.2 (which is inclination-affected);
(b) corrected for the auto-eclipse by the envelope (half depth of primary eclipse = 0.4mag);
(c) for fitting the companion's luminosity: 1.6 m.brighter
(d) black-body radius r_B (envelope's radius r_2 is given on Tab.2.2);
(e) derived from M-L relation (not satisfying the mass function of the system! See Tab. 2.1).

can be due to macroturbulence; (ii) a different behaviour of the radial velocity of the Balmer lines with a time interval of 2 months, which indicates variations in the characteristics of the external layers of the atmosphere. Such kind of activity, which is common in supergiants, could be possibly related with the cepheid-like photometric fluctuations (2.8) affecting the light curve. Moreover it was evidenced an asymmetry in almost all the strongest line profiles, with a red sharp edge and a violet wing.

Spectral analysis of the F-star's atmosphere was finally improved by Castelli herself (1978). A radiative-equilibrium plane-parallel LTE standard model atmosphere was computed, and fitted with observational data. By this procedure abundances were derived, which resulted not significantly different from solar ones. Asymmetry of line profiles (Fig 2.7a) was attributed to negative acceleration in the outer atmospheric layers. The final parameters provided by the model for the F star are listed in Tab. 2.3, together with the parameters (2.9) suggested for the companion B star on the basis of UV observations. As one can see by comparison with the values derived in Tab. 2.1, the primary's mass $m_1 = 28M_\odot$ given by the model implies a problematically high mass $m_2 \simeq 15M_\odot$ for the secondary.

A comparison between the observed and synthetic spectrum shows that generally the observed line-profiles are very well reproduced by the computed ones; the only significant disagreement concernes the slight observed asymmetry due to deceleration, quoted above. There are however some remarkable exceptions, concerning in particular the H and K lines of CaII (Fig. 2.7 b) and the H_α feature (Fig. 2.7 c). As regards the K line, for example, an additional multiple absorption

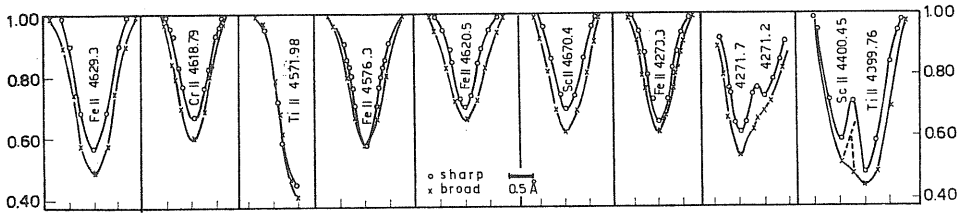

Fig. 2.6 - Sharp and broad-line spectrum. Comparison of line profiles is shown (Hack, 1959).

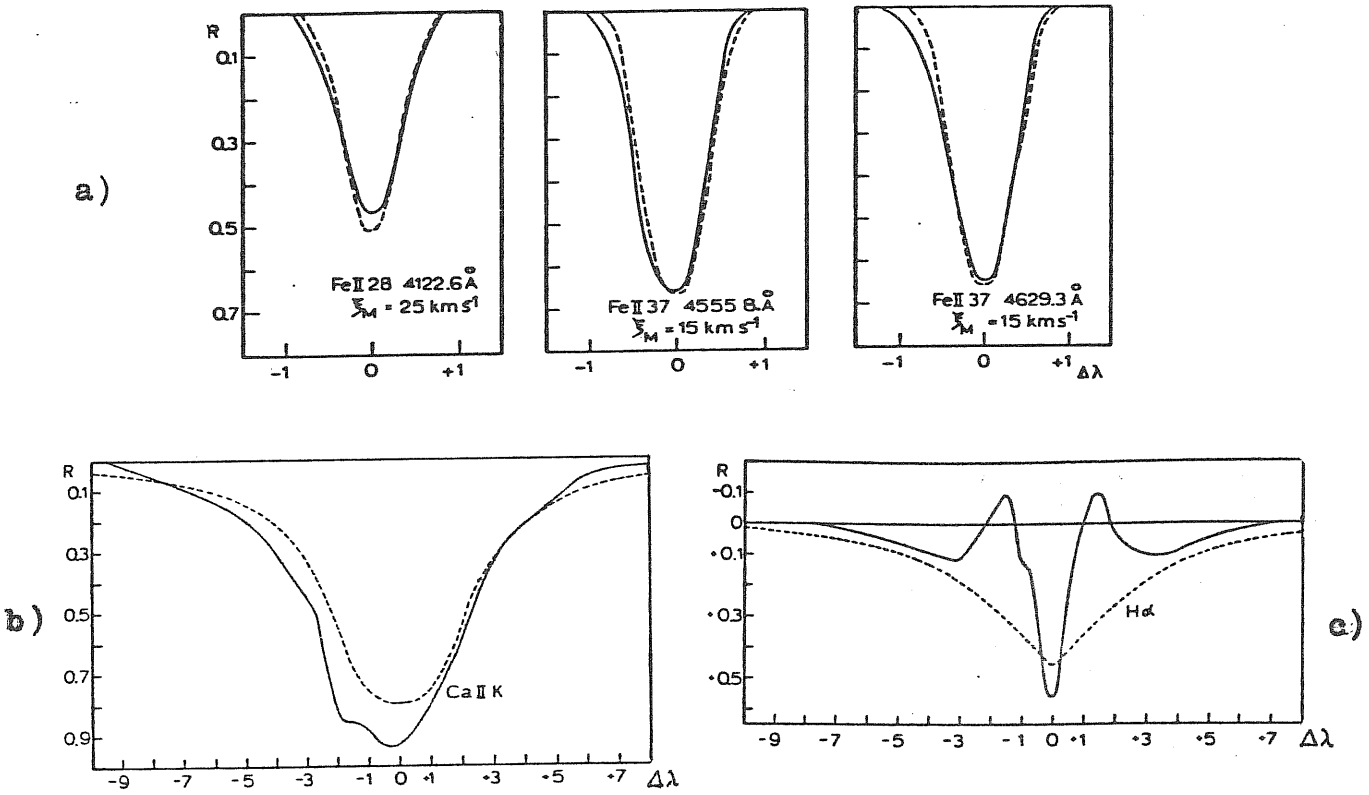

Fig. 2.7 - Out-of-eclipse line profiles. Comparison between observed (————) and computed (----------) profiles (Castelli, 1978).

a) Asymmetry of metallic absorption lines: sharp red edge + violet wing

b) CaII K-line shows complex absorption feature superimposed on the violet side (maybe variable)

c) Hα displays emission peaks displaced by about -70 and + 60 km/s.

component is superimposed over the violet wing; such effect can be interpreted as a circumstellar contribution, which might be also variable with time.

The H_α line of hydrogen exibits a still more interesting structure. A central core with a total half-width of about 1 Å is flanked by a couple of sharp emission features extending about 2 ÷ 3 Å from the line centre ; beyond the emissions there are two shallow absorption wings, broad at least 8 Å on either side of the line centre. Such extended wings are a normal feature of the hydrogen lines. The core absorption feature has a central intensity of about 40÷50% of the continuum , and the emission features rise to about 20 ÷ 30% above the continuum; the broad absorption wings have a depth of about 10% below the continuum and are clearly seen only on tracings. The whole H_α structure as seen outside of eclipse is roughly symmetrical, but changes do do occur most noticeably in the emission features, which exhibit marked variations in total and relative strengths (Castelli, 1977).

3. - THE ECLIPSED SPECTRUM

Fundamental information, concerning the structure and the physical condition of the eclipsing body, can be derived by examining the behaviour of the visible spectrum during the eclipse. In fact, characteristic variations of the line profiles appear in correlation with the eclipse phase, and are thus interpreted as produced by the interposed object. It is surprising that, although such behaviour is known by almost half a century, generally theoreticians (allowing for some exceptions) did not take it in any consideration while building up models of ε Aur. By presenting in this section the information available from earlier eclipses, let us say in advance that the importance of visible spectroscopy, as a tool for investigating the nature of the eclipsing object, has been confirmed once more during the last 1982-84 eclipse, providing most of the results obtained by the author and discussed in Part 2 of this book.

3.1 The Shell Lines

The most outstanding feature of the eclipsed spectrum consists in a doubling of the majority of the F-star's lines, depending on the eclipse phase (its detection by Adams and Sanford dates back to 1930). Shortly before the 1st contact, it appears on the F-star's spectrum a new set of lines, usually called "shell lines" because of their origin, as we shall see. These lines are first weak and sharp, and

red-shifted with respect of the corresponding stellar lines. Then they strengthen at the 1st contact and during the first partial phase. As the 2nd contact is approached, the shell lines become broader and weaker, and cease to be visible shortly after the 2nd contact. About two months before the 3rd contact, the same shell lines become visible again; at this time they are violet-shifted with respect to the stellar lines and broad again, having roughly the same width as the stellar lines. The shell lines become sharper and stronger during the second partial phase, then weaker again as the 4th contact is approached. After the 4th contact, the shell lines continue to weaken, but remain visible for at least four months during the post-eclipse phase.

The foregoing description applies specially to the shell lines of neutral and ionized metals (Fig. 3.1). Anyway, it is difficult to state unequivocally whether such shell lines actually disappear near mid-totality, since a shell line usually manifests itself only as an asymmetry of the corresponding stellar line. Unless the asymmetry is pronounced, it is indistinguishable from a normal variation of the stellar line profile, such as those seen out of eclipse; and just towards mid-totality the shell lines give no asymmetry, being superimposed centrally over the stellar lines' cores. Certainly, however, the metallic shell lines become too difficult to be measured during the total phase except towards the beginning and the end (that is at 2nd and 3rd contacts).

The shell lines of hydrogen display a rather different behaviour. They persist throughout the eclipse, and they are fairly broad and strong most of the time. In particular, they appear to increase in strength until mid-eclipse, and to decrease after.

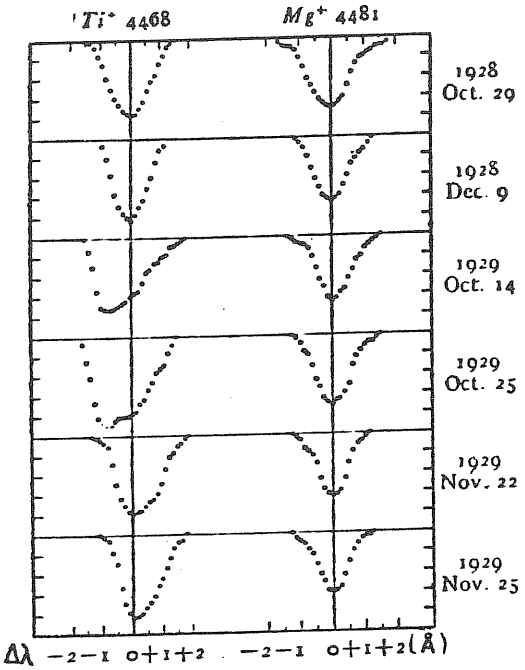

Fig. 3.1 - Metallic lines on the egress phase (as first illustrated by Struve and Elvey, 1930). The typical behaviour is displayed by TiIIλ4468, showing the shell line superimposed on the violet side. On the contrary, MgIIλ4481 is significantly peculiar, showing no shell line.

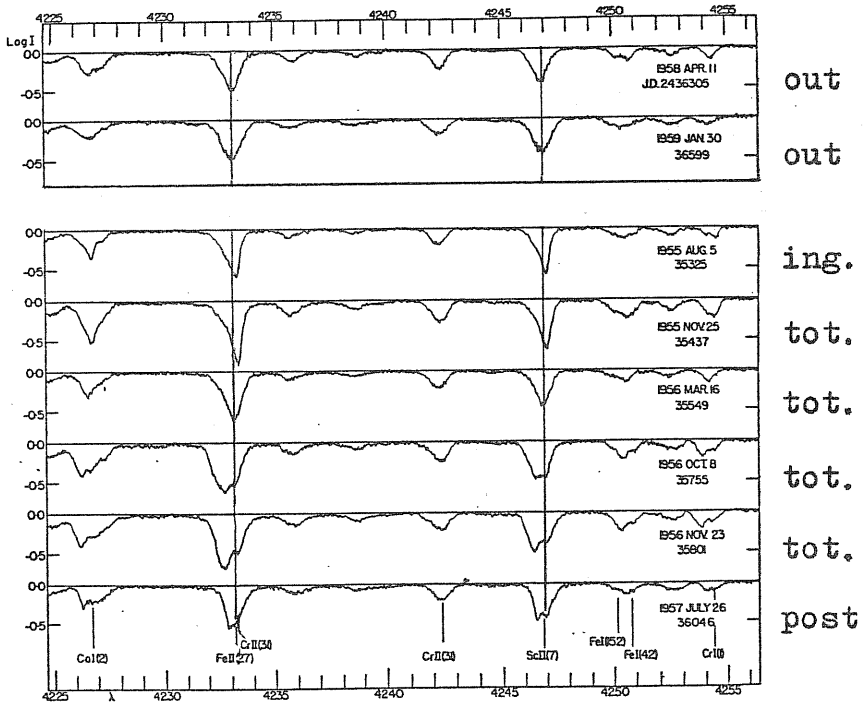

Fig. 3.2 - Typical behaviour of the lines during the 1955-57 eclipse. The shell component drifts from the red to the violet and persists also post eclipse (Morris,1963).

The observed behaviour of the eclipsed spectrum has been interpreted by Kuiper et al. (1937), assuming that the shell lines are formed in an outer gaseous shell of the eclipsing body. The absorption spectrum of this region has to reproduce the spectrum of the primary, since these layers are supposed to be excited by the primary's radiation. The shift toward the red before totality, and toward the violet after it (Fig. 3.2), can then be attributed to a rotation of the eclipsing body, supposing it rotates in the same sense as the orbital motion. Similar considerations may also explain the behaviour of the broader shell-components of Balmer lines. For metals, v_{rot} is about 20 Km/s on ingress and 35 on egress.

The physics of the shell spectrum has been first discussed by Kraft (1954), and then extensively analyzed by Hack (1959, 1961) on the basis of the curve of growth method. The physical problem concerns the presence of exciting diluted radiation in the shell region. From the geometry of the system one finds that the F star, seen from the companion, covers a fraction of celestial sphere equal about to 10^{-4} ; that is to say by definition that the geometrical dilution factor is 10^{-4}, for the primary's radiation in the shell region. If no other effects are present, this geometrical factor 10^{-4} should also represent the effective physical dilution factor; that is, in the shell region one should have the normal (non-metastable) atomic levels depopulated by a factor of 10^4. With such a strong depopulation, Kraft (1954) showed that the eclipsing body had to be 10^3 times less opaque than observed during the eclipse.

The problem could be overcome, by directly measuring the effective physical dilution factor in the shell region. Hack (1961), examining high-dispersion spectrograms of the

1955-57 eclipse, found in the shell spectrum evidence of diluted radiation by a factor of 10^{-1}, since normal levels of Ca I, Mg I and Fe I were depopulated by a factor of 10 with respect to metastable ones. The difference, between the physical and geometrical dilution factors in the eclipsing body, was interpreted as indicating the presence of a source of additional UV radiation; this radiation could be able of populating the non-metastable levels with more efficency than the geometrically diluted radiation of the F star.

Anyway it was rather difficult to explain how an F super-giant could be the source of a strong UV excess such as the one required for the above mechanism. To solve this last problem, on 1961 it was proposed by Hack that the UV ionizating source could be a hot dwarf, embedded in the central region of the eclipsing body itself. This model of ε Aur (§4.1) has received a strong experimental confirmations on 1979, by the discovery of the UV excess.

3.2 The H_α Feature

Observations of the H_α line show that this feature, during eclipse, undergoes a sequence of changes which are more complex than those observed for the other lines. These changes have been described in detail by Wright and Kushwaha (1957); here they are illustrated in Fig. 3.3, and should be compared with the observed out-of-eclipse profile of Fig. 2.7c. The most outstanding changes during the eclipse concern the emission wings: on ingress the red wing is sobstituted by an absorption component, on mid-totality both wings are sobstituted by a broad absorption feature, and on egress the violet emission

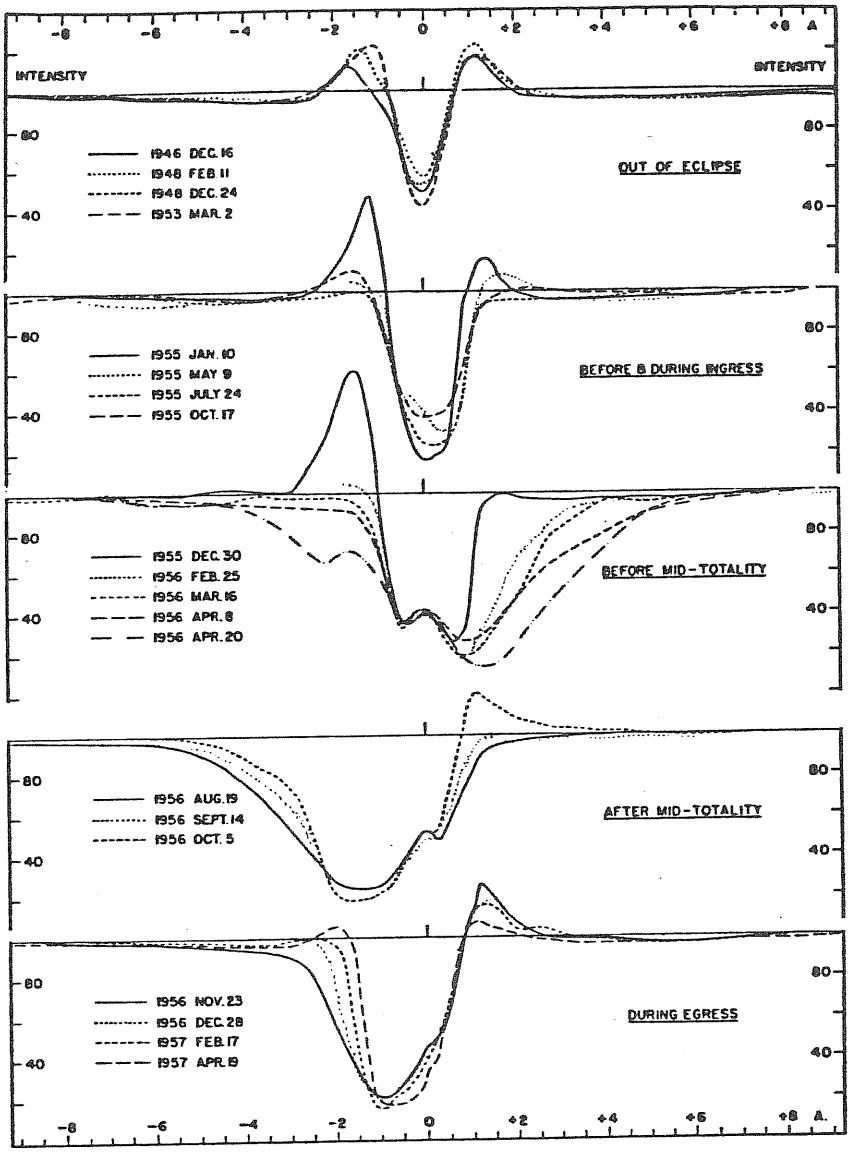

Fig. 3.3 - Observed intensity profiles of Hα in the spectrum of ϵ Aurigae. The continuum (at intensity 100) is relative to the F star, determined at wave-lengths more than 10 Å from Hα . The terrestrial absorption lines have been eliminated from the intensity tracings (Wright, Kushwaha, 1957).

wing is sobstituted by an absorption component. Clearly, these phenomena are explained by the superposition of a (broad) absorption feature, which drifts from a red-shifted toward a violet-shifted position as the eclipse goes on. Such behaviour is the same as the one observed for the other (sharper) shell lines; hence also this effect can be explained as due to the interposition of an eclipsing body, which rotates in the same sense as the orbital motion.

Let us now discuss briefly the physical processes, by which the $H\alpha$ absorption feature may be originated in the eclipsing body. The mechanism by which the H_α line is excited is not immediately apparent. One may consider radiation by the surface of the F star, as a possible exciting mechanism; but applying the computations by Morris (1963) it results that, for a reasonable F-star surface temperature of 7300 °K, the effect is by far too small to account for the observed intensity. The problem is similar to the one already described, about the formation of the metallic shell spectrum in presence of diluted radiation from the F star. Therefore, it remains the possibility that the hypothized central <u>hot star</u> of the secondary component (§2.5) radiates enough UV light, to produce the necessary excitation.

A further clue to the nature of the excitation mechanism is the fact that no large shell absorption is seen at $H\beta$. There is thus an indication that the Balmer decrement in the shell spectrum is very steep, which is a characteristic of collisional excitation (Aller 1956). This fact suggest that the broad H_α feature in the shell spectrum could be excited also by <u>collisions</u>.

4. - CLASSICAL MODELS OF EPSILON AURIGAE

In this section we shall briefly review-without entering into mathematical details - the different models which have been proposed for ε Aur, in a historical perspective extending from the early 1920s until just before the last eclipse, which was awaited as the definite test for selecting the "correct" model. But, remarkably, such a relection did not take place: apart from the details, at least three basically different models (those by Hack, Huang and Wilson) were confirmed at the same time, as describing different aspects of the same composite structure (§ 5). The various models are illustrated on the next Figure 4.1, evidentiating their hypothetical visual appearance

4.1 First Ideas

The first astronomer, who tried to give a hypothesis about the nature of the mysterious body, which at intervals of 27 years eclipsed the visible component of ε Aur, was Ludendorff himself in 1924. He suggested that the eclipsing body could be a swarm of meteorites, but after he gave up developing further this idea, perhaps because he was not very sure of it. But today, after 60 years of research, we can realize that probably Ludendorff was much nearer to the truth, than he himself and his contemporaries could imagine.

In 1937 Kuiper, Struve and Stromgren produced the first real model of Epsilon Aurigae (Ap.J. 86 , 570).

Figure 4.1 - Classical models of ε Aur (artist's conception):

a) Ludendorff, 1924
b) Kuiper et al., 1937
c) Struve, 1955
d) Hack, 1961
e) Huang, 1965
f) Kopal, 1971
g) Handbury, Williams, 1976
h) Plavec, 1981
i) Cameron, 1971
j) Wilson, 1971

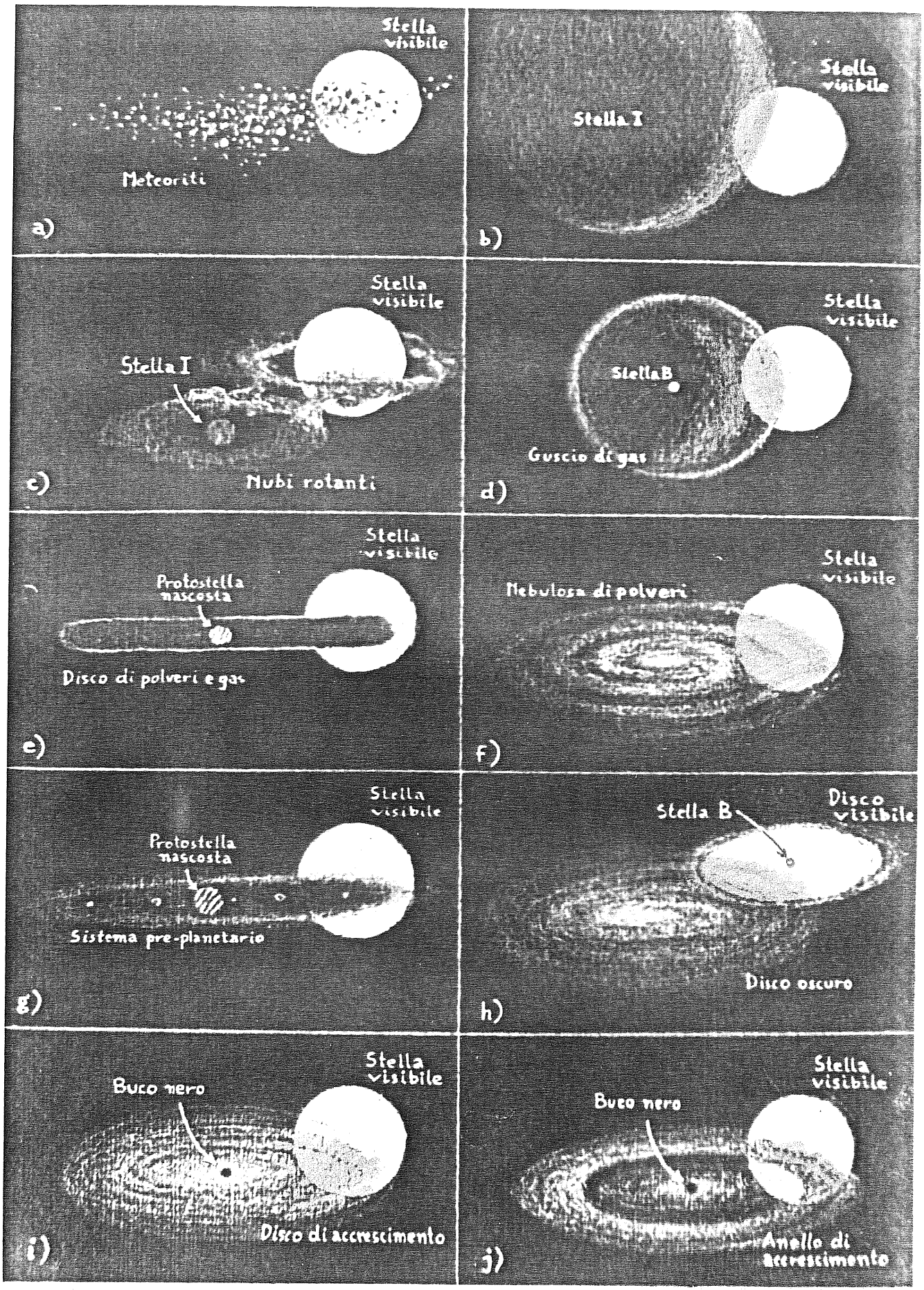
Stella visibile
Meteoriti
a)
Stella visibile
Stella I
b)
Stella visibile
Stella I
Nubi rotanti
c)
Stella visibile
Stella B
Guscio di gas
d)
Stella visibile
Protostella nascosta
Disco di polveri e gas
e)
Stella visibile
Nebulosa di polveri
f)
Stella visibile
Protostella nascosta
Sistema pre-planetario
g)
Stella B
Disco visibile
Disco oscuro
h)
Stella visibile
Buco nero
Disco di accrescimento
i)
Stella visibile
Buco nero
Anello di accrescimento
j)

Fig. 4.1

They imagined that a huge fading "infrared super-star", of low temperature and density, existed. Such body, called "I Star", should rotate round the visible component of Epsilon Aurigae, and be much larger (2 800 solar radii). Passing in front of the visible companion, this body should completely eclipse the visible star, but still should let its light partly filter; in fact, the layers of I Star were supposed to be semi-opaque. Even if this model became soon popular, it showed some weak points, from the very beginning. For instance, during the eclipse, the thicker internal zones of I Star should have partly absorbed the light of the primary, and some characteristic spectral lines would have appeared; but these lines (or molecular bands) have never been observed. Furthermore, owing to the temperature that the "I Star" was supposed to have (little above 1 000 K), this huge body should have produced an intense infra-red emission. This radiation, in spite of repeated researches with more and more sensitive instruments, had never been revealed.

For these reasons, Otto Struve had revised in 1955 the first model, drastically reducing the dimensions of cumber some "I Star", and embedding it in a very large system of gas clouds (Struve, 1956); these clouds were supposed to move, in a complicated shape of an "eight", wrapping up also the visible star. In spite of these argumentations,it remained the fact, already discovered by Kraft one year before (Kraft, 1954), that the gas could hardly be opaque enough, as to produce the observed eclipse.

4.2 Basic Conceptions: Shell and Disk

A new generation of models appeared after the 1955-57 eclipse. Basically, they all descended from two different configurations proposed in the early '60s. As described hereafter, the one explained in particular the existence of the shell spectrum, while the other accounted for the dark nature of the eclipsing body.

Margherita Hack, after analysing (Hack, 1959) a sample of spectra obtained during the 1955-57 eclipse, proposed in 1961 the first of these new models. She suggested that the object, orbiting around the bright visible star, could be a hot dwarf presumably of type B (too weak, compared with the primary, to be observable), surrounded by a semi-transparent gas shell. This secondary component, with its gaseous envelope, eclipsed periodically its bright companion star, which remained anyway observable in transparence. Such a structure, where the gaseous shell could maybe have an elliptic, discoidal or ring-like shape (Fig 4.2) produced naturally the characteristics of the observed eclipse. Moreover, it was very reasonable that a B star could possess a gaseous envelope, as this fact had already been observed in other cases. Also the semi-transparence of the gas found a convincing physical motivation, since the ultraviolet radiations emitted by the B Star were enough energetic to ionise the gas in the shell; as a consequence, the shell should become semi-opaque and grey, due to electron scattering (a mechanism that Struve had already suggested, although he didn't find the source which could ionise the gas. The UV excess observed on 1978 (§2.5) gave a strong support to this model; notwithstanding, it was rather difficult to explain why the hot source resulted underluminous by about one order of magnitude, both for ionising the shell and for fitting the mass-function of the system.

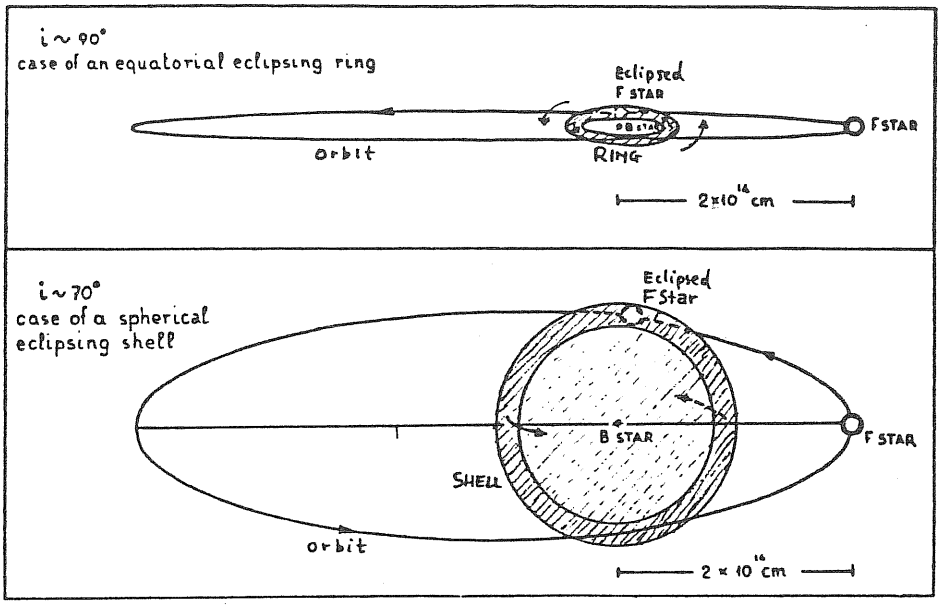

Figure 4.2 - Geometry of Hack's model ; the shell/ring is semitransparent.

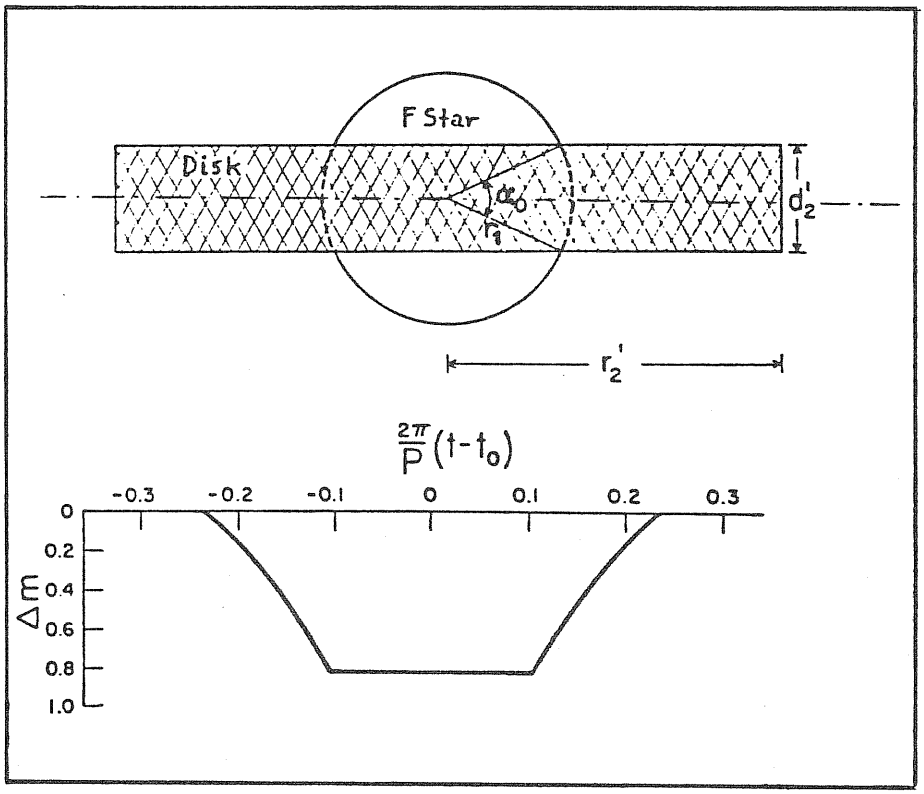

Figure 4.3 - Geometry of Huang's model ; the band is opaque. Predicted light-curve is also shown.

Su-Shu Huang suggested in 1965 another possible configuration for the system of Epsilon Aurigae, which could explain many of the pecularities observed, and had the merit of remarkable conceptual simplicity (Huang, 1965). He imagined that, round the visible star, there was rotating a secondary companion embedded in a discoid nebula, supposed to be seen in section due to prospectic effect. This nebula, which Huang compared to the one originating the solar system, should anyway have resulted completely opaque, just owing to the fact that it appeared in section that is in the direction of its maximum thickness. In this way, the problem of the invisibility of the secondary component was solved, since it could be well hidden in the center of the opaque disk. Then the eclipse must have occurred when, in front the visible star, the nebular disk had passed; such a disk, seen in section, must have appeared like a dark band, on the body of the primary star (Fig 4.3). During the transit, the light arriving on the Earth would then diminish by a constant factor, while the colour and the spectral characteristics should obviously remain unchanged. By this mean , both the "flatness" and "greyness" of the eclipse were explained. Huang contested the electron scattering as a cause for the opacity of the disk, saying that it should have been accompanied by other effects, which had not been observed (such as light polarization). In turn, he proposed that the material which caused the nebula to be opaque consisted of dust particles, formed out of nebular gas itself; he went as far as to state that the nebula could contain also bigger conglomerates, solid bodies, or even bodies with planetary sizes. Although it was in good agreement with infrared data (§2.4), Huang's model had a basic deficiency: it did not account for the observed shell spectrum.

4.3 The Ring Model

On the early 1970s, it seemed that the solution for the problem of ε Aur - a system containing a dark object of about ten solar masses - had been found at last. A.G.W Cameron (1971) proposed that, orbiting around the visible star, it could exist a black hole of ten solar masses surrounded by a disk of solid particles. But such an idea was abandoned in a short time, as soon as it was realized that no sign of a black hole existed on ε Aur, since no X-ray or γ-ray emissions were observed.

Though still considering the short-lived idea of a black hole for secondary, Robert Wilson at the same time (1971) proposed also a new interesting model for the eclipsing body. He suggested that around the secondary it was rotating an opaque ring of dust seen obliquely, flat and thin, and with a semitransparent opening in the middle (similar in appearance to the rings of Saturn). Such a geometry reproduced very well the light-curve of both eclipses on 1929 and 1956 (Fig. 4.4, dashed lines), and suggested a higher transparency on the latter eclipse. The negative bump near mid-eclipse on 1956 was moreover interpreted as due to a smaller transient cloud embedding the massive object at the center of the ring.

Later, the same model was generalized by Huang himself (1974), who computed the theoretical light-curves for semi transparent discoidal structures, assuming different thickness, different radial distributions of opacity, and different inclinations. By a suitable (although not univocal) choice of the parameters, the observed light-curves could be fitted very precisely (Fig. 4.4, solid lines); and also in this case, the central transparency resulted higher on 1956 . Finally, let us enticipate that the ring model received nowadays a striking confirmation, by the mid- eclipse brightening clearly observed on 1983 (cf. § 9.2).

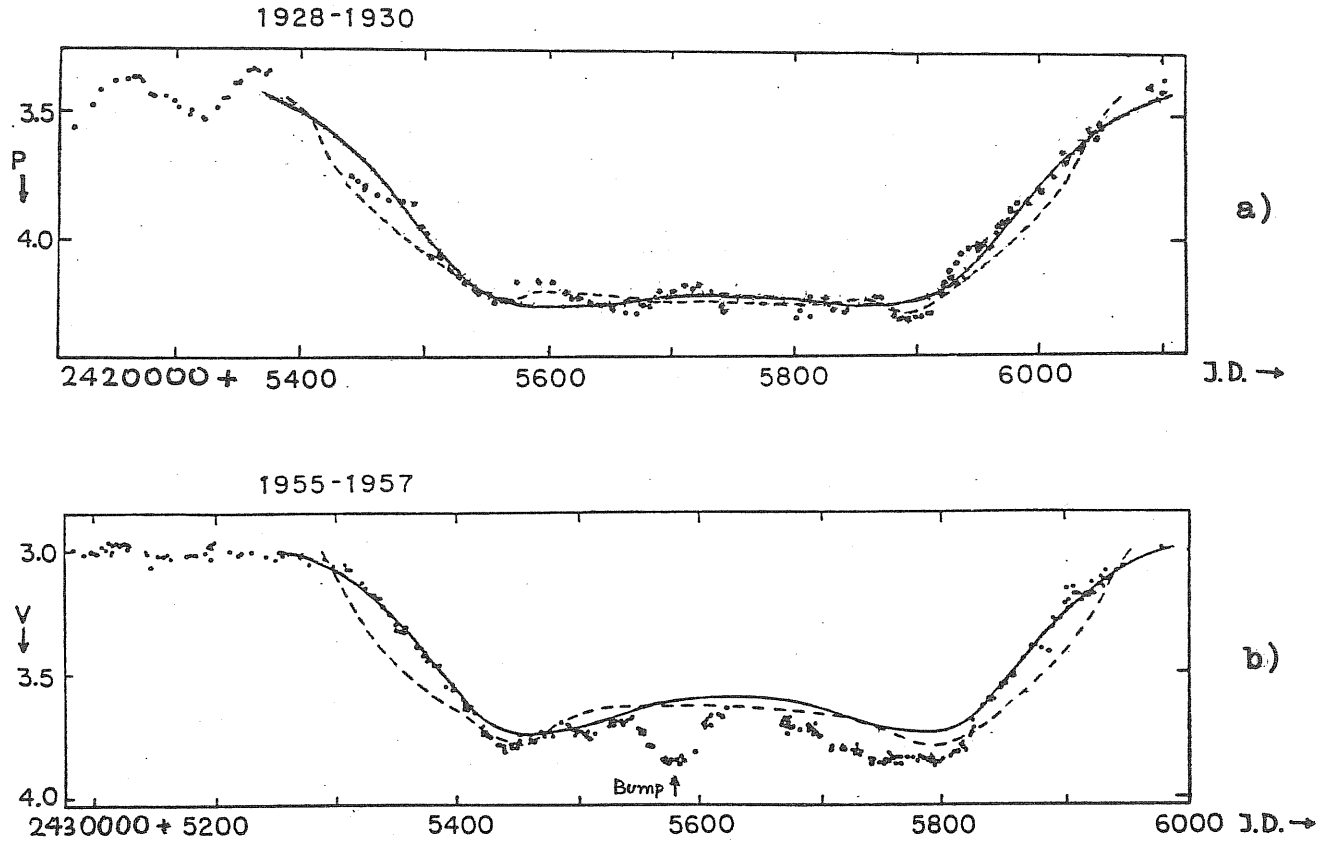

Fig. 4.4 - Ring model fitting: a)eclipse of 1929; b)eclipse of 1956.

Dashed curves: Wilson,1971 (inclined, thin, opaque ring with central semitransparent hole).

Solid curves: Huang,1974 (edge-on, thick, semitransparent disk with central rarefaction).

4.4 Implementations and Variants

Zdenek Kopal, who already since the 1950's had maintained that the object causing the eclipse in the ε Aur system was a dust cloud, presented his own improved model also on 1971 . As to the geometry of the eclipse, Kopal's idea followed partially Hack's model: the eclipsing body was identified with a large nebular discoid, homogeneous and semi-transparent, seen obliquely. This nebula , which was supposed to be formed by coarse circumstellar dust, and maybe by larger solid fragments, was more like the one imagined by Huang (or even by Ludendorff, half a century before). In particular Kopal was convinced that the nebular object was a real pre-planetary system, similar to the nebula which gave origin to the solar system; moreover he thought that the object was only in the very first stages of evolution, so that in the center of the nebula the star formation process was just to begin. Hence, according to Kopal, in the ε Aur system the secondary component didn't exist as a star yet, and simply this fact should have been the reason for the unobservability of the secondary.

Handbury and Williams tackled the problem in 1976, presenting a model which was somewhat more sophisticated than the previous ones (Handbury and Williams, 1976). Improving the idea that the eclipsing body was a nebular disk seen in section, they stated that it should appear like an opaque disk , semi-transparent at the edges, being presumably more rarefied in its outer parts. Without putting special constraints on its composition, they suggested it might be a mixture of gas and dust. Then, from the presence of this nebular material, one could infer that the ε Aur

system was of very recent formation. Therefore, the two researchers believed that the visible primary supergiant was in its first stages of evolution (pre-main sequence phases), instead of being in the final stages, like the ordinary supergiants are (and like it was thought in the other models). As regards the eclipsing disk, also Handbury and Williams thought it was a pre-planetary nebula, in the middle of which a protostar should be hidden, ready to make itself visible as soon as it would become a real star. The two authors suggested we should expect this occurring, so that their model would be confirmed; it's a pity we'll need waiting perhaps some ten thousands years!

Mirek Plavec finally produced the most exotic idea : two pseudostellar discoids seen obliquely, revolving the one around the other (Plavec, 1982). He presumed that the visible star, instead of being an ordinary supergiant, was actually a hot rotating disk which only simulated a stellar behaviour, and contained in its center a B-type dwarf. Around this whole, a large ellipsoidal grey body, more or less flat should rotate, and be responsible for the eclipse (vaguely like Struve's "I Star"). This strange model overturned the classical image of the ε Aur system, by identifying the disk and the B Star with the primary component, and not with the secondary one. But, along with the interest of originality, Plavec's model had also the little attracting characteristic, of explaining the observed phenomena in the most complicated way. This would not mean, however, that such a model should have been discarded "a priori".

5. - THE 1982-1984 ECLIPSE

We shall not review here all the recent literature about this eclipse, since the basic works are already organically collected and commented in the proceedings of the two workshops, which were held on the subject in 1985 : the first in Tucson,AZ in occasion of an AAS meeting (°), the second in N.Delhi in occasion of the IAU General Assembly (°°). But in the following pages we shall present some figures, synthetising the most outstanding results of the observational "Eclipse Campaign".

5.1 Important Notice

The times of contact for this eclipse have been slightly different from those predicted by Gyldenkerne (1970), so that ambiguity may arise about the denomination of the phases. Since most results were published when the eclipse was still on course, and the exact contact dates were not yet known by that time, in most of the literature and also in the present work, the terminology is referred to the predicted times, and not to the observed ones. Hereafter, for example, spectra labelled F12, F13 and H7 will be classified "early egress", with respect to the predicted 3rd contact; but they should be classified "late totality", considering the really observed time of the 3rd contact. As a basic reference, we report on Table 5.1 the predicted and observed contact times, as given by Schmidtke (°).

(°) Stencel,R.E.(ed.): "1982-1984 Eclipse of ε Aur", NASA Conf.Publ.2384
(°°) Swings,J.P.(ed.): IAU Highlights of Astronomy, 7 , pp. 143-206 (1986)

Table 5.1 - Times of Contact for the 1982-84 Eclipse

Contact	Predicted		Observed	
	Date	JD	Date	JD
1st	82 Jul 29	2 445 180	82 Jul 14	2 445 165
2nd	Dec 11	315	Nov 28	302
3rd	84 Jan 9	709	84 Feb 17	748
4th	May 29	850	Apr 21	812

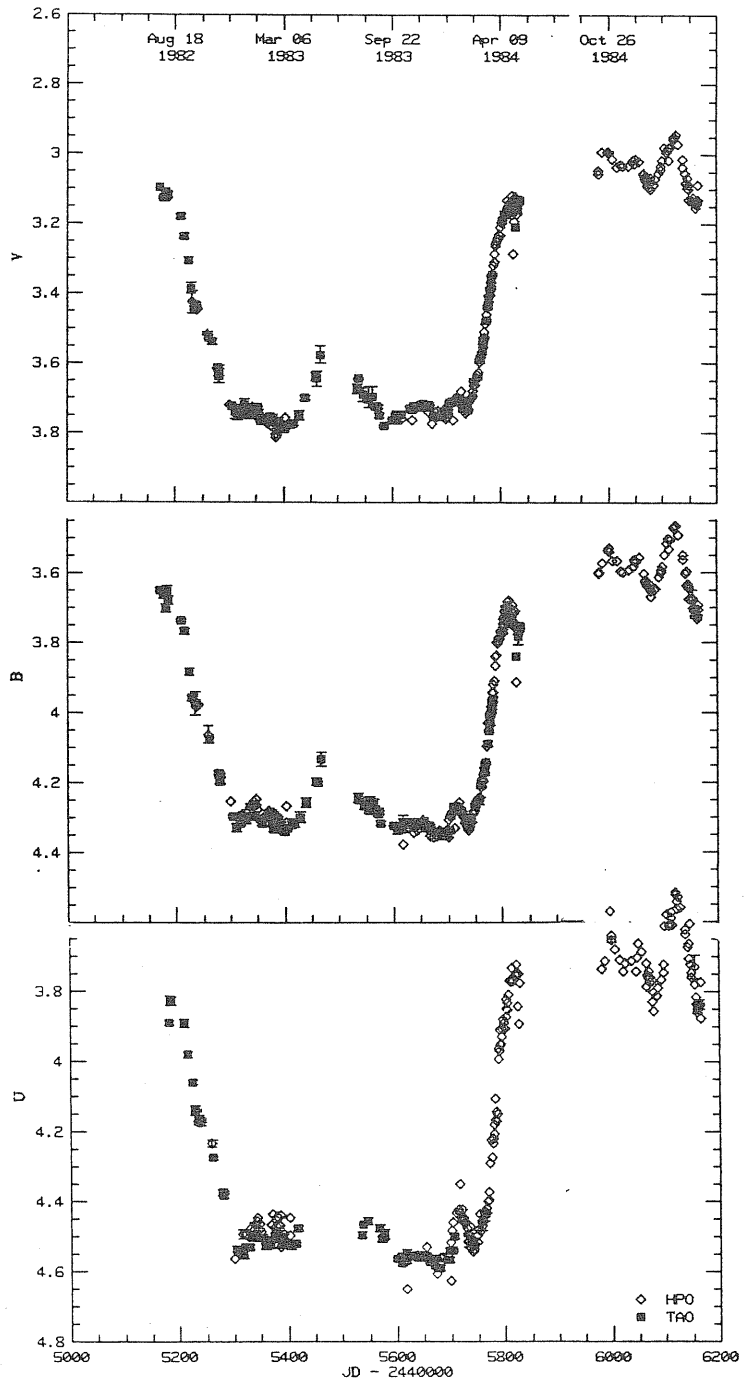

Fig. 5.1 - UBV photometry

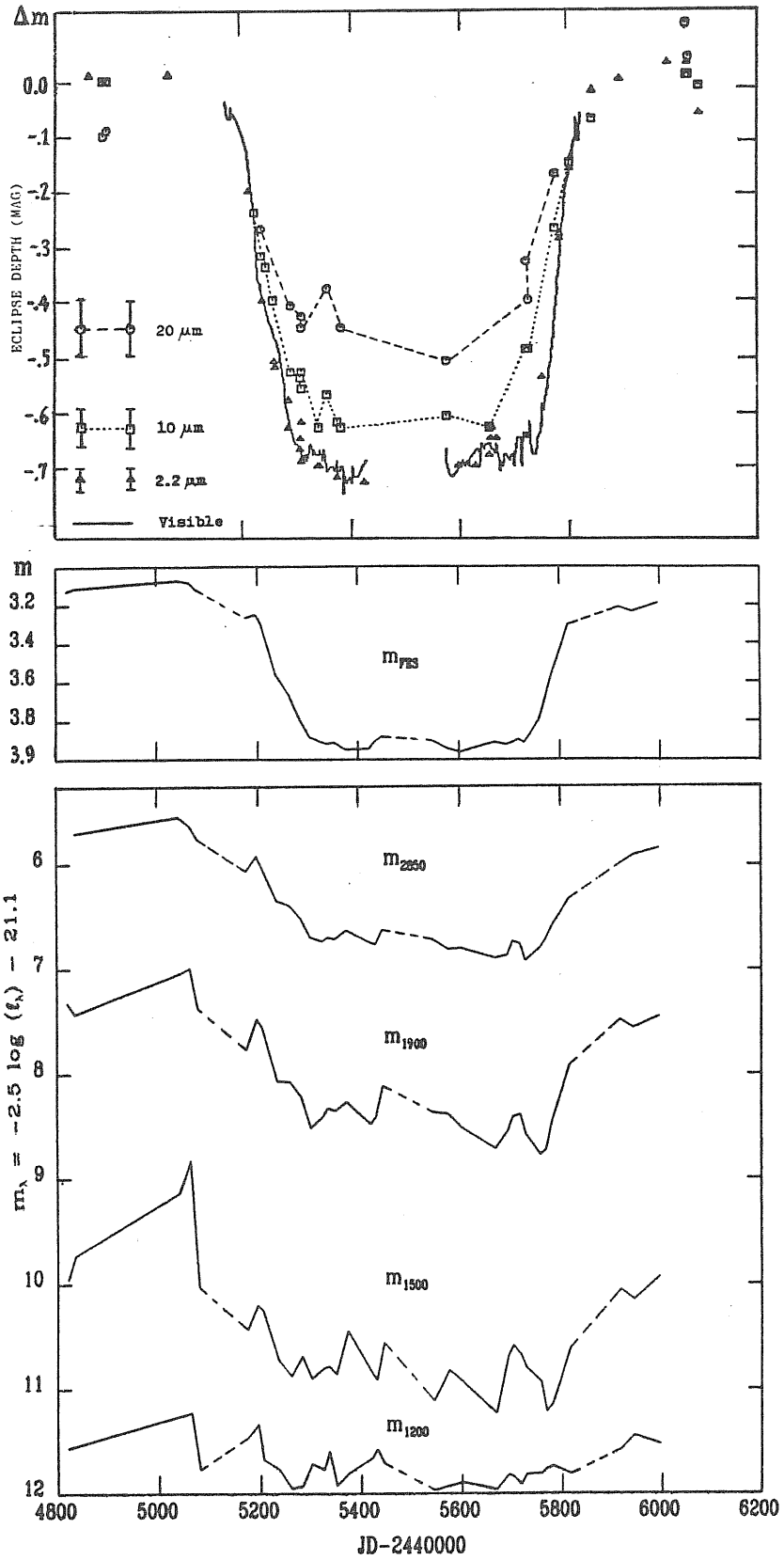

Fig. 5.2 - Multi-wavelengths light curves

a) Infrared
b) Visible
c) Ultraviolet

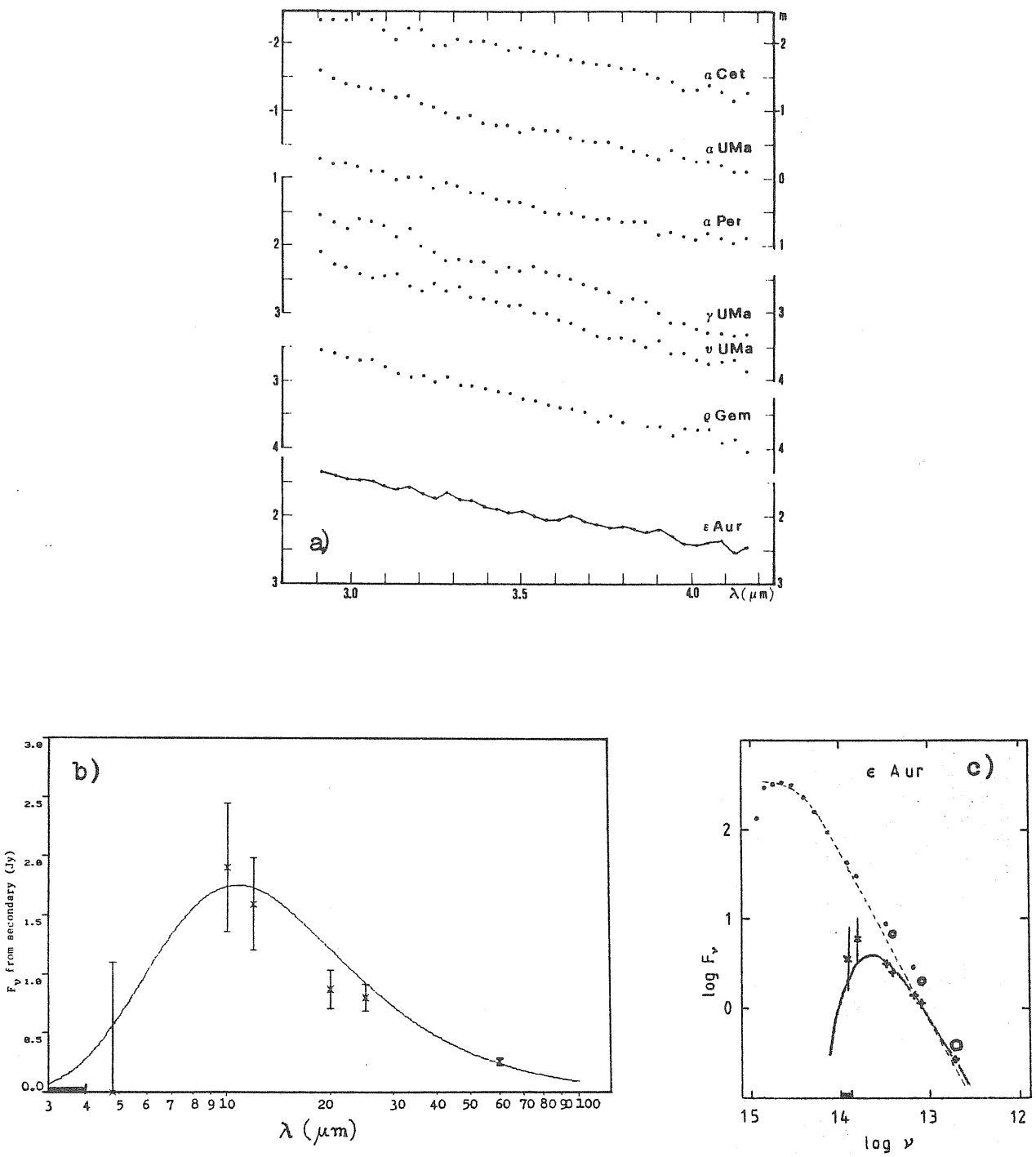

Fig. 5.3 - Temperature determinations of the cool body

a) Boehm & Cester: 700 K
b) Backman: 450 K
c) Stickland: 750 K

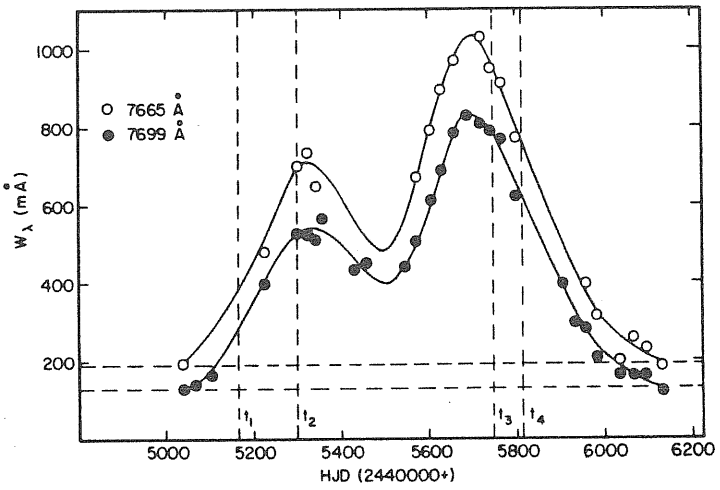

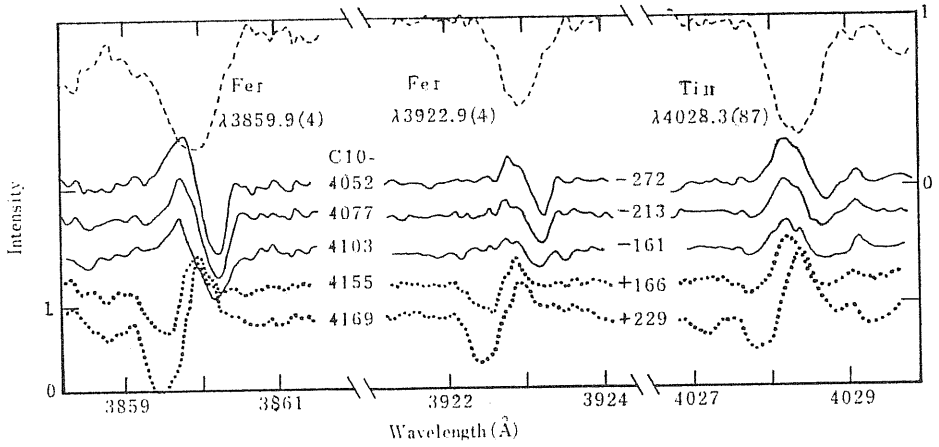

Fig 5.4 - Visible Spectroscopy

a) Lambert: Eq. width of shell lines
b) Kawabata: Extracted (spurious) shell lines

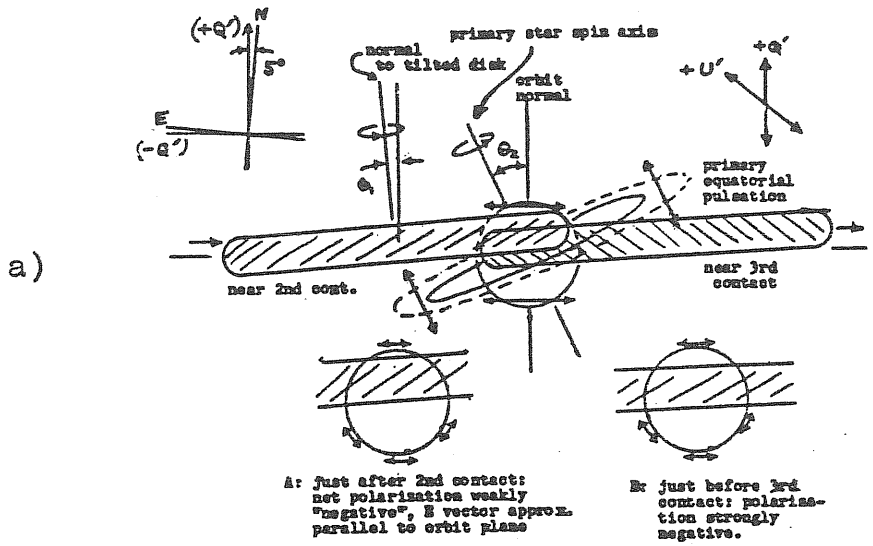

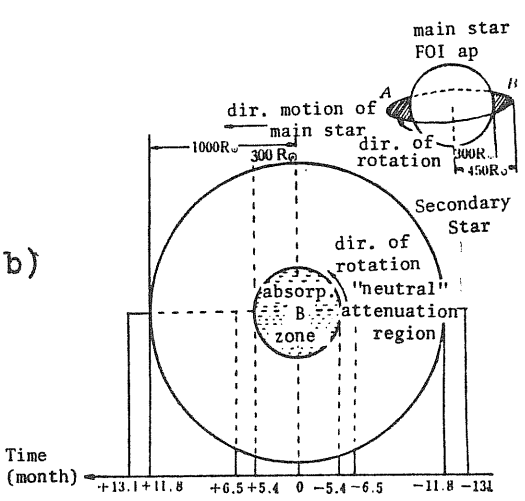

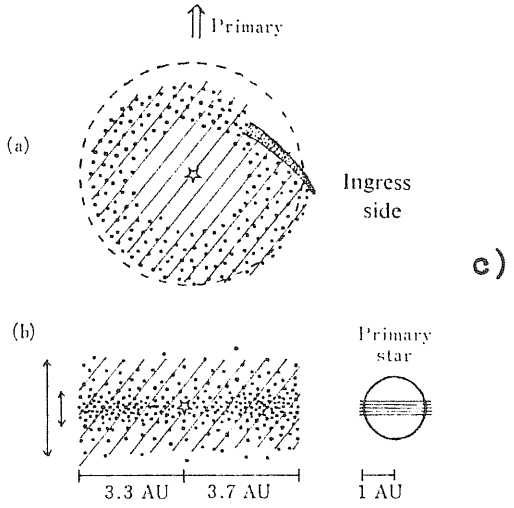

Fig 5.5 - Models

a) Kemp
b) Tan
c) Saito et al.

PART II

CONTRIBUTIONS

6. - THE BEHAVIOUR OF Hα ON ECLIPSE

We shall first briefly introduce the complete observational material concerning visible spectroscopy, upon which this study of the eclipse is extensively based, including the present investigation of the behaviour of H-alpha.

6.1 Visible spectra of Epsilon Aurigae

Observations were performed at the "Observatoire de Haute Provence" (OHP) in France, by collaborators and partly by the writer, fully covering all the phases of the eclipse and both pre-eclipse and post-eclipse epochs, from 1981 to 1987. Globally 21 observational runs (~1 week each) were carried out, including elder observations on 1970-71; in total 89 high-resolution spectrographic plates were obtained, 60 in the blue (λ3600-4950 Å) and 29 in the red (λ4800-6700 Å) region of the spectrum.

The instrument normally used was the 152-cm Coudè Telescope equipped with the large grating spectrograph, reaching at high dispersion 7 Å/mm with a corresponding resolution of about 0.14 Å (GC plates); at medium dispersion, i.e. 12.4 Å/mm, a resolution of 0.25 Å is achieved (GB plates). The larger 193-cm Telescope with its own Coudè spectrograph was also used in one occasion, obtaining spectra at dispersion of 4.1 Å/mm (X plates) and of 12.4 Å/mm (W plates).

Emulsions utilized were Kodak IIaO (usually non-baked) for the blue plates, and IIIaF (usually hypersensibilized) for the red ones; when possible, for each spectrogram a

corresponding calibration of the mother-plate was obtained. Normally GC spectra are 0.6 mm high, and GB spectra 0.2 mm, so that (if equally exposed) the noise is about $\sqrt{3}$ times lower on GC plates. Full details of the spectrograms are on the log-sheets of the OHP observations.

At first, selected blue plates were measured manually, providing an early recognition of the behaviour of the shell lines , described in the further Section 7.1 . Later , extensive data processing was performed at the "Astronet" Com_ puter Center of Trieste. For all the blue and for some red plates, digitization with the PDS microdensitometer and standard ELSPEC/11 procedure (*) were completed, providing heliocentric spectra, calibrated (intensity vs. wavelength), and continuum-normalized. Red plates (less rich in spectral lines) are partly still to be digitized.

The complete sample of visible OHP spectrograms is listed on Table 6.1 . Spectra used for early investigations of the eclipse discussed in Sections 6, 7 , 9 are underlined. Further deep analysis of the shell spectrum (Section 10) is based upon the whole sample of well-exposed blue spectra.

(*) ELSPEC is a software package for the processing of PDS-digitized spectrograms, including particular algorythms for the analysis of spectral parameters (Pasian et al., 1982).

Table 6.1 - OHP Spectrographic Observations

Phase no.	Dates	Blue plates	Red plates	Observers	Epoch
FØ1	1970, Dec. 8-11	GC 60 61 (66)		Hack, Stalio	Out of eclipse
FØ2	1971, Feb.11-12	GC 105 106 107 110 111 112		Stalio, Pucillo	Out of eclipse
FØ3	1981, Jan. 3-5	GC 1219 1220 1223 1224 1226 1228	GC 1221 1222 1227	Faraggiana	Pre-eclipse
FØ4	1982, Jul. 31	GC 7313		Boehm, Franco	Early ingress
FØ5	1982, Sep. 21 22 26 28 30	GC 1349 1350 1354 1355 1357	GB 7459 7463 7471 7474 7480	Ferluga, Boehm, Vladilo	Ingress
FØ6	1982, Nov. 18 19 20 21	GC 1358 1360 1362 (1363)	GC 1359 GB 7512 7514	Ferluga	Late ingress
FØ7	1983, Mar. 18 18 19 19 20 21	GB 7747 7749 GC (1410) 1413 GC 1416	GB 7748 GC 1409 GC 1412 1415	Ferluga	Totality
FØ8	1983, Aug. 2 7	GB 7972 7983	GB 7970 7984	Boehm	Mid totality
FØ9	1983, Sep. 27	GB 8052	GB 8051	Boehm	Totality
F1Ø	1983, Oct. 20	GB 8084	GB 8085	Boehm	Totality
F11	1983, Dec. 21 21 22 23	GB 8120 8122 8130 8136	GB 8121 GB 8137	Boehm	Late totality
F12	1984, Jan. 24 25 29	GB 8177 GC 1538 GB 8205	GB 8178 8181	Morossi, Persic, Ramella	Early egress
F13	1984, Feb. 7 7 9 10 11	W (7484) W (7485) W (7492) X 1218 X (1219)	W 7491	Persic (193cm-telescope)	Early egress
F14	1984, Mar. 17 17	GB (8238) 8239		Persic	Early egress
F15	1984, Mar. 29	GC 1563	GC 8253	Ferluga	Egress
F16	1984, Jul. 9	GB 8369		Boehm, Morossi	Post-eclipse
F17	1984, Nov. 23 23 23 24 27	GB 8574 8575 8576 GC 1606 1613	GB 8577 8578 GB 8589	Ramella	Post-eclipse
F18	1985, Jan. 25	GC 1630	GC 1631	Boehm	Post-eclipse
F19	1987, Jan. 22 25	GC 1756 1757		Denizman	Out of eclipse
F2Ø	1987, Apr. 14,18	GC 1789		Denizman	Out of eclipse
F21	1987, May 14	GB 7549		Denizman	Out of eclipse

Underlined : spectrum used for early investigation.

(Parenthesis) : spectrum ill-exposed, or redundant.

6.2 Narrow Band H-Alpha Photometry

Let us first examine the behaviour of the integrated flux through the Hα feature, during ingress and totality. These measurements were performed at the Astronomical Observatory of Trieste (OAT) by the writer and C.Boehm, using the 30 cm telescope with its photoelectric photometer, equipped with two interferential filters of 30 Å half-width. The first one is centered on the laboratory wavelength of the Hα line of hydrogen, at 6653 Å; the other is located on a nearby region of the continuum, at about 6620 Å.

Differential measurements of Δm (Hα - 6620 Å) provide a direct indication of the net flux through the Hα feature, which spectroscopically (§ 3.2) is composed by an absorption core flanked by a couple of emission wings, undergoing complex modifications during the eclipse. Moreover, by assuming as a comparison star λ Aur (m_V = 4.7; sp. GØ V), which is routinely used as a reference for photometry of ε Aur, one can trace the light-curve of the eclipse in the red continuum, based on the difference $\Delta m_{6620}(\varepsilon - \lambda)$.

Medium values of these differential magnitudes, for 6 observing nights, on ingress and totality are reported on Table 6.2; each value is obtained by averaging over one night several measurements, with a typical integration-time of 1 min. Whereas, short time-scale behaviour during a 4^h -long interval, over a single night, is shown on Figure 6.1.

At short time-scales, no remarkable variation of Hα is detected, since the situation on Fig. 6.1 is more or less the same, as during the other observing nights. The flux at Hα, measured at intervals of minutes, remains constant

Table 6.2 - Photometric light-curve of H_α

(1) Date	(2) Δm (H_α - 6620 Å)	(3) $\Delta m_{6620}(\varepsilon-\lambda)$	(4) Phase
Nov. 19, 1982	- 0.05 ± 0.01	- 1.02 ± 0.01	Ingress
Jan. 11, 1983 †	- 0.06 ± 0.02	- 0.98 ± 0.01	Totality
Jan. 17, 1983	- 0.04 ± 0.01	- 0.98 ± 0.01	Totality
Jan. 23, 1983	- 0.05 ± 0.01	- 0.92 ± 0.01	Totality
Mar. 17, 1983	+ 0.13 ± 0.02	- -	Tot.(*)
Mar. 18, 1983	+ 0.09 ± 0.01	- 0.94 ± 0.01	Tot.(*)

(*) H_α in absorption (elsewhere in emission).

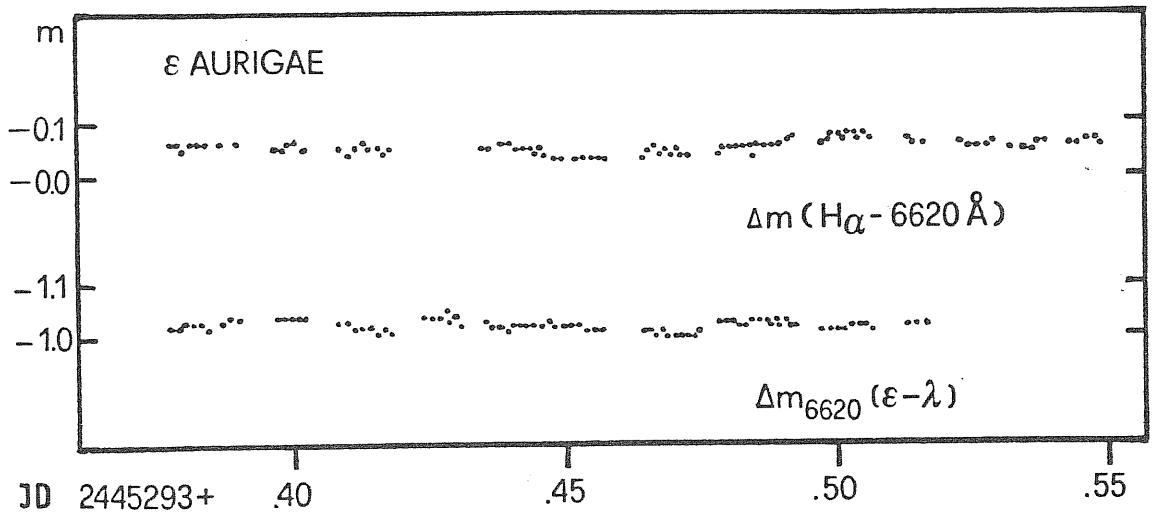

Figure 6.1 - Short time-scale photometry of H_α during one night (Nov.11, 1982; 9pm-1am), with a time-resolution of 2 min. No significant variability is observed.

within a few hundredths of a magnitude, that is the instrumental accuracy. However, on a time-scale of about one hour, a systematic variation of about 0.02 mag amplitude seems to occur, affecting at the same time the difference Δm (H_α-6620 Å) and the comparison $\Delta m_{6620}(\varepsilon - \lambda)$. This may suggest a variation of the continuum of ε Aur, which could be also of intrinsic nature, if not probably due to terrestrial H_2O absorption bands.

The photometric measurements of $H\alpha$ on eclipse, reported on Table 6.2, provide two interesting results. First, on ingress and early totality, the $H\alpha$ feature appears globally in <u>emission</u>, since the integrated flux through the $H\alpha$ band is higher than through the nearby continuum band (signs "-" on column 2); this is surprising, because in general the $H\alpha$ feature appears globally in absorption even out of eclipse, as one can see from the spectroscopic profile of Fig. 2.7c (the two emission peaks are not sufficient to balance the deep absorption core). Second, there is an evident <u>drop</u> on totality, about two months after the 2nd contact, with the $H\alpha$ feature changing abruptly into absorption; this is also surprising, since - naively - one would expect such a drop before the 2nd contact, and not two months later. Although we know that $H\alpha$ undergoes intrinsically some irregular variations, these outstanding photometric effects appear cor<u></u>related (but dephased) with respect to the eclipse. Such phenomena may provide a deeper insight into the ε Aur system, if well understood and implemented with the aid of spectroscopic observations of the line-profile behaviour.

6.3 High Resolution H-Alpha Spectroscopy

The modifications of the Hα feature during this eclipse can be followed by inspecting the digital tracings of different spectrograms taken at various phases (red plates underlined on Tab. 6.1), which are plotted together on Figure 6.2 . As one can see, the tracings are very similar to those of the preceding 1955-57 eclipse, already shown on Figure 3.3.

We shall then describe these modifications in the classical terms of the eclipsed spectrum of ε Aur. Precisely, like the other spectral lines, the Hα line of the visible F star undergoes the superposition of an absorption component, which drifts from the red to the violet, as the eclipsing body with its rotating gaseous shell passes in front of the star (§3). Phase by phase, the following characteristic sequence of phenomena is observed.

FØ5: ingress (Sep.82). The red emission wing of Hα starts weakening, because an incoming faint absorption component is overimposed.

FØ6: ingress (Nov.82). The red emission wing is much fainter than the violet one, because the absorption component by the eclipsing shell is enhanced.

FØ7: totality (Mar.83). The red emission wing is no longer observable, while the violet one is still unaffected; the strongest absorption component is the red-shifted shell line.

FØ8: mid totality (Aug.83). The profile is very broad with several faint violet-shifted and red-shifted absorption components; no emissions are observable.

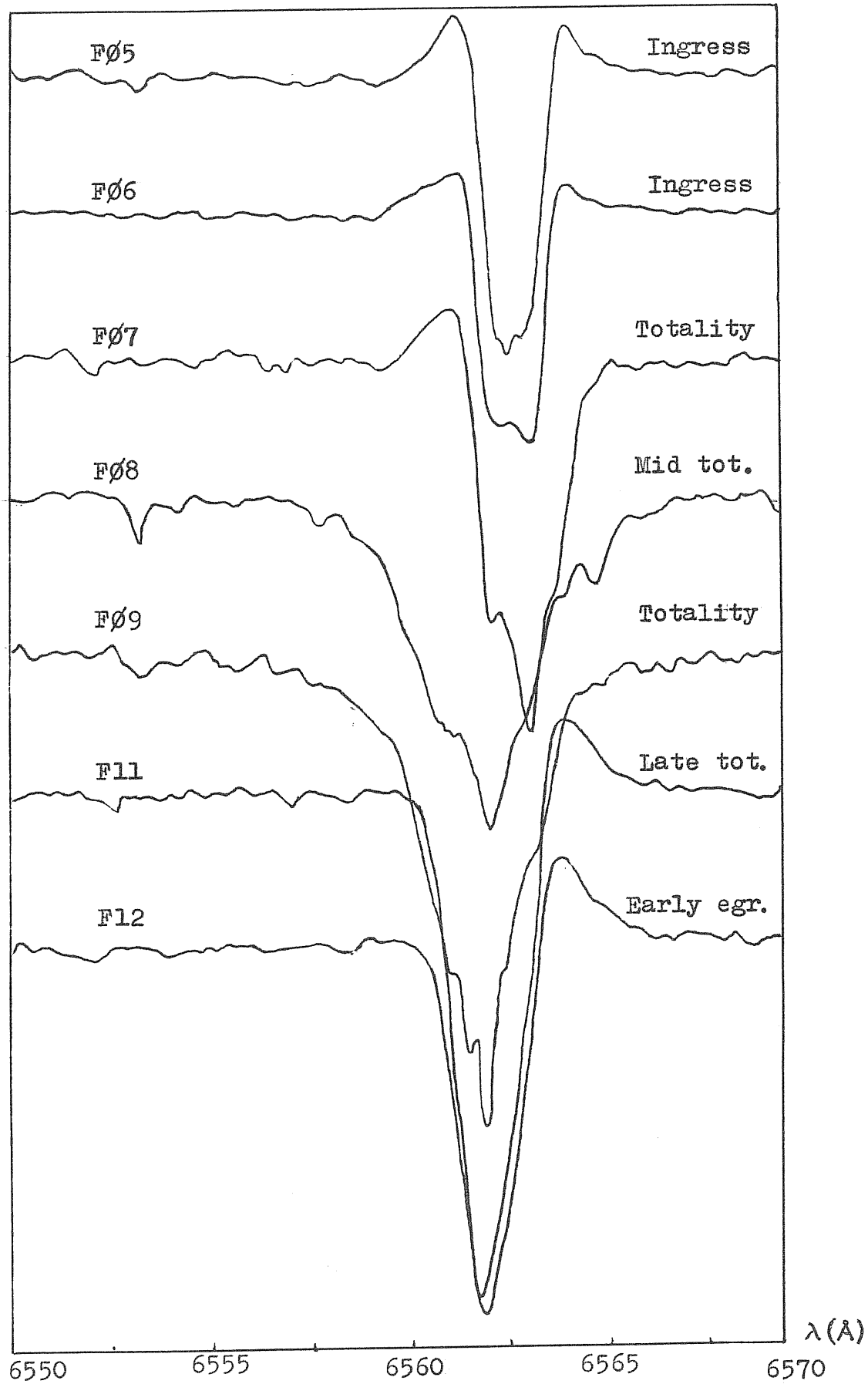

Figure 6.2 - H-alpha profiles

FØ9: totality (Sep.83). Several violet-shifted and red-shifted absorption components, and no emissions, are observable.

F11: late totality (Dec.83). The absorption line is almost symmetrical; the presence of a violet-shifted shell component is suggested by the absence of the violet emission wing, while the red wing has returned into emission.

F12: early egress (Jan.84). The profile is asymmetric, sharper on the violet side, and there is still no violet emission.

F15: egress (Mar.84). The violet wing is returning into emission, but it is still fainter than the red wing, because a fading absorption component by the shell is still overimposed.

F17: post-eclipse (Nov.84). The profile has returned symmetric and both emission wings are present, as they always are out-of-eclipse, having about the same intensity.

The correspondence of this behaviour with the one observed on the last eclipse (Wright and Kushwaha, 1957) is complete. Morphological differences are allowed, since the Hα profile is intrinsically variable also out-of-eclipse (Castelli, 1977), so that two distinct eclipses can never reproduce themselves exactly in the same way. Also short time-scale variability is observed, and in the same weak form, on both eclipses.

Finally, quantitative measurements of the Hα feature, made upon the same digitized spectra, are reported on Table 6.3. It lists at different epochs the radial velocity of the various components of the line, the total half-width, together with the depth of the absorption core and the intensity of emission wings, with respect to the continuum (out-of-eclipse emission wings have variable intensity ≈ 1.2). The unexpectedly weak absorption core can be explained as due to filling-in by emission, also occurring probably on Hα, Hβ, Hγ, but not on higher Balmer lines (Castelli, 1978).

Table 6.3 - Compnents of the Hα profile

Phase no.	Date	Radial velocity (km/s) of absorption components (b)	(c)	(r)	Half-width (km/s) at ½ log I (t)	Absorption depth relative to cont. (c)	Emission intens. relative to cont. (b)	(r)	Days from mid-eclipse	Eclipse phase
FØ5	1982, Sep.30		+ 1.4	+21.9	59	0.71	1.29	1.23	-277	Ingress
FØ6	1982, Nov.19	- 3.2	+28.8		69	0.65	1.17	1.10	-227	Late ingress
FØ7	1983, Mar.18	-10.1	+31.1		91	0.82	1.26	-	-108	Totality
FØ8	1983, Aug. 7	-92.3 -83.2 -74.0	-30.6	+56.2 +88.2	137	0.78	-	-	+ 34	Mid totality
FØ9	1983, Sep.27	-83.2 -60.3	-42.1	-19.2 +12.8	100	0.86	-	-	+ 85	Totality
F11	1983, Dec.23		-46.6		73	0.90	-	1.41	+172	Late totality
F12	1984, Jan.24		-42.1		73	0.81	-	1.45	+204	Early egress

Notes: (b) 'blue' features ; (c) core feature ; (r) 'red' features ; (t) total line .

6.4 Discussion

The observed modifications of the Hα profile are fully consistent with the behaviour of the other lines on eclipse, being affected by absorption from the rotating gaseous shell of the secondary. Since the part of the shell which is interposed on ingress is the receding one, and the opposite on egress, the absorption feature drifts from the red to the violet during the eclipse.

In case of Hα, there are also emission features to be considered. The total width of the emission is most probably produced by the rotation of the primary (in the same sense as the orbital motion), combined with turbulence in the emitting region. But also counter-rotation of the primary (retrograde motion) has been suggested (Tan, 1985), in order to account for the observed behaviour on eclipse.

In particular, one should explain the enhancement of the uneclipsed emission wing during the partial phases, and the fact that totality is shorter for Hα than for the continuum (°).

(°) "Totality" for Hα means that the whole profile of the out-of-eclipse line (including both emission wings) is replaced by a broad absorption feature.

Both effects have been detected on this eclipse photometrically, and verified spectroscopically (Tab. 6.3). Moreover, both phenomena were observed also on the preceding eclipse by Wright and Kushwaha (Fig. 3.3), and thus probably they are not simply produced by intrinsic $H\alpha$ variability.

The simplest explanation assumes that the primary star is directly rotating, and surrounded by a rather extended $H\alpha$-emitting region (the existence of an envelope in confirmed by UV observations). When the obscure secondary eclipses the primary star, this larger region (which could be simply an inclined ring, § 5.2) remains mostly uneclipsed, and both emission wings should appear enhanced, with respect to the continuum. But only the violet wing on ingress and the red wing on egress can be observed, because also the strong absorption feature by the secondary's shell (drifting from the red to the violet) is superimposed.

The same geometrical configuration most naturally explains also the reduced duration of totality for $H\alpha$. In fact, the entire $H\alpha$ feature will be completely absorbed only when the primary's emitting envelope (or ring) and the secondary's absorbing shell will be overimposed - coherently rotating - along the line of sight, and this particular condition is verified only around mid-eclipse, Figure 6.3. Its duration, about three times a partial phase, may suggest that the $H\alpha$-emitting structure surrounding the primary could be about three times larger than the star's photosphere.

Anyway such evaluation is very uncertain, since also the absorption over the photosphere is enhanced near mid-eclipse, and a remarkable deepening and broadening of all hydrogen lines occurs on totality (§ 7.2). This is due to the particular conditions (higher temperature and turbulence) existing in the central regions of the eclipsing body, which near mid-eclipse are projected upon the primary's photosphere. Thus,

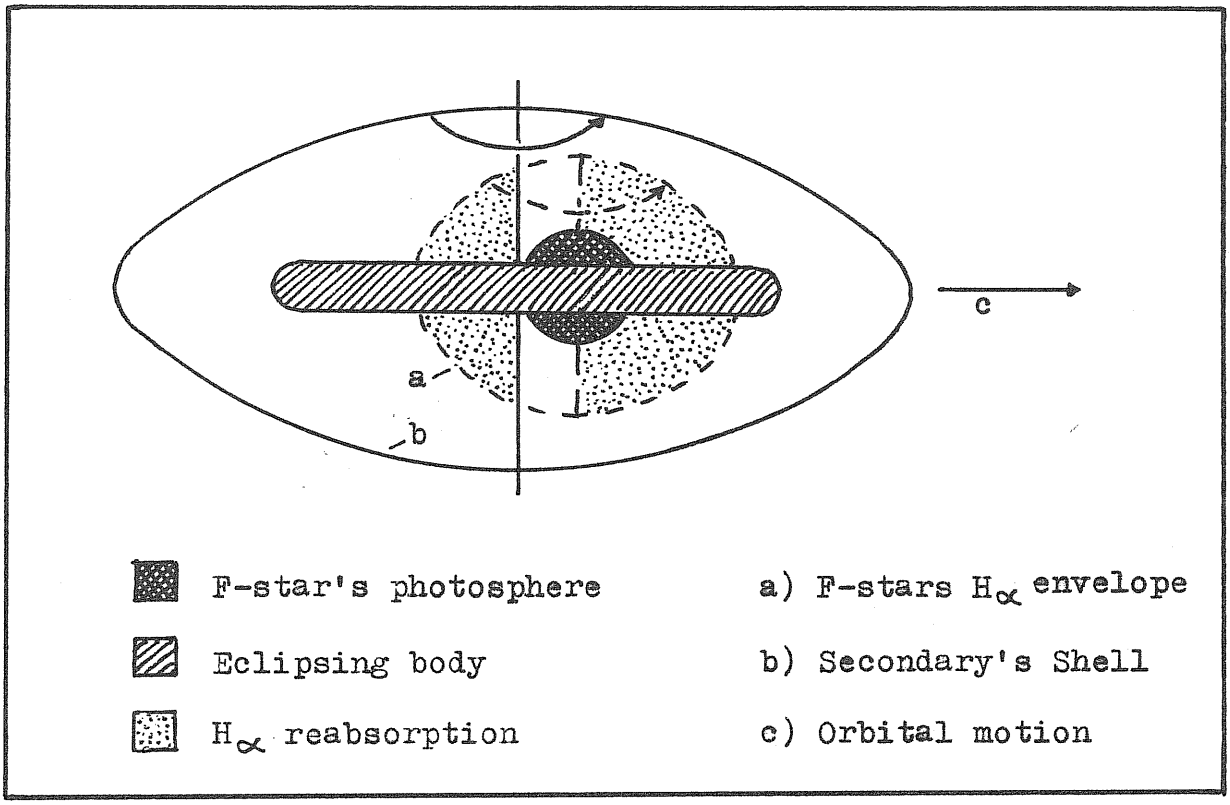

Figure 6.3 - Geometry of the eclipse. H_α absorption is maximized around mid-totaliy, when emitting and reabsorbing regions are superimposed with parallel rotational velocities (schematic).
Moreover, the H_α absorption over the photosphere is enhanced near mid-eclipse, since the F star passes behind the central region of the eclipsing body, where temperature and turbulence are higher.

the observed behaviour of H_α is a composite effect, in which it is difficult to discriminate the contribution of the intrinsically peculiar (and variable) conditions of the eclipsing body, from the pure geometrical effects of the eclipse, and also from the intrinsic H_α variability of the primary supergiant.

Let us finally consider the physical reason, for the observed great broadening of the H_α absorption feature, produced by the eclipsing body. The kinematic effect of combined rotation of the components may be responsible for a total breadth of about 2 or 3 Å, but the observed width of the H_α profile on totality is about double. This effect is caused more probably by turbulent motions than by Stark broadening, since Stark broadening would require a high density in the secondary component, of the same order of magnitude as the density found in the atmosphere of the F star. Turbulent broadening instead demands high turbulent velocities, of the order of 300 km/sec in the outer regions of the secondary component, and a similar situation is already known to exist in the shell stars.

Moreover, the presence of multiple components of $H\alpha$ during totality suggests the existence of multiple condensations in the inner regions of the eclipsig body. In conclusion, let us notice that the strong enhancement of the $H\alpha$ absorption on mid totality can be also interpreted as an indication of an off-plane bipolar flow, from the hot source at the center of the eclipsing object.

7. - THE APPEARANCE OF THE SHELL SPECTRUM

This is an early spectroscopic investigation which first provided, for the 1982-84 eclipse, the rotational-velocity curve of the eclipsing body, and general information about its constitution (papers VI and VII).

Among the rather large set of optical spectrograms taken at the Obs. de Haute Provence (OHP), it was selected a representative sample of blue plates (underlined on Tab. 6.1). The spectrographic dispersion is the highest available with the 152-cm telescope (7.2 Å/mm), except on mid-totality phase (12.4 Å/mm), when only short exposures could be obtained (°).

The first indications were derived by preliminary (analogical) treatement of some plates taken on ingress (Master th., p.91), as summarized in the next Section 7.1. Then, four spectrograms taken on ingress, totality, egress, and out-of-eclipse respectively (Tab. 7.1), were digitally processed (PDS+ELSPEC) and analysed, providing results described in further Sections 7.2 and 7.3.

7.1 Preliminary measurements

A limited program of radial-velocity measurements was carried out, with the ABBE comparator, as soon as the first spectra were available at the beginning of the eclipse. In particular, plates GC 1354-57-58-62 (obtained by the writer at OHP) were measured. So, it was possible to derive preliminary indications about the doppler-shifts of the lines, produced by the overposition of the shell obsorption components, upon the spectrum of the visible primary star.

(°) At that time, ε Aur was observable just before dawn.

Most of the measured lines (that in total are about 120) are due to metallic elements, in neutral or single-ionized states, which are common in the spectrum of ε Aur. In particular Fe I, Fe II and TiII are present with a large number of multiplets; this permits to measure radial velocities v_{rad} of those lines, which correspond to transitions starting from different values of the excitation potential χ_e.

From a first examination of the measured radial velocities, one finds immediately that, in general, they don't agree with the (small) values predicted by the primary's radial velocity curve (Morris, 1963), for the observed early-eclipse phases. Figure 7.1 shows some indicative results for the end-ingress phase: values of v_{rad} are found to be spread in an interval (vertical scale in figure), about from 0 km/sec to +30 km/sec toward the red, while the orbital expected value should be near to the baricentric velocity $v_0 = -1.4$ km/sec. Moreover, a relation between v_{rad} and χ_e is well established, in particular for FeI and for TiII, in terms of a decrement of v_{rad} for increasing χ_e.

The other metallic lines (AlI, MgI, YI, SrII, VaII, BaII, CrII, NiII) are situated at intermediate velocities; a remarkable exception is the one of MgII ($\chi_e > 8$ eV), having a radial velocity consistent with the orbital (baricentric) one. Lines of the Balmer series (which often are not easy to be measured) do not show any clear dependance on progressive number n, but have always rather high values of v_{rad}, about +30 km/s.

The observed differential radial velocities could mean that some kind of stratification is present in the eclipsing body, so that the hotter regions are rotating slowlier. But the same behaviour could also be produced by a simple temperature effect: the eclipsing body, being little cooler than the primary star, has weaker high-excitation lines, so that they are more blended with the F-star's stationary component.

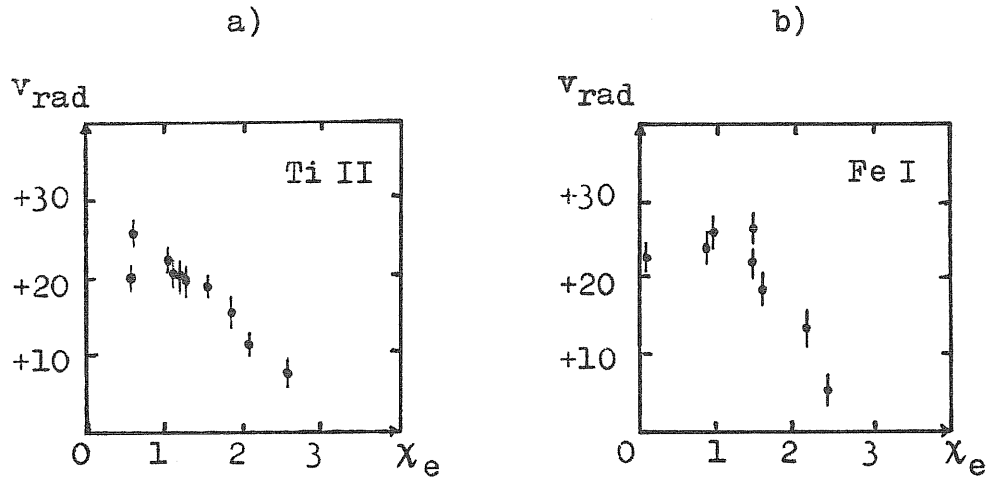

Fig. 7.1 - Radial velocities at ingress: v_{rad}(km/s), plotted vs. excitation potential χ_e(eV), of the lower level of transition. Velocities are positve, since the shell lines are red-shifted on ingress. The decrement of v_{rad} is roughly prportional to χ_e.

a) spectrum GC 1358 on Nov.18,1982;
b) spectrum GC 1362 on Nov.20,1982.

Table 7.1 - Digtized spectra discussed in this section

PLATE No.	D A T E	JULIAN DAY	P H A S E	Φ
GC 1224	Jan. 4, 1981	2444609.36	911 days before mid-eclipse, FØ3 out	0.91
GC 1360	Nov.19, 1982	5293.54	227 days before mid-eclipse, FØ6 ing.	0.98
GB 7983	Aug. 7, 1983	5554.52	34 days after mid-eclipse , FØ8 tot.	0.003
GC 1563	Mar.29, 1984	5789.36	269 days after-mid-eclipse , F15 egr.	0.03

7.2 General Conditions Of The Shell

By examining a set of spectra taken at different eclipse-phases, as listed on Table 7.1, one can observe - like during the previous eclipses - the appearance of sharp absorption components on the red side of the strong low-excitation lines during the ingress phase, and on the violet side during the egress phase. This additional spectrum can be axplained - as usual - by a gaseous shell associated with the eclipsing body, and rotating in the same direction as the orbital motion.

The shell has a slightly lower excitation temperature with respect to the photosphere of the FØ Ia primary, but a much lower density and optical depth. This is indicated by the fact that the quantum number of the last resolved Balmer line is n = 31 in the photospheric spectrum, and $n \approx 55$ in the shell spectrum. From the Inglis and Teller relation, it can be derived the electron density: $N = 1.2 \cdot 10^{12}$, and $N \approx 1.6 \cdot 10^{10}$ cm^{-3} respectively. Moreover, the high-excitation lines as Mg II λ4481, and all the faint lines, do not present the shell component (Fig. 7.2).

The spctrum during totality is very similar to the one taken out of eclipse. The presence of the additional absorption component is revealed by the slightly increased depth of the lines. Such component is very evident only in correspondence to the Balmer lines, which have very deep cores during totality (Fig. 7.3). Possibly, this contribution may come from the central region of the eclipsing body, which indeed is passing in front of the primary at mid-eclipse.

A comparison of the central depths R of the shell lines, at ingress and egress phases, shows that the ratio R(egress)/R(ingress) presents a rough dependence on the wavelength. At wavelengths shorter than about 4200 or 4300 Å, the majority of the shell lines have about the same intensity at ingress and at egress; while, at longer wavelengths, the shell lines at egress are generally

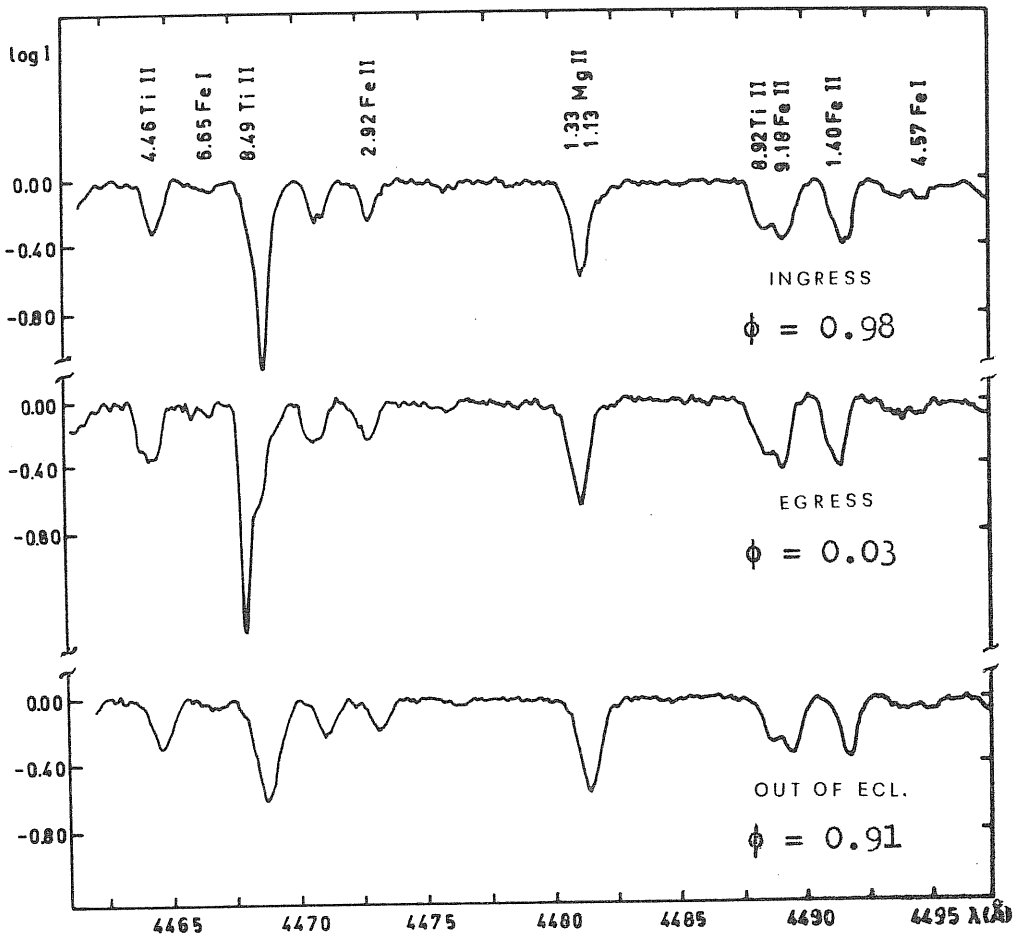

Fig 7.2 - The spectral region of Mg II λ 4481. Top: Nov. 19, 1982, 227 days before mid-eclipse. Middle: Mar. 29, 1984, 269 days after mid-eclipse. Bottom: Jan. 4, 1981; out of eclipse. The two lines Ti II λ 4468.49 and Mg II λ 4481 have about the same intensity, in the spectrum taken out of eclipse. At the phases of ingress and egress only the line of Ti II, which has a low excitation potential of 1.13 eV, presents the shell component, while the line of Mg II (EP = 8.83 eV) is a pure photospheric line.

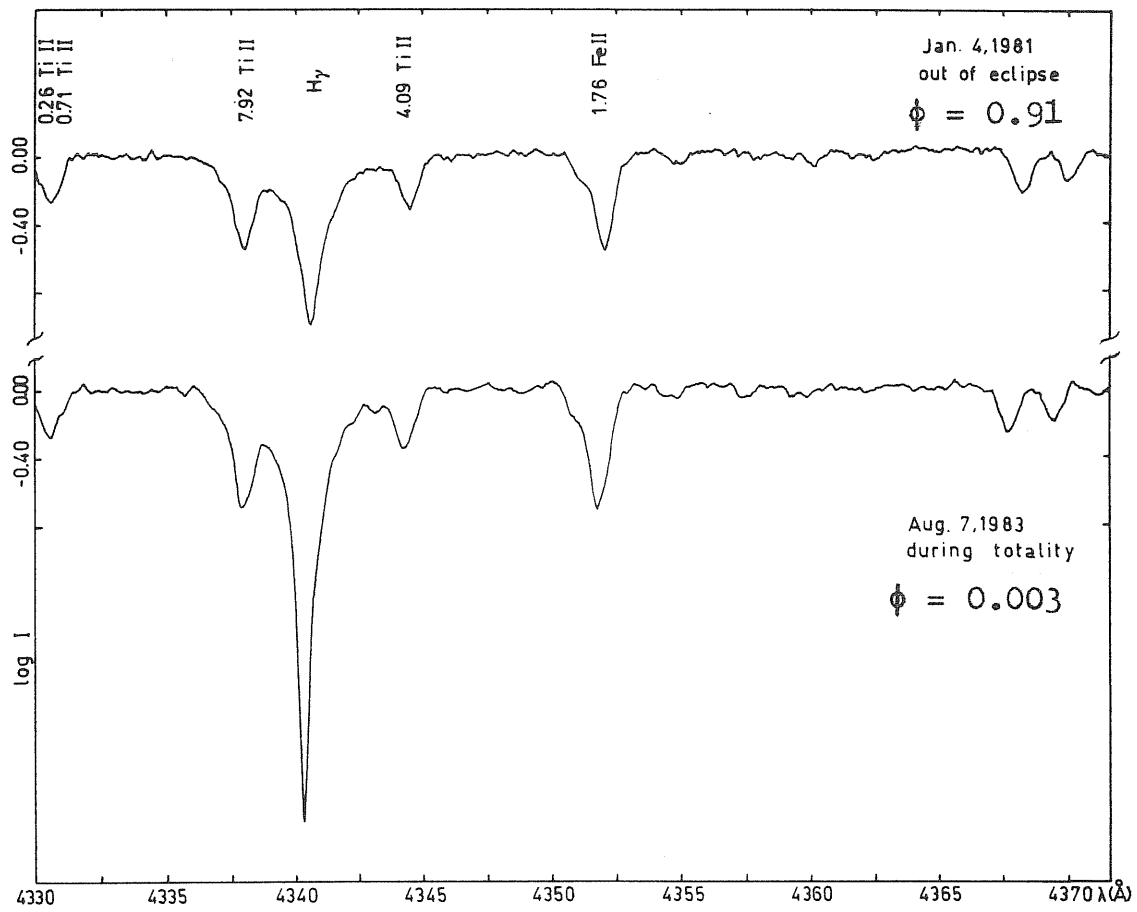

Fig 7.3 - One spectrum taken during totality (Aug. 7, 1983) is compared with one taken out eclipse (Jan. 4, 1981) . The lines, which during the ingress and egress phases present a red-shifted and violet-shifted component respectively, during totality are deeper than out of eclipse. The shell component of H_γ is clearly visible during totality.

deeper than at ingress. The Balmer lines show a clear dependence on wavelength: $H\beta$ is stronger at egress; $H\gamma$, $H\delta$, $H7$ have about the same intensity at the two epochs; and the upper terms of the series are generally stronger on ingress.

A possible explanation for these facts may be the following: let us suppose that the shell is thicker at egress than at ingress; in addition to producing the spectral lines by absorbing the spectrum of the primary, it scatters the light of the blue companion, more efficiently than at ingress. This scattered light partially fills the shell lines, and because of the energy distribution of the light of the blue companion,the effect is stronger on the shorter wavelengths side.

The physical mechanism responsible for the scattering in the shell could be simply electron scattering, as discussed on §8.4; however, infrared observations by Backman et al. (1984) indicate that also dust has to be present in the eclipsing body. This dust, which must be non-typical in size and/or in composition (no effect is observed at 2200 Å during the eclipse), could also produce the observed slight deepening of the eclipse towards the far-UV (if it is not caused by a blending of the shell lines as suggested on the next section 8).

7.3 The Shell's Rotation

The primary's photospheric lines have a difference in radial velocity between phase 0.91 and phase 0.03 of about +18 km/s ; and between phase 0.003 and phase 0.03 the difference is about + 4km/s. This is in good agreement with the values predicted from the orbital radial-velocity curve by Struve et al, 1937 (Fig. 2.2), also showing that the absolute radial velocity at reference phase 0.03 should be about zero.

The secondary's shell lines have a radial velocity which, measured with respect to the primary, at ingress is about

+15 km/s, and at egress is about -35 km/s .
The difference ΔRV, between the radial velocites of the shell lines at ingress (ϕ = 0.98) and at egress (ϕ = 0.03), are given on Table 7.2 .

The strongest lines in the spectrum, which are H and K of Ca II, have much lower ΔRV than the other lines. This may be due to the blending of shell, photospheric and circumstellar lines. In fact, the spectrum on Jan. 1981 shows that the H and K lines have a complex structure with a violet-shifted component at about -30 km/s, probably of circumstellar origin, which was observed also by Struve on 1950 (Struve 1951) and by Adams on 1940. The Fe I and FeII lines, and H_β, present a slightly lower ΔRV than the other lines. The presence of a circumstellar envelope is confirmed by UV observations (§ 8).

The complete rotational-velocity curve, covering all the eclipse phases, is given on Figure 7.4 ; the primary's photospheric line Mg II λ 4481 (+), and the other lines with a dominant stellar component (x), are consistent with the primary's orbital velocity (dashed line). Whereas , the shell components of H_α , H_β , H_γ (●), and of the other strong low-excitation lines (o), show a remarkable positive displacement on ingress, and still more evident negative displacement on egress; this is due to the combined effect of the secondary's rotational and orbital motions.

In particular, 277 days before mid-eclipse (FØ5) the radial velocity of the shell is +15 km/s, and 269 days after it (F15) the velocity is -35 km/s ; 227 days before mid-eclipse (FØ6) the shell velocity is +17 km/s, and 221 days after it (F13) the velocity is -37 km/s. That is, the frontal part of the shell in the orbital motion, appears to rotate slowier than the back part. Moreover, both parts of the shell show a rotational velocity which increases from the outer portion of the shell to the inner one, then reaches a maximum, and finally decreases again. The general behaviour, and also the values of the radial velocity in the shell are about the same as observed by Struve et al. (1958) during the 1955-57 eclipse.

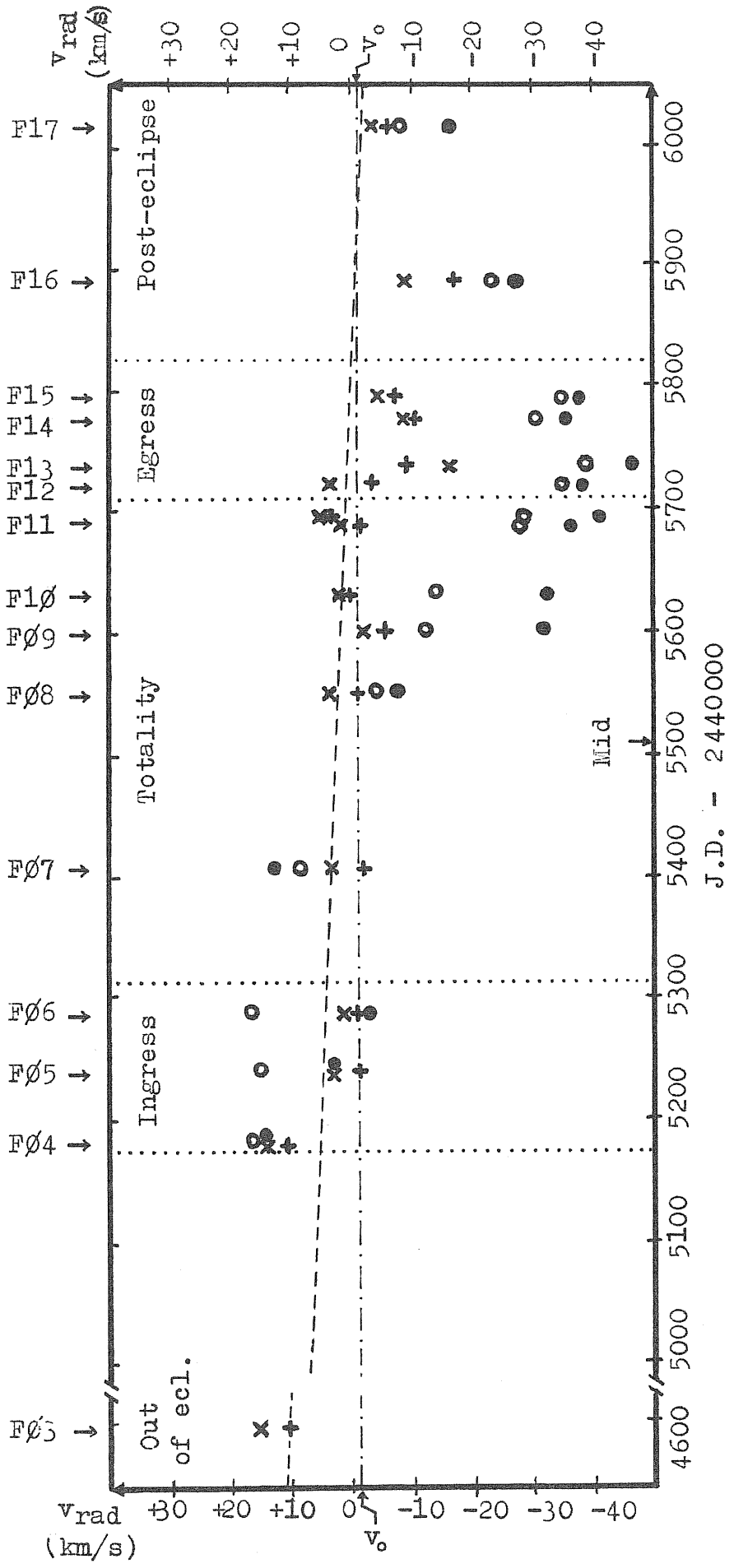

Figure 7.4 - Radial velocities of the lines during the eclipse.

+ Mg II 4481 } Primary
× other lines }
● Hα, Hβ, Hγ } Shell
o other lines }

(—·—·—) Baricentric velocity of the System, v_o
(— — —) Orbital velocity of the Primary

F// → Progressive number of observed eclipse-phase.

Table 7.2 - Difference ΔRV in radial velocity of the shell lines, between ingress and egress

LINES	NO. OF LINES USED IN THE AVERAGE	Δ RV (Km/s)
Mg I	2	54.75 ± 0.05
Ca I	1	53.2
Ca II H	1	26.4
Ca II K	1	22.8
Sc II	4	52.3 ± 0.2
Ti II	30	51.2 ± 0.6
Cr I	2	56.2 ± 3.3
Cr II	2	57.0 ± 0.5
Fe I	43	50.5 ± 0.7
Fe II	12	47.5 ± 1.4
Sr II	2	48.8 ± 1.0
Y II	1	58.7
H β	1	49.4
H γ	1	55.3
H δ	1	51.2
H 7	1	56.7
H 8	1	61.7
H 9	1	58.7
H 10	1	59.2
H 11	1	47.7
H 12	1	64.0
H 13	1	56.2
H 14	1	60.4
H 15	1	64.7
H 18	1	52.8
H 38-H 43	6	49.0 ± 1.0

Near the third contact, at the epoch of the brightening on Jan. 1984 (Ôki et al., 1984), the shell has the maximum negative radial velocity and also the maximum intensity. Even weak low-excitation lines, which generally do not show the shell components, show it at phase F12 (for example in the spectrum GB 8177 taken at OHP on Jan. 24); moreover the same behaviour in displayed also in the ultraviolet, by the spectrum LWP 2673 obtained with the IUE on Jan. 20 (high-resolution shift H7, Tab.8.4). This fact could mean that we are observing the absorption lines from a part of the shell close to the orbital plane, where the density and the rotational velocity are probably higher than above or below the plane itself.

8. - THE ECLIPSE AT ULTRAVIOLET WAVELENGTHS

The behaviour of Epsilon Aurigae in the ultraviolet has been investigated extensively, studying the epoch from 1979 to 1984 that is before and during the whole eclipse. For this research, the International Ultraviolet Explorer (IUE) satellite was employed, both at low and at high resolution spectrographic modes. Results and straightforward interpretation are presented in the following sections. Let us here remark that ultraviolet observations have provided strong constraints and fundamental indications about the structure and the nature of the eclipsing body, and about the presence of a variable hot component in the system, dominating the far-UV behaviour of ϵ Aur. Timely recognition of such far-UV activity (paper II) also permitted to avoid some misleading interpretations, about the eclipse-depth at short wavelength, which were proposed by contemporary investigators (Chapman et al., 1983).

8.1 Low Resolution Observations

We shall start examining the set of low-resolution IUE observations that have been considered, and which are listed in Table 8.1 . Spectra (7), (8), (12) and (13) were obtained by the writer and collaborators, at the VILSPA Satellite Tracking Station of the European Space Agency (ESA) in Spain. Whereas, the observational material concerning the other spectra is from different authors, and has been made available

Table 8.1 - IUE low-resolution Observations

Spectrum (no.)	IUE Configuration Cam. Image, Ap.	Date Observer (*)	Spectral Range (Å) λmin, λmax
(1)	LWR 6005, L	1979, Nov. 1 Gilra (*)	1900, 2500
(2)	SWP 14647, L LWR 11238, L	1981, Aug. 4 Plavec (*)	1200, 1700 1900, 3200

(3)	SWP 14654, L
	SWP 14654, S
	LWR 11246, L
	LWR 11246, S
		1981, Aug. 5
		Stickland (*)
			1200, 1690
			1690, 1910
			1910, 2415
			2415, 3200

(4)	SWP 16522, L LWR 12776, L	1982, Mar. 12 Chapman (*)	1500, 1950 2400, 3200

(5)	SWP 16628, L
	SWP 16628, S
	LWR 12864, L
	LWR 12864, S
		1982, Mar. 26
		Stickland (*)
			1200, 1570
			1570, 1940
			1940, 2420
			2420, 3200

(6)	SWP 18137, L	1982, Sep. 27 Stickland (*)	1200, 1700
(7)	SWP 18570, L SWP 18570, S	1982, Nov. 16 Molaro	1200, 1695 1695, 1950

(8)	SWP 19492, L
	SWP 19492, S
	LWR 15523, L
	LWR 15524, L
		1983, Mar. 20
		Morossi
			1200, 1725
			1725, 1900
			1900, 2425
			2425, 3200

(9)	SWP 19671, L
	SWP 19672, L
	LWR 15674, L
	LWR 15673, L
		1983,Apr. 7
		Ake (*)
			1200, 1600
			1600, 1900
			1900, 2520
			2520, 3300

(10)	SWP 19751, L LWR 15767, L	1983, Apr. 18 Chapman (*)	1500, 1900 1900, 2520

(11)	SWP 19782, L
	SWP 19780, L
	LWR 15790, L
	LWR 15788, L
		1983, Apr. 21
		Ake (*)
			1200, 1600
			1600, 1900
			1900, 2520
			2520, 3300

(12)	SWP 20643, L
	SWP 20644, L
	LWR 16552, L
	LWR 16551, L
		1983, Aug. 8
		Ferluga
			1200, 1700
			1700, 1900
			1900, 2400
			2400, 3200

(13)	SWP 22055, L
	SWP 22054, L
	LWP 2671, L
	LWP 2672, L
		1984, Jan. 20
		Boehm
			1200, 1680
			1680, 1980
			2340, 2640
			2640, 3300

(*) Spectra released by VILSPA Data Bank.

by the VILSPA Data Bank.

The dates of the observations, given on the third column of Table 8.1, show that the first spectra from (1) to (5) were all taken out of eclipse; spectrum (6) corresponds roughly to mid ingress, while spectra (7) and (8) correspond to late ingress and early totality respectively; the spectra from (9) to (12) were all taken around mid totality, and finally spectrum (13) corresponds to early egress. Symbols L and S on the second column stand for large (10"x20") and small (3") aperture. Only the best exposed part of each image, indicated on the last column, has been utilized.

In order to be shure in excluding possible spurious effects (e.g. due to evolving IUE calibration techniques), which could in principle simulate stellar variability, special controls of VILSPA spectra were performed at the computer center of Trieste Observatory. Careful reprocessing with the IUEARM software procedure ruled out the possibility of any spurious effect, thus conferming the full reliability of the available sample of spectra (Master th., p.61).

Moreover, since the small aperture does not gather all the light of the star, it allows no absolute flux calibration. Therefore, small-aperture images have been considered only when they partially overlap with a large-aperture image, taken nearly at the same time, which can provide its own flux calibration. Anyway, the flux derived by the small-aperture images is affected by a systematic error, estimated on of the order of 5%, caused by the uncertainty in the vertical shift necessary to fit the spectra obtained with the large and small apertures.

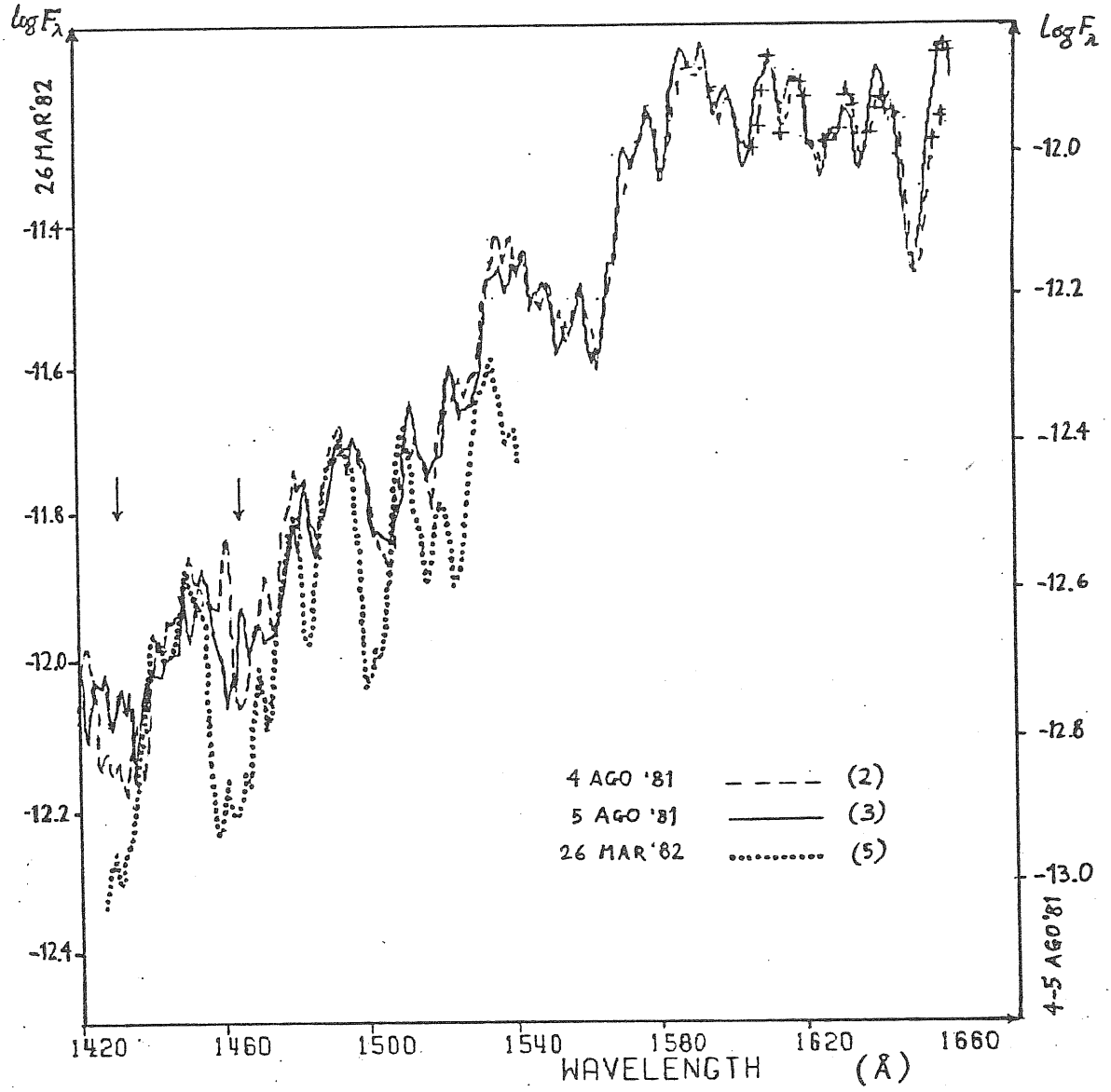

Fig. 8.1 - Line variability in far-UV; see text at point 8.2 b) for detailed description. In the figure, the "active" spectrum (5) has been shifted downwards (left-side ordinate), with respect to the other two "quiescent" spectra (2) and (3) (right-side ordinate), in order to make direct comparison possible. Short-time variabity (3)-(2) is clearly present in the regions showed by the arrows (F_λ is in erg $s^{-1}cm^{-2}Å^{-1}$).

8.2 Basic Results

A comparison between eclipsed and uneclipsed spectra is shown in Figure 8.2 . Four selected spectra are plotted, providing significant indications (*):

a) Out-of-eclipse flux variability. Spectra (3) and (5), both taken out of eclipse, show remarkable variations of the flux in the spectral range 1300-2150 Å. Spectrum (5) on 1982 is higher than spectrum (3) on 1981; the difference increases towards shorter wavelengths, while at $\lambda \gtrsim$ 2150 Å there are practically no flux variations.

b) Out-of-eclipse line variability. In the range 1400-1600 Å, the spectral absorption lines are systematically deeper in the "active" phase (5), than at all other epochs. Moreover, in the same spectral range a detailed comparison between spectra (3) and (2), reported in Figure 8.1 , shows variations of the line profiles on a time-scale of 15 hours.

c) Greyness of the eclipse. In the wavelength range 2150-3200 Å, the totally eclipsed spectrum (8) on March 20, 1983 differs from the nearly identical out-of-eclipse spectra, (3) and (5), only by a shift in the logarithmic flux scale. This means that the UV depth of the eclipse is almost constant with wavelength (as it is in the visible).

d) Invariance of the λ 2200 absorption feature. Comparing spectrum (8) with spectra (3) and (5), it appears no

(*) NOTE. It should be remarked that, when these results were first derived (Paper II), only the earlier spectra from (1) to (8) were available; that is to say, only the data concerning out-of-eclipse, ingress, and early-totality were known. Finally, when also spectrum (12) was taken, the new mid-totality data provided full confirmation of all the early results.

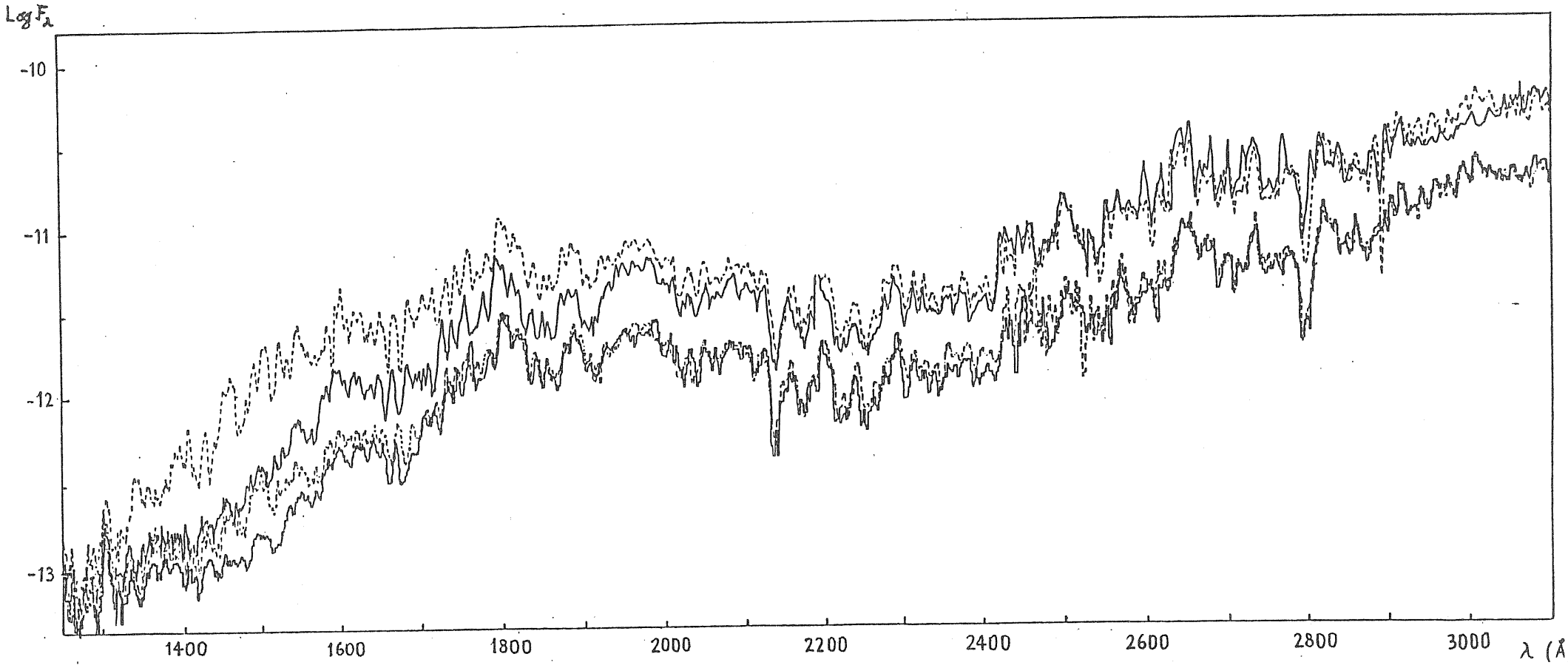

Fig. 8.2 - Four significant spectra of ε Aur, taken before and during the eclipse, which are analysed in the text (fluxes F_λ are in erg $cm^{-2}\ s^{-1}\ Å^{-1}$)

Upper lines (out of eclipse) ---- (5) active (1982, Mar 26)
——— (3) quiescent (1981, Aug 5)

Lower lines (total eclipse) ---- (8) active (1983, Mar 20)
——— (12) quiescent (1983, Aug 8)

remarkable deepening of the wide absorption feature at $\lambda \simeq 2200$ Å, in correspondence with the eclipse phase.

e) Eclipse vanishing at short wavelengths. Complex behaviour is displayed in the range 1300-1700 Å ; activity described in a) is there evident. Moreover, by comparing the eclipsed spectra (8) and (12) with non-eclipsed ones (3) and (5), it appears that the depth of the eclipse decreases and gradually vanishes towards the shortest wavelengths.

f) Behaviour on totality. Let us finally examine spectrum (12), taken in phase of mid-totality on 1983, August 8. One can see that the couple of eclipsed spectra (8) and (12) display exactly the same kind of far-UV variability, which was previously detected out of eclipse on the couple (3) and (5). Moreover, in the range 1700-3200 Å , the couple of totally eclipsed continua (8) and (12) are coincident; this shows that, from early totality (8) to mid totality (12), the eclipse remained of constant depth in time. Greyness of the eclipse is outstanding in the mid UV and near UV, from the overall parallelism of the couple (8), (12) with respect to the couple (3), (5).

8.3 The Continuum

Quantitative measurements of the continuum fluxes, for all the 8 spectra considered, are given in the left part of Table 8.2 . Values of monochromatic fluxes are tabulated for selected wavelengths, representing "windows" over the continuum, which is supposed to be matched by a curve passing through the highest points of the spectrum (Castelli et al., 1982); the adopted continuum was shown extensively, for each spectrum, on Master Thesis (p.96-109).

Table 8.2 - Continuum fluxes and variations

Sp. / Date / λ (Å)	- log F_λ (erg cm^{-2} s^{-1} Å^{-1})								Δ m (mag)			
	(1) 1.11.79	(2) 4.8.81	(3) 5.8.81	(4) 12.3.82	(5) 26.3.82	(6) 27.9.82	(7) 16.11.82	(8) 20.3.83	(5)-(3) Δm_{out}	(5)-(4) Δm_{act}	(8)-(3) Δm_{tot}	(8)-(7) Δm_{ing}
3200	-	10.37	10.30[a]	10.34	10.30[a]	-	-	10.74	.00	-	1.10	-
3110	-	10.44[b]	10.27[ab]	10.31	10.31[a]	-	-	10.72	.10	-	1.12	-
3005	-	-	10.38[ab]	10.22[b]	10.24[ab]	-	-	10.63	-.35	-	.70	-
2905	-	-	10.45[ab]	10.46[b]	10.45[ab]	-	-	10.88	.00	-	1.07	-
2820	-	-	10.50[ab]	10.50[b]	10.51[a]	-	-	10.97	.00	-	1.17	-
2735	-	-	10.53[ab]	10.61[b]	10.58[a]	-	-	10.98	.12	-	1.12	-
2615	-	-	10.81[ab]	10.95	10.81[a]	-	-	11.26	.00	-	1.12	-
2495	11.11[b]	10.95[b]	10.84[a]	10.83	10.86[a]	-	-	11.35	.05	-	1.27	-
2405	11.38	11.31	11.43	11.21[c]	11.33	-	-	11.78	-.25	-	.87	-
2295	11.29	11.32	11.33	-	11.26	-	-	11.70	-.32	-	1.07	-
2205	11.40	11.35	11.46	-	11.34	-	-	11.76	-.30	-	.75	-
2120	11.36	11.35	11.38	-	11.28	-	-	11.78	-.25	-	1.00	-
2035	11.31	11.33	11.42	-	11.26	-	-	11.76	-.40	-	.85	-
1950	11.20	11.21	11.22	11.09	11.10[ab]	-	11.66[a]	11.62[a]	-.30	.02	1.00	-.10
1795	-	-	11.18[a]	11.05	10.94[ab]	-	11.55[a]	11.51[a]	-.60	-.11	.82	-.10
1685	-	11.91[b]	11.82[b]	11.57	11.43	12.22	12.30	12.17	-.97	-.35	.87	-.32
1595	-	11.87[b]	11.84	11.59[c]	11.36	12.26	12.31	12.20	-1.20	-.57	.90	-.27
1500	-	12.38	12.41	11.91[c]	11.71	12.71	12.74	12.43	-1.75	-.50	.05	-.77
1405	-	12.72	12.73	-	12.17	12.96[c]	12.97[c]	12.82[c]	-1.40	-	.22	-.37
1335	-	12.92[c]	12.86[c]	-	12.47	13.04[c]	13.03[c]	12.89[c]	-.97	-	.07	-.35
1304	-	12.62	12.66	-	12.59	12.72[c]	12.74[c]	12.71[c]	-.17	-	.12	-.07
1240	-	12.90[c]	12.89[c]	-	12.80[c]	13.04[c]	13.03[c]	12.98[c]	-.22	-	.22	-.12
m_{FES}	-	3.25	3.25	3.20	3.22	3.69	3.98	4.10	-.03	.03	.85	.12

Notes :

a) Small aperture
b) Over-exposed
c) Under-exposed

On the last line , visual magnitudes obtained from IUE Fine Error Sensor (FES) are reported; values from (1) to (6) are taken from Chapman et al. (*) , while (7) and (8) are derived from our observations using the same calibration (°°).

Flux variations, for significant couples of spectra, were computed; they are given, in terms of differences of monochromatic magnitudes, on the right part of Table 8.2 and are plotted on Figure 8.3 . In particular, "(5)-(3)" is the amplitude of the activity observed out of eclipse, reaching a maximum of 1.75 mag at 1500 Å. Then, "(8)-(3)" represents the depth of total eclipse, which is about 1 mag in the mid UV (slightly larger than the 0.85 mag observed in the visible), but under 1500 Å is masked by intrinsic variability prevaling in the far UV. For instance, "(8)-(7)" shows that at 1500 Å the flux measured during totality is surprisingly 0.8 mag larger than the flux in the partial phase.

Monochromatic light curves from Tab. 8.2, updated to sp.(13), are shown in Figure 8.4 . At long wavelength the drop due to the eclipse is evident, while at short wavelength the behaviour is complicated because of intrinsic activity. The light curve at λ 1304 Å , corresponding to the O I (em.) line , shows little or no evidence of the eclipse; moreover, it is practically insensitive to the out-of-eclipse activity.

Error bars, in Figures 8.3 and 8.4 are estimated taking into account the uncertainty due to the small-aperture fitting procedure, and the effects of over-exposure and under-exposure.

(*) Ap.J. L.269, 17.
(°°) Holm & Rice, 1981; IUE Newsl. 15, 74.

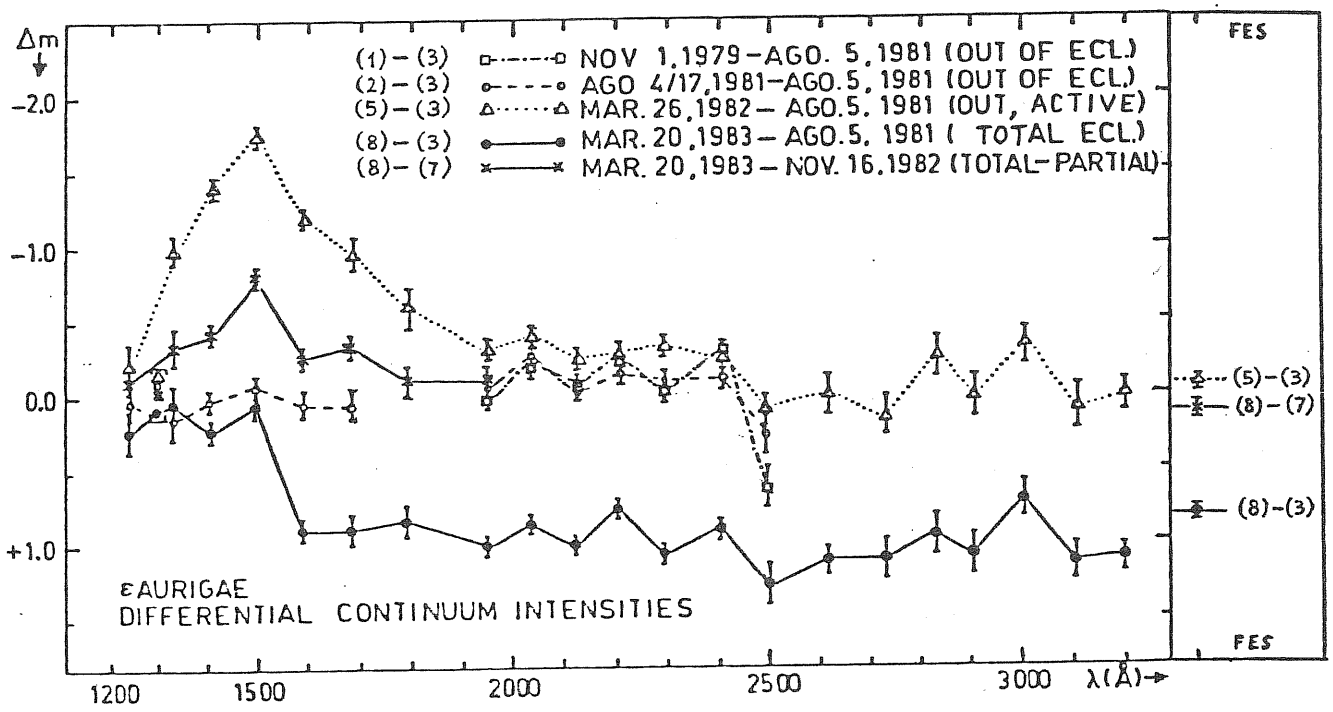

Fig. 8.3 - UV variability. The differences in magnitude between various phases, vs. wavelength, are given. The lower solid line represents the depth of total eclipse, while the dotted line shows out-of-eclipse activity. In the right part of the figure the corresponding values for visible wavelengths are reported, as they were measured by the Fine Error Sensor (FES) of IUE.

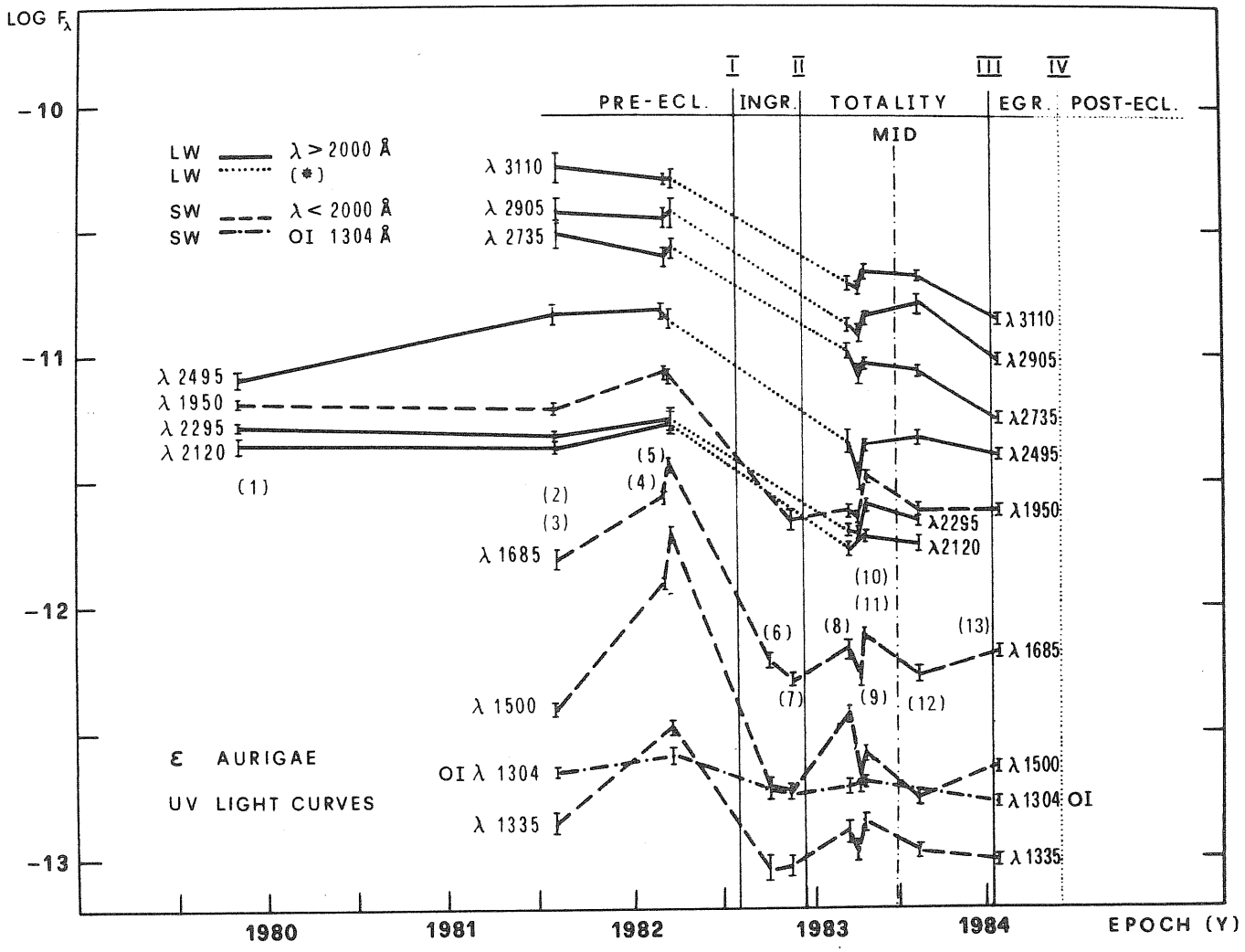

Fig. 8.4 - Monochromatic UV light curves, based on our sample of IUE low-resolution spectra (Tab. 8.1). Numbers in parenthesis indicate the spectra, from which the experimental points are derived. Fluxes F_λ are in erg $s^{-1} cm^{-2} Å^{-1}$.
(*) Dotted lines: ingress data are now better covered by other observers (cf. § 5.3).

8.4 Interpretation

From the set of eclipsed and uneclipsed spectra, one gets the basic result that the amplitude of the eclipse is reduced at $\lambda \lesssim 1400$ Å. Probably the contradiction with the data reported by Chapman et al. (1983), who found an opposite trend in the wavelength dependance of the eclipse, is only apparent. In fact, Chapman et al. consider a spectrum taken out of eclipse on April 13, 1982 during an active period (near spectrum (5)), and compare it with a partially eclipsed spectrum taken on Sept. 21, 1982 during a quiescent period (near spectrum (6)). This causes an apparent deepening of the eclipse in the short wavelength range, which is dominated by intrinsic variability (see further discussion on § 8.7).

The decreasing of the eclipse-depth at short λ gives a strong support to those models of ε Aur that predict the existence of a hot secondary component, dominant in the far UV and not affected by the eclipse because it passes in front of the primary. For the same reason Plavec's model (1982), which locates the hot object inside the primary component (supposed to be a disk simulating an F supergiant), seems to be contradicted by observation.

Let us come to the source of far-UV variability. Continuum fluctuations could be simply an intrinsic property of the hot secondary, but we need a mechanism also for line variations. Probably this variability could come from a non-homogeneous hot internal region of the extended body surrounding the secondary (and already responsible for the eclipse of the primary); in this case, according to the degree of clumpiness, the light of the secondary should be more or less attenuated, so that its spectral lines could be more or less filled by continuous emission of the extended body. Another possibility is the intrinsic vari-

ability of the extended body itself; an increase in its opacity may explain both the increase in the flux emitted (getting closer to black body conditions), and the deepening of the absorption lines (supposing they are formed in the body itself). An attempt for analyzing the variability of the UV excess is made hereafter in Section 9.1 .

Since there is no remarkable deepening of the λ 2200 Å absorption feature, associated with the eclipse, this fact puts serious constraints on the nature of the eclipsing body. Shurely, the eclipsing object cannot be a semitransparent veil (e.g. thin disk seen obliquely) made of standard-composition dust. Notwithstanding this important conclusion, in case the eclipsing body is an opaque structure (e.g. thick disk seen edge-on) whatever composition remains possible. In priciple, dust could be also present all around the whole system, inside a circumstellar envelope (supposed to extend beyond the secondary's orbit). Anyway, a gaseous envelope exists around the F star, and it is larger in size than the eclipsing object, as revealed by the emission line OI λ 1304 which is practically independent of the eclipse and of UV variability.

Finally, let us examine the greyness of the eclipse. There are indications that, in the near and mid UV, the eclipse is deeper than in the visible (Ake and Simon, IAU Circ. 3763). Also the values given in our Table 8.2 confirm this trend, but the observed disagreement between optical and UV depths may be reduced to about 0.1 mag, if only well exposed regions of the large aperture-spectra are considered. Anyway in addition to electron scattering, which may provide the grey component of the eclipse (as suggested by Hack, 1959), another contribution to the opacity of the eclipsing body must be present the ultraviolet. This could be produced by strong blended absorption lines from the eclipsing body, affecting the position of the continuum (particularly on low-resolution spectra).

8.5 High Resolution Observations

In order to study the behaviour of the ultraviolet lines during the eclipse, a sample of 9 high-resolution IUE spectra, taken at different eclipse-phases, has been analysed; such observations are listed on Table 8.3 . In particular, 4 observational shifts with IUE (providing spectra labelled H2, H3, H6, H7) were carried out by the writer and collaborators, almost simultaneously with 4 corresponding spectrographic runs in the visible, performed at the Obs. de Haute Provence (France). The rest of the sample, consisting of 5 high-resolution ultraviolet spectra taken by other observers, has been obtained from the VILSPA Data Bank.

Moreover, because of instrumental opportunity, most IUE observers obtained spectra at the same time, both at low and at high resolution (cf. Tabs. 8.1 and 8.3). Thus, also including visible OHP observations (Tab. 6.1), the set of contemporary spectra at different wavelengths, is listed on Table 8.4 together with the corresponding eclipse-phases. It should be noticed that in the far UV only low-resolution spectra of ε Aur are well exposed, while in the mid UV high-resolution spectra can be taken, providing most information. Finally, as regards the timing of observations, one can see that the phase-coverage of the eclipse is complete, at all spectral ranges under study.

Table 8.3 - IUE High-Resolution Observations

Date	Observer	Images	t_{exp}	Spectrum
1981,Aug. 5	(*) Stickland	LWR 11247	-	H1
1982,Mar.12	(*) Chapman	SWP 16523 LWR 12777	70^m 9^m	H1a
1982,Mar.26	(*) Stickland	SWP 16629 LWR 12865 " 12866	60^m 50^m 8^m	H1b
1982,Nov.16	Molaro	SWP 18751 LWR 14645 " 14646	55^m 15^m 50^m	H2
1983,Mar.20	Morossi	LWR 15522	60^m	H3
1983,Apr. 8	(*) Ake	LWR 15675 " 15676	55^m 15^m	H4
1983,Apr.18	(*) Chapman	SWP 19749 LWR 15766	300^m 18^m	H5
1983,Aug. 8	Ferluga	LWR 16553	15^m	H6
1984,Jan.20	Boehm	LWP 2763	12^m	H7
1984, Sep. 6	Ferluga-Stickl	LWP 4158	-	H8

(*) Spectra released by Vilspa Data Bank

Table 8.4 - Corresponding Spectra and Eclipse-Phases

Epoch	Far UV (1300-1900Å)	Mid UV (1900-3200Å)	Visible (3600-6700Å)	Eclipse-phase
Aug 81	(3)	H1		Pre-eclipse
Mar 82	(4)	H1a (°)		Pre-eclipse 'activity'
Mar 82	(5)	H1b (°)		Pre-eclipse 'activity'
Nov 82	(7)	H2 (°)	FØ6	Late ingress
Mar 83	(8)	H3	FØ7	Totality
Apr 83	(9)	H4		Totality 'brigtening'
Apr 83	(10)	H5 (°°)		Totality 'brigtening'
Aug 83	(12)	H6	FØ8	Totality (mid)
Jan 84	(13)	H7	F12	Early egress

Notes: (°) well-exposed towards the far-UV until 1700 Å.
(°°) well-exposed towards the far-UV until 1600 Å.

8.6 The Mid-UV lines

The 1982-84 eclipse of ε Aur was the first one to be observed at ultraviolet wavelengths; so that, as soon as high-resolution spectra H2, H3 and H6 were obtained, an early comparison made possible the first detection of the shell spectrum in the UV (Paper III). Neverthless, the resolution of IUE's high-dispersion spectrograph is not sufficient for separating the shell components from the corresponding stellar lines. As a consequence, it can be observed only a (more or less evident) distorsion of the instrumentally-convoluted profile, towards that side of the line where the shell component is present.

However, by studying the full sample of spectra (Table 8.3) in their best exposed part (λ2400-3200 Å), one realizes that not all the profiles behave in the same way with respect to the eclipse-phase, thus revealing different origins with respect to the eclipsing body. In particular it is possible to identify 2 distinct classes of spectral lines, which we shall call "normal" and "special" respectively, since the first ones behave like in the visible (and are the majority) while the others show significant anomalies.

a) Normal lines. Almost all the lines - with only a few exceptions - display the same kind of phase dependence (Fig. 8.6), exactly reproducing at IUE's resolution the already familiar behaviour of the visible eclipsed spectrum (Section 7).

- At ingress (H2) a widening of the profile on the red side appears, suggesting the presence of an additional

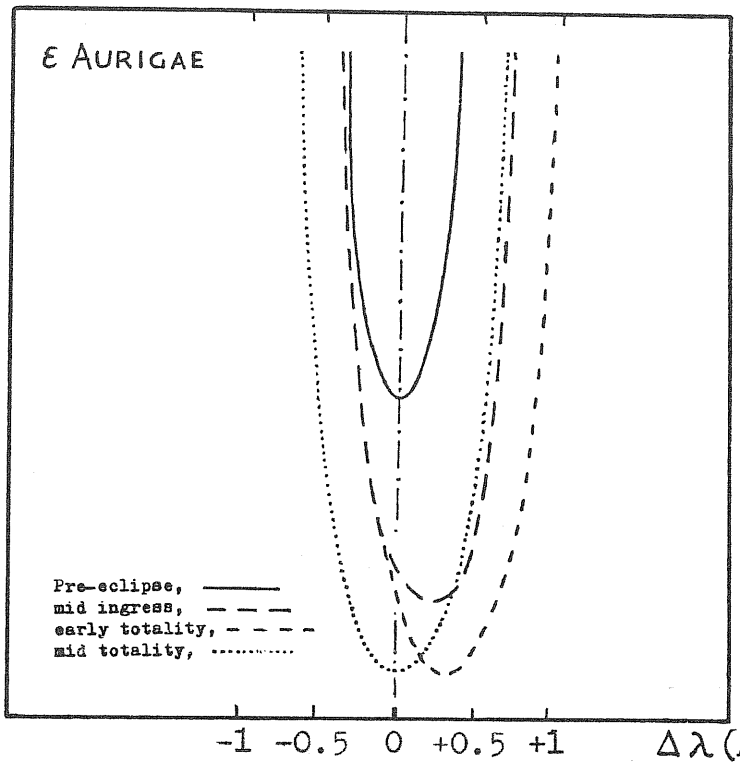

Figure 8.6 - Normal lines . The typical phase-dependence of the profile, on ingress and totality (schematic).

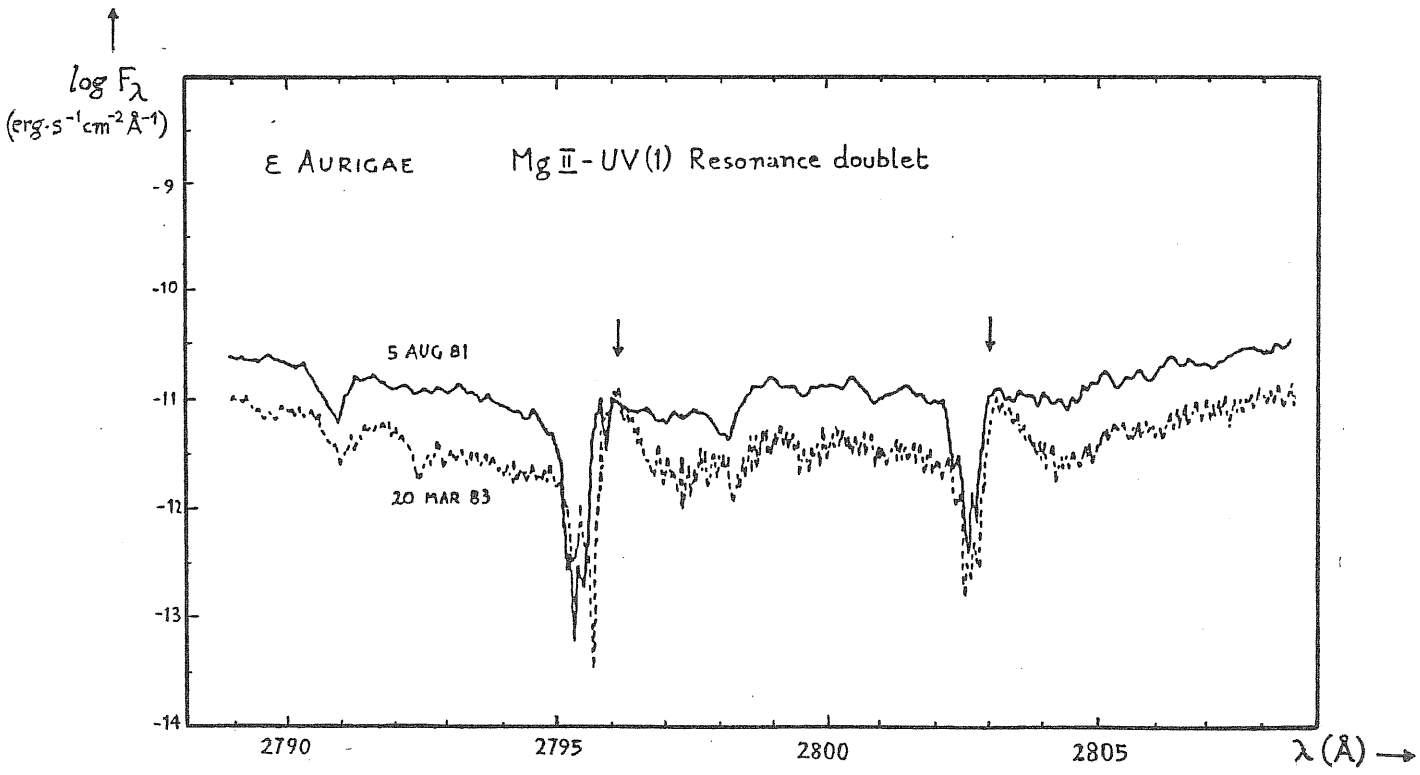

Figure 8.7 - Special lines. The outcoming of the P-Cygni component on the MgII λ2800 doublet. Solid trace: out of eclipse; dashed trace: totality.

unresolved absorption component, with a redshift corresponding to about + 30 km/s.

- At early totality (H3) the effect is even more evident, presumably because of a corresponding enhancement of the red-shifted component. Although generally the two components are unresolved, giving the global appearance of a single larger and red-shifted line, there are also cases in which a double-core structure can be directly observed.

- At mid totality (H6) the lines remain deeper and larger with respect to out-of-eclipse ones (H1) but no evident shift is present, suggesting the two components are superimposed. In some cases a complex structure appears to be convoluted with the instrumental profile, and occasionally some usually weak lines may undergo particular enhancement.

- At egress (H7) the widening of the profile appears on the violet side of the line, and the effect is symmetrical to the one at ingress, but more pronounced.

b) Special lines. Some isolated lines in the mid UV, such as the resonance lines of MgI, MgII and FeII, do not participate to the general "oscillation" of profiles during the eclipse. Among these special lines there are some features, which moreover seem not to participate in the general lowering of the continuum, corresponding to the depth of the eclipse; as an effect, these features "come out" in the eclipsed spectra, appearing as emission components of P Cygni-like profiles (Fig. 8.7). Accounting for these and other peculiarities, the following classification is proposed:

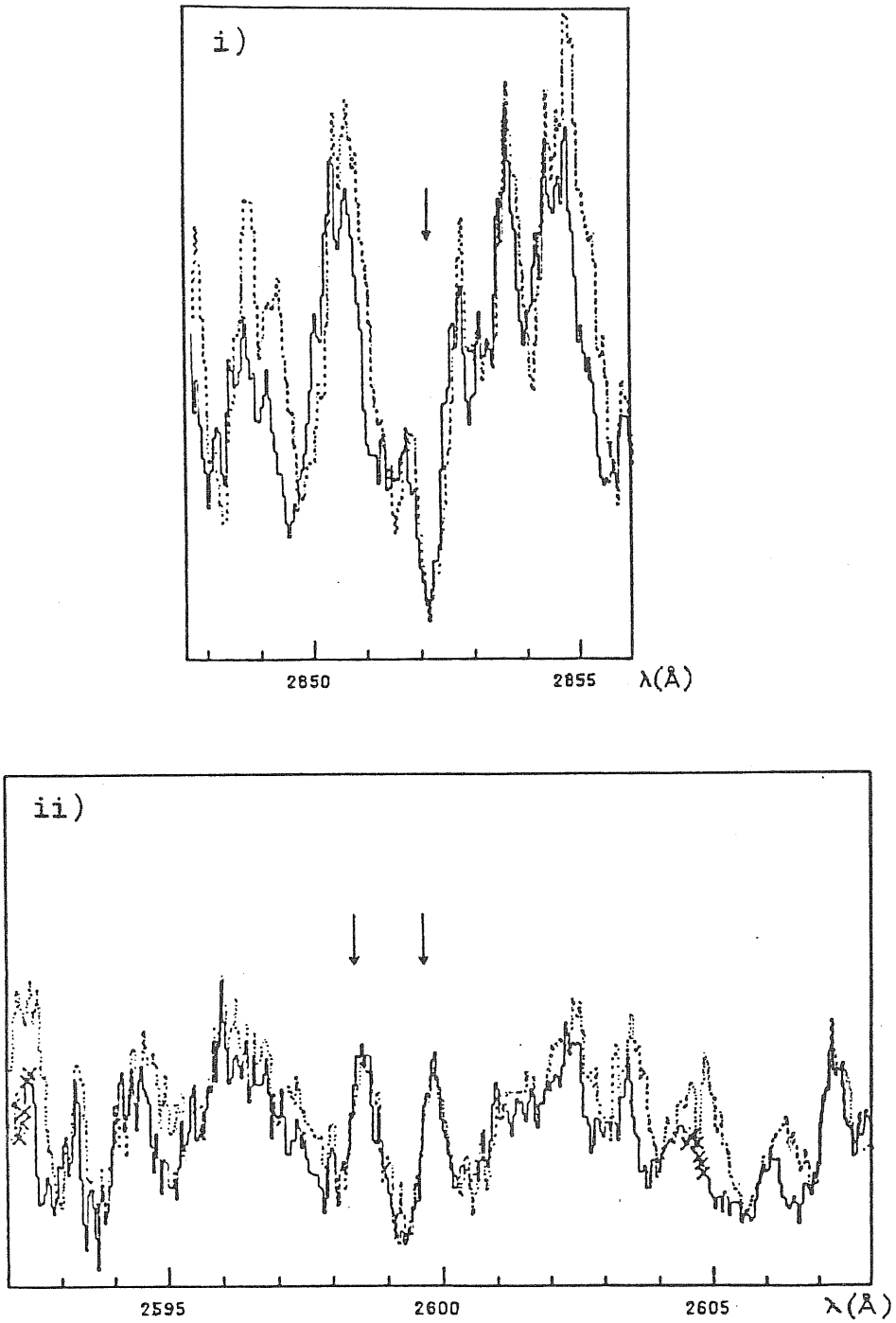

Figure 8.8 - Special lines at end-ingress (·····) and mid-totality (——); vertical scale linear. Note that these features are not affected in wavelength by the eclipse phase.

i) Pure absorption : Mg I λ2852 resonance

ii) Outcoming emission : FeII λ2598-99 resonances

- Pure absorptions. The profile of these absorption lines remains unsensitive to the eclipse; they are rare to be found, and the best example (Fig. 8.8a) is the strong resonance line of MgI at 2852 Å. Intermediate cases, displaying a more or less reduced oscillation during the eclipse, are rather common; examples can be MnII resonance lines at 2570 and 2590 Å.

- Outcoming emissions. In these cases the position of the emission feature is unaffected by the eclipse phase. The most evident example is given by the MgII resonance doublet at 2800 Å (Fig. 8.8b), and also FeII resonances at 2598 and 2599 Å show the presence of a steady emission component.

In order to give an interpretation to such phenomena, the basic point is the following: all these special lines, which do not to take part in the eclipse mechanism, were classified peculiar also out of the eclipse by Castelli et al. (1982), because the observed profile did not fit their synthetic spectrum, as shown on Fig 8.9. Lines exhibiting a stable pure absorption feature on eclipse, showed out-of-eclipse an enhanced core shifted towards the violet (at about -30 km/s). On the other hand, lines displaying an outcoming emission with a P Cygni-like profile during the eclipse, showed out-of-eclipse both the violet-shifted core, and a raised profile on the opposite side of the line (at about + 10 km/s or some more).

Clearly, these out-of-eclipse features are interpreted as the effects of an expanding envelope around the primary, with $v_{exp} \approx 30$ km/s. The evidence that these features are not significantly eclipsed by the secondary companion has the following explanation: the primary's envelope producing the

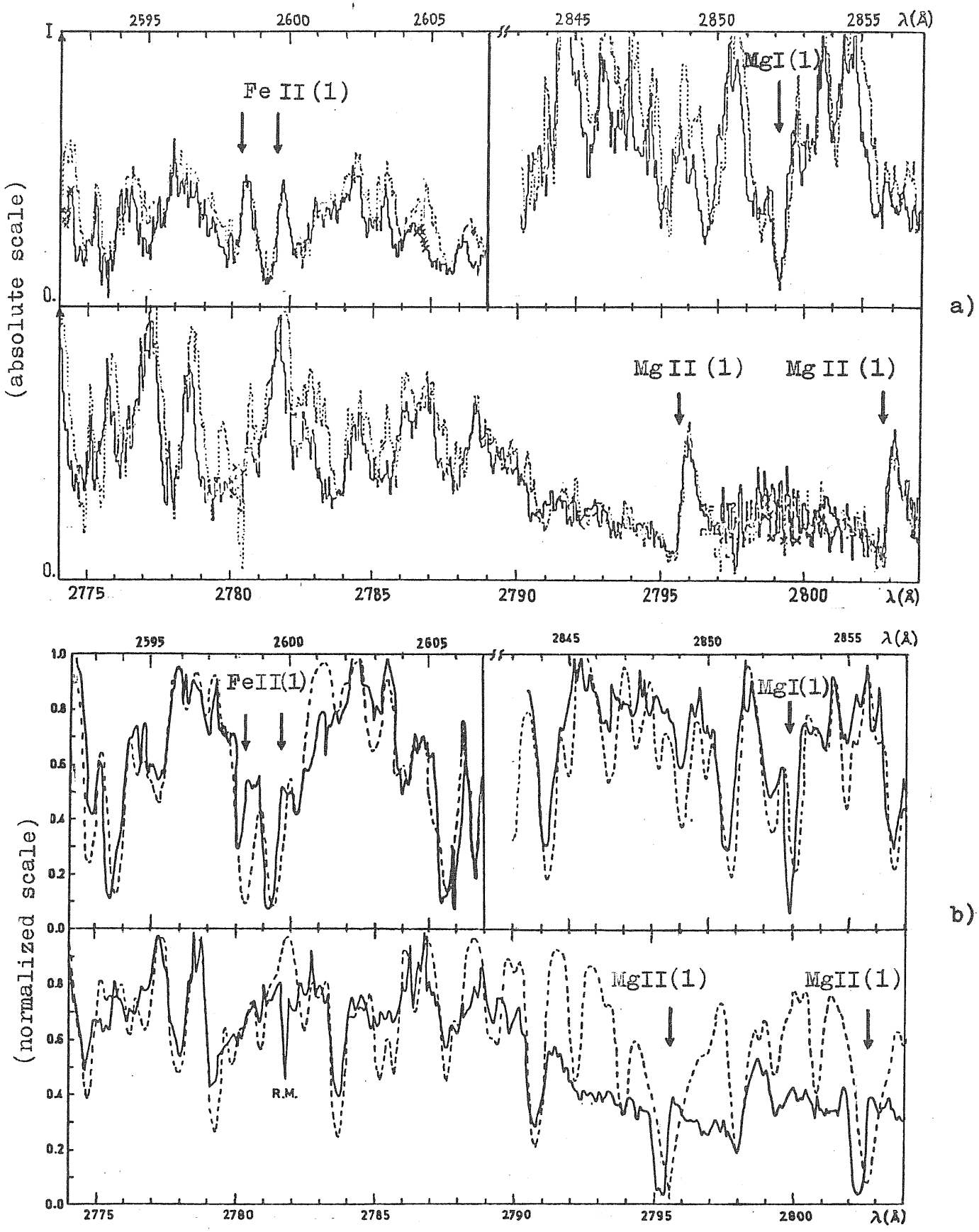

Fig. 8.9 - Special lines on eclipse are peculiar lines out of eclipse (see text).

a) eclipse { ····· end ingress, sp.H2
—— mid totality, sp.H6

b) out of eclipse { ---- IUE spectrum
—— LTE model (Castelli et al., 1982)

emission components must have a much larger size than the interposed companion, so that such envelope remains mostly uneclipsed also during totality. Moreover it is observed that the whole P-Cygni profile, as well as the pure absorption features, during the eclipse show an apparently lower expansion velocity; this could be due to the fact that the opaque body (producing the photometric eclipse) occults the central part of the F star, which is just responsible for the highest projected velocity.

As we have seen, all the lines which have a special behaviour as in b) during the eclipse, are observed to be peculiar also out of eclipse; the reverse, however, is not always true. In fact, about 50% of the lines which are peculiar out of eclipse, display a rather normal phase-dependence on eclipse, as in a). Among this group, we find for instance the UV multiplets CrII(5)(6) and MnII(5), and the multiplet TiII(5V). Intermediate cases, showing only a reduced phase-dependence effect, are also common.

This phenomenology is due to the superposition of two contributions, by the secondary's rotating shell and by the primary's expanding envelope, with comparable intensities. The more pronounced is the observed phase-dependence, the more intense must be the shell component with respect to the envelope component. Such contribution from the F-star's envelope can be evaluated line-by-line, by measuring the discrepancy between the observed out-of-eclipse profile and the model. Detailed comparison with phase-dependence is on Master Th.,pag.111-120.

For the majority of the lines, one finds that the envelope component is negligible or rather weak. These lines are precisely those resulting <u>normal</u> on eclipse, since the shell component prevails producing the typical phase-dependent

oscillation. On the other hand, for some particular features such as the resonance lines, one finds that the envelope component is dominant (Fig. 8.9) and it has the shape of an absorption feature (MgI λ2852) or of P-Cygni profiles (MgII $\lambda\lambda$2800). Such lines are exactly those observed to be special on eclipse, since the envelope features grow up enhanced by the eclipse itself, which occults the F star but not its envelope. Let us finally notice that the most remarkable spectral feature, revealing the presence of an envelope, is the OI emission line at 1304 Å observed at low resolution, which remains practically uneclipsed and unaffected by far-UV activity (§ 8.4).

8.7 The Question of Non-greyness

It is well known (§ 2.3) that the eclipse of ε Aur is substantially grey at visible wavelengths, since the whole spectrum is lowered by a wavelength-independent factor, and only sharp absorption features (shell lines) are superimposed. However, along the mid-UV spectrum, regions of enhanced deepening are observed towards the shorter wavelengths (where the density of lines is particularly high), while at longer wavelengths (where the continuum can be unambiguously recognized) no significant wavelength-dependence is found in the depth of the eclipse. This fact has a possible trivial explanation: the deviation from greyness could come simply from the integrated contribution of the superimposed shell line-spectrum, which is richer in lines towards the shorter wavelengths.

But, if the eclipse is really non-grey in UV, in the sense

of a true deepening of the continuum towards the shorter wavelengths, this should be interpreted as a clear sign of the presence of dust in the eclipsing body. Despite other researchers (Chapman et al., 1983; Altner et al., 1984) claim to have found such a deepening, absolutely no evidence of dust is observed on our full sample of low-resolution eclipsed spectra (6) to (13), when compared with the out-of-eclipse spectrum (2) assumed as a reference (Aug'81). In fact, deviations from greyness which are found on our sample are so small (or even absent), that they can be easily produced by simple blending of the shell absorption lines, or by effects of far-UV variability. Intrinsic variability is probably also the reason for such a severe discrepancy, about the evaluation of the eclipse greyness, and ultimately about dust. Let us now discuss this point in more detail.

Determinations of the eclipse-depth can differ substantially, since they depend on the choice of the out-of-eclipse reference spectrum. As it was noticed by Altner et al. themselves, this is a delicate choice, because of the primary's cepheid-like variability. But still more critical is the problem of far-UV activity, coming from the hot source (probably embedded in the eclipsing body), and affecting in particular the region from 1300 Å to 1700 Å with a peak around 1500 Å. If the assumed out-of-eclipse reference spectrum were taken for example near the activity period of March 1982, when the luminosity was enhanced in the far-UV (by 1.5 mag at 1500 Å), then the depth of the eclipse at the various phases would appear systematically deeper in the far-UV (by 1.5 mag at 1500 Å). Such a deepening of the eclipse at short wavelengths is precisely the result obtained by Altner et al., assuming a reference spectrum taken on April '82, right near the active period: at all phases,

their curves of eclipse-depth vs. λ are exactly the mirror image of the curve of activity vs. λ shown on Figure 8.2 (dotted line).

Probably all the evaluations of the non-greyness of the eclipse, which are referred to uneclipsed spectra taken around March '82 (near the highest peak of far-UV activity) are misleading. Unfortunately, it is always difficult to distinguish the pure effect of the eclipse from the superimposed contribution of intrinsic variability. And anyway the problem remains open, since Altner et al. (priv.comm.) confirm that, after carefully re-examining the IUE archival data, they still find that the eclipse was non-grey (!), using different pre-eclipse spectra for comparison.

In conclusion, let us mention one more problem concerning the wavelength-dependence of the eclipse. As one can see from Fig. 8.4, the low-resolution spectrum (13), providing the last point of each light-curve just near the 3rd contact, shows an apparent deepening of the eclipse at the longer wavelengths (λ2500-3100 Å). Although it might be due in part to the intensification of unresolved shell-absorption lines at egress (§ 8.6a), if real this deepening would be in contrast with the UBV photometry results (Ôki et al., 1984), showing in the same period (J.D. 2245700-5740) a brightening of about 0.15 mag in the U band, decreasing towards B and V. In fact, while this brightening could be related with a corresponding far-UV activity shown by spectrum (13) itself, there is no way to match such general brightening with the near-UV "dimming". But since spectrum (13) is the only case in our sample, for which LWP camera of IUE was used in place of LWR, the most reasonable possibility is that such discrepancy is nothing but an instrumental effect, due to different calibration of IUE cameras.

9. - STRUCTURE OF THE ECLIPSING BODY

9.1 The Hot Source

The observed far-UV variability was interpreted as due to the activity of a hot source embedded in the system of ε Aur (§ 8.4). For studying this variable UV excess, one has to measure the observed continuum F_o at various epochs, and compare it with expected flux distribution F_e which should be received from ε Aur, if not embedding a hot component. The UV excess is then defined as the quantity

$$\eta = \frac{F_o}{F_e} - 1 \quad . \qquad (9.1)$$

Moreover, indicating with L_A and L_B the (monochromatic) luminosities of the primary star and of the hot component respectively, the ratio F_o/F_e is equal to $(L_A+L_B)/L_A$. Hence the UV excess

$$\eta = \frac{L_B}{L_A} \qquad (9.2)$$

can be also regarded as the luminosity of the peculiar hot component, with respect to the primary star, at a given wavelength.

We shall now analyse the emission of this hot source, as a function of wavelength and time, referring to a set of low-resolution IUE spectra taken during the years 1981-83, and already labelled from (2) to (8) on Tab 8.1. The values of the observed continuum F_o for these spectra have been already listed on Tab. 8.2 (where they were indicated as F_λ).

For computing the expected flux F_e at different wavelengths, we shall follow here the same method adopted by Hack and Selvelli (1979); this enables us to include in the present analysis also their first observation of the UV excess (§2.5), dating back to Apr 19, 1978 and hereafter labelled spectrum (0).

The procedure is based upon the quantities F_{obs}, F_{corr} and F_{pred} referring to that determination, which are tabulated (vs. wavelength) on the same paper.

By definition, F_{obs} is the observed continuum on spectrum (O); while F_{corr} is the same observed flux, corrected in order to neutralize the effect of interstellar extinction. That is to say, interstellar extinction is responsible for the reduction factor F_{obs}/F_{corr}. Moreover, F_{pred} is the flux predicted from ε Aur (same spectrum as ∝ Car), supposing no hot component, and neglecting interstellar extinction.

Hence, out of eclipse, it is by definition

$$F_e = F_{pred} \frac{F_{obs}}{F_{corr}} \quad , \qquad (9.3)$$

so that we can derive directly F_e at the different wavelengths, simply from the tabulated values of F_{obs}, F_{corr} and F_{pred}. Whereas, during the eclipse, it is obviously

$$F_e = F_{pred} \frac{F_{obs}}{F_{corr}} 10^{-0.4\Delta m} \quad , \qquad (9.4)$$

where Δm is the eclipse depth, given on Tab 8.2 for the various phases.

Kowing the observed continuum F_o and the expected flux distribution F_e for our sample of spectra, we can finally compute the UV excess η from (9.1). The resulting values of η (at wavelengths in the range 1300-1850 Å) are listed on Tab. 9.1, for epochs before and during the eclipse.

It is evident that, at the shortest wavelengths, the excess is rising over 2 orders of magnitude. On the contrary, longward 1700 Å the excess is generally 0 (negative values are probably due to imperfections in continuum tracing and in

compensating the interstellar absorption).

Figure 9.1 plots the secular variability of the excess η at λ1450 Å, where the effect is particularly evident, and at λ1650 Å, where it is weaker. As one can see, the timescale of these fluctuations appears not to exceed a few months. On the other hand, at short timescales, no appreciable variation is revealed over a one-day interval, comparing spectra (2) and (3).

Figure 9.2 shows the behaviour of the excess η as a function of wavelength, from 1300 to 1650 Å, for selected spectra taken at different epochs before and during the eclipse (*). It is outstanding that the excess is not related to the eclipse. Moreover, some kind of parallelism of the curves can be noticed; this should mean that the variability is not significantly depending on temperature, and hence it can rather be caused by inhomogeneities of the opaque body, rotating around the hot source and variably occulting its surface (provided the hot component is really located in the middle of the extended body which causes the primary eclipse).

In fact, expliciting effective temperature T and radius r in the black-body approximation, equation (9.2) becomes

$$\eta = \frac{r_B^2}{r_A^2} \frac{e^{C/\lambda T_A} - 1}{e^{C/\lambda T_B} - 1} \quad , \qquad (9.5)$$

where C is a constant, and the indexes A and B stay for the primary star and the hot component respectively. Parallel

(*) Erratum. On paper V (partly anticipating this discussion), the corresponding Figure 1 shows unproper plot for spectrum (5).

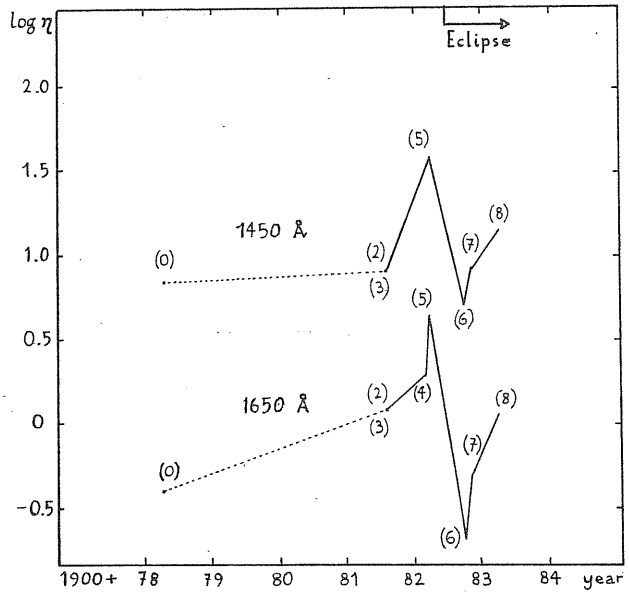

Figure 9.1 The variable UV excess, as a function of time.

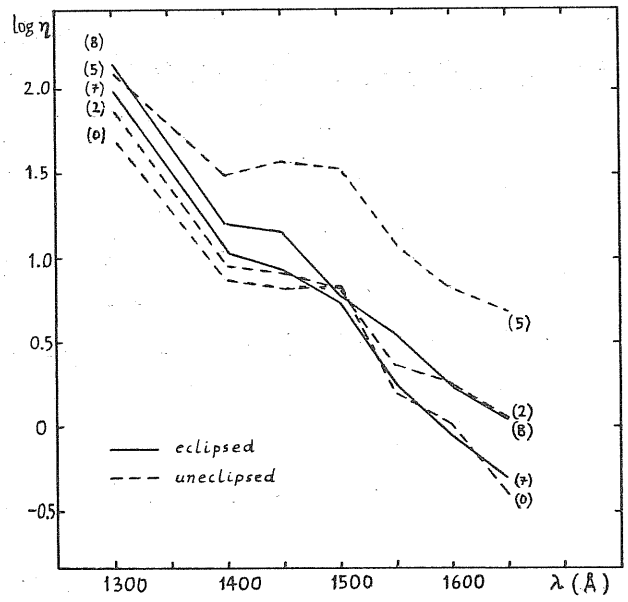

Figure 9.2 The variable UV excess, as a function of wavelength.

curves on Fig. 9.2, which shows the variability of the function

$$\log\eta = \log \frac{r_B^2}{r_A^2} + \log \frac{e^{C/\lambda T_A} - 1}{e^{C/\lambda T_B} - 1} \quad , \qquad (9.6)$$

should imply that the 2nd term remains constant (dependence on λ), while the 1st term adds a variable contribution (vertical shift). This would mean that the effective temperature T_B of the hot source remains constant, while its effective radius r_B is responsible for the observed variations (obviously supposing that the primary star does not vary!). For example, in the largest variation "(8)-(0)" shown on Fig. 9.2, $\log\eta$ undergoes an increment of about 0.8; this should mean that $\log r_B^2$ undergoes the same increment, implying that the effective surface should vary in this case by a factor of about 6, and r_B by a factor of about 2.5 .

More explicitely, if T_B is constant with time, we can use eq. (9.5) for comparing the values of a general spectrum (t) with those of reference spectrum (0), obtaining at all wavelengths the same ratio

$$\frac{\eta(t)}{\eta(0)} = \frac{r_B^2\,(t)}{r_B^2\,(0)} \quad . \qquad (9.7)$$

Thus we can compute the effective radius of the hot source

$$r_B(t) = r_B(0) \sqrt{\frac{\eta(t)}{\eta(0)}} \quad , \qquad (9.8)$$

simply referring to the value $r_B(0) = 1.1 \cdot 10^{11}$ cm known by (2.9), and by comparing the excess η of the two spectra; such determination will be independent of wavelength, if T_B is constant. Values of $r_B(t)$ determined in this way at different

Table 9.1 - The variable UV excess η

Sp. / λ(Å)	(0) 1.4.78	(2) 4.8.81	(3) 5.8.81	(4) 12.3.82	(5) 26.3.82	(6) 27.9.82	(7) 16.11.82	(8) 20.3.83
1300	52	77	77	-	127	79	106	149
1400	7.5	9.0	9.0	-	32	6.7	11	17
1450	6.8	8.2	8.2	-	38	4.9	8.3	14
1500	6.9	6.8	6.8	18	34	3.2	5.7	6.2
1550	1.6	2.3	2.3	5.6	13	0.8	1.8	3.5
1600	1.0	1.8	-	3.1	6.6	0.5	0.9	1.7
1650	0.4	1.2	-	1.9	4.4	0.2	0.5	1.1
1700	-.4	-.1	-	0.3	0.9	-.4	-.3	-.2
1750	0.0	-.1	-	0.6	0.8	-	-.2	-.1
1800	-.3	0.0	-	0.4	0.7	-	-.1	0.0
1850	-.3	-.1	-	0.3	0.6	-	-.2	0.0

Table 9.2 - Effective radius r_B

Sp. / λ(Å)	(0) 1.4.78	(2) 4.8.81	(3) 5.8.81	(4) 12.3.82	(5) 26.3.82	(6) 27.9.82	(7) 16.11.82	(8) 20.3.83
1300	1.1	1.34	1.34	-	1.72	1.34	1.57	1.84
1400	1.1	1.20	1.20	-	2.27	0.98	1.33	1.66
1450	1.1	1.21	1.21	-	2.60	0.93	1.22	1.58
1500	1.1	1.02	1.02	1.78	2.44	0.75	1.00	1.75
1550	1.1	1.32	1.32	1.61	3.14	0.78	1.17	1.63
1600	1.1	-	1.48	1.94	2.83	0.78	1.04	1.43
1650	1.1	-	1.91	2.40	3.65	0.78	1.23	1.82
Mean	1.1	1.23	1.36	1.93	2.66	0.91	1.22	1.67
$\pm\sigma$	(°)	±.10	±.27	±.34	±.62	±.21	±.19	±.14

(°) Note: $r_B(0)$ is assumed; values are in units of 10^{11} cm.

wavelengths, for each spectrum (t), are listed on Table 9.2: a substantial wavelength-independence can be seen, conferming constant temperature. That is, we can assume at any time T_B = 15 000 K as given by (2.9).

Then, by averaging upon wavelength, the definite value of r_B can be derived for each epoch. Moreover, Pogson's formula provides the values of absolute bolometric and apparent visual mag!s $M(bol)_B, m(vis)_B$ for each epoch, derived from the initial quantities (2.10). The resulting values of the effective radius, bolometric and visual magnitudes for the hot component at different epochs, are reported on Table 9.3. Interpreting these values as indicative of a main-sequence B star variably occulted by a surrounding opaque body, observation (5) implies that it should have <u>at least</u> a radius of nearly $4R_\odot$, correspond ing to a mass of about $7M_\odot$.

Table 9.3 - Parameters of the variable hot component (°)

Sp. / B comp.	(0) 1.4.78	(2) 4.8.81	(3) 5.8.81	(4) 12.3.82	(5) 26.3.82	(6) 27.9.82	(7) 16.11.82	(8) 20.3.83
$r_B/R_\odot$	1.6	1.8	1.9	2.8	3.8	1.3	1.7	2.4
$M(bol)_B$	-2.2	-2.5	-2.7	-3.4	-4.1	-1.8	-2.4	-3.1
$m(vis)_B$	9.2	8.9	8.7	8.0	7.3	9.6	9.0	8.3

(°) Note: T_B = 15000 K, constant

9.2 The Opaque Ring

A rather complete light curve of the present eclipse (Fig.5.1) is available from UBV photometry (Schmidtke 1985). The most outstanding feature is an apparent brightening of more than 0.2 mag centered at mid totality, and having a duration of about 5 months. Unfortunately, the data coverage of the light curve at mid totality is very poor in the present eclipse, as well as in the past ones, because of seasonal observational constraints (proximity of the sun). This could have caused the phenomenon not to be so evident during the past eclipses.

Small fluctuations, already observed on past eclipses, were generally interpreted as intrinsic cepheid-like activity of the F star (§ 2.3). Anyway, it was noticed that fluctuations were larger on totality than out of eclipse, and hence a possible relation with the eclipsing body was suspected. Now, the colourless nature, the strong intensity, and the exact mid-totality collocation of the present brightening, clearly require the latter explanation.

In particular, the eclipsing body should display a variable or differential trasparency, as it happens in the case of a ring-like structure with a raefaction in the center. Such a geometry was already proposed by Wilson (1971) and Huang (1974) for explaining the similar, but less pronunced, behaviour of the last eclipses (§ 4.3).

A crucial test for this interpretation is provided by ultraviolet observations. By considering (Tab 8.4) the high-resolution spectra H4-5-6-7 and the contemporary low-resolution ones (9,10, 12,13), important complementary information can be derived about the correlation between the continuum and the lines during the brightening. Obviously, this analysis is limited to the mid-UV spectral region ($\lambda > 2000$ Å), since at short wavelength the phase-dependent behaviour is perturbed by the contribution of the variable far-UV source.

In conclusion, one obtains the following results:

a) The mid-eclipse brigthening appears also in the UV, and it is even more pronunced towards the shorter wavelengths. This effect seems to follow the general trend, of the "quasi-greyness" of the eclipse; that is, one observes a slight deepening of the light-curve features, in the sense of decreasing λ (for instance, the average depth of the eclipse in the near IR is 0.7 mag, while in the visible it becomes 0.8 mag and in the UV it ranges between 0.9 and 1.0 mag). In particular the eclipse depth, at 2nd and 3rd contact, seems to be enhanced towards the shorter wavelengths.

b) The mid-eclipse brightening depends only on the continuum, which undergoes a general raising, while no significant variations occur to profiles of the lines, or to their normalized intensity. Such phenomenon can be observed in particular by comparing the couple of high-resolution spectra H4 and H5, taken during the increasing phase of the brightening (*). This fact fully confirms that, at mid totality, the almost grey eclipsing body has reduced its optical thickness, and/or its projected area over the F star.

Very interesting deductions can be made, from the lucky occurrence that the central brightening of this eclipse has been short, as well as very bright. Precisely, it lasted about 200 days and it reached an intensity $\Delta m \approx -2.5$ mag, with respect to the bottom of totality. First of all, since we know that the brightening must depend on a central rarefaction of the eclipsing body, its time duration - which is about twice a partial phase - implies that the size of this "hole" cannot exceed the size of the primary.

In particular, it is the shorpness of this brightening which allows us, finally, to discriminate among the long-

---

(*) since the spectra H4 and H5 were taken at a time interval of only 10 days (that is short with respect to the time-scale of the brightening), the effect which is observed is very small, though systematic.

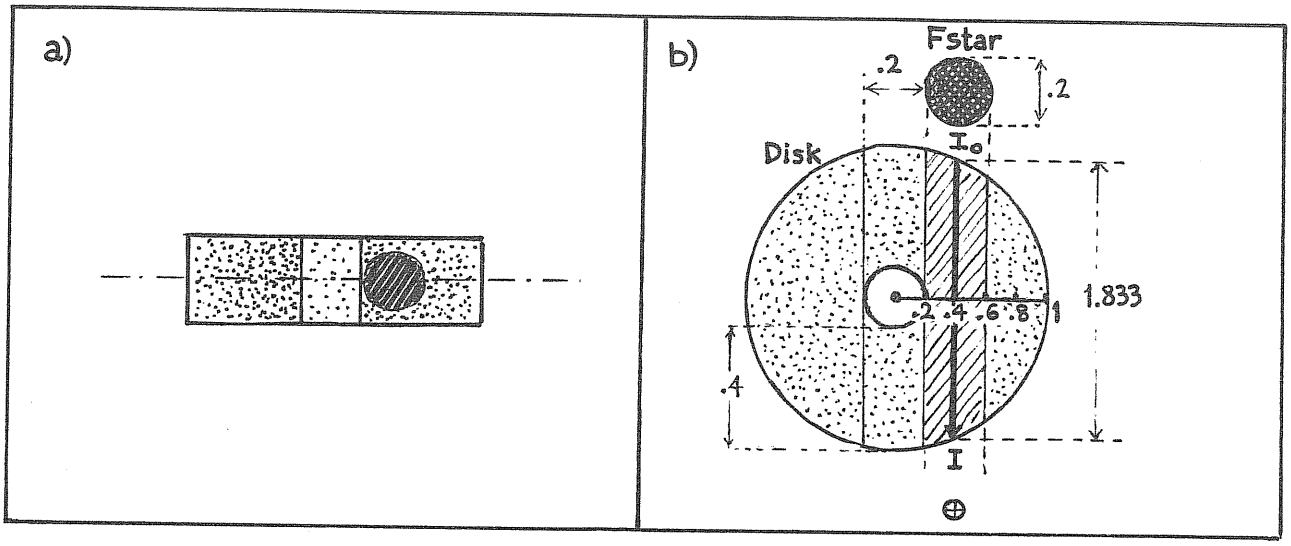

Figure 9.3 - Thick disk model. a)Equatorial view, as it is seen from Earth, on totality. b)Pole-on view, with geometrical parameters, discussed in the text.

discussed alternative between the two possible geometries for the eclipsing component: a thin opaque disk seen obliquely with a central aperture (Wilson, 1971), or a thick semitransparent disk seen edge-on with a central cavity (Huang, 1974). Now the second alternative can be ruled out. In fact - also supposing the central cavity totally void - it is impossible to produce, with the edge-on geometry, such a (short) brightening of 2.5 mag at mid eclipse.

Let us show it. For maximizing the contrast at mid eclipse, we shall consider a totally transparent cavity at the center of a uniform semitransparent disk, so thick that the whole primary's disk can be covered by it; see Figure 9.3a. The extinction law through the disk is

$$I = I_o e^{-\mu x} \quad , \tag{9.9}$$

where x is the optical path through the plane of the disk, μ is the extinction coefficient per unit lenght of the semitransparent region, I and I_o are the eclipsed and uneclipsed intensities, respectively. The value of

$$\mu = -\frac{1}{x} \cdot \ln \frac{I}{I_o} \tag{9.10}$$

is easy to be determined. Precisely, on the bottom of totality, we have $I/I_o=0.5$, with an optical path $x=1.833 \cdot r$ where r is the external radius of the disk, as shown on Figure 9.3b. Hence, it must be

$$\mu = 0.378/r \qquad (9.11)$$

Then, at mid eclipse, when the optical path through the semitransparent region is $x=1.6\,r$ we shall have

$$I = 0.546\ I_o \ , \qquad (9.12)$$

which corresponds to an eclipse-depth of 0.66 mag. Whereas, on the bottom of totality, we know that the depth is 0.75 mag. In conclusion, the height of the mid-eclipse brightening would not exceed

$$\Delta m \approx -1 \text{ mag} \ ; \qquad (9.13)$$

while, on the contrary, the observed height of the brightening is

$$\Delta m \approx -2.5 \text{ mag} \qquad (9.14)$$

This is enough, for excluding the possibility that the eclipsing object could be a thick semitransparent ring, seen edge-on (*).

So, it remains the possibility that the eclipsing body is a thin opaque disk with a central aperture, seen obliquely: briefly, an inclined flat ring. The geometrical parameters of the ring, which reproduce the observed light-curve of the last 1983 eclipse, have been determined, and they are reported on Table 9.4. For comparison, the ring-model values for the preceding eclipses, on 1956 and 1929, are also listed (symbols are the same used by Huang, 1974).

(*) Note that this striking conclusion could be obtained only because the observed brightening on this eclipse has been so short in duration, implying a corresponding small size for the central cavity. Such particular condition was not verified on the preceding eclipses, allowing for ambiguities in the models.

Table 9.4 - The Flat Opaque Ring

Parameters*)	1929 ; 1956	1983
t_o	30 ; 65±3	100 (!)
r'_2	99 ± 1	35 (!)
r''_2	197 ± 12	175
r_1	34 ± 18	35
j	84.4 ± 3.4	85.4
i	89.9 ± 0.1	90 (91)
Ψ	0.4 ± 0.4	0 (5.6)

Symbols

t_o Transmittance of the hole, %

r'_2 Radius of the hole } ring

r''_2 Radius of the disk }

r_1 Radius of the primary star

j Inclination angle of the ring plane

i Inclination angle of the orbital plane

Ψ Position angle of projected ring vs. projected orbit

*) Thickness $\ll r'_2$.

- Angles are in degrees;
  Radii are in units of $10^{-3}a$, where a is the separation.
- Errors are the difference between Huang's and Wilson's values, when the "thin disk" option by Huang 1974 and an average "adjustement" by Wilson 1971, are considered.
- (!) indicate the quantities that have changed remarkably; all others are consitent with the preceding eclipses.
- (Parenthesis) indicate values for the 'tilted' option, implying an 8° inclination of ring plane vs. orbital plane

Table 9.5 - Fitting of the Flat Ring Model

Quantity	Computed *)	Observed, 1983
Eclipse duration	660 d	647 d
Totality duration	440 d	446 d
Partial phases (aver.)	110 d	100 (± 37) d
Brightening (FWMH)	110 d	100 d
Brightening intensity	-.25 m	-.25 m
Eclipse depth	.75 m	.75 m

*) Non-tilted option

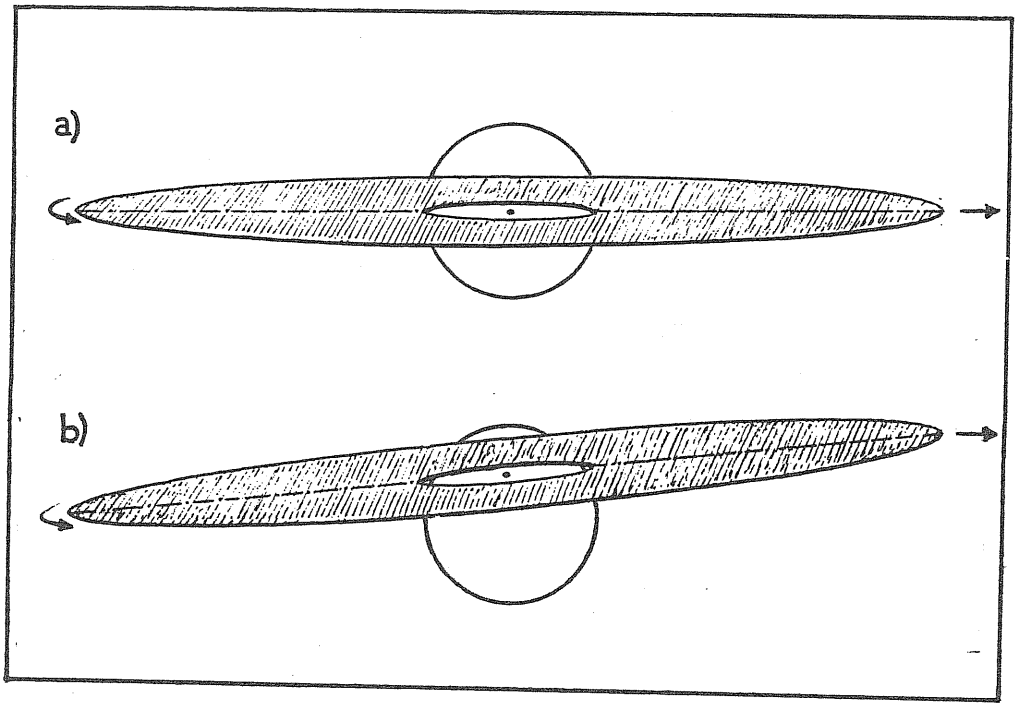

Fig. 9.4 - Flat Ring Model: visual appearance at mid-eclipse
a) non-tilted;
b) tilted as in Tab. 9.4 (values in parenthesis).

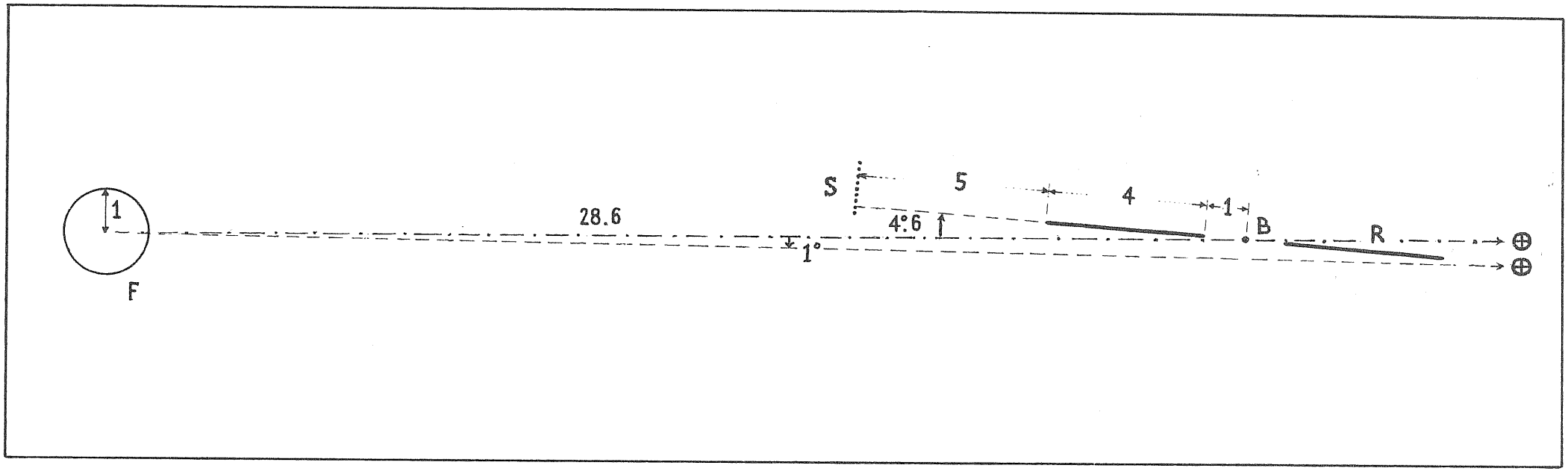

Figure 9.5 - Geometry of the system, corresponding to the model parameters listed on Table 9.4, for the 1983 eclipse. Lengths are expressed in units of the primary's radius, which is about 1 AU (dash-dotted: orbital plane). Lower position of ⊕ is that assumed for the "tilted" option

F - Primary star, FØ Ia
B - Secondary component, hot source
S - Shell of the secondary, outer limit
R - Ring of dust (thick bar)

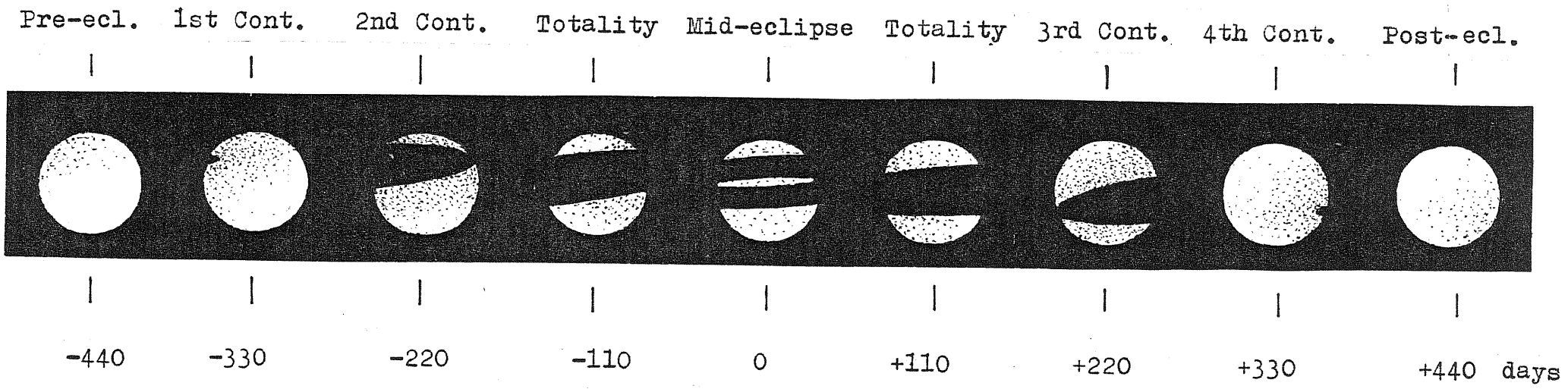

Fig. 9.6 - A visual simulation of the eclipse, in "tilted" conditions (i=90°.5 , j=5°); dots indicate the gas.

9.3 The Gaseous Shell

In this section we shall study in particular how the shell is related with the far-UV source; behaviour in the visible is discussed in §§ 7 and 10. As happens for the depth of the eclipse, also the determination of the shell spectrum, in principle, is affected by the problem of separating the effects of the eclipse from those related with the intrinsic far-UV activity. The influence of this activity, over the spectral lines of the system, can be studied in correspondence of active periods which have been observed in the UV: the first occurred before the eclipse on March 1982, the second occurred during totality on March 1983, and the third occurred near the third contact, on January 1984. Since for theactive periods in totality it is difficult, if not impossible, to separate the effects of the eclipse and of the activity, here we shall analyse in particular the activity period which occurred out of eclipse.

The activity phase in 1982 was the strongest and reached its observed maximum, Δm = 1.75 mag at 155 Å, on March 26 (Tab 8.2); two weeks before, on March 12, the activity was weaker, Δm = 1.25 mag at 1500 Å. It is then particulary interesting to compare the two IUE highresolution spectra, Hla and Hlb, taken in 1982 on March 12 and March 26 respectively (spectral range $\lambda\lambda$ 2600 ÷ 3100 Å); unfortunately, we do not have optical spectrograms at that epoch (Table 8.4). Since both spectra are "active", there are no large variations in the line profiles; but a detailed inspection reveals that some groups of lines appear to change their relative intensities slightly.

In particular we may notice that, in correspondence of a higher degree of activity, the stronger mid-UV lines of Fe I, such as $\lambda\lambda$ 2966.9 - 2973.1 Å resonances or the multiplet V9, seem to be partially "filled". The same thing happens to several low-excitation lines of Ti II, and in particular to the strong low-excitation lines of V II belonging to the multiplets UV 3-10-11-12 (EP $\leq$ 0.4 eV) and V 26-27-34-42. Also the absorption wings of the Fe II λ 2599 Å

resonance line, and particularly the large absorption wings of the Mg II 2800 Å resonance doublet, appear to be flattened by the effect of activity. The filling occurs generally on the red side of the lines, and on both wings of the Fe II and Mg II resonances; the effect is about 0.2 - 0.3 magnitudes, between March 12 and March 26, 1982. At the same time, the continuum is raised by about 0.1 mag, in the "window" around 3080 - 3087 Å.

Such effects are greatly enlarged, if we compare these active pre-eclipse spectra, with a quiescent post-eclipse spectrum: in our case let us consider the high resolution spectrum H8 on September 6, 1984. After overcoming some calibration problems (this spectrum was taken with a different IUE camera), there still remains a difference of about 0.5 mag, between the mid-UV continuum enhanced by activity (1982), and the quiescent one (1984); then, while the continuum is raised, the behaviour of the line components of the mid-UV spectrum, with respect to activity, can be classified as follows.

(i) Normal. The majority of the lines apparently follow the variation of the continuum, increasing their central flux by ~ 0.5 mag in activity, with no remarkable in the profile.

(ii) Filled. This is the case (Fig. 9.6) of the already-mentioned lines of Fe I, Ti II, V II, and wings of Fe II - Mg II resonance lines, which are filled in pre-eclipse activity by 1 mag. (*)

(*) Note. The behaviour of an even larger number of low-excitation lines, know to possess a violet-shifted shell component in the post-eclipse spectrum of Sep 1984, is apparently similar. The same behaviour is shown, symmetrically, in the pre-eclipse spectra of March 1982. Just because the shell absorption is weaker at ingress, on comparing a pre-eclipse spectrum with a post-eclipse one, these lines appear to be "filled" on the violet side before the eclipse: this effect has nothing to do with activity, and it should be distinguished from case (ii).

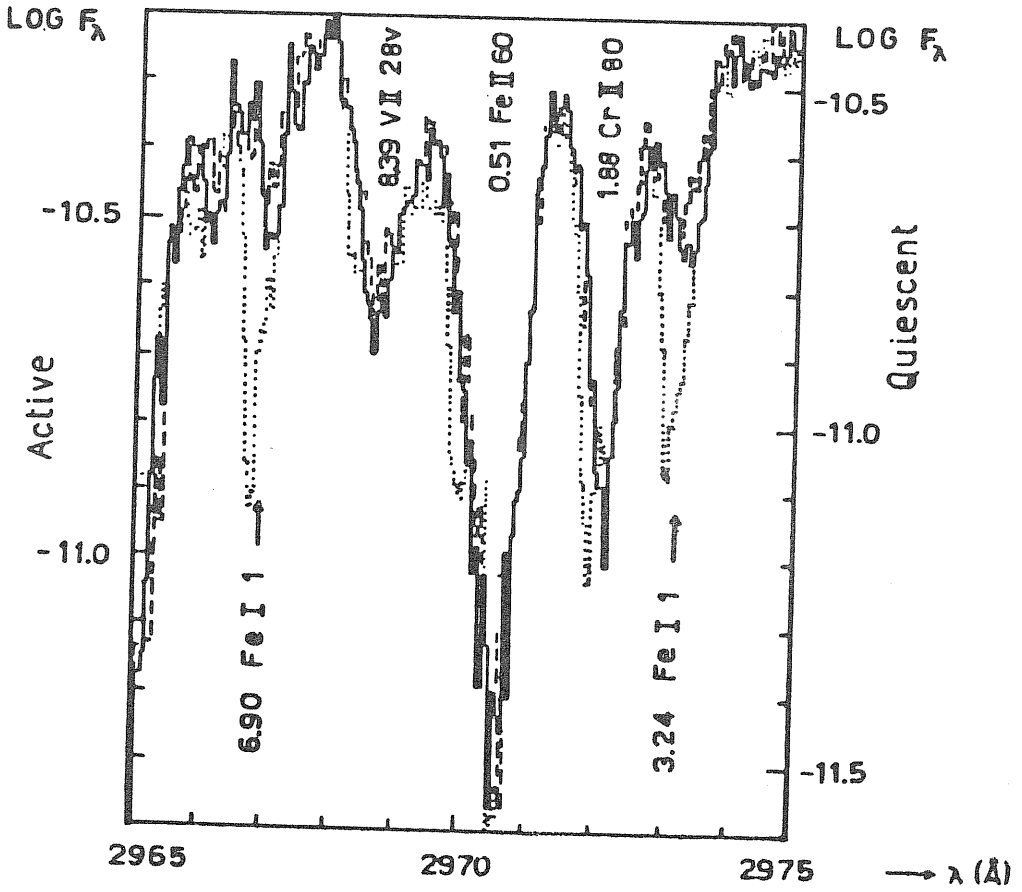

Fig. 9.6 - Line variations during UV activity. With respect to the quiescent phase on Sep 6, 1984 (·····), the profiles of Fe I UV 1 resonance lines are "filled" during activity on March 12, 1982 (———), and they are still more filled during the activity peak on March 26, 1982 (----). Note that the "filling" acts on the doppler-shifted part of the lines.

(iii) Unchanged. Activity does not affect remarkably the central flux of some high-excitation lines, such as Fe II multiplets UV 62 and higher (EP $\gtrsim$ 1 eV), or Cr II multiplets UV 5 and higher (EP $\gtrsim$ 1.5 eV); so these lines appear to be deepened, with respect to the enhanced continuum. This effect should be dominant in the far UV, producing the deepening of lines observed at low resolution. Moreover, these lines do not show any remarkable doppier shift depending on activity (or on eclipse phase).
(iv) Circumstellar. Also the circumstellar emission components of strong resonance lines, such as Fe II λ2599 Å and Mg II λ 2800 Å, remain unchanged by activity, as well as O I λ1302 Å (§8.4).

These observed effects can be easily explained by the presence of an additional spectrum, produced by the source of far-UV variability, and superimposed over the spectrum of the system. This active spectrum should be very similar to that of the primary, in order lo leave it practically identical; the only difference should be a slightly higher temperature (together with the absence of absorption wings in Fe II and Mg II resonance lines).

As a consequence, one would have (ii) fainter low-excitation lines, producing the observed filling (and the wings of Fe II and Mg II resonances would be filled as well); moreover, one would also have stronger high-excitation lines, adding no appreciable flux (iii) to the underlying stellar spectrum. Intermediate situations would generate case (i), while circumstellar emission components (iv) would clearly remain unaffected. Finally, we note that in case (ii) the residual line is not red-shifted in pre-eclipse activity, since the"filling" acts on the doppier-shifted part of the line (Fig.9.6). This fact is of basic importance, since it means that the active hot source does not undergo absorption by the doppler-shifted shell component, as instead does the primary. So, we are finally facing a long-sought experimental evidence : the hot source cannot be associated with the primary, and hence it must be located at the center of the secondary.

9.4 The Complete Structure

From the results of the present and previous eclipses of Epsilon Aur it is evident that the spectroscopic and photometric observations are completely explained by the presence of the following bodies:

a) the F0 Ia primary, whose spectrum is always observable;

b) a cool body ($T \sim 750$ K) which is responsible for the photometric eclipse of the primary (§ 5.1). This dusty ring must be made of particles much larger than present in the interstellar dust, because no additional reddening is observed at 2200 Å during the eclipse;

c) a gaseous shell, more extended than the dusty disk, which is responsible for the additional spectrum appearing during the eclipse;

d) an extended envelope surrounding the primary, where the emissions of OIλ 1302 and Mg IIλ 2800 are formed;

e) a faint hot body which is not eclipsed and whose radiation dominates at $\lambda \leq 1500$ Å. In fact the depth of the eclipse tend to become zero at $\lambda \leq$ 1500 Å, thus indicating that the excess in the UV is real and not due simply to scattered light from longer wavelengths in the spectrum of the primary, or in other-words, it is not simply an instrumental effect. This hot body may be a star (as suggested by Hack and Selvelli, 1979) or a binary system (as suggested by Lissauer and Backman, 1984), whose radiation escaping from the poles excites and ionizes the gaseous envelope, producing theshell spectrum; but it is not a hot spot on that part of the surface of the primary which isn't occulted by the eclipsing body (as suggested by Parthasarthy and Lambert, 1983). The hot body (single star or close binary) is variable in light.

One may wonder how it is possible for the gaseous, partially ionized, shell to coexist with the cool object. Possibly, the light of the hot secondary escaping from the poles is able to excite and ionize the thin gaseous shell which extends farther out of the orbital plane, while a cool disk / ring surrounding the secondary and eclipsing the primary lies in the vicinity of the orbital plane,

10. - THE SPECTRUM OF THE ECLIPSING BODY

10.1 First Extraction of the Shell Spectrum

Reduction of the whole sample of available blue spectrograms of ε Aur (Tab. 6.1) was performed at the ASTRONET pole of Trieste, starting with the digitation at the PDS microdensitometer, and then following the standard ELSPEC/11 procedure (Pasian et al.,1982) which provides calibrated, heliocentric and normalized intensity spectra, and also allows further mathematical treatment.

In order to minimize the noise, groups of spectra taken at the same phase, with only a few days' interval, were averaged together. Average spectra for phases FØ3 to F18, from 1981 to 1984 covering the whole eclipse, were then obtained. As a reference, it was available the almost noise-free spectrum FØ3, which is an average of 6 normalized spectra taken out of eclipse on January 1981. Doppler shift correction was finally applied, reducing to zero the orbital velocity of the F star at all phases.

The shell spectrum is formed in the eclipsing body, by absorbing the radiation of the primary F star. Hence the local continuum, for a general shell line, is given by the profile of the corresponding line of the F star, on which the shell component is superimposed. So, if one divides an eclipsed spectrum containing the shell components, by a pure uneclipsed reference spectrum of the F star, one obtains a normalized spectrum of the eclipsing body. Such a method, taking the spectrum of the F star as the continuum for the shell lines, was already used in a single case for the extraction of the Hδ shell line during the previous 1955-57 eclipse (Hack,1959).

Taking the FØ3 uneclipsed spectrum as reference, it was applied the extraction procedure to our sample of phase-averaged eclipsed spectra, after careful equalization of their zero-intensity levels. As a result, it was obtained the first individual spectra of the gaseous component of the eclipsing body, at all phases of the eclipse.

A portion of the shell spectrum, extracted at different eclipse phases, is shown in Figure 10.1. All the properties of the shell lines, already detected by previous investigations, clearly appear at the first inspection of the shell spectra. One observes for example the sharpness of metallic lines, the prevalence of low-excitation features, the redward and blueward shift (depending on phase), and the deepening on egress. The dilution is evident, since the Fe I multiplet 152 is extremely weak, in particular at ingress.

However, undesired spurious effects, appearing in the extracted shell spectrum because of stellar variability, are generally present. Residual absorptions or over-compensations of stellar lines (pseudo-emissions) can appear during partial eclipse phases (because of shrinking line-profiles), or can affect the H and K lines of calcium which are intrinsically variable in the F star (Castelli, 1978).

Particularly interesting is the fact that a lot of new physical phenomena can be identified for the first time in the eclipsing body, by analyzing the extracted shell spectra. There is one striking difference between the shell spectra at mid-eclipse, and those in the partial phases: the Balmer series. It clearly dominates during the whole totality, showing broad lines with very steep profiles and no wings (width at half-depth corresponds to a velocity dispersion of $\sim$90 km/s); on the contrary at mid-ingress the Balmer series, for $n \geq 4$, is much sharper (corresponding to a velocity of $\sim$30 km/s). Also the metallic lines are slightly broader in

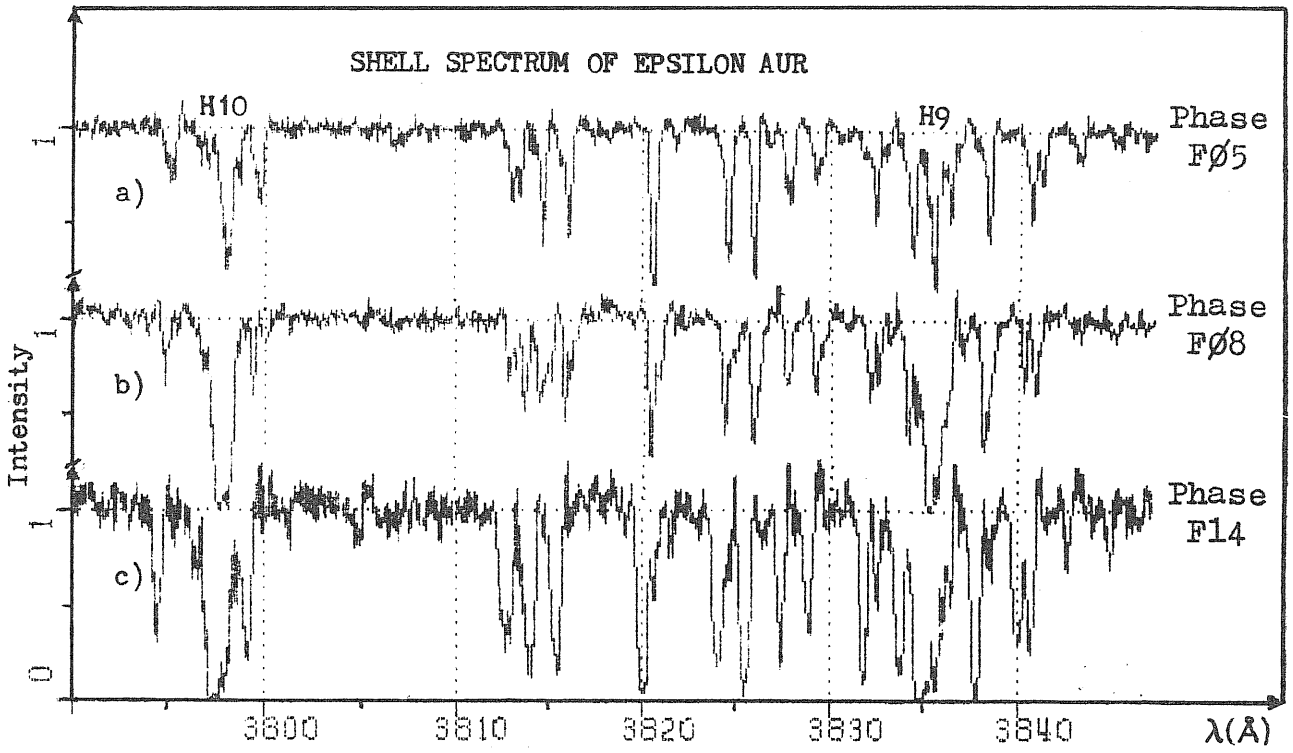

Fig. 10.1 - Extracted spectrum of the eclipsing companion of εAur:

a) Mid ingress, Sep.82
b) Mid totality, Aug.83
c) Early egress, Mar.84 .

totality, than in the partial phases. Profile variations of the shell lines during the eclipse are reported on Table 4.1.

During the various phases of the eclipse, different parts of the eclipsing body pass in front of the F star; this means that the phase-dependence of the shell spectrum provides a natural scanning of the inner parts of the eclipsing body. The interpretation of the observed behaviour of the shell spectra during totality is then clear: the internal regions of the eclipsing body show evidence of low density, high rotational velocity, and a remarkably higher temperature, that is of the order of an A-type star. This is a further evidence that the hot source, causing the far-UV excess of ε Aur, should then be located at the center of the shell.

10.2 Special Data Processing

The extraction procedure operates on logarythmic spectra (F=logI), in principle because in this way the shell spectrum is obtained simply by subtracting the stellar contribution from the eclipsed spectrum. But, as we know, this contribution is considerably variable (Fig.2.6); so that, in order to remove it properly, one has to find an out-of-eclipse spectrum which reproduces the stellar contribution at best.

This can be done, for example, by performing a weighted average of a couple of uneclipsed spectra, displaying on "extreme" degree of variation. In our sample, such a couple is (FØ1, FØ2), which shows outstanding variations specially in the Balmer lines; the weight of FØ1 in the average will be indicated by w. Moreover, sometimes the stellar spectrum does not very much selectively, but rather in the sense of general enhacement of all the metallic lines, as if their (logarythmic) intensity would be multiplied by a constant factor c. In conclusion, the stellar spectrum can be approximated

at a given phase, by the linear conbination:

$$L = w \cdot cF\emptyset 1 + (1-w) \cdot cF\emptyset 2 \quad . \qquad (10.1)$$

This method, which we may call "interpolated extraction", has provided the first complete sample of (logarythmic) shell spectra:

$$S = F - L_z \quad , \qquad (10.2)$$

where L_z indicates that L has been shifted for compensating the star's orbital (and atmospheric) radial velocity. Table 10.2 lists the adopted coefficients c and w, and the radial velocity shift for all the phases; parameters m , h and h', used to compute c and w are also listed (°).

Despite a generally good appearance of the extracted shell spectra, though in some cases it is not possible to compensate all the stellar features, so that negative residuals are left (in form of fictitious absorptions) and positive residuals appear (as fictitious emissions). Particularly disturbing is the fact that by this extraction procedure it is not possible to discriminate, in principle, between the real shell features and the artifacts of the extraction itself; thus ambiguities may arise, specially concerning the weaker lines and the shape of the profiles. Moreover, at the edge of the spectrum (λ 3600-3700 Å), standard calibration and normalization are very poor, so that the opportunity of directly measuring the Balmer discontinuity in the shell, is missed.

(°) The derivation of the coefficients c and w , for a given phase, is made by measuring the intensity of the stellar contribution, in correspondence of selected spectral features which are indicative of the general behaviour. In particular, one can measure the core of MgII λ4481 (metallic lines), the "saddle" between H23 and H24 (Balmer series), or Hδ; their logarythmic intensity is indicated by m , h and h' respectively (eventually with an index specifying the phase), and h' is used in alternative to h when the latter is not measurable. Then, for "renormalizing" the intensity of the metallic lines, it is sufficient to multiply the reference spectra FØ1 and FØ2 by $c = m/m_1$; and finally, for reproducing the Balmer series, it has to be used the weight $w = (h-h_2c)/(h_1-h_2)c$. In conclusion, introducing the numerical values, we have: $c = m/.3$; $w = (h+.16c)/.1c$.

Finally, an optimized method of shell-spectrum extraction was realized, overcoming all such problems. As a reference spectrum, it is used the average of all the out-of-eclipse spectra available (FØØ). Metallic line-depth is reproduced, by multiplying this spectrum by a suitable coefficient E. Balmer series compensation is achieved by adding, to the reference spectrum, a special correction-spectrum COR (which is nothing but FØ1-FØ2), multiplied by a factor B. Radial-velocity shift compensation Z is also considered. Final values of E, B, Z are determined by a best-fit procedure, minimizing the residuals. General statistics of the residuals, for all the out-of-eclipse spectra, was performed; this allowed to determine an error factor ($\pm\sigma$ band) associated with the extraction procedure. Thus, for each shell spectrum it is now possible to associate its uncertainity band $\pm$ R, which allows to discriminate between pure shell features, and possible spurious artifacts. Such a sophisticated extraction technique made it possible to detect the shell spectrum also on post-eclipse phase F18, that is at a distance from the secondary 's center, more than double of the radius of the eclipsing disk. Results are presented in Fig. 10.2 and Tab.10.2; details of the procedure are given on Table 10.3; values of the parameters E, F, Z (and R in units of σ), are listed on Tab. 10.2 .

In the special Supplement section, a complete Spectral Atlas of the eclipsing body is presented. Spectra SØ4, SØ8, S14, S17 provide a set of scans through the eclipsing body, at different positions covering almost the entire structure, as shown in the picture at the beginning of the Atlas. Positions of the spectra within the page, reproduce the position of the scans with respect to the eclipsing body, as shown in the initial picture. Identifications, together with the reference spectrum FØØ, are also given; wavelength range is from 3600 to 4950 Å. Shell spectra SØ8 and S14 were extracted with the interpolation procedure; whereas spectra SØ4 and S17 were obtained with the optimized best-fit extraction, providing also the corresponding error bands.

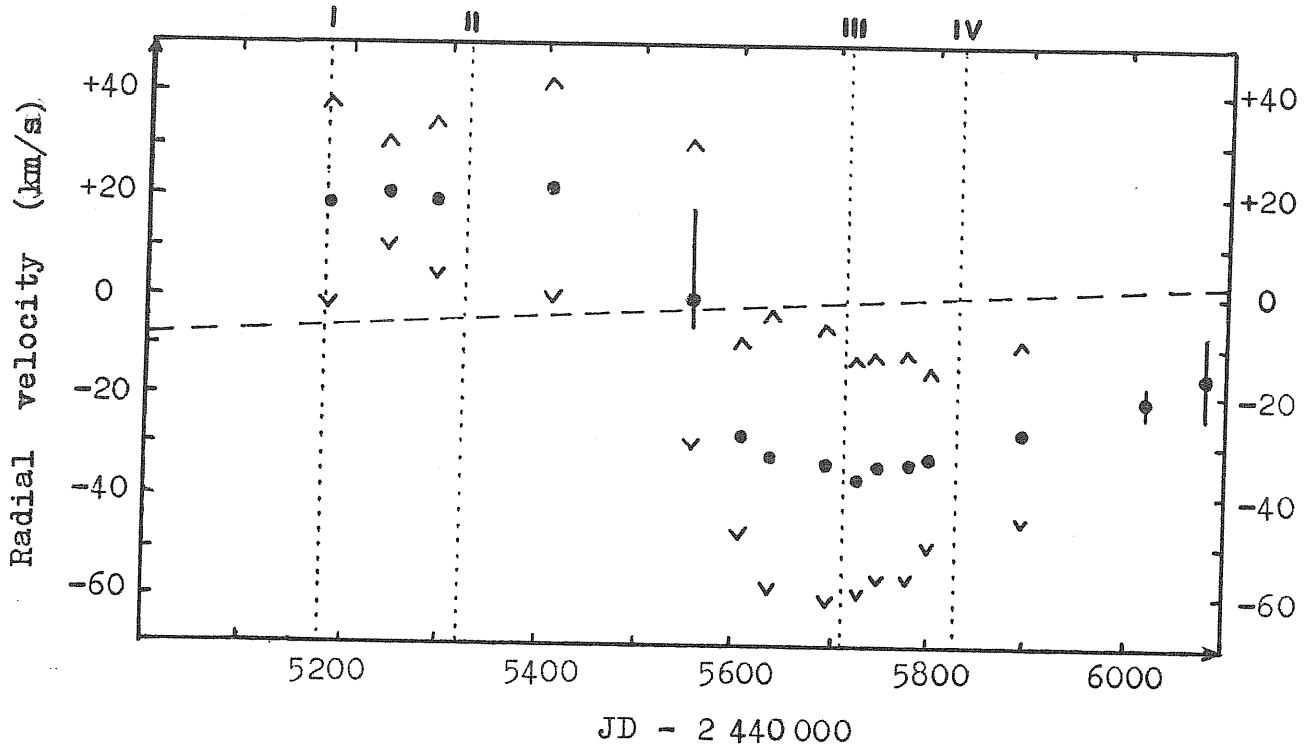

Fig. 10.2 - Rotation of the eclipsing body is better determined, from metallic lines, after shell-spectrum extraction (cf. Fig. 7.4): the velocity is slightly larger, since the blended stellar lines are removed. Moreover, the rotation of the shell can be traced as far as twice the radius of the eclipsing disk. Variations of the halfwidth of the shell line-profiles (^v) can also be evidenced.
Note that the asymmetry between ingress and egress almost disappears, if one considers, for the secondary, an orbital velocity corresponding to a mass m_2 equal to m_1 (dashed line). The small residual difference can then be explained as a simple effect due to expansion ($v_{exp} \sim 10$km/s), in a geometric configuration as shown on Figure 9.4b.
The assumption $m_2 = m_1$ is also consistent with the observed radial velocities in the shell. In fact, the shell is empty internally (~ no metallic lines on totality), and is also very extended. Hence the observed velocities do not represent the rotational motion on that part of the line-of-sight which is closer to the center, but on the contrary they are the projected velocities of the slow-rotating external regions.

Table 10.1 Profile Variations of the Shell Lines

FEATURE	INGRESS FØ5	EARLY TOTALITY FØ7	EARLY EGRESS F14
BALMER JUMP $\Delta I/I_c$	Absent ~ 0	Remarkable 0.3	Underexposed ~ 0.5
BALMER LINES Width (at P/2) Wings	Weak and sharp ±20 km/s Absent	Strong and large ±40 km/s Absent	Strong and large ±40 km/s Absent
H, K LINES Masked by FØ intrinsic variations	Apparent absorption (stellar lines deeper than in reference sp.)	Apparent emission (stellar lines less deep than in reference sp.)	Apparent absorption (stellar lines deeper than in reference sp.)
METALLIC LINES Width (at P/2) Effect of FØ profile variations	Sharp $\lesssim$±10 km/s (res.limit) fictitious blue-side emission winglet	large and weak ±30 km/s fictitious blue-side emission winglet	sharp and strong ±15 km/s fictitious red-side emission spike
MgII λ4481 Only FØ profile variations	Fictitious absorption at stellar $v_{rad.}$ FØ line sharpened	fictitious absorption at stellar $v_{rad.}$ FØ line sharpened	
FeI mult.152 observed λλ	Undetectable Only FØ contribution	Undetectable Only FØ contribution	Present in the shell λλ4236, 4260
MgI λ4702	Undetectable	Undetectable	Present in the shell
Low/High EP features	Normal behaviour	FeII(27),(38)...stronger SrII,TiII(50),(82)...weaker	Same as in ingress
Blends at resolution limit	λ3856 SiII1+FeI4 $\Delta\lambda$=0.35Å	λ4417-8 (FeII27-TiII40) $\Delta\lambda$=0.9Å	λ4400(TiII51-ScII14) $\Delta\lambda$=0.6Å

Tab. 10.2 Shell - spectrum Extraction Parameters

	Spectra				Radial Velocties			Interpolated Extraction					Best-fit Extraction				
O	no.	Epoch		Plates·scans	Orbit	Atm.	Tot.	m	h	h'	c	w	D	E	B	Z	R
	F01	Dec	70	2 x GC3	-5.2	-3.8	-9	-.30	-.06	-.42	1	1	0	.6	.1	+9	2
Out	F02	Feb	71	6 x GC3	-4.8	+0.8	-4	-.30:	-.16	-.57	1	0	0	.6	1.1	+4	2
	F03	Ian	81	6 x GC3	+11.0	+1.0	+12	-.48	-.14		1.60	.73	...	1.1	.4	-10	2
	F04	Iul	82	1 x GB	+5.3	-1.3	+4	-.44	-.11		1.47	.85	.3	.8	.6	+8	2
Ing	F05	Sep	82	5 x GC2	+4.7	-2.7	+2	-.48	-.11		1.60	.91(1.0)			NE		
	F06	Nov	82	3 x GC3	+4.2	-7.2	-3	-.48	-.17		1.60	.54			"		
	F07	Mar	83	2 x GB+2 x GC3	+3.0	0.0	+3	-.42		-.49	1.40	1.47			"		
	F08	Aug	83	2 x GB	+1.6	+4.4	+6	-.35	-.06		1.17	1.09(.9)			"		
Tot	F09	Sep	83	1 x GB	+1.1	-4.1	-3	-.47	-.10		1.57	.96			"		
	F10	Oct	83	1 x GB	+0.9	+3.1	+4(0)	-.43		-.88	1.43	-.30			"		
	F11	Dec	83	4 x GB	+0.3	+3.7	+4	-.43	-.11		1.43	.83(1.3)			"		
	F12	Ian	84	2 x GB+1 x GC3	0.0	+4.0	+4(2)	-.26	-.13		.87	.11			"		
	F13	Feb	84	1 x X3	-0.2	+3.2	+3	-.22		-.40	.73	.15			"		
Egr	F14	Mar	84	1 x GB	-0.5	-1.5	-2	-.35	-.08		1.17	.92(1.0)			"		
	F15	Mar	84	1 x GC3	-0.7	-4.3	-5	-.47	-.14		1.57	.71(1.1)			"		
	F16	Iul	84	1 x GB	-1.3	-4.7	-6	-.44		-.99	1.47	-.69			"		
	F17	Nov	84	3 x GB+2 x GC3	-3.0	-5.0	-8	-.48	-.10		1.60	.98	.2	1.0	.2	-6	2
Post	F18	Ian	85	1 x GC3	-3.7	-2.3	-6	-.59		-.85	1.97	.92	0	1.3	0	-6	3
	F19	Ian	87	2 x GC3	...	...	-16	-.64	-.09		2.13	1.18	1.0	1.3	-.1	+15	3
Out	F20	Apr	87	1 x GC3	...	...	-19	-.66	-.15		2.20	.92	...	1.3	0	+19	2
	F21	May	87	1 x GB	...	...	-14	...	...		...	...	0	1.1	.4	+14	2

Notes. NE: Not Extracted (work in progress)
(parentesis): values giving better results

Table 10.3 Best-fit Extraction Sequence

Step	Operation	Param.
1	Standard Elspec processing (SCN)	
2	Phase-average & Plot	
3	Zero reset (if needed)	
4	Cosmetics (if needed)	
5	Edge-distorsion rectification	D
6	Metallic line fitting	E
7	Balmer series correction	B
8	Velocity compensation	Z
9	Residuals' amplitude check	R
10	Best-fit iterative procedure (6 ÷ 9)	
11	Error band factor (1±R)	
12	Final overplot	

1÷4 ... Preliminary phase

5÷9 ... Extraction phase

10÷12 ... Optimization phase

A P P E N D I X E S

A. - NEAR-INFRARED MICHELSON INTERFEROMETRY

By combining spectroscopic (§ 2.6) and astrometric (§2.1) measurements of the visible component of ε Aur, its angular diameter is expected to be about 4 m". Hence one could attempt to resolve directly its disk, by using the largest available optical interferometer: the 70m-baseline two-telescope Michelson interferometer "I2T", located at the CERGA Observatory in France (Blazit et al., 1977; Ap.J.217,L55). Also the other ζ Aur-type supergiants present very similar angual diameters and apparent luminosities, just at the limit of the instrumental capabilities of the I2T interferometer, equipped with the IR beam recombination table (Di Benedetto & Conti, 1983; Ap.J. 268, 309). In order to observe these objects, a remarkable observational effort has been substained on 1984-85, in collaboration with G.P. Di Benedetto and the French equipe, pioneering the limit of current-generation optical interferometry.

A.1 A puzzling Observation of Epsilon Aurigae

Measuring directly the effective angular diameter of ε Aur on eclipse, would have been of capital importance, since it could provide an experimental determination of the nature of the eclipsing body. In fact the instrumental response is predicted to be different, if the source has the shape of a normal disk, or of a disk splitted in two parts; that is if the eclipsing body acts as a semitransparent veil, or as a dark bar respectively (Fig. A.1).

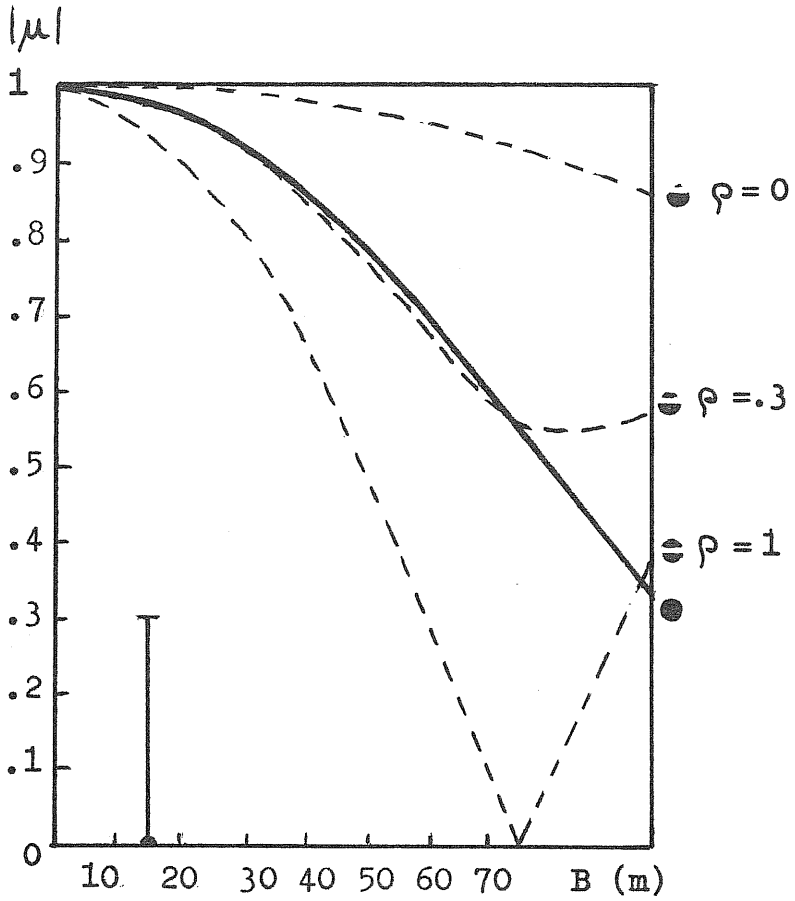

Fig. A.1 - The visibility function, computed for different possible configurations of ε Aur on eclipse. The angular diameter of the disk is supposed to be ϕ=4m". Solid line: increasing the baselength B, one starts getting a lower fringe contrast $|\mu|$, because of partial resolution of the source (μ=0 is reached for ϕ=1.22 λ/B). Dashed lines: predicted behaviour in case of a splitted disk, for different luminosity ratios ρ between the two parts.
Observations consist of measuring the contrast $|\mu|$ at different baselengths B, in order to find the curve on which the experimental points are distributed. Our experimental result is puzzling, since an upper limit $|\mu| \leq 0.3$ at B=16m was obtained from one single measurement, in total disagreement with the expectations. If reliable, it would imply an angular diameter $\phi \gtrsim 25$m".

Unfortunately, after overcoming severe instrumental problems, due to the low luminosity of the source, an ambiguous response was obtained from observation, performed at 2.2 μm with 16 m baseline, on 15.2.84 (near 3rd contact): no interferometric signal was detected. Statistics of such kind of results, based on previous observations of different sources with I2T, give no more than 80% confidence that this result is reliable.

However, if taken seriously, it would mean that the source is $\gtrsim$ 25 m" in diameter, maybe because of an extended envelope (scattering IR radiation at 2.2 μm). More prudently, one should not take in consideration such result, attributing our negative detection of the interferometric signal, to the low luminosity of the source combined with non-optimum seeing conditions.

After this puzzling result, no more attempts were made for observing ε Aur interferometrically, in consideration of the extreme technical difficulties of measuring this source, by forcing the sensitivity limits of the instrument.

A.2 An extension to ζ Aur-type stars

Much more encouraging, since the beginning, have been the measurements of the other ζ Aur-type supergiants: 31 and 32 Cyg, and ζ Aur itself (paper IX). The interest of measuring directly the angular diameters of these stars is considerable, since they are the only double-lined spectrophotometric binaries containing a supergiant, and thus providing its absolute parameters (the companion is a hot dwarf). Moreover, there are still strong discrepancies between the determinations of the

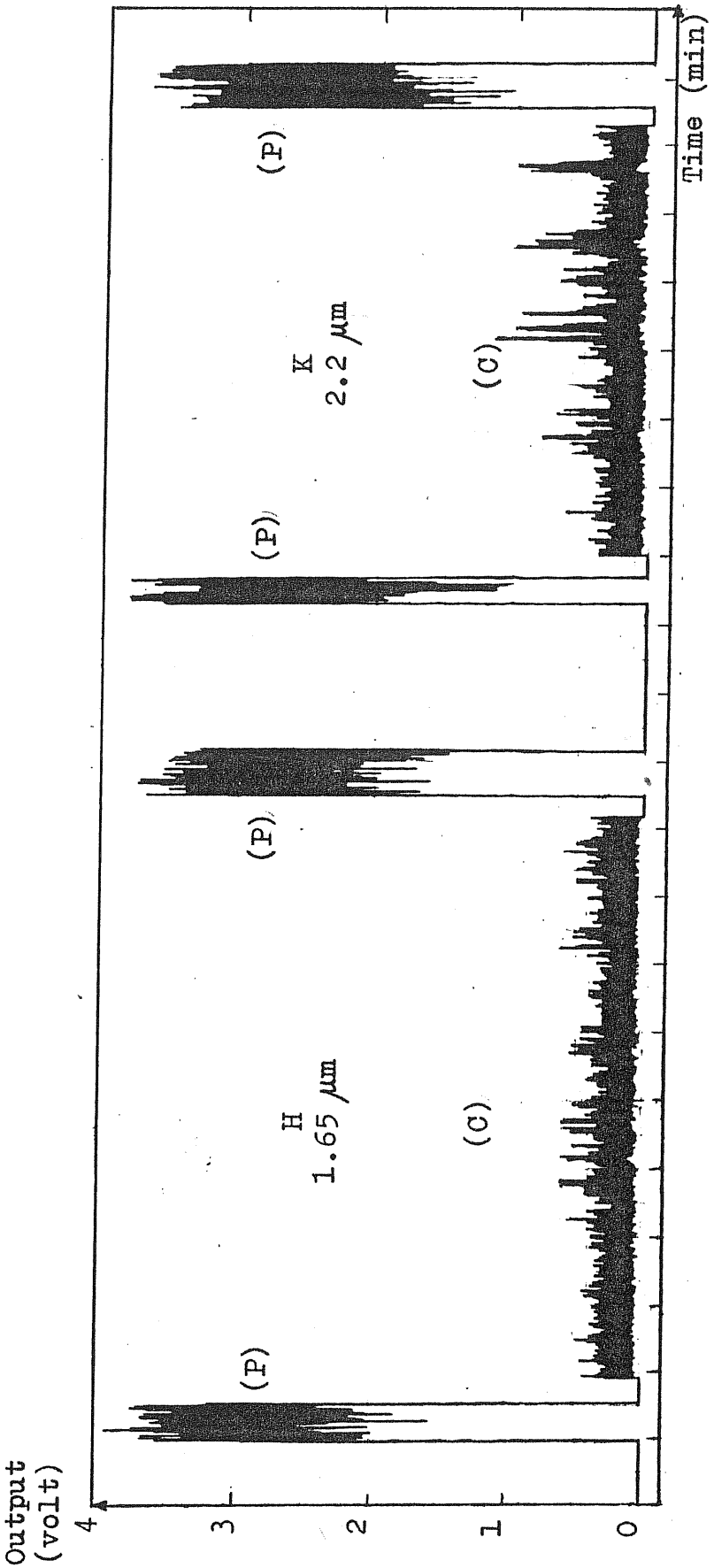

Fig. A.2 — Total photometric energy (P) and coherent energy (C), recorded from 32 Cyg with 50m baselength, on 11/10/85. The spikes in (C) show the fringe signal detected in a scan of the coherence region (FWMH~10 μm): the signal is lower in H than in K, while the mean photom. energy is almost the same in the two cases. This indicates that the source is clearly resolved in H, the point-source transfert function being about the same for H and K.

supergiant's diameter obtained with different indirect methods.

In the infrared, the contribution of the hot dwarf is almost negligible, and so one observes the interferometric effects depending on the supergiant's finite angular size. The fringe visibility in the H and K atmospheric windows was measured with different baseline lengths, up to 55 m. Already from rough data, it appears that $\mathcal{J}$ Aur, 31 Cyg and 32 Cyg are all clearly resolved at 1.65 μm with the longest baselines (an example is given in Fig. A.2). This means that such measurements can provide angular diameters of these supergiants, with well established reliability (G.P. Di Benedetto, 1985; A.Ap.148,169).

Repeated measurements at different wavelengths and baselines were performed, in order to emprove the accuracy of the determinations. Finally, after performing the analysis of the data, it was obtained the set of results, listed on Table A.1. Clearly, the measured angular diameters ϕ_{obs} are systematically larger by about 2σ, with respect to the predicted ones ϕ_{pred} obtained from indirect estimations in the literature (Schröder, 1985; A.Ap.147,103). The reasons - and the implications - of this underestimation of the angular diameters in the literature, are still under study (Di Benedetto and Ferluga, in preparation).

Table A.1 - Angular Diameters

Star	ε Aur	$\mathcal{J}$ Aur	31 Cyg	32 Cyg
ϕ_{pred}(m")	4.4	4.8	4.5	4.4
ϕ_{obs}(m")	($\gtrsim$ 25 ?)	5.4$\pm$.4	5.5$\pm$.6	5.3$\pm$.5

B. - PROPOSED SPACE-BORN OBSERVATIONS

A few short-exposure observations with the Space Telescope should finally give a clear answer to the main still unresolved problems concerning the peculiar binary ϵ Aur, in particular about the nature of the eclipsing body and of the variable far-UV source. In occasion of the quadrature phase occurring in the years 1990-'92, when the difference in radial velocity, and the angular separation, between the components will be at maximum, a set of observations with the HRS and the FOC can be suggested.

A proposal for using the HRS has been already sent to the STScI, by M.Hack together with the writer and other collaborators, and we shall not discuss it here in detail. Simply, the idea is to observe the line spectrum of the hot source (too faint for IUE) at time intervals of 1-2 years, in order to measure its radial velocity curve, and to test if it is consistent with that of the secondary; then, also its mass could be directly determined.

In the next section, we shall consider another opportunity: that of employing the FOC, both in the imaging and objective-prism modes. Finally (§ B.2), we shall examine the possibility of using the projected EXPLORER satellite, for extreme-UV and far-UV monitoring. A schedule of future eclipses to be observed is also given (from now to year 2000), for all the ζ Aur-type systems, including ϵ Aur.

B.1 Faint Object Camera

Taking advantage form the exceptionally high angular resolution available with the FOC, the single components of the ε Aur system should be directly observable , by obtaining a set of high-resolution images, with the shortest exposure time possible on FOC (read-out time) and with the following instrumental configuration:

- Optical relay: f/96
- Imaging mode: f/288 apodizer (2)
- Attenuator: 8 mag (+ narrow-band filters, or Prism)
- Format: 64 x 64 pixels. (3)

It will be necessary to work at the limits of the resolution power of the ST; in fact the pixel size of 7.5 m", combined with the expected diffraction-limited resolution $1.22\lambda/D = 15$m" (at 1500 Å), should be just sufficient (4) to resolve the two components of the system, when (in the phase of quadrature) their angular separation (5) will be of about 45 m". In particular, the following images sould be taken.

a) Set of monochromatic images with narrow-band filters

Prioritary bands: (i) $\lambda \sim 1250$ Å, isolating the UV source (6)

(ii) $\lambda \sim 1500$ Å, showing both the UV source and the primary (7)

NOTES:

(2) giving highest available angular resolution

(3) allowing brightest observable m_v (=6 with attenuator and no filters; Macchetto et al. 1984)

(4) Taking into account also 7 m" pointing accuracy, possible optical aberrations, etc...

(5) expected, from measurements by van de Kamp (1978; AJ 83,975).

(6) and showing whether it is really coincident with the position of the secondary (or with that of the primary, as suggested by Parhasarathy and Lambert in 1983; PASP 95,1012).

(7) At short λ ,eventually,less dense attenuators can be used.

(iii) λ 2000÷3000Å, isolating the FØ Ia primary;

(iv) filters for: Mg IIλ2800; OI λ1304 (lines with circumstellar emission) + polarizers 0°, 60°, 120°.

Expected results. - At least: Test of the existence of the hot secondary, by measuring a displacement of the centers of the images in the cases (i) and (iii). Angular separation between the components.

- At best: Accurate (1%) photometry of the single components in the far UV. Test for extended shell around the components, by comparing images (iv) with (i), (ii), (iii).

b) One single image with the <u>far-UV objective prism</u>

- Dispersion: $\lambda/\Delta\lambda = 50$, perpendicular to the line connecting the components.
- Range: $\sim$ 1250÷3000 Å (covering the spectra of both components).
- Length of the spectrum: $\sim$50 pixels (contained in the 64 x 64 format).
- Read-out: in time-resolution mode, since the shortest allowed pose is required for the λ 2000÷3000Å region, while integration is neeeded to reveal the far-UV part of the spectrum.

Expected results. - At least: measurement of the variable UV excess of the system, if no separation of the two spectra is possible (for physical or instrumental reasons).

- At best: Separation and direct analysis of the spectrum of the hot secondary.

c) Set of coronographic images with interference and narrow-band filters

-New f/96 configuration,with:

- coronographic mask inserted
- f/288 apodizer removed
- Attenuator removed
- Format 512 x 512.

-Filters, isolating circumstellar emission:

H_α ; Mg II λ 2800 ; OI λ 1304 + polarizers: 0°,60°,120°.

-Coronographic "fingers", occulting the stellar components:

0".4 finger : short pose (inner envelope),
0".8 finger : longer pose (outer envelope).

Expected results. - At least (no detection): upper limit, for the extension of the circumstellar envelope.
- At best: structure of the circumstellar medium, around the system of ε Aur.

B.2 Monitoring the ζ Aur/ VV Cep Systems

The astronomical interest of the ζ Aur/ VV Cep systems (in particular ζ Aur, 31 Cyg, 32 Cyg, VV Cep and ε Aur) is well known, since they are the only case of spectrophotometric binaries involving late supergiant components, and hence providing absolute parmeters for these stars. The companion is generally a hot dwarf, moving at the edge of the primary's extended envelope, and sometimes affected by morphological peculiarities, such as a frontal shock-bow in ζ Aur, (Chapman, 1981; ApJ.248,1043), or a surrounding dark disk in ε Aur (Ferluga, Hack, 1985; A.A.144,395). When the secondary is eclipsed by the supergiant, it gradually disappears behind the limb, allowing to study the primary's turbulent atmosphere; by this mean a large prominence has been detected in 32 Cyg (Schröder, 1983; A.A.124,L16).

Clearly, the optimum spectral range to observe the hot secondary is the UV, and so far the most reliable determinations of the systems' elements are based on IUE observations (Schröder, 1985; A.A.147,103); however remarkable uncertainities remain, concerning in particular the radii of the components. Angular diameters of the supergiants, measured in the IR by long-base Michelson interferometry (Di Benedetto, Ferluga, 1986; Highlights in Astr. 7,in press) suggest that absolute luminosities of the components might have been so far mis-extimated, so that the secondary could be generally an underluminous object. Monitoring the ζ Aur/VV Cep binaries in the UV,during the future eclipses, will allow to determine the proper nature of the dwarf secondary, the complex structure of the supergiant's atmosphere, and finally more precise absolute elements for the systems.

The problem of the secondary's real nature is particularly interesting in ε Aur, since it eclipses the primary supergiant behind its own extended surrounding disk; moreover, it displies a large far-UV variability (Boehm,Ferluga,Hack, 1984; A.A.130, 419), and it is so strongly underluminous that it could be a close binary instead of a single star (Lissauer,Backman, 1984; Ap.J.286,L39). Single obdervations with the Space Telescope at high resolution - both spectral and spatial - are already scheduled (GTO's) and/or proposed,for the ζ Aur / VV Cep systems. Monitoring the eclipse phases with the Explorer (short exposures will be sufficient since these objects are enough bright) will ensure a continuous time-coverage (e.g. with daily observations), and will then provide the ideal implementation for the ST research programs. A list of the future eclipses, to be observed in the next decade, is given in the following table (in parenthesis the suggested monitoring time for best coverage of eclipse).

ζ Aur	31 Cyg	32 Cyg	VV Cep	ε Aur B
Mideclipse	Midecl.	Midecl.	Midecl.	Ingress
5. 8.90	21.2.93	6. 9.90	18.1.98	~1999
3. 4.93		27.10.93		
1.12.95	(10 months)	18.12.96	(20 months)	(2 years)
3. 7.98				
		(6 months)		
(4 months)				

Supplement

S P E C T R A L A T L A S

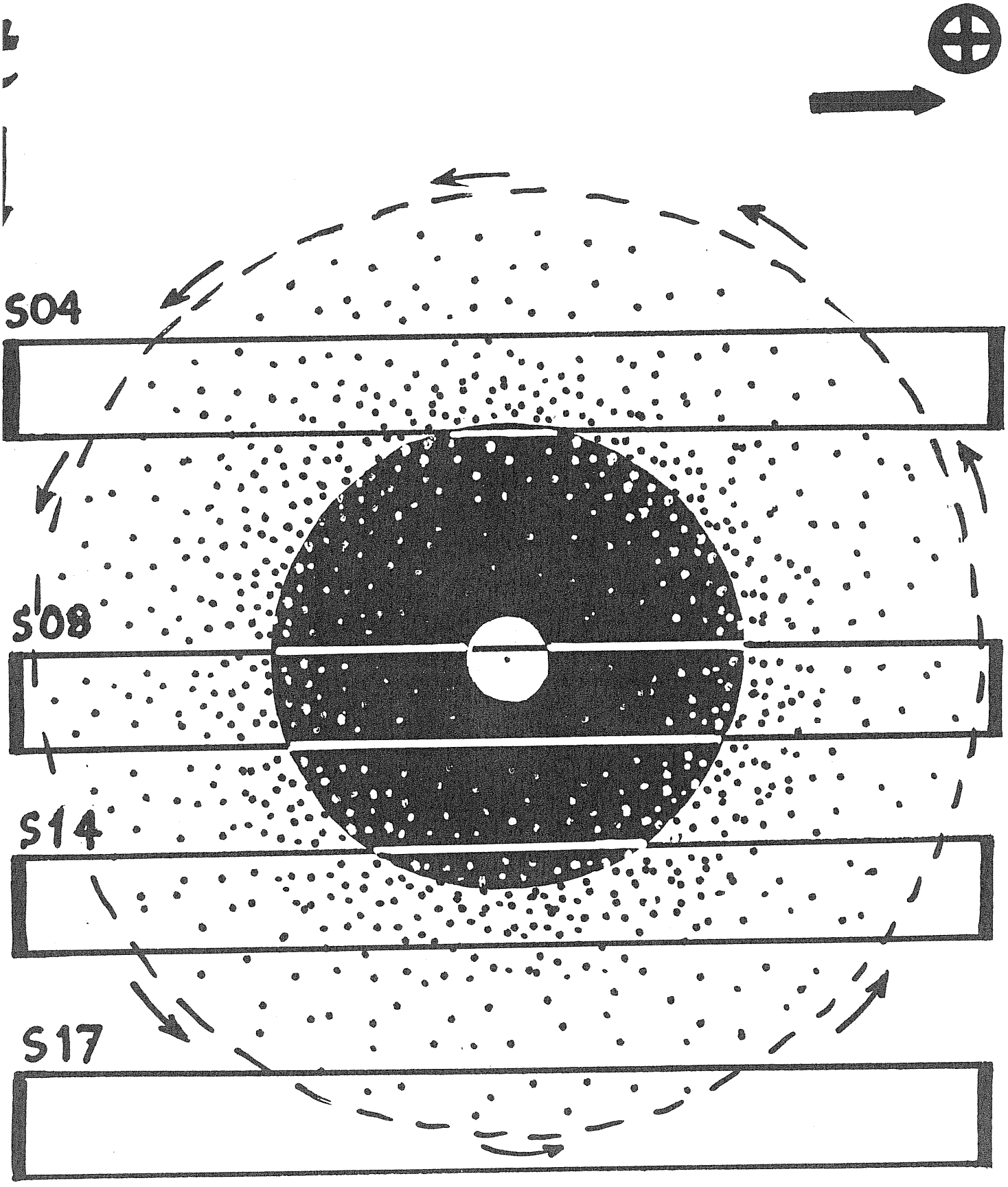
S04
S08
S14
S17

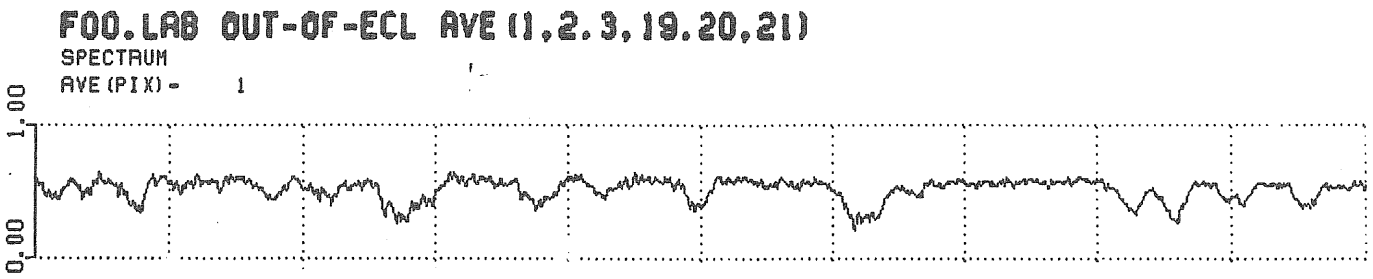
F00.LAB OUT-OF-ECL AVE(1,2,3,19,20,21)
SPECTRUM
AVE(PIX)- 1
1.00
0.00

EXPOSURE

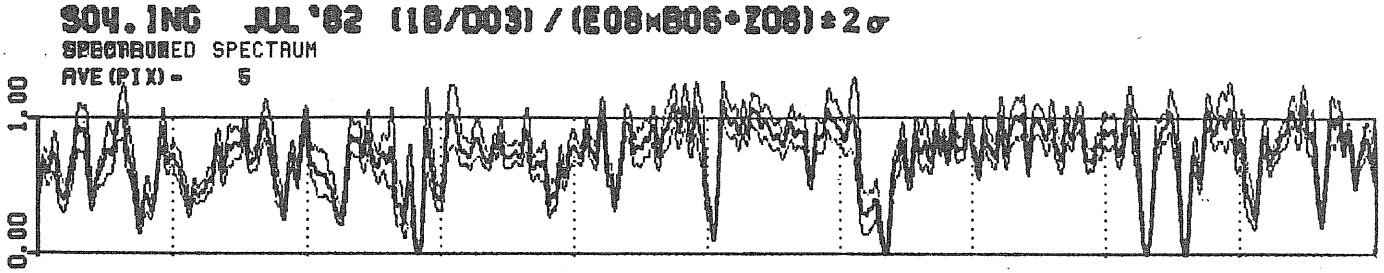
S04.ING JUL'82 (1B/D03)/(E08×B06•Z06)±2σ
SPECTRUM
AVE(PIX)- 5
1.00
0.00

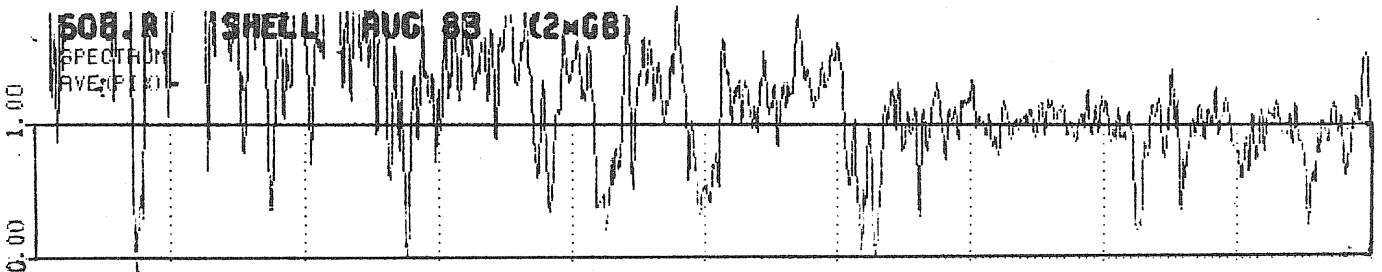
S08.A SHELL AUG 83 (2×GB)
SPECTRUM
AVE(PIX)-
1.00
0.00

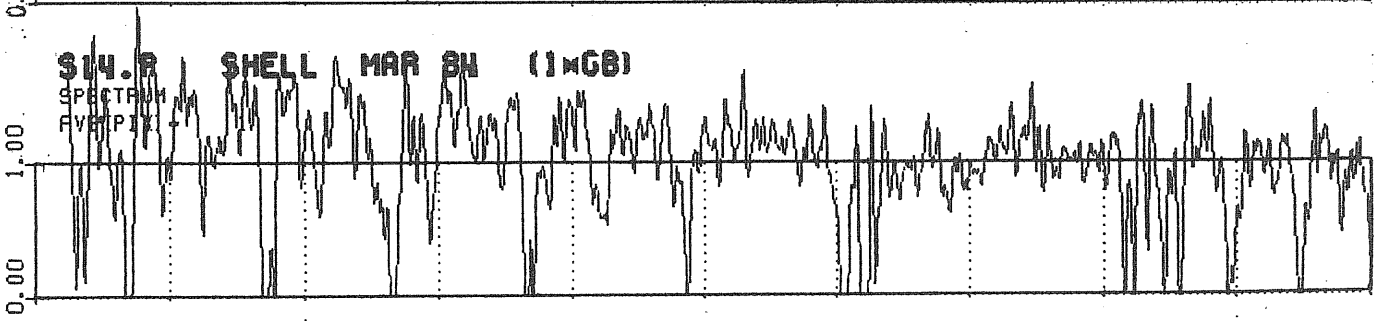
S14.A SHELL MAR 84 (1×GB)
SPECTRUM
AVE(PIX)-
1.00
0.00

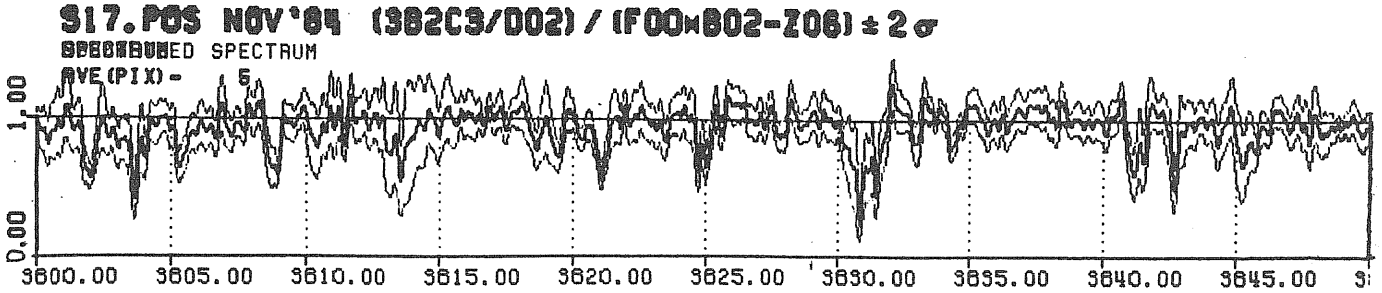
S17.POS NOV'84 (3B2C9/D02)/(F00×B02-Z06)±2σ
SPECTRUM
AVE(PIX)- 5
1.00
0.00
3600.00
3605.00
3610.00
3615.00
3620.00
3625.00
3630.00
3635.00
3640.00
3645.00

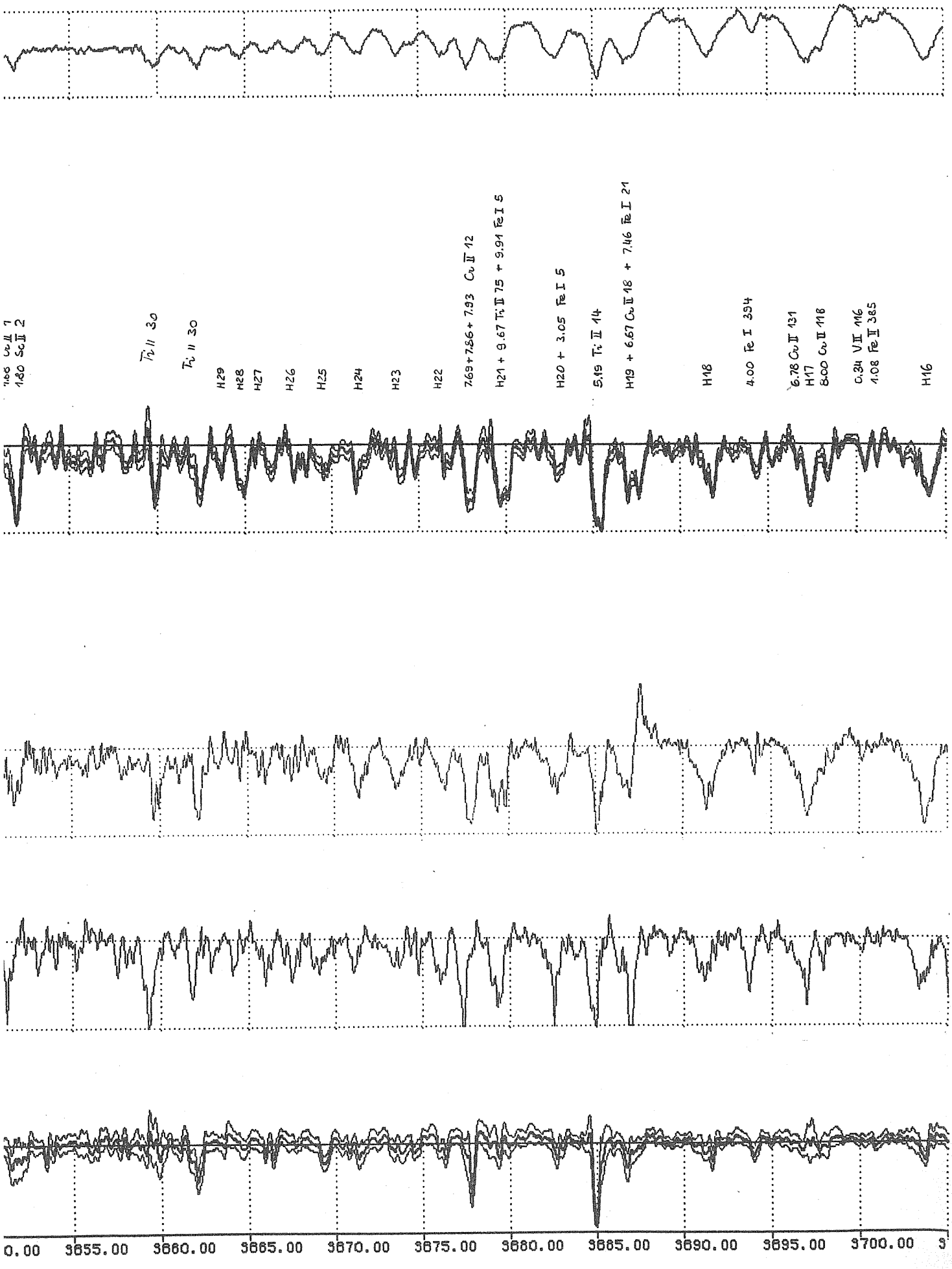
1.85 Cr II 7
1.80 Sc II 2
Ti II 30
Ti II 30
H29
H28
H27
H26
H25
H24
H23
H22
7.69+7.86+7.93 Cr II 12
H21 + 9.67 Ti II 75 + 9.91 Fe I 5
H20 + 3.05 Fe I 5
5.19 Ti II 14
H19 + 6.67 Cr II 18 + 7.46 Fe I 21
H18
4.00 Fe I 354
6.78 Cr II 131
H17
8.00 Cr II 118
0.34 V II 116
1.08 Fe II 385
H16
0.00
3855.00
3860.00
3865.00
3870.00
3875.00
3880.00
3885.00
3890.00
3895.00
3700.00

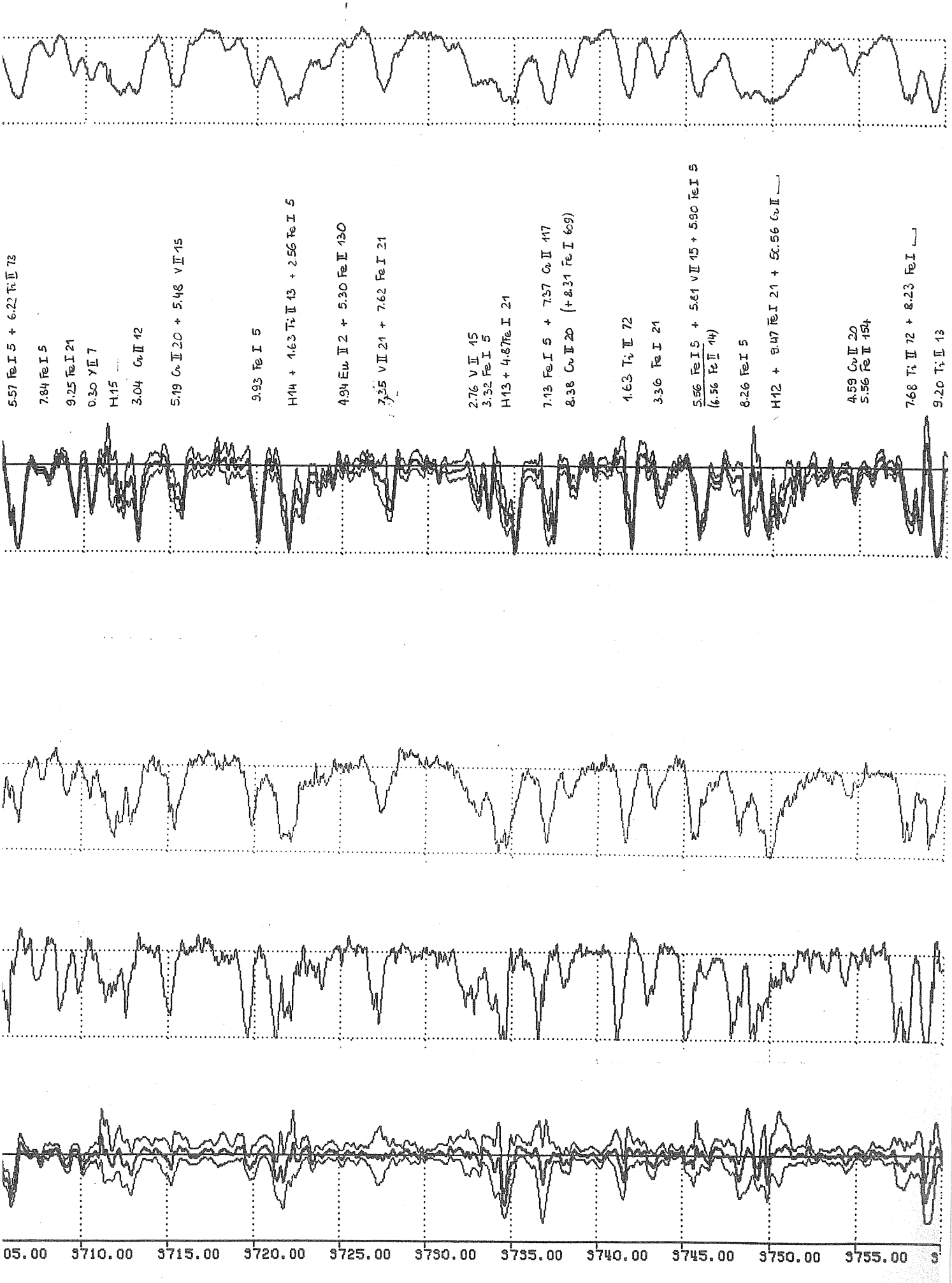
5.57 Fe I 5 + 6.22 Ti II 73
7.84 Fe I 5
9.25 Fe I 21
0.30 Y II 7
H 15
3.04 Ca II 12
5.19 Ca II 20 + 5.48 V II 15
9.93 Fe I 5
H 14 + 1.63 Ti II 13 + 2.56 Fe I 5
4.94 Eu II 2 + 5.30 Fe II 130
7.35 V II 21 + 7.62 Fe I 21
2.76 V II 15
3.32 Fe I 5
H 13 + 4.87 Fe I 21
7.13 Fe I 5 + 7.37 Ca II 117
8.38 Ca II 20 (+8.31 Fe I 609)
1.63 Ti II 72
3.36 Fe I 21
5.56 Fe I 5 + 5.61 V II 15 + 5.90 Fe I 5
(6.56 Fe II 14)
8.26 Fe I 5
H 12 + 8.47 Fe I 21 + 50.56 Ca II
4.59 Ca II 20
5.56 Fe II 154
7.68 Ti II 72 + 8.23 Fe I
9.20 Ti II 13
05.00
3710.00
3715.00
3720.00
3725.00
3730.00
3735.00
3740.00
3745.00
3750.00
3755.00

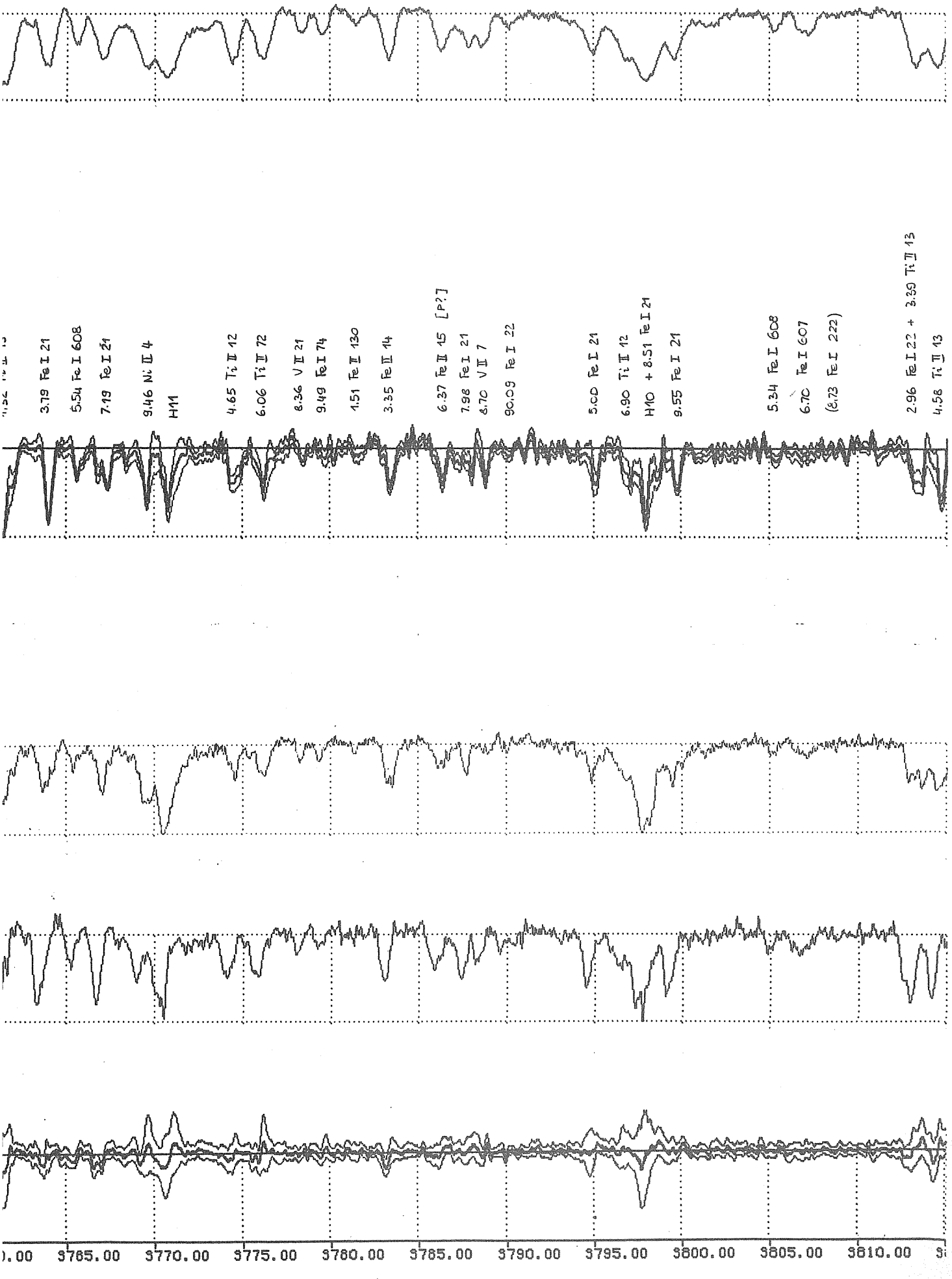
3.19 Fe I 21
5.54 Fe I 608
7.19 Fe I 21
9.46 Ni II 4
H11
4.65 Ti II 12
6.06 Ti II 72
8.36 V II 21
9.49 Fe I 74
1.51 Fe II 130
3.35 Fe II 14
6.37 Fe II 15 [P?]
7.98 Fe I 21
8.70 V II 7
90.09 Fe I 22
5.00 Fe I 21
6.90 Ti II 12
H10 + 8.51 Fe I 21
9.55 Fe I 21
5.34 Fe I 608
6.70 Fe I 607
(8.73 Fe I 222)
2.96 Fe I 22 + 3.39 Ti II 13
4.58 Ti II 13
3765.00
3770.00
3775.00
3780.00
3785.00
3790.00
3795.00
3800.00
3805.00
3810.00

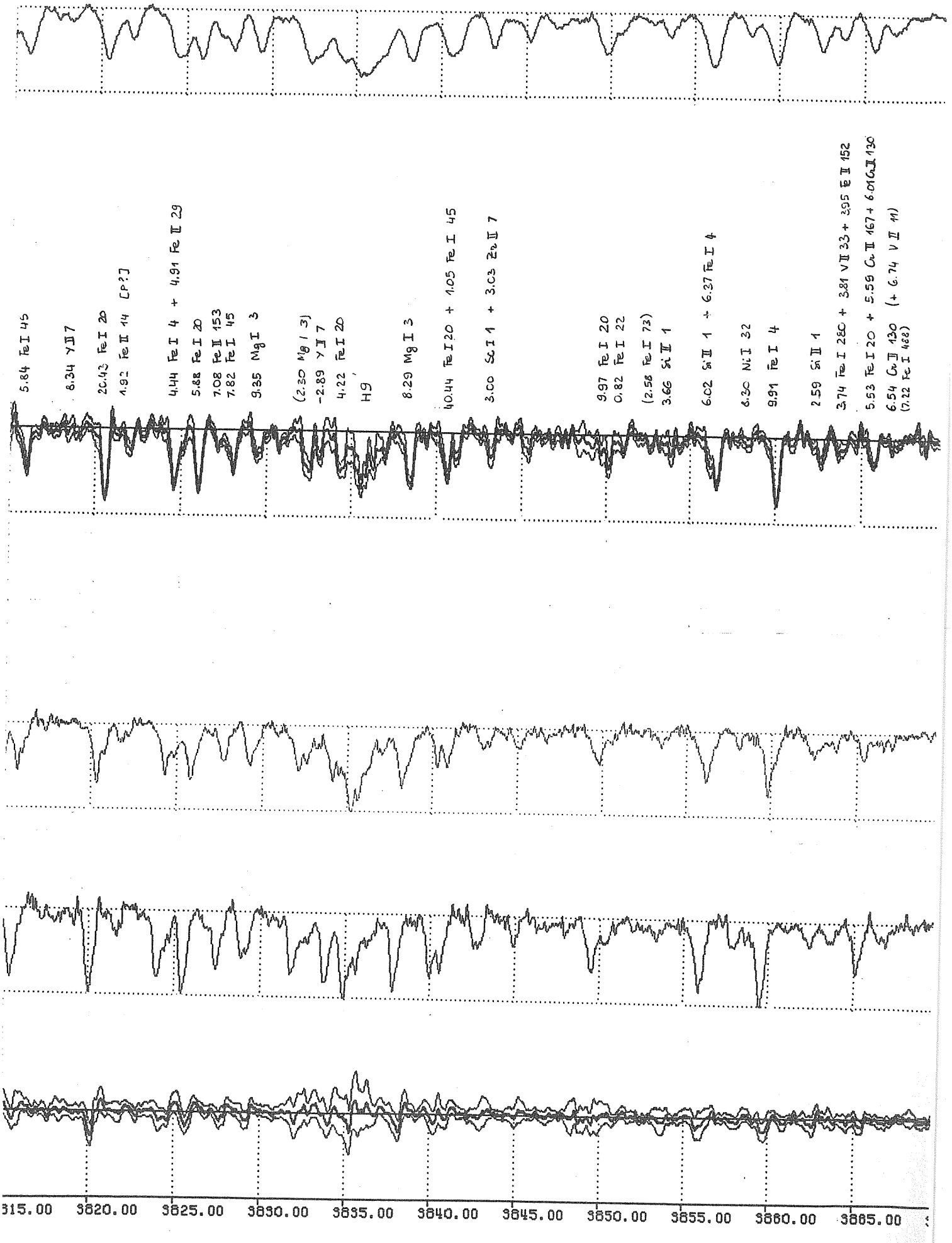
5.84 Fe I 45
8.34 Y II 7
20.43 Fe I 20
1.92 Fe II 14 CP?]
4.44 Fe I 4 + 4.91 Fe II 29
5.88 Fe I 20
7.08 Fe II 153
7.82 Fe I 45
9.35 Mg I 3
(2.30 Mg I 3]
-2.89 Y I 7
4.22 Fe I 20
Hγ
8.29 Mg I 3
10.44 Fe I 20 + 1.05 Fe I 45
3.00 Sc I 1 + 3.03 Zr II 7
9.97 Fe I 20
0.82 Fe I 22
(2.58 Fe I 73)
3.66 Si II 1
6.02 Si II 1 + 6.37 Fe I 4
8.30 Ni I 32
9.91 Fe I 4
2.59 Si II 1
3.74 Fe I 280 + 3.81 V II 33 + 3.95 Fe II 152
5.53 Fe I 20 + 5.59 Cr II 167 + 6.01 Cr I 130
6.54 Cr II 130 (+ 6.74 V II 11)
(7.22 Fe I 488)
3815.00
3820.00
3825.00
3830.00
3835.00
3840.00
3845.00
3850.00
3855.00
3860.00
3865.00

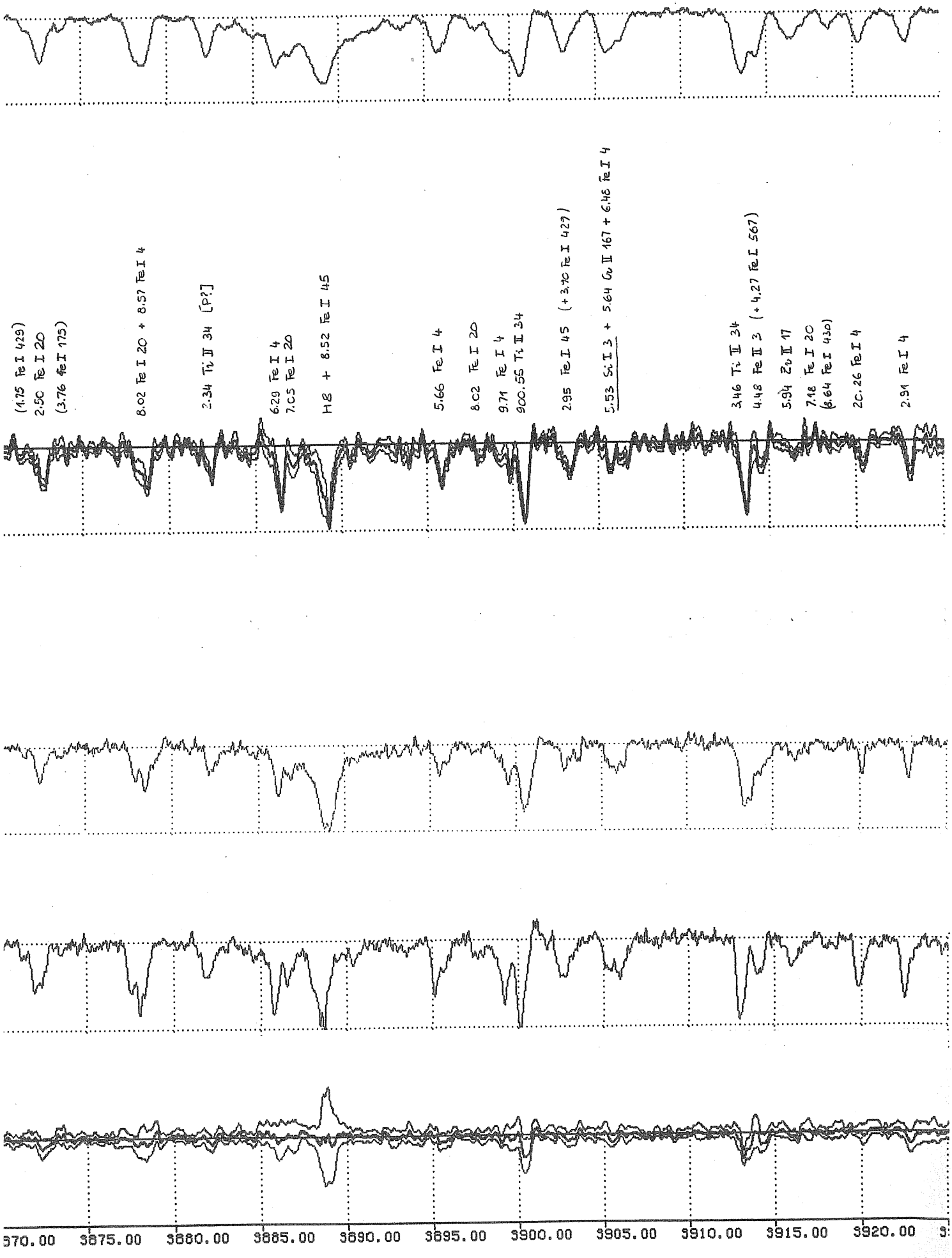
(1.15 Fe I 429)
2.50 Fe I 20
(3.76 Fe I 175)
8.02 Fe I 20 + 8.57 Fe I 4
2.34 Ti II 34 [P?]
6.29 Fe I 4
7.05 Fe I 20
H8 + 8.52 Fe I 45
5.66 Fe I 4
8.02 Fe I 20
9.71 Fe I 4
900.55 Ti II 34
2.95 Fe I 45 (+3.70 Fe I 427)
5.53 Si I 3 + 5.64 Co II 167 + 6.46 Fe I 4
3.46 Ti II 34
4.48 Fe II 2 (+4.27 Fe I 567)
5.94 Zr II 17
7.18 Fe I 20
(8.64 Fe I 430)
20.26 Fe I 4
2.91 Fe I 4
3870.00
3875.00
3880.00
3885.00
3890.00
3895.00
3900.00
3905.00
3910.00
3915.00
3920.00

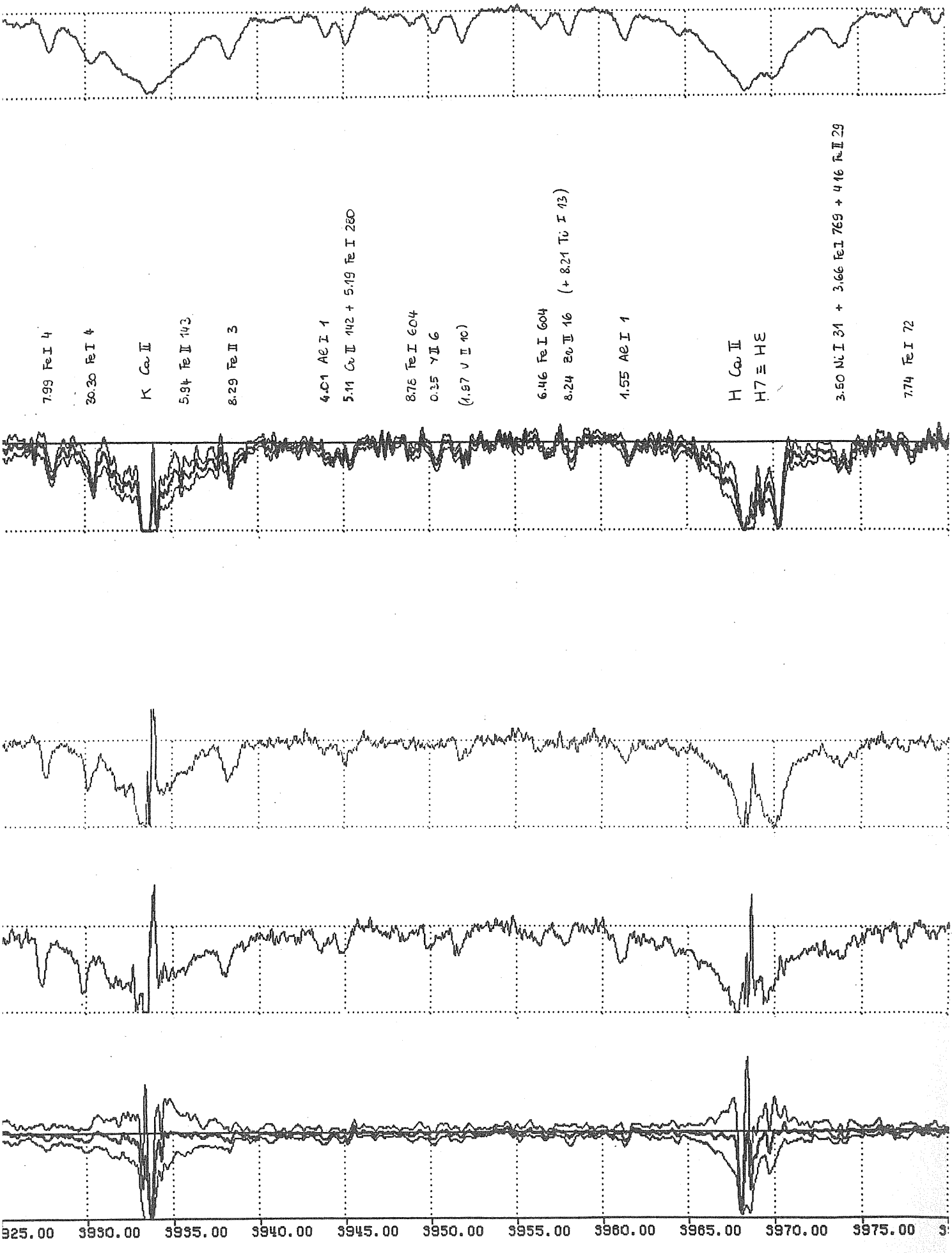
7.99 Fe I 4
30.30 Fe I 4
K Ca II
5.94 Fe II 143
8.29 Fe II 3
4.01 Ae I 1
5.11 Ca II 142 + 5.19 Fe I 280
8.76 Fe I 604
0.35 Y II 6
(1.97 V II 10)
6.46 Fe I 604
8.24 Zr II 16 (+ 8.21 Ti I 13)
1.55 Ae I 1
H Ca II
H7 ≡ Hε
3.50 Ni I 31 + 3.66 Fe I 769 + 4.16 Fe II 29
7.74 Fe I 72
3925.00
3930.00
3935.00
3940.00
3945.00
3950.00
3955.00
3960.00
3965.00
3970.00
3975.00

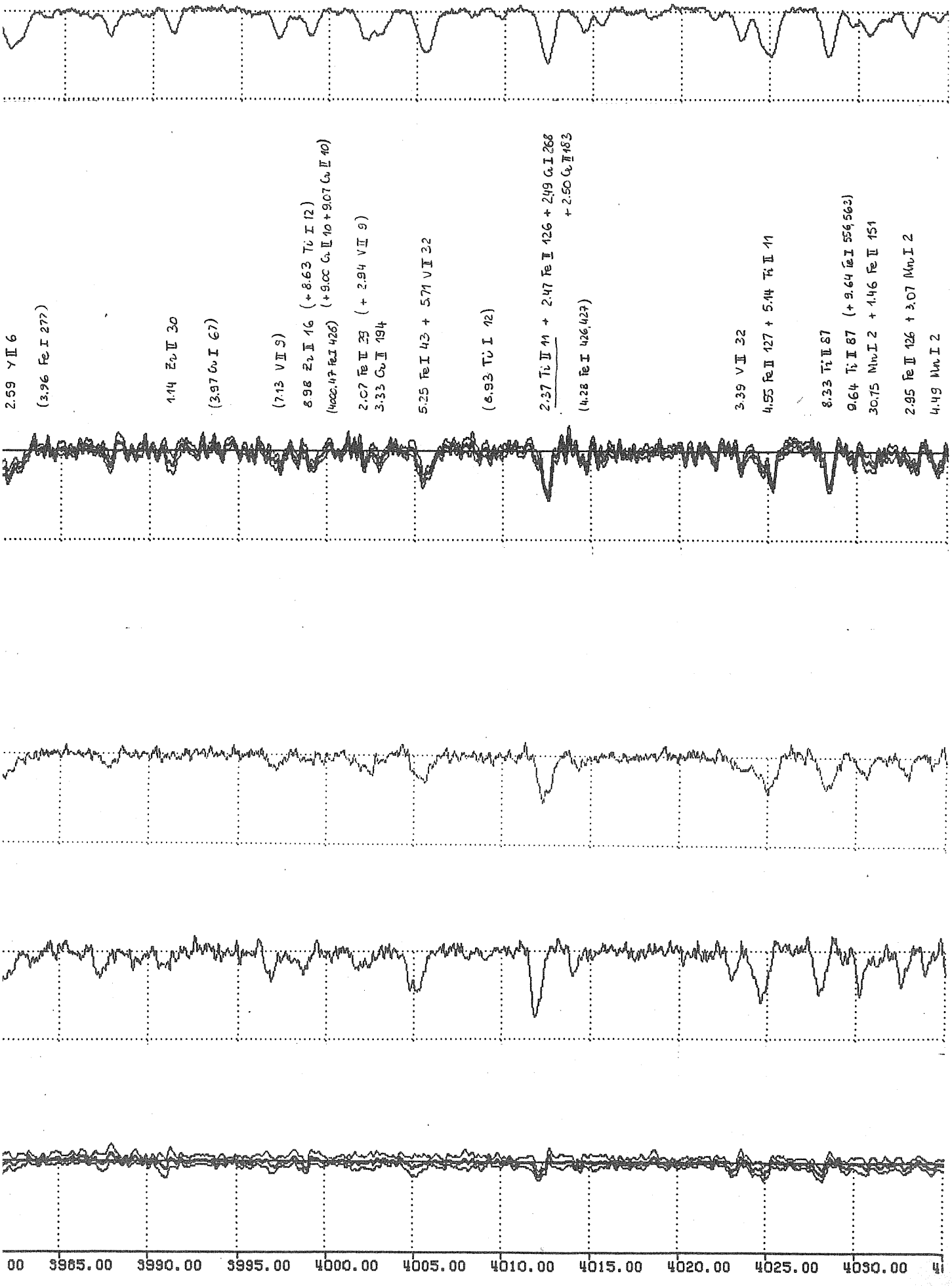
2.59 Y II 6
(3.96 Fe I 277)
1.14 Zr II 30
(3.97 Cu I 67)
(7.13 V II 9)
8.98 Zr II 16 (+8.63 Ti I 12)
(4002.47 Fe I 426) (+9.00 Cu II 10 +9.07 Cu II 10)
2.07 Fe II 29 (+2.94 V II 9)
3.33 Cu II 194
5.25 Fe I 43 + 5.71 V I 32
(8.93 Ti I 12)
2.37 Ti II 11 + 2.47 Fe II 126 + 2.49 Cu I 268 + 2.50 Cu II 163
(4.28 Fe I 426,427)
3.39 V II 32
4.55 Fe II 127 + 5.14 Ti II 11
8.33 Ti II 87
9.64 Ti II 87 (+9.64 Fe I 556,563)
30.75 Mn I 2 + 1.46 Fe II 151
2.95 Fe II 126 + 3.07 Mn I 2
4.49 Mn I 2
00
3985.00
3990.00
3995.00
4000.00
4005.00
4010.00
4015.00
4020.00
4025.00
4030.00

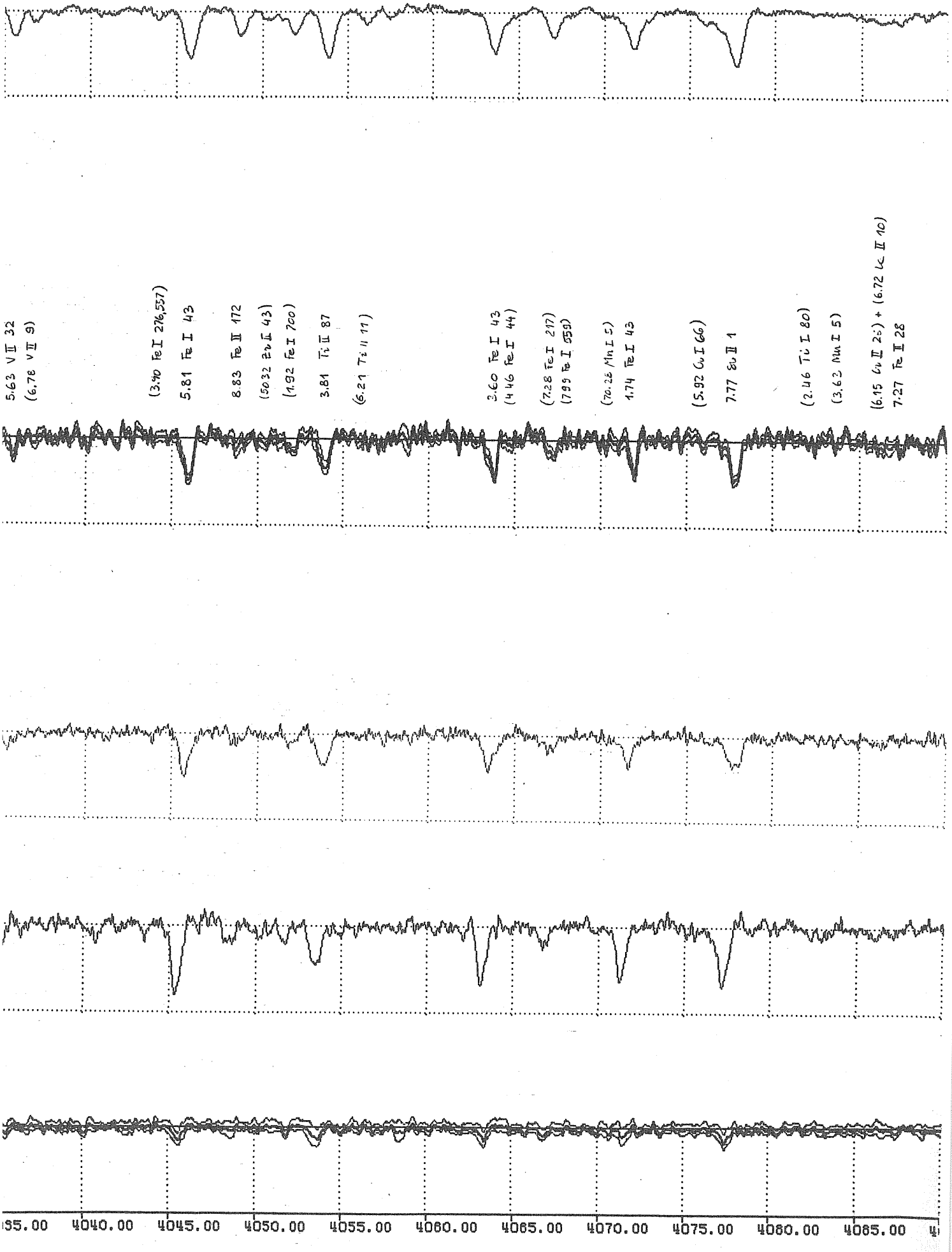
5.63 V II 32
(6.78 V II 9)
(3.90 Fe I 276,557)
5.81 Fe I 43
8.83 Fe II 172
(5032 Sm II 43)
(1.92 Fe I 700)
3.81 Ti II 87
(6.21 Ti II 11)
3.60 Fe I 43
(4 46 Fe I 44)
(7.28 Fe I 217)
(799 Fe I 559)
(70.28 Mn I 5)
1.74 Fe I 43
(5.92 Cu I 66)
7.77 Sm II 1
(2.46 Ti I 80)
(3.62 Mn I 5)
(6.15 Cu II 26) + (6.72 Cu II 10)
7.27 Fe II 28
4035.00
4040.00
4045.00
4050.00
4055.00
4060.00
4065.00
4070.00
4075.00
4080.00
4085.00

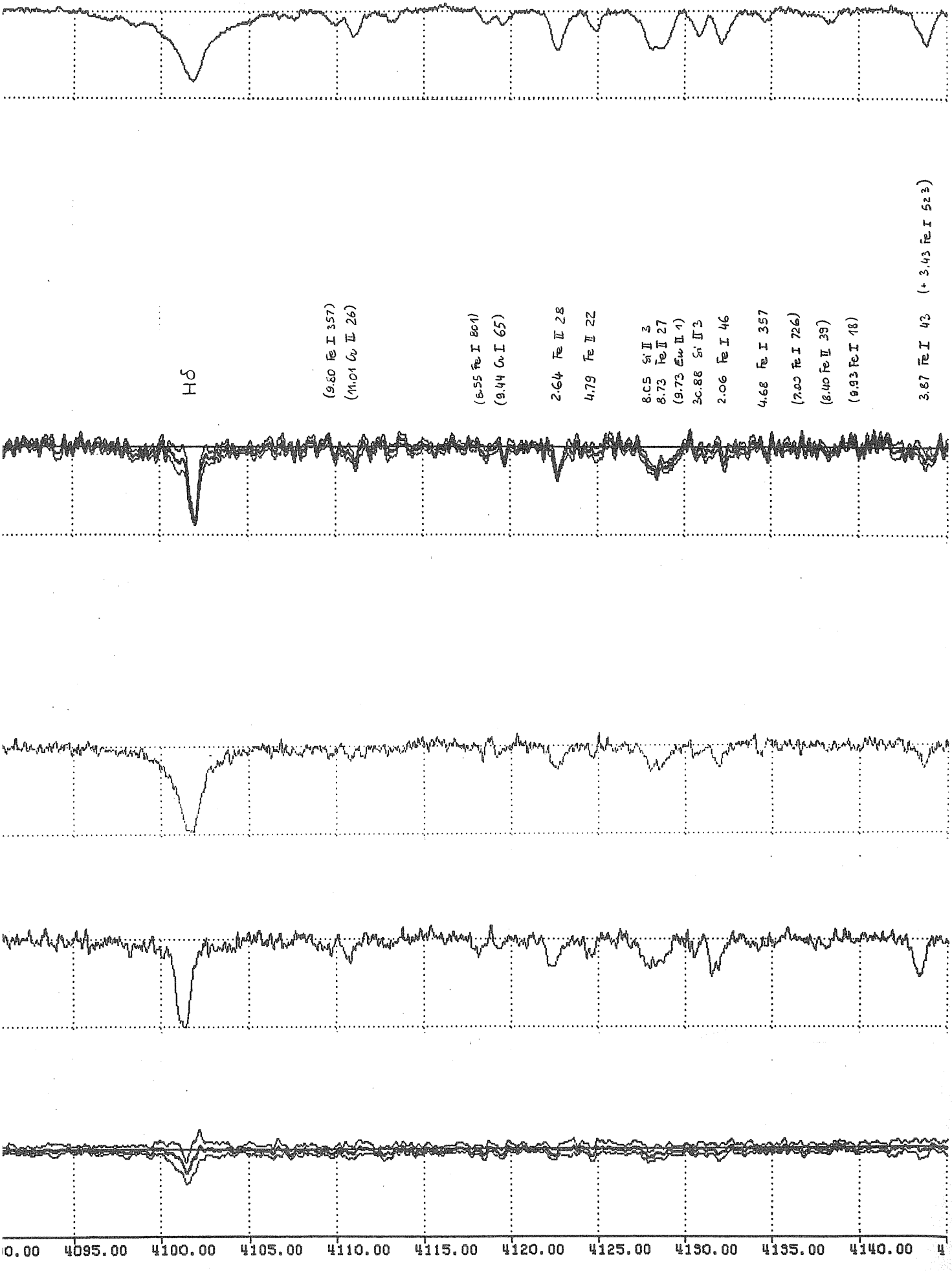
Hδ
(9.60 Fe I 357)
(11.01 Cr II 26)
(6.55 Fe I 801)
(9.44 Ca I 65)
2.64 Fe II 28
4.79 Fe II 22
8.65 Si II 3
8.73 Fe II 27
(9.73 Ew II 1)
30.88 Si II 3
2.06 Fe I 46
4.68 Fe I 357
(7.80 Fe I 726)
(8.40 Fe II 39)
(9.93 Fe I 18)
3.87 Fe I 43
(+ 3.43 Fe I 523)
0.00
4095.00
4100.00
4105.00
4110.00
4115.00
4120.00
4125.00
4130.00
4135.00
4140.00

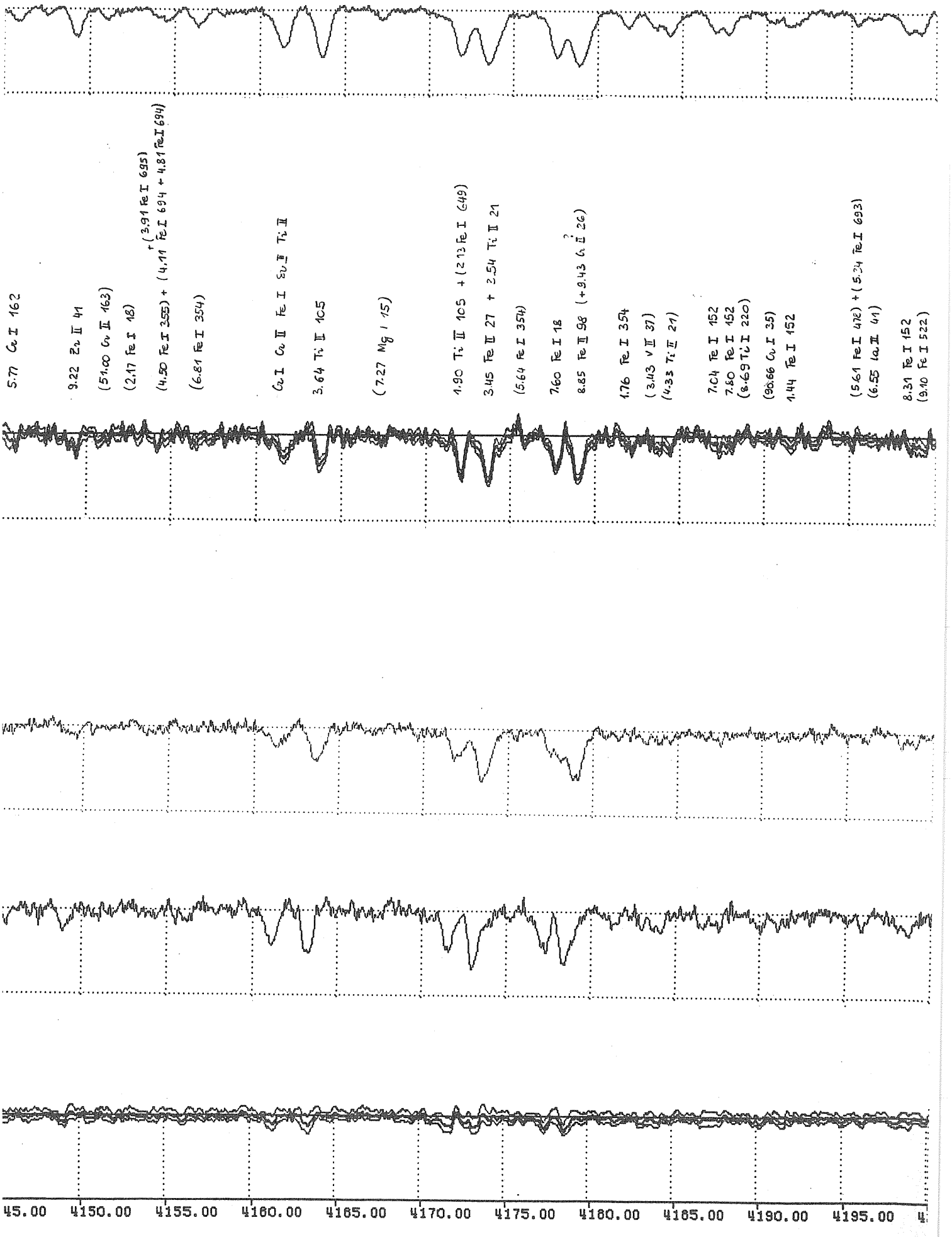
5.77 Ca I 162
9.22 Zr II 41
(51.00 Cr II 163)
(2.17 Fe I 18)
(4.50 Fe I 355) + (4.11 Fe I 694 + 4.81 Fe I 694)
(3.91 Fe I 695)
(6.81 Fe I 354)
Ca I Ca II Fe I Sc II Ti II
3.64 Ti II 105
(7.27 Mg I 15)
1.90 Ti II 105 + (2.13 Fe I 649)
3.45 Fe II 27 + 2.54 Ti II 21
(5.64 Fe I 354)
7.60 Fe I 18
8.85 Fe II 98 (+9.43 Cr II 26)
1.76 Fe I 354
(3.43 V II 37)
(4.33 Ti II 21)
7.04 Fe I 152
7.80 Fe I 152
(8.69 Ti I 220)
(90.66 Cr I 35)
1.44 Fe I 152
(5.61 Fe I 472) + (5.24 Fe I 693)
(6.55 La II 41)
8.31 Fe I 152
(9.10 Fe I 522)
4145.00
4150.00
4155.00
4160.00
4165.00
4170.00
4175.00
4180.00
4185.00
4190.00
4195.00

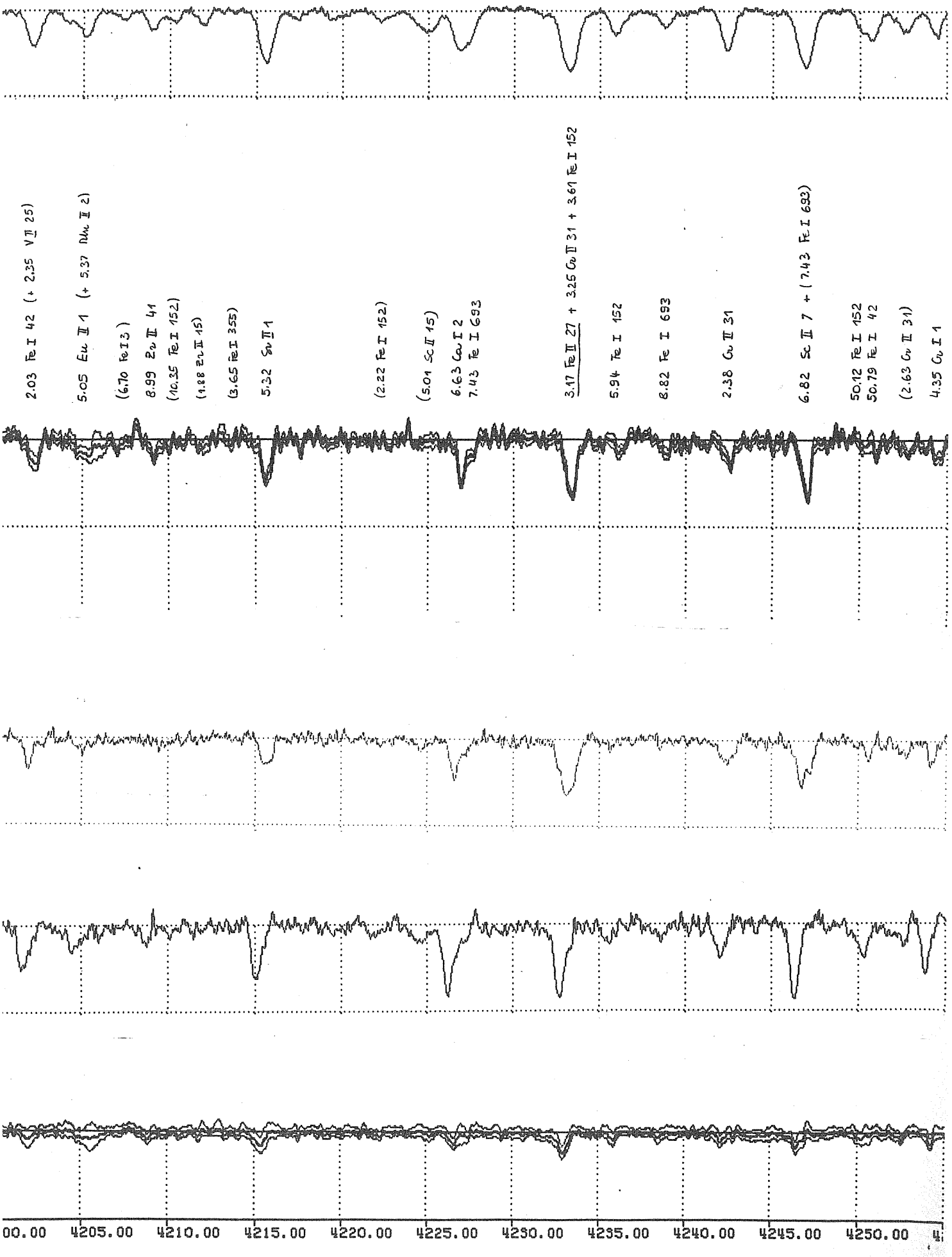
2.03 Fe I 42 (+ 2.35 V II 25)
5.05 Eu II 1 (+ 5.37 Nd II 2)
(6.70 Fe I 3)
8.99 Zr II 41
(10.35 Fe I 152)
(1.88 Zr II 15)
(3.65 Fe I 355)
5.32 Sr II 1
(2.22 Fe I 152)
(5.01 Sc II 15)
6.63 Co I 2
7.43 Fe I 693
3.17 Fe II 27 + 3.25 Cr II 31 + 3.61 Fe I 152
5.94 Fe I 152
8.82 Fe I 693
2.38 Cr II 31
6.82 Sc II 7 + (7.43 Fe I 693)
50.12 Fe I 152
50.79 Fe I 42
(2.63 Cr II 31)
4.35 Cr I 1
00.00
4205.00
4210.00
4215.00
4220.00
4225.00
4230.00
4235.00
4240.00
4245.00
4250.00

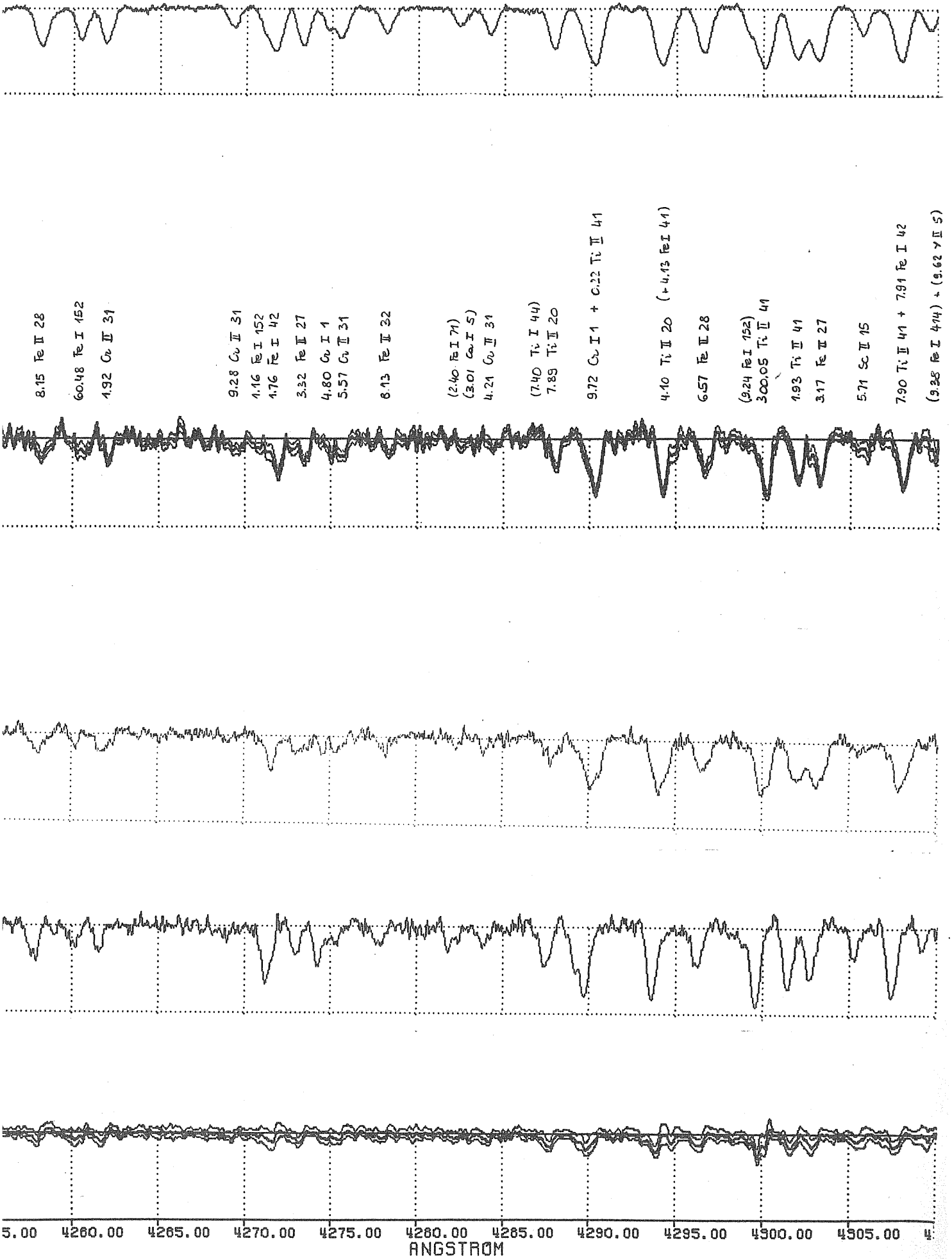
8.15 Fe II 28
60.48 Fe I 152
1.92 Cr II 31
9.28 Cr II 31
1.16 Fe I 152
1.76 Fe I 42
3.32 Fe II 27
4.80 Cr I 1
5.57 Cr II 31
8.13 Fe II 32
(2.40 Fe I 71)
(3.01 Cr I 5)
4.21 Cr II 31
(7.40 Ti I 44)
7.89 Ti II 20
9.72 Cr I 1 + 6.22 Ti II 41
4.10 Ti II 20 (+4.13 Fe I 41)
6.57 Fe II 28
(9.24 Fe I 152)
300.05 Ti II 41
1.93 Ti II 41
3.17 Fe II 27
5.71 Sc II 15
7.90 Ti II 41 + 7.91 Fe I 42
(9.38 Fe I 414) + (9.62 Y II 5)
5.00
4260.00
4265.00
4270.00
4275.00
4280.00
4285.00
4290.00
4295.00
4300.00
4305.00
ANGSTROM

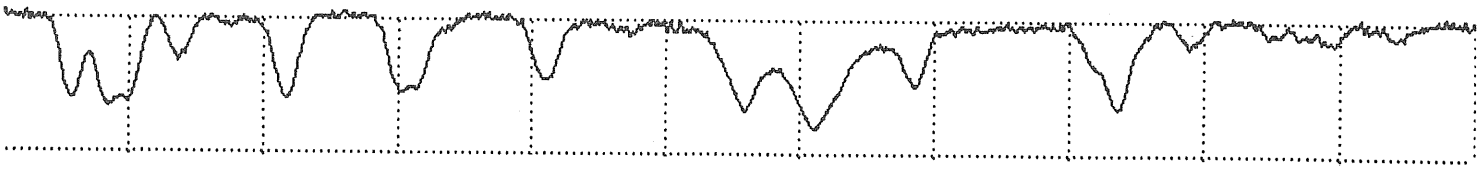

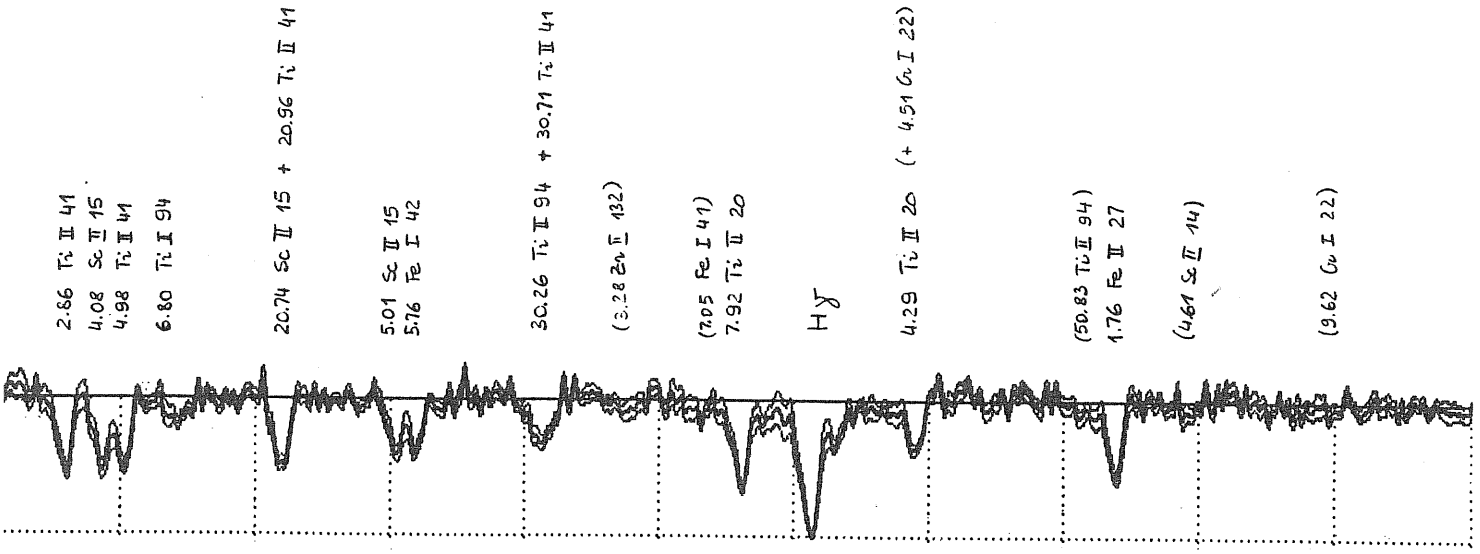
2.86 Ti II 41
4.08 Sc II 15
4.98 Ti II 41
6.80 Ti I 94
20.74 Sc II 15 + 20.96 Ti II 41
5.01 Sc II 15
5.76 Fe I 42
30.26 Ti II 94 + 30.71 Ti II 41
(3.28 Zn I 132)
(7.05 Fe I 41)
7.92 Ti II 20
Hγ
4.29 Ti II 20 (+ 4.51 Cr I 22)
(50.83 Ti II 94)
1.76 Fe II 27
(4.61 Sc II 14)
(9.62 Cr I 22)

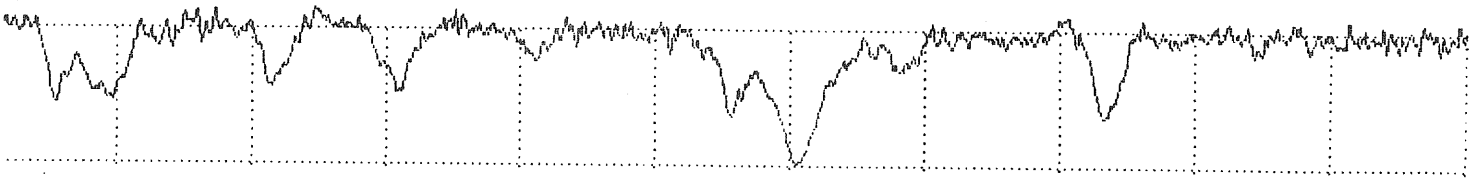

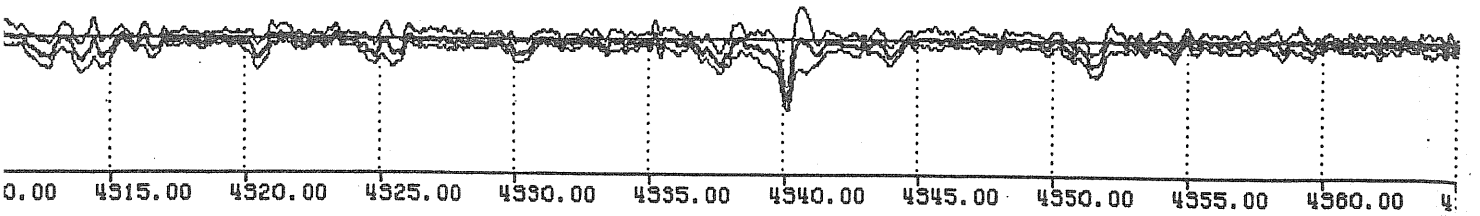
0.00
4315.00
4320.00
4325.00
4330.00
4335.00
4340.00
4345.00
4350.00
4355.00
4360.00

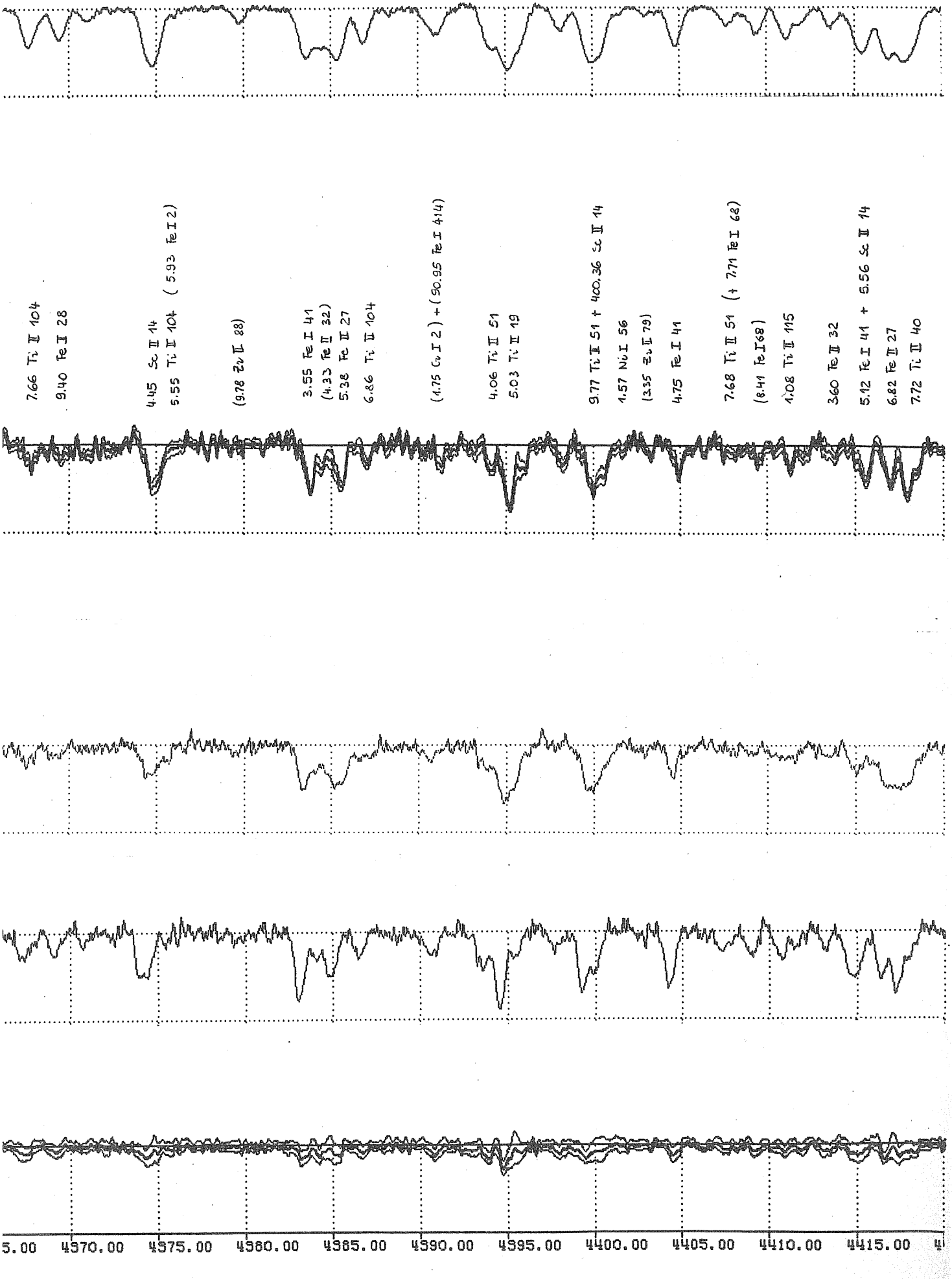
7.66 Ti II 104
9.40 Fe I 28
4.45 Sc II 14
5.55 Ti II 104 (5.93 Fe I 2)
(9.78 Zr II 88)
3.55 Fe I 41
(4.33 Fe I 32)
5.38 Fe II 27
6.86 Ti II 104
(1.75 Cr I 2) + (90.95 Fe I 414)
4.06 Ti II 51
5.03 Ti II 19
9.77 Ti I 51 + 400.36 Sc II 14
1.57 Ni I 56
(3.35 Zr II 79)
4.75 Fe I 41
7.68 Ti II 51 (+ 7.71 Fe I 68)
(8.41 Fe I 68)
1.08 Ti II 115
3.60 Fe II 32
5.12 Fe I 41 + 5.56 Sc II 14
6.82 Fe II 27
7.72 Ti II 40
5.00
4370.00
4375.00
4380.00
4385.00
4390.00
4395.00
4400.00
4405.00
4410.00
4415.00

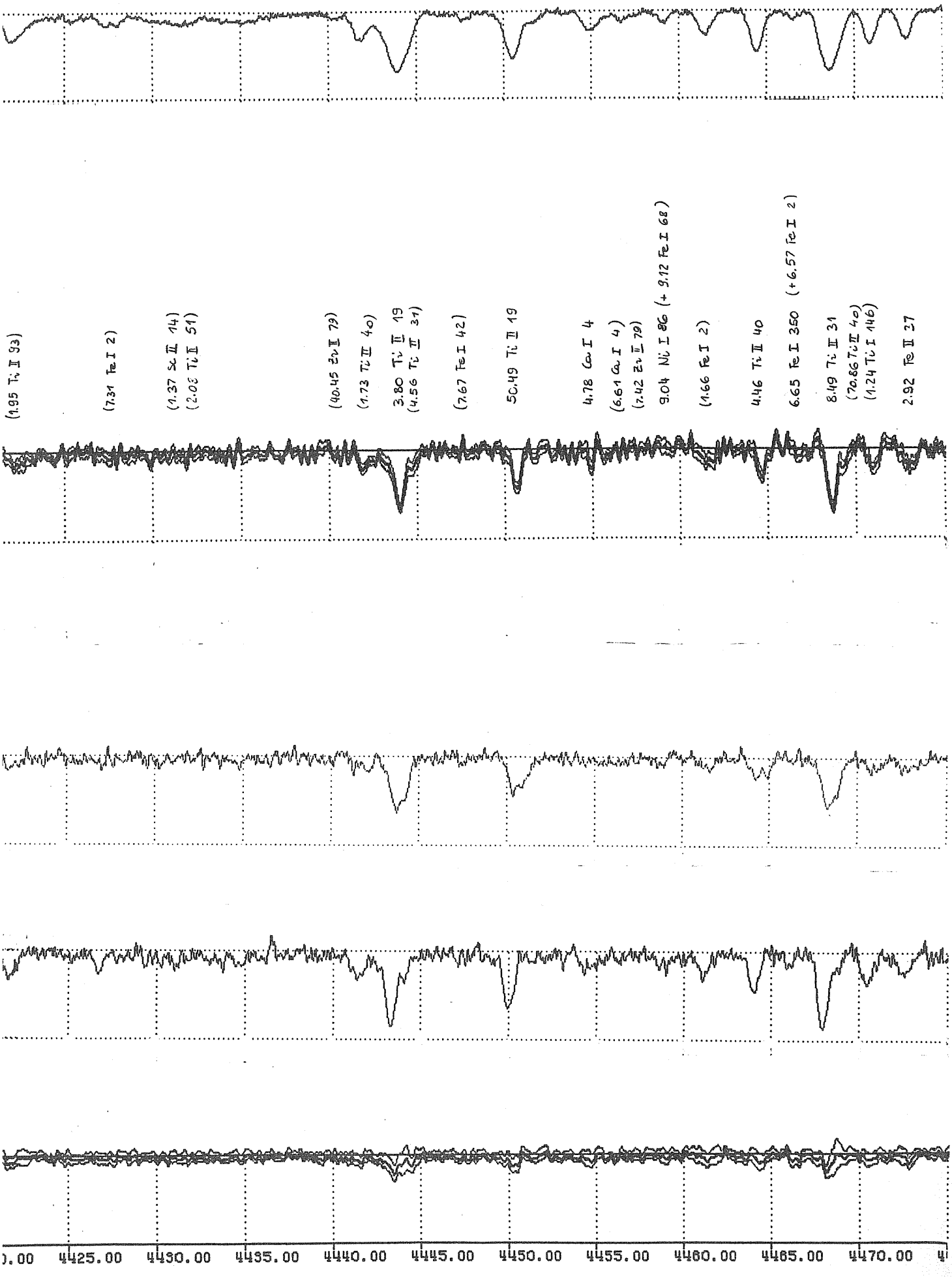
(1.95 Ti II 93)
(7.31 Fe I 2)
(1.37 Sc II 14)
(2.08 Ti II 51)
(40.45 Zn I 79)
(1.73 Ti II 40)
3.80 Ti II 19
(4.56 Ti II 31)
(7.67 Fe I 42)
50.49 Ti II 19
4.78 Ca I 4
(6.61 Ca I 4)
(7.42 Zn I 79)
9.04 Ni I 86 (+ 9.12 Fe I 68)
(1.66 Fe I 2)
4.46 Ti II 40
6.65 Fe I 350 (+6.57 Fe I 2)
8.49 Ti II 31
(70.86 Ti II 40)
(1.24 Ti I 146)
2.92 Fe II 27
.00
4425.00
4430.00
4435.00
4440.00
4445.00
4450.00
4455.00
4460.00
4465.00
4470.00

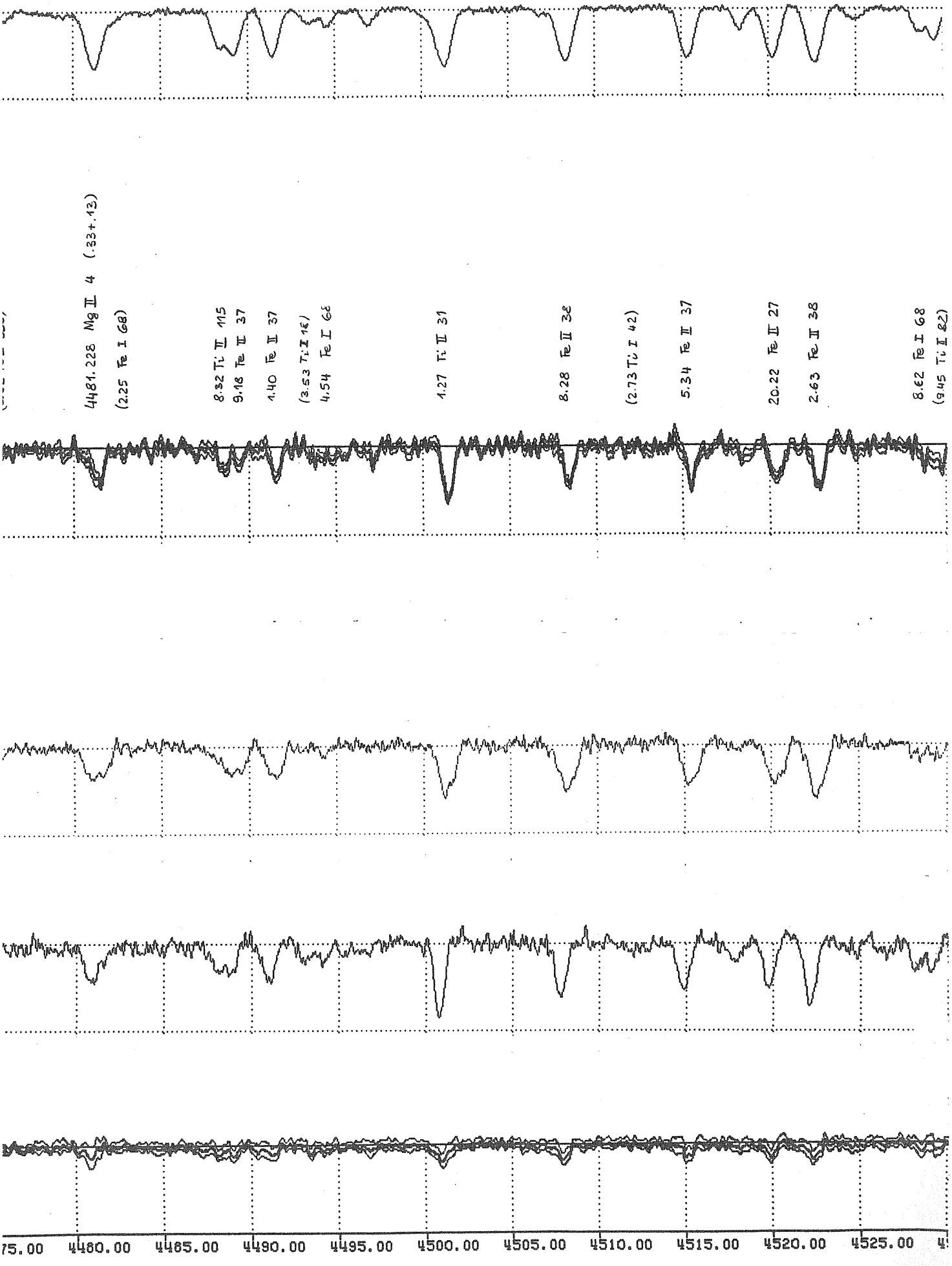
4481.228 Mg II 4 (.33+.13)
(2.25 Fe I 68)
8.32 Ti II 115
9.18 Fe II 37
1.40 Fe II 37
(3.53 Ti I 16)
4.54 Fe I 68
1.27 Ti II 31
8.28 Fe II 38
(2.73 Ti I 42)
5.34 Fe II 37
20.22 Fe II 27
2.63 Fe II 38
8.62 Fe I 68
(9.45 Ti II 82)
75.00
4480.00
4485.00
4490.00
4495.00
4500.00
4505.00
4510.00
4515.00
4520.00
4525.00

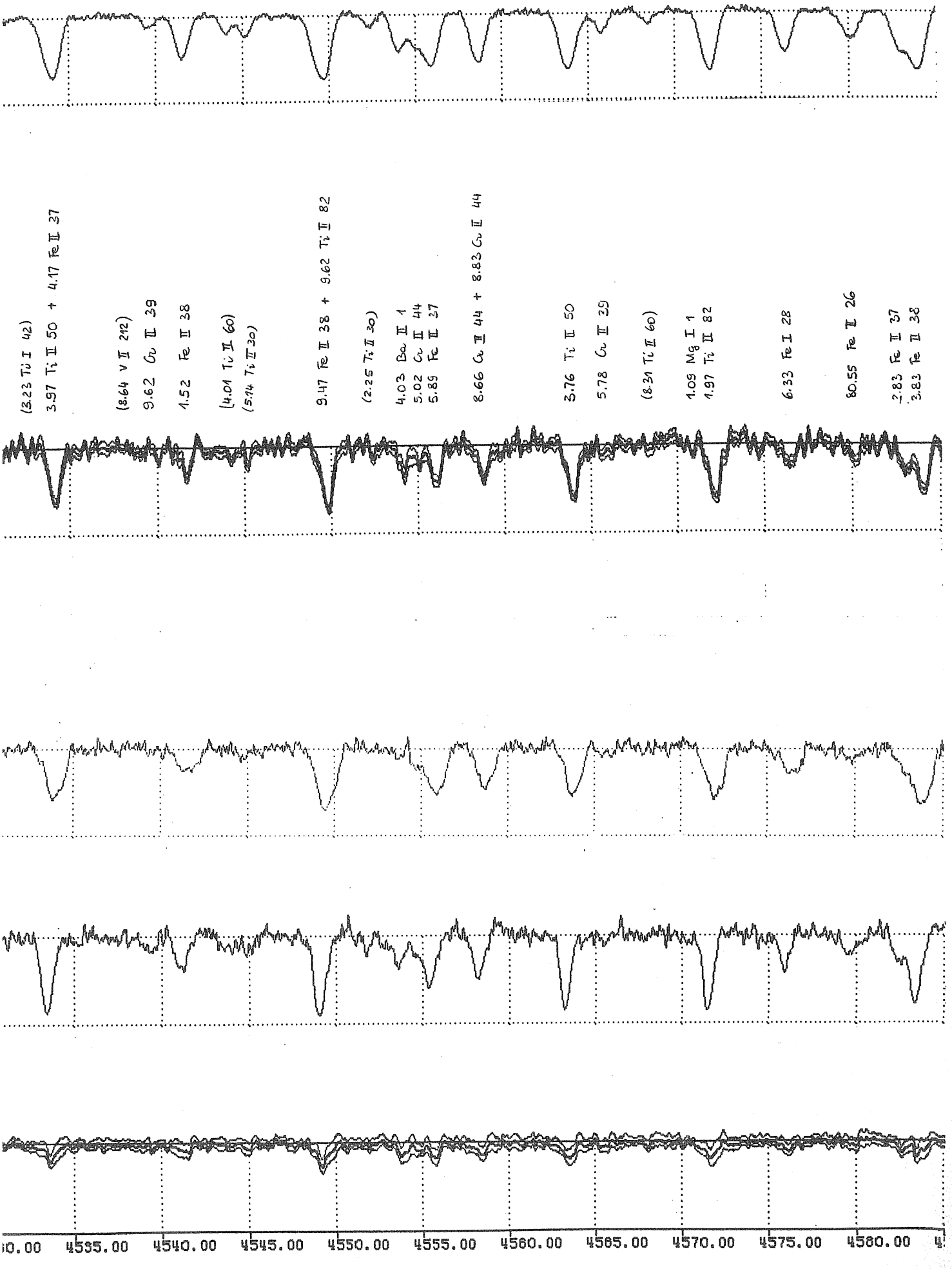
(3.23 Ti I 42)
3.97 Ti II 50 + 4.17 Fe II 37
(8.64 v II 212)
9.62 Cr II 39
1.52 Fe II 38
(4.01 Ti II 60)
(5.14 Ti II 30)
9.47 Fe II 38 + 9.62 Ti II 82
(2.25 Ti II 30)
4.03 Ba II 1
5.02 Cr II 44
5.89 Fe II 37
8.66 Cr II 44 + 8.83 Cr II 44
3.76 Ti II 50
5.78 Cr II 39
(8.31 Ti II 60)
1.09 Mg I 1
1.97 Ti II 82
6.33 Fe I 28
80.55 Fe II 26
-2.83 Fe II 37
3.83 Fe II 38
0.00
4535.00
4540.00
4545.00
4550.00
4555.00
4560.00
4565.00
4570.00
4575.00
4580.00

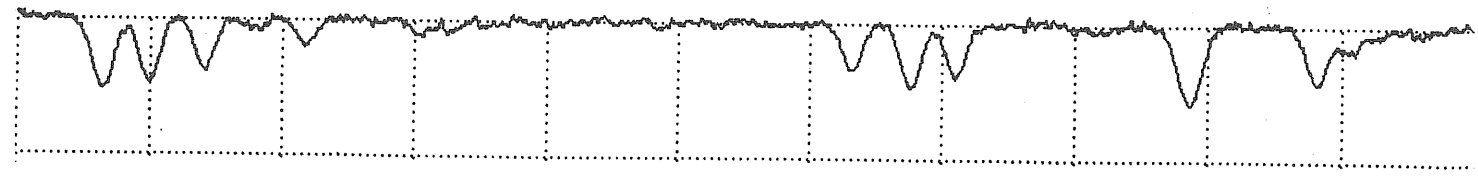

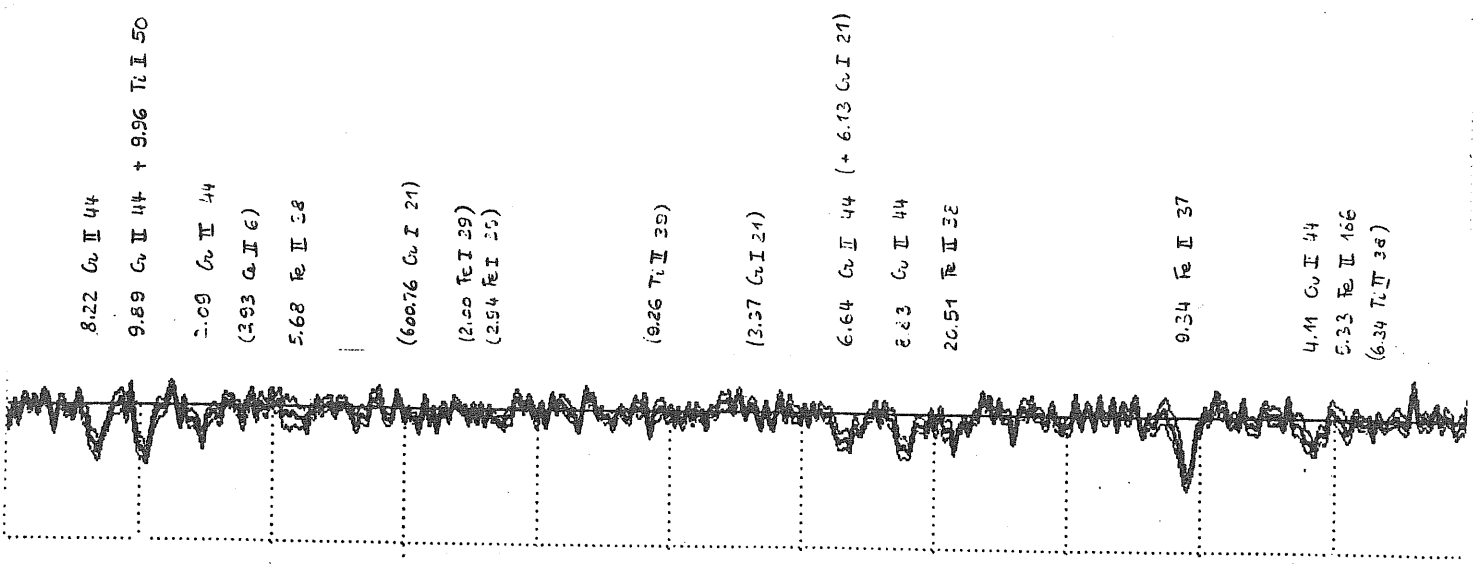
8.22 Cu II 44
9.89 Cu II 44 + 9.96 Ti I 50
2.09 Cu II 44
(2.93 Cu II 6)
5.68 Fe II 38
(6.76 Cu I 21)
(2.00 Fe I 29)
(2.54 Fe I 25)
(9.26 Ti II 39)
(3.37 Cu I 21)
6.64 Cu II 44 (+ 6.13 Cu I 21)
8.43 Cu II 44
20.51 Fe II 32
9.34 Fe II 37
4.11 Cu II 44
5.33 Fe II 166
(6.34 Ti II 38)

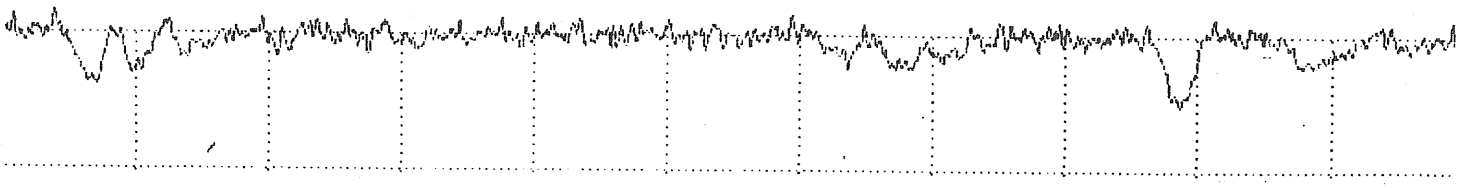

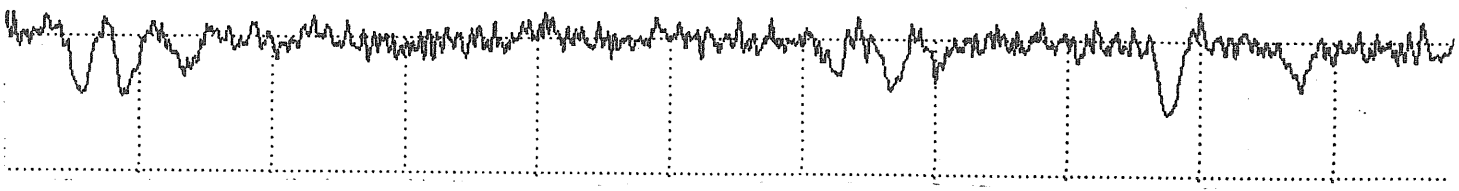

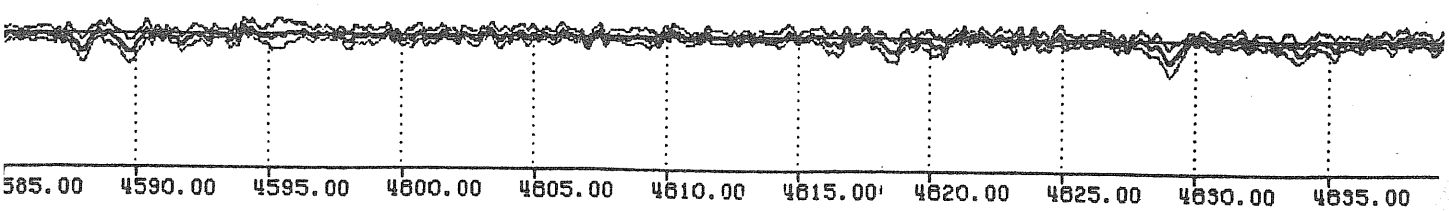
585.00
4590.00
4595.00
4600.00
4605.00
4610.00
4615.00
4620.00
4625.00
4630.00
4635.00

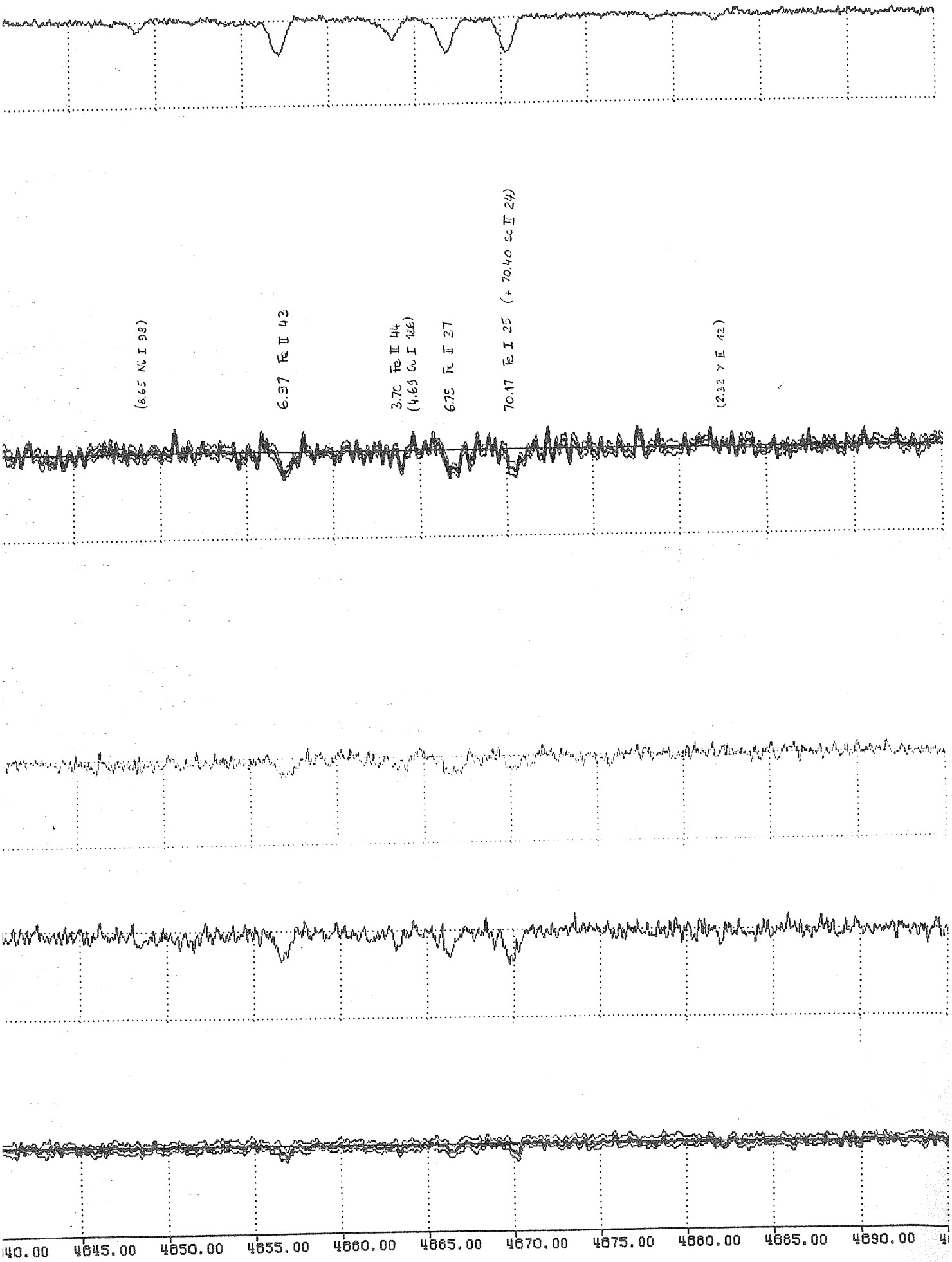
(8.65 Ni I 98)
6.97 Fe II 42
3.70 Fe II 44
(4.69 Cu I 166)
6.75 Fe II 37
70.17 Fe I 25
(+ 70.40 Sc II 24)
(2.32 Y II 12)
4640.00
4645.00
4650.00
4655.00
4660.00
4665.00
4670.00
4675.00
4680.00
4685.00
4690.00

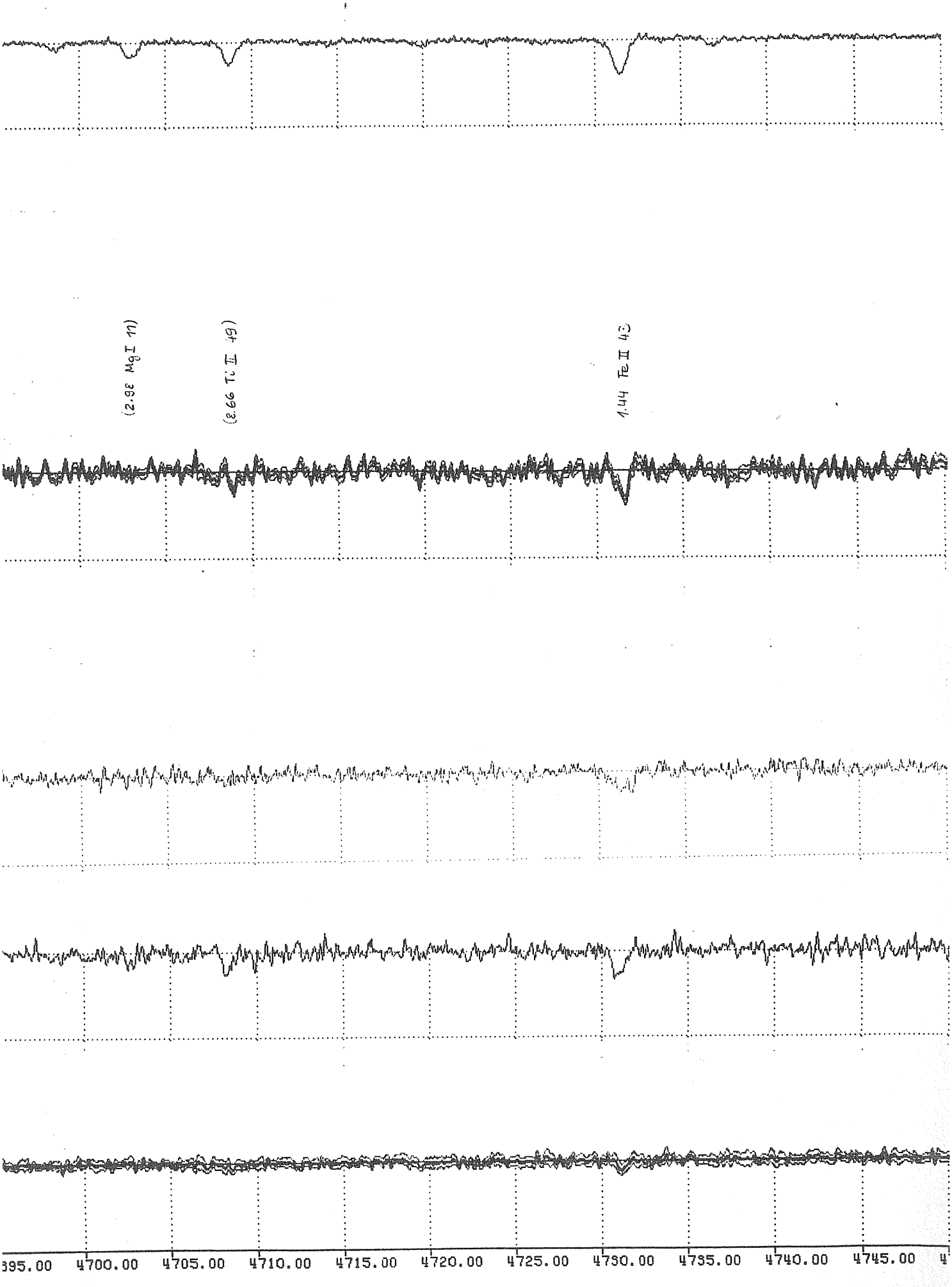
(2.98 Mg I 11)
(3.66 Ti II 49)
1.44 Fe II 43
4695.00
4700.00
4705.00
4710.00
4715.00
4720.00
4725.00
4730.00
4735.00
4740.00
4745.00

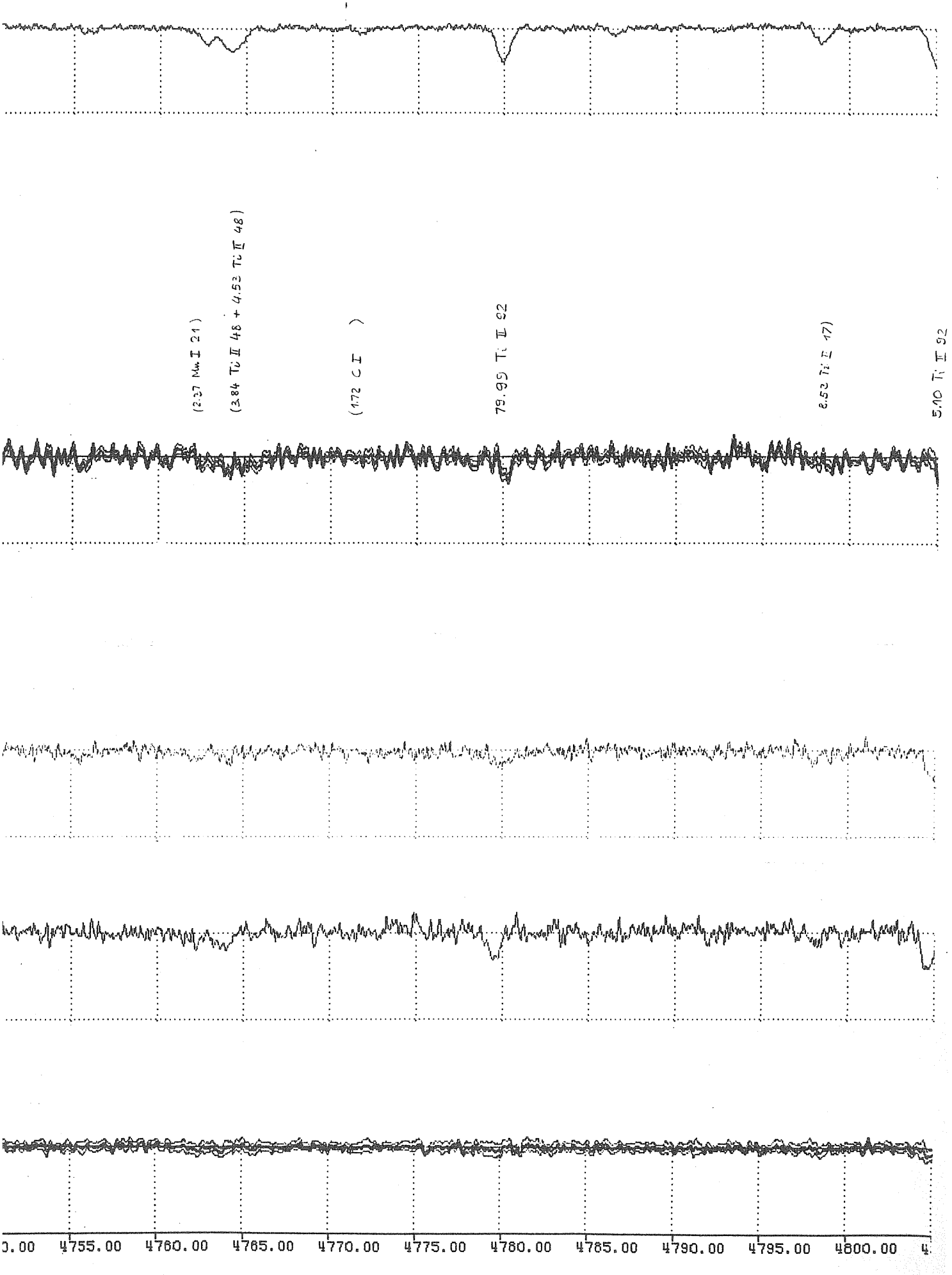
(2.37 Mn I 21)
(3.84 Ti II 48 + 4.53 Ti II 48)
(1.72 C I)
79.95 Ti II 92
8.53 Ti II 17)
5.10 Ti II 92
4755.00
4760.00
4765.00
4770.00
4775.00
4780.00
4785.00
4790.00
4795.00
4800.00

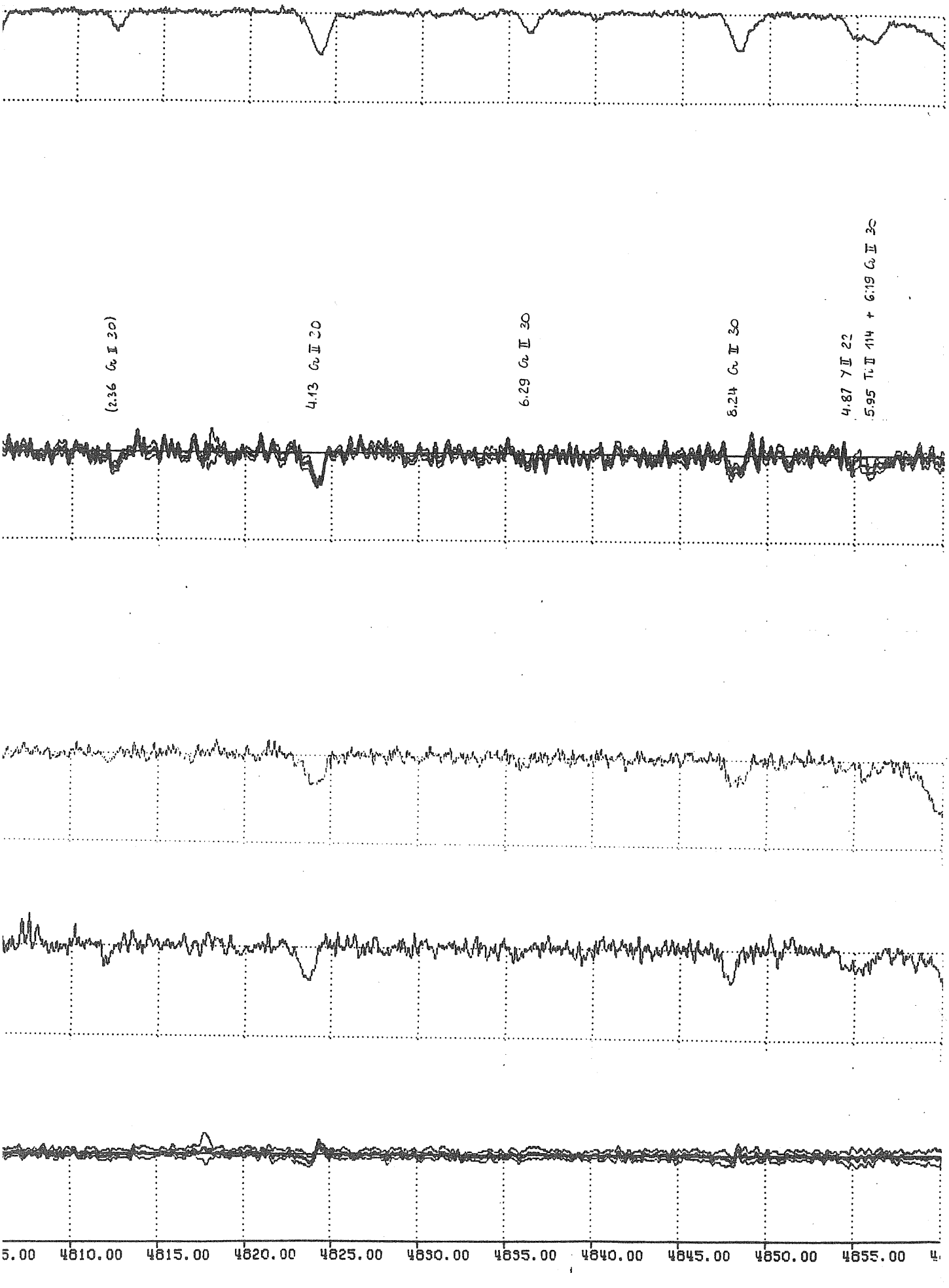
(2.36 Ca I 30)
4.13 Ca II 20
6.29 Ca II 30
8.24 Ca II 30
4.87 Y II 22
5.95 Ti II 114 + 6.19 Ca II 30
5.00
4810.00
4815.00
4820.00
4825.00
4830.00
4835.00
4840.00
4845.00
4850.00
4855.00

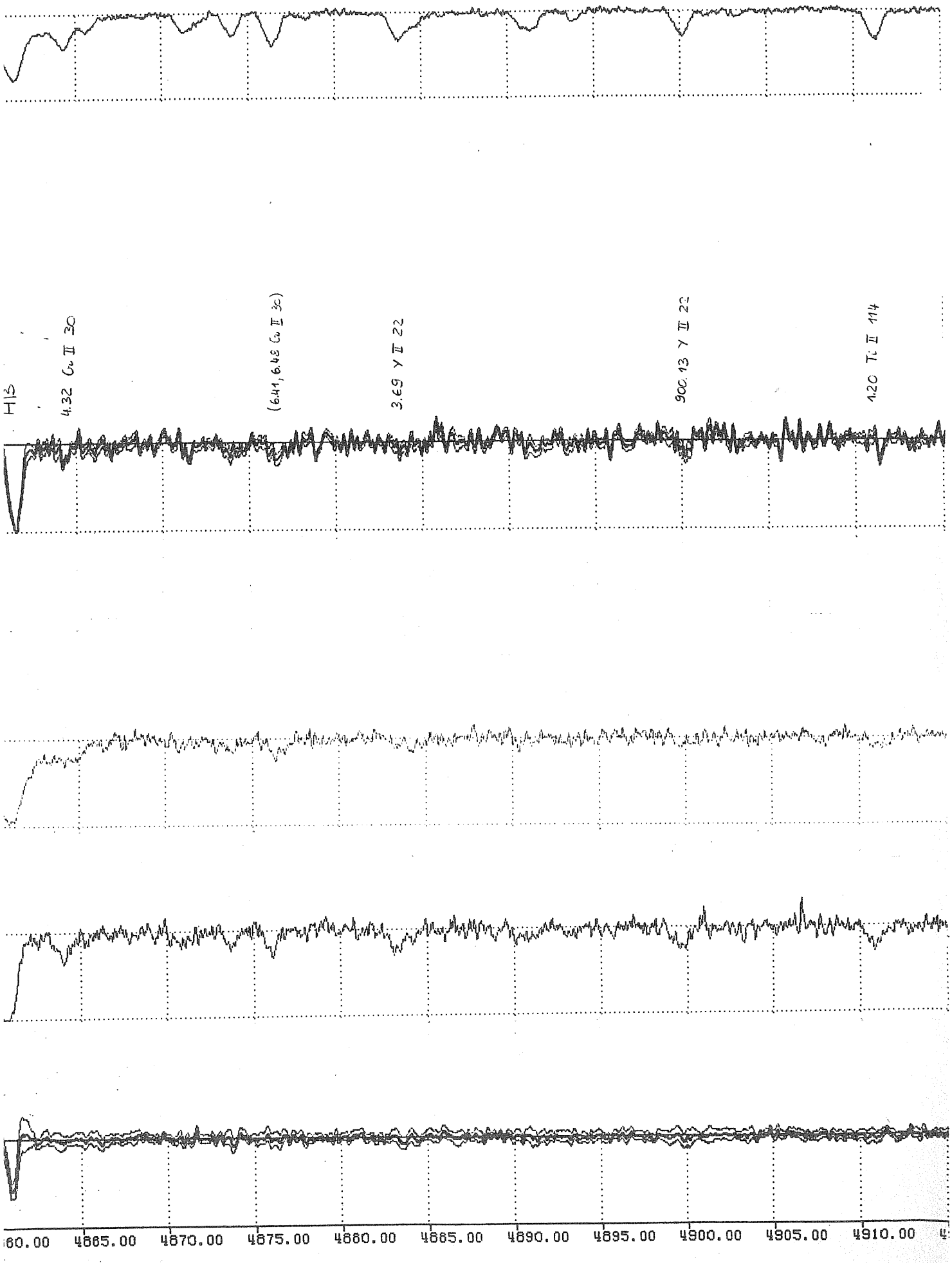
H13
4.32 Cu II 30
(6.41, 6.48 Cu II 30)
3.69 Y II 22
900.13 Y II 22
1.20 Ti II 114
4860.00
4865.00
4870.00
4875.00
4880.00
4885.00
4890.00
4895.00
4900.00
4905.00
4910.00

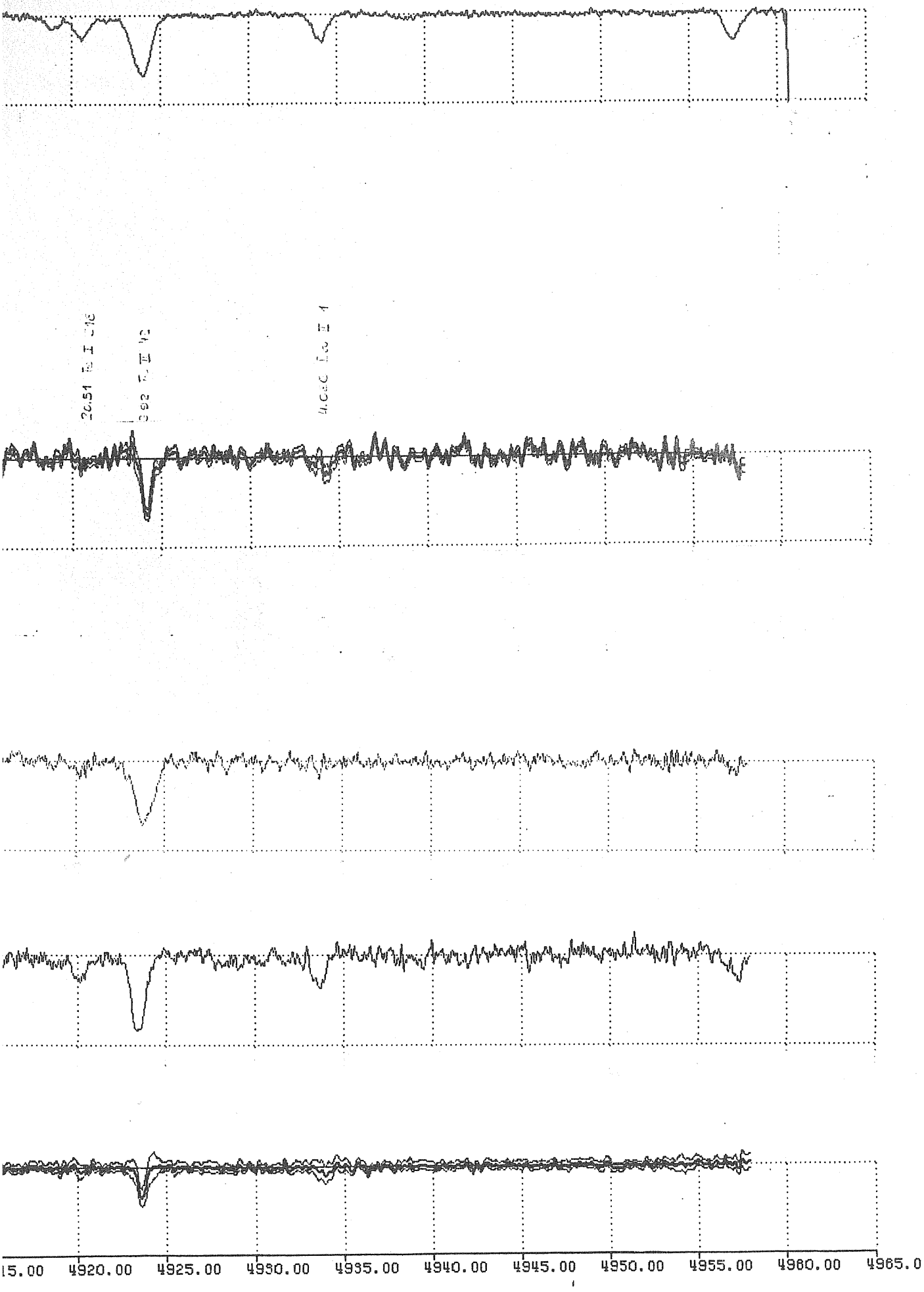
15.00
4920.00
4925.00
4930.00
4935.00
4940.00
4945.00
4950.00
4955.00
4960.00
4965.0

Addendum

PUBLISHED PAPERS ON EPSILON AURIGAE

Paper I

COMMISSION 27 OF THE I. A. U.
INFORMATION BULLETIN ON VARIABLE STARS
Number 2326

Konkoly Observatory
Budapest
4 May 1983
HU ISSN 0374 - 0676

H ALPHA OBSERVATIONS OF EPSILON AURIGAE

The binary system ε Aur (= HR 1605) is now passing through the phase of its total eclipse. This system has an orbital period of 27.1 years; the primary star is an FOIa supergiant and the secondary component is an object of unknown nature.

ε Aur has been well studied photoelectrically (Gyldenkerne 1970). The light curve shows only the primary minimum, with a totality phase of roughly constant magnitude that lasts about one year. The secondary component gives no observable contribution, at least in the visible bands, to the luminosity of the system at any time. In spite of this, during the totality phase, the difference in magnitude is restricted within less than one magnitude, so that it is supposed to be caused by a disk-shaped or by a semitransparent object.

At the Trieste Observatory ε Aur has been observed with a photoelectric photometer equipped with two interferometric filters of 30 Å halfwidth. One of them is centered on the Hα 6653 Å line of neutral hydrogen, the other being centered on a nearby continuum region, say 6620 Å. The comparison star, λ Aurigae, is a solar type dwarf (GOV). Table I shows the magnitude of the line minus the magnitude of the red continuum, together with the differences between ε and the comparison. Every value is an average of several particular measurements, made with a time resolution of, typically, 1 minute.

The first fact that these measurements seem to reveal is an evident decrease in the relative flux emitted by the line.

2

Table I

Date	Δm ($H\alpha$ - 6620 Å)	Δm_{6620} ($\varepsilon - \lambda$)
Nov. 19, 1982	- 0.05 ± 0.01	- 1.02 ± 0.01
Jan. 11, 1983	- 0.06 ± 0.02	- 0.98 ± 0.01
Jan. 17, 1983	- 0.04 ± 0.01	- 0.98 ± 0.01
Jan. 23, 1983	- 0.05 ± 0.01	- 0.92 ± 0.01
Mar. 17, 1983	+ 0.13 ± 0.02	- -
Mar. 18, 1983	+ 0.09 ± 0.01	- 0.94 ± 0.01

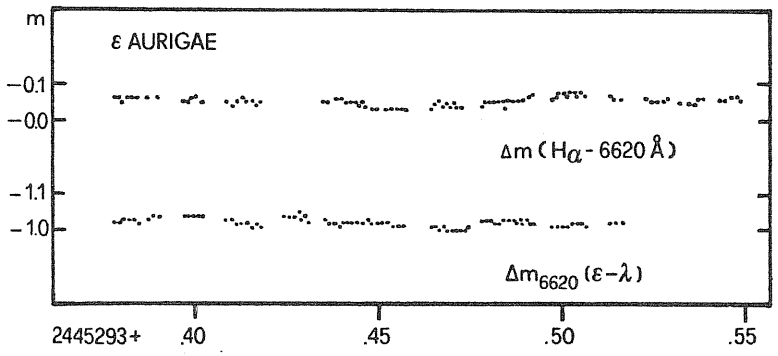

Figure 1. Photoelectric measurements of ε Aurigae during one night, Nov. 19, 1982. The methods used are described in the text.

It may be important to note that this drop happened only well after the beginning of totality, which probably occurred at the end of last year (Stencel 1983). Figure 1 shows one complete run of observations; the behaviour was similar on all the other observing nights, so we can exclude the occurrence of systematic short-time-scale variations in the red flux.

In addition, some high-resolution spectra have been obtained with the 152 cm coudé telescope of the Observatory

3

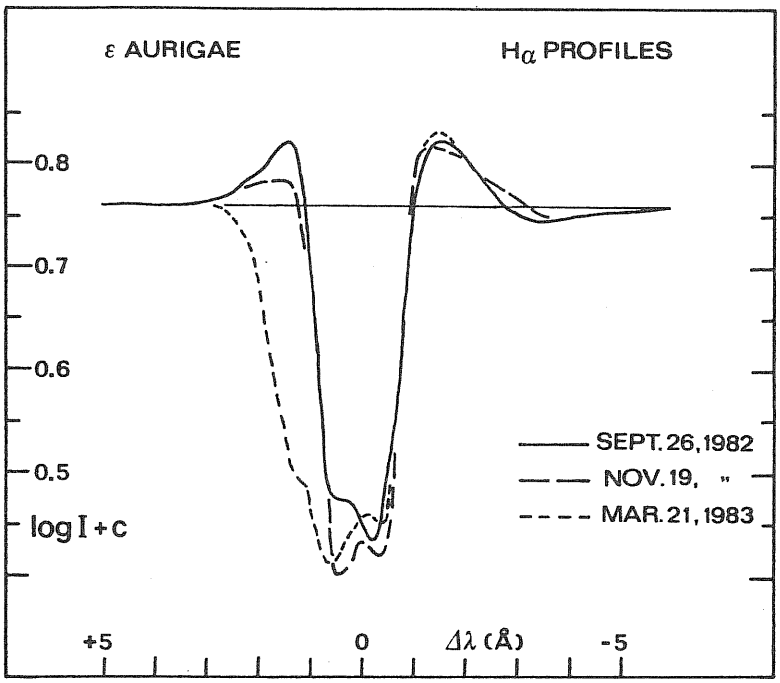

Figure 2. Comparison between H alpha profiles at mid ingress, end ingress and totality phases, plotted in logarithmic scale of intensity.

Haute Provence. One of the most noticeable variations in the spectral features is the change in the profile of the Hα line. In Figure 2 we have plotted the profiles at various epochs. In particular, we can see that the blueward emission wing seemed to remain unperturbed, while the redward one was gradually reduced until it disappeared during last March. In its place, a corresponding broadening of the absorption towards the red can be noted. This observational evidence explains and confirms the analogous decrease observed photoelectrically in the Hα band (30 Å wide).

4

A similar phenomenon was detected during the corresponding phase of the 1956 eclipse (Wright and Kushwaha 1957), superimposed on strong variations in the blueward emission (occurring, at that time, on the occasion of the first and second contacts). Since significant variations in the Hα profile were seen also out of eclipse (Castelli 1977), one is led to view the observed Hα behaviour in terms of a composite phenomenon. An eclipse effect, generated by combined rotations of the supergiant and of the eclipsing body can produce the Hα inverse P Cygni-like profile, that we observed in March, before mid totality. Irregular variations, probably due to inhomogeneities, both of the primary shell and of the eclipsing object, may then be superimposed.

CONRAD BOEHM
Osservatorio Astronomico
casella postale
succursale Trieste 5
I-34131 Trieste Italy

STENO FERLUGA
S.I.S.S.A.
strada Costiera 11
I-34136 Trieste Italy

References:

Castelli, F. (1977): Astroph.Space Sci. 49, 179
Gyldenkerne, K. (1970): Vistas Astron. 12, 199
Stencel, R.E. (1983): Epsilon Aur Campaign Newsletter, n°6
Wright, K.O. and Kushwaha, R.S. (1957): VIII Coll. de Liège, p. 421.

Paper II

Astron. Astrophys. 130, 419–423 (1984)

ASTRONOMY AND ASTROPHYSICS

The eclipse of Epsilon Aurigae in the ultraviolet*

C. Boehm[1], S. Ferluga[2,3], and M. Hack[1,2]

[1] Osservatorio Astronomico di Trieste, via G. B. Tiepolo 11, I-34131 Trieste, Italy
[2] Università degli Studi di Trieste, P.le Europa 1, I-34100 Trieste, Italy
[3] Scuola Internazionale Superiore di Studi Avanzati (SISSA), Str. Costiera 11, I-34136 Trieste, Italy

Received June 20, accepted August 10, 1983

Summary. Ultraviolet low-resolution spectra of ε Aurigae (F0Ia +?) have been taken with IUE during the partial and total phase of the present eclipse; they are compared with a set of corresponding pre-eclipse spectra.

The following conclusions are derived. A hot component, dominant in far UV, is associated with the extended body that eclipses the primary. Far UV variability, observed also out of eclipse, may originate from this component or from the extended object itself; possible mechanisms are suggested. The eclipsing body cannot be made of dust, since no deepening of the λ 2200 feature is observed during the eclipse. Electron scattering is thus supposed to be responsible for the greyness of the eclipse; an additional contribution by blending of absorption lines in the eclipsing body is possible. The system is embedded in a large rarefied gaseous envelope, which is responsible for the O I λ 1304 emission, remaining practically unaffected by the eclipse.

Key words: UV spectroscopy – eclipsing binaries – Epsilon Aurigae

Introduction

The binary sytem ε Aurigae (HD 31964), having a period of 27.1 yr, is now undergoing the one-year-long total eclipse phase; the first and second contacts occurred in July and December 1982, respectively.

Optical observations of past eclipses (Gyldenkerne, 1970) show a very peculiar behaviour. The primary F0Ia star undergoes a quasi-total eclipse (flat minimum), during which its spectrum remains visible; the depth is constant with wavelength (~ 0.8 mag), while the secondary component is not individually observable (single-lined spectrum, no secondary minimum).

Many different models have been proposed in order to explain the observed data. Among them the less exotic ones posit a small secondary star surrounded by an ionised envelope or disk (Hack, 1961), or an opaque dust disk (Huang, 1965), or maybe a semitransparent pre-stellar cloud (Handbury and Williams, 1976) absorbing and/or scattering the light of the primary. In order to explain the greyness of the eclipse, Hack attributes the opacity to electron scattering, while Huang attributes it to dust scattering.

When the first ultraviolet observations of ε Aur were taken, the system was out of eclipse (Hack and Selvelli, 1979), and a noticeable UV excess was discovered, suggesting the existence of a hot dwarf secondary component. The UV behaviour of ε Aur in the phases preceding, on entering and during the present eclipse, appears then to be particularly interesting.

Observations

Our study is based on the analysis of the UV monochromatic fluxes at different wavelengths, observed in various epochs before and during the eclipse phase of ε Aur, with the International Ultraviolet Explorer (IUE), set on the low-resolution mode.

Table 1 lists the observations we have considered. Spectra (7) and (8) were obtained by members of our group (P. Molaro and C. Morossi), while the observational material concerning spectra from (1) to (6) is from different authors, and has been made available to us by the VILSPA Data Bank; moreover, the procedure of deconvolution and calibration, for all the spectra considered, has been performed with VILSPA software, in the updated version. The dates, in the third column of Table 1, show that the first observations, from (1) to (5), were all taken outside eclipse; spectrum (6) corresponds roughly to mid ingress; the last two, (7) and (8), represent the end of partial phase and early totality, respectively. Symbols *L* and *S* in Column 2 stand for *large* (10″ × 20″) and *small* (3″) aperture. Only the best exposed part of each image, indicated in the last column, has been utilized.

Since the *small* aperture does not gather all the light of the star, it allows no absolute flux calibration. Therefore, small-aperture images have been considered only when they partially overlap with a large-aperture image, taken nearly at the same time, which can provide its own flux calibration. Anyway, the flux derived by the small-aperture images is affected by a systematic error, estimated to be of the order of 5 %, caused by the uncertainty in the vertical shift necessary to fit the spectra obtained with the *large* and *small* apertures.

Results

A comparison between eclipsed and uneclipsed spectra is shown in Fig. 1. Four selected spectra are plotted, providing significant indications:

Send offprint requests to: S. Ferluga

* Based on observations by the International Ultraviolet Explorer (IUE) collected at the Villafranca Satellite Tracking Station (VILSPA) of the European Space Agency, and on data released by the VILSPA Data Bank

(420)

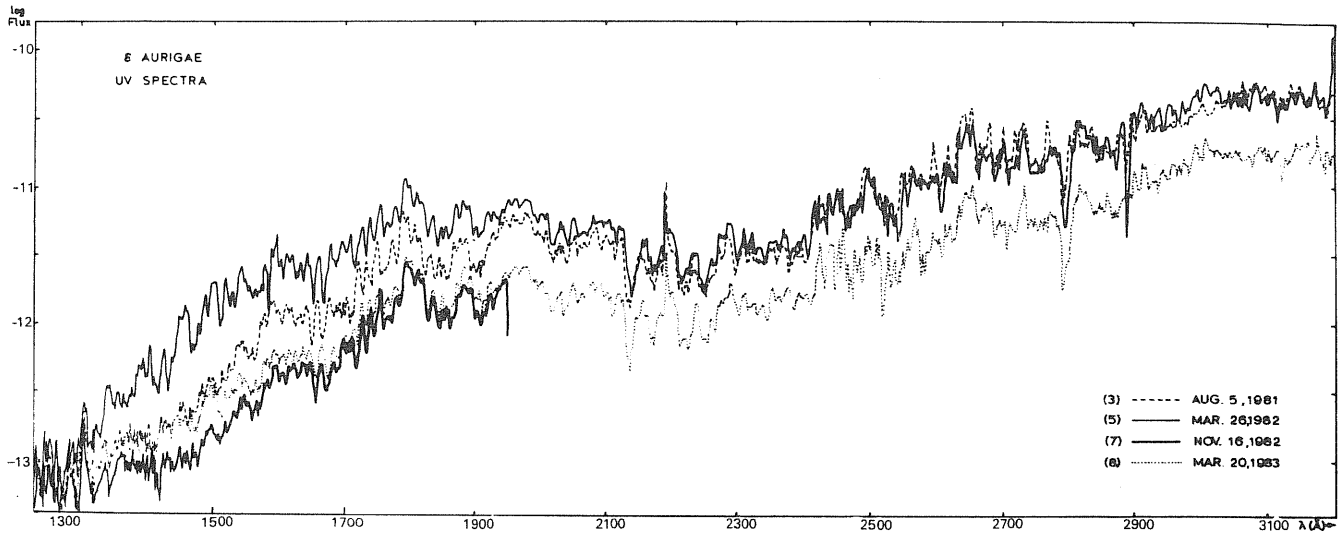

Fig. 1. Four significant spectra of ε Aur, taken before and during the eclipse, are plotted together. Fluxes are in erg cm^{-2} s^{-1} $Å^{-1}$. A detailed comparison is described in the text [section "Results", a)–e)]. The spectrum taken in totality (dotted line) is higher than the one taken in the partial phase (lower solid line)

Table 1. Observations

1 No. of Spectrum	2 IUE Image & Apert.	3 Exposure (s)	4 Date Observer	5 Spectral Range λ min, λ max (Å)
(1)	LWR 6005, L	120	1979, Nov. 1; 9^h 23^m Gilra	1900, 2500
(2)	SWP 14647, L	1800	1981, Aug. 4; 9 22	1200, 1700
	LWR 11238, L	50	Plavec 9 42	1900, 3200
(3)	SWP 14654, L	1200	1981, Aug. 5; 0 51	1200, 1690
	SWP 14654, S	300	Stickland 0 51	1690, 1910
	LWR 11246, L	120	0 9	1910, 2415
	LWR 11246, S	60	0 9	2415, 3200
(4)	SWP 16522, L	35	1982, Mar. 12; 19 54	1500, 1950
	LWR 12776, L	9	Chapman 19 59	2400, 3200
(5)	SWP 16628, L	1200	1982, Mar. 26; 7 33	1200, 1570
	SWP 16628, S	420	Stickland 7 33	1570, 1940
	LWR 12864, L	30	7 7	1940, 2420
	LWR 12864, S	30	7 7	2420, 3200
(6)	SWP 18137, L	1500	1982, Sep. 27; 18 24 Stickland	1200, 1700
(7)	SWP 18570, L	2400	1982, Nov. 16; 15 35	1200, 1695
	SWP 18570, S	600	Molaro 15 35	1695, 1950
(8)	SWP 19492, L	1800	1983, Mar. 20; 5 12	1200, 1725
	SWP 19492, S	600	Morossi 5 12	1725, 1900
	LWR 15523, L	300	6 9	1900, 2425
	LWR 15524, L	20	6 9	2425, 3200

Table 2. Continuum fluxes

Sp. / Date / λ (Å)	$-\log F_\lambda$ (erg cm^{-2} s^{-1} Å^{-1})								Δ m (mag)			
	(1)	(2)	(3)	(4)	(5)	(6)	(7)	(8)	(5)-(3)	(5)-(4)	(8)-(3)	(8)-(7)
	1.11.79	4.8.81	5.8.81	12.3.82	26.3.82	27.9.82	16.11.82	20.3.83	Δm_{out}	Δm_{bur}	Δm_{tot}	Δm_{in}
3200	-	10.37	10.30[a]	10.34	10.30[a]	-	-	10.74	.00	-	1.10	-
3110	-	10.44[b]	10.27[ab]	10.31	10.31[a]	-	-	10.72	.10	-	1.12	-
3005	-	-	10.38[ab]	10.22	10.24[ab]	-	-	10.63	-.35	-	.70	-
2905	-	-	10.45[ab]	10.46[b]	10.45[ab]	-	-	10.88	.00	-	1.07	-
2820	-	-	10.50[ab]	10.50	10.51[a]	-	-	10.97	.00	-	1.17	-
2735	-	-	10.53[ab]	10.61[b]	10.58[a]	-	-	10.98	.12	-	1.12	-
2615	-	-	10.81[ab]	10.95	10.81[a]	-	-	11.26	.00	-	1.12	-
2495	11.11[b]	10.95[b]	10.84[a]	10.83	10.86[a]	-	-	11.35	.05	-	1.27	-
2405	11.38	11.31	11.43	11.21[c]	11.33	-	-	11.78	-.25	-	.87	-
2295	11.29	11.32	11.33	-	11.26	-	-	11.70	-.32	-	1.07	-
2205	11.40	11.35	11.46	-	11.34	-	-	11.76	-.30	-	.75	-
2120	11.36	11.35	11.38	-	11.28	-	-	11.78	-.25	-	1.00	-
2035	11.31	11.33	11.42	-	11.26	-	-	11.76	-.40	-	.85	-
1950	11.20	11.21	11.22	11.09	11.10	-	11.66[a]	11.62	-.30	.02	1.00	-.10
1795	-	-	11.18[a]	11.05	10.94[ab]	-	11.55[a]	11.51[a]	-.60	-.11	.82	-.10
1685	-	11.91[b]	11.82[b]	11.57	11.43	12.22	12.30	12.17	-.97	-.35	.87	-.32
1595	-	11.87[b]	11.84	11.59[c]	11.36	12.26	12.31	12.20	-1.20	-.57	.90	-.27
1500	-	12.38	12.41	11.91[c]	11.71	12.71	12.74	12.43	-1.75	-.50	.05	-.77
1405	-	12.72	12.73	-	12.17	12.96	12.97	12.82	-1.40	-	.22	-.37
1335	-	12.92[c]	12.86[c]	-	12.47	13.04[c]	13.03[c]	12.89[c]	-.97	-	.07	-.35
1304	-	12.62	12.66	-	12.59	12.72	12.74	12.71	-.17	-	.12	-.07
1240	-	12.90[c]	12.89[c]	-	12.80[c]	13.04[c]	13.03[c]	12.98[c]	-.22	-	.22	-.12
m_{FES}	-	3.25	3.25	3.20	3.22	3.69	3.98	4.10	-.03	.03	.85	.12

Notes to Table 2.
a) Small aperture
b) Over-exposed
c) Under-exposed

a) Out-of eclipse flux variability

Spectra (3) and (5), both taken out of eclipse, show remarkable variations of the flux in the spectral range 1300–2150 Å. The flux on March 26, 1982 (5) is higher than the flux on August 5, 1981 (3); the difference increases towards shorter wavelengths, while at $\lambda \gtrsim 2150$ Å there are practically no flux variations.

b) Out-of-eclipse line variability

In the range 1400–1600 Å, the spectral absorption lines are systematically deeper in the "active" phase (5) than at all other epochs. Moreover, in the same spectral range, a detailed comparison between spectra (3) and (2), not reported in Fig. 1, shows variations of the line profiles, on a timescale of 15 h.

c) Greyness of the eclipse

In the wavelength range 2150–3200 Å the totally eclipsed spectrum (8) on March 20, 1983 differs from the nearly identical out-of-eclipse spectra, (3) and (5), only by a shift in the logarithmic flux scale. This means that the UV depth of the eclipse is almost constant with wavelength (as it is in the visible).

d) Invariance of the λ 2200 absorption feature

Comparing spectrum (8), with (3) and (5), the wide absorption feature at $\lambda \simeq 2200$ Å shows no obvious phase-dependent variation, and no deepening during the eclipse.

e) Eclipse vanishing at short wavelengths

Complex behaviour is displayed in the range 1300–1700 Å. The flux during the partial phase on Nov. 16, 1982 (7) is lower than during totality (8); the effect of the variability described in a) is thus evident. Moreover, by comparing eclipsed spectra (7) and (8) with non-eclipsed ones (3) and (5), it appears that the depth of the eclipse decreases, and gradually vanishes, towards the shortest wavelengths.

Quantitative measurements of the continuum fluxes, for all the 8 spectra considered, are given in Table 2 (left part). Values of monochromatic fluxes are tabulated for selected wavelengths representing "windows" over the continuum, which is supposed to be matched by a curve passing through the highest points of the spectrum (Castelli et al., 1982). On the last line the corresponding visual magnitudes, obtained from Fine Error Sensor (FES), are reported; values from (1) to (6) are taken from Chapman et al. (1983), while (7) and (8) are derived from our observations, using the same calibration (Holm and Rice, 1981).

(422)

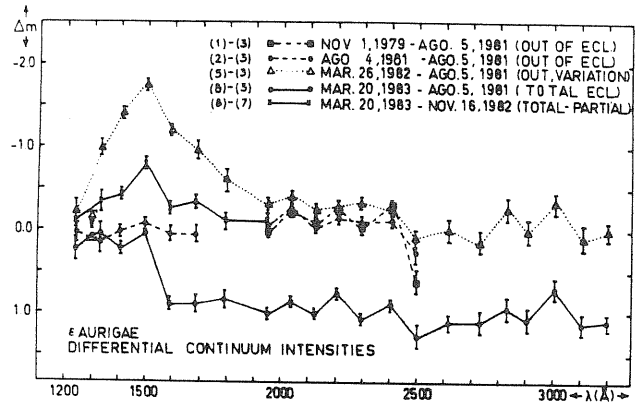

Fig. 2. UV variability. The differences in magnitude between various phases, vs. wavelength, are given. The lower solid line represents the depth of total eclipse, while the dotted line shows out-of-eclipse activity

Flux variations, for significant pairs of spectra, are given in terms of differences of monochromatic magnitudes in Table 2 (right part), and are plotted in Fig. 2. In particular, "(5)–(3)" is the amplitude of the "activity" observed out of eclipse, reaching a maximum of 1.75 mag at 1500 Å. "(8)–(3)" represents the depth of total eclipse, which is about 1 mag in the mid UV (slightly larger than 0.85 mag observed in the visible), but shortward of 1500 Å is masked by intrinsic variability prevailing in the far UV. For instance, "(8)–(7)" shows that at 1500 Å the flux measured during totality is surprisingly 0.8 mag larger than the flux in the partial phase.

Monochromatic light curves, derived from Table 2, are shown in Fig. 3. At long wavelengths the drop due to the eclipse is evident, while at short wavelengths the behaviour is complicated because of intrinsic activity. The light curve at λ 1304, corresponding to the O I lines, shows little or no evidence of the eclipse; moreover, it is practically insensitive to the out-of-eclipse activity.

Error bars, in Figs. 2 and 3, are estimated taking into account the uncertainty due to the small-aperture fitting procedure, and the effects of over-exposure or under-exposure.

Discussion and conclusions

From our set of eclipsed and uneclipsed spectra, we derive the basic result that the amplitude of the eclipse of ε Aur is reduced at $\lambda \lesssim 1400$ Å. We think that the contradiction with the data reported by Chapman et al. (1983), who found an opposite trend in the wavelength dependence of the eclipse, is only apparent. In fact, Chapman et al. consider a spectrum taken out of eclipse on April 13, 1982, during an "active" period [near spectrum (5)], and compare it with a partially eclipsed spectrum taken on Sept. 21, 1982, during a "quiescent" period [near spectrum (6)]. This causes an apparent deepening of the eclipse in the short-wavelength range, which is dominated by intrinsic variability.

Eclipse depth decreasing at short wavelengths gives strong support to those models of ε Aur that predict the existence of a hot secondary component dominant in the far UV, and not affected by the eclipse because it passes in front of the primary. For the same reason, Plavec's model (Plavec, 1982), which locates the hot object inside the primary component (supposed to be a disk simulating an F supergiant), seems to be contradicted by observation.

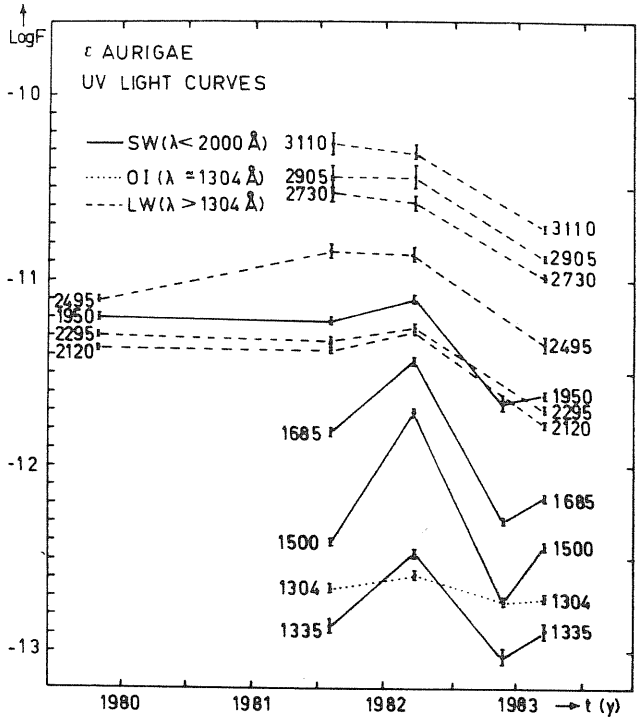

Fig. 3. Monochromatic UV light curves. Fluxes are in erg $cm^{-2} s^{-1} Å^{-1}$. The O I λ 1304 curve (dotted line) seems to be unaffected both by the eclipse and by intrinsic activity

Let us come to the source of far UV variability. Continuum fluctuations could be simply an intrinsic property of the hot secondary, but we need a mechanism also for line variations. Probably, variability could come from a presumed non-homogeneous structure of the extended body surrounding the secondary (and already responsible for the eclipse of the primary); in this case, according to the degree of clumpiness, the light of the secondary should be more or less attenuated, so that its spectral lines could be more or less filled by continuous emission of the extended body. Another possibility is the intrinsic variability of the extended body itself; an increase in its opacity may explain both the increase in the flux emitted (getting closer to black body conditions), and the deepening of the absorption lines (supposing they are formed in the body itself).

Since there is no remarkable deepening of the λ 2200 absorption feature, associated with the eclipse, this fact puts serious constraints on the nature of the eclipsing body, ruling out its being made of standard-composition dust. Therefore, if dust is present, it can be found only in small quantities around the secondary; otherwise it may be located in an external envelope surrounding the whole system. The existence of this extended structure is suggested by the emission line O I λ 1304, which is practically independent of the eclipse and of UV variability; a similar behaviour is also shown by the emission wings of the chromospheric lines of Mg II $\lambda \sim 2800$, which are observable on IUE high-resolution spectra.

Finally, let us examine the greyness of the eclipse. There are indications that, in the near and mid UV, the eclipse is deeper than in the visible (Ake and Simon, IAU Circ. 3763); also the values given in our Table 2 confirm this trend, but the observed disagreement between optical and UV depths may be reduced to about 0.1 mag if only well exposed regions of the large aperture-

spectra are considered. Anyway, in addition to electron scattering, which may provide the grey component of the eclipse (as suggested by Hack, 1961), another contribution to the opacity of the eclipsing body must be present in the ultraviolet. This could be produced by strong blended absorption lines from the eclipsing body, affecting the position of the continuum (particularly on low-resolution spectra).

Acknowledgements. The procedures of decoding and plotting the IUE spectra were performed at the Computing Center of the Trieste Astronomical Observatory.

Programs by C. Morossi, M. Ramella, C. Allocchio, and L. Crivellari were used. We thank Mrs. L. Canziani for kindly typing the manuscript.

References

Castelli, F., Hoekstra, R., Kondo, Y.: 1982, *Astron. Astrophys. Suppl.* **50**, 233

Chapman, R.D., Kondo, Y., Stencel, R.E.: 1983, *Astrophys. J. Letters* **269**, 17

Gyldenkerne, K.: 1970, *Vistas in Astronomy* **22**, 199

Hack, M.: 1961, *Mem. S. A. It.* **32**, 351

Hack, M., Selvelli, P.L.: 1979, *Astron. Astrophys.* **75**, 316

Handbury, M.J., Williams, I.P.: 1976, *Astrophys. Space Sci.* **45**, 439

Holm, A., Rice, G.: 1981, IUE *Newsletters* **15**, 74

Huang, S.: 1965, *Astrophys. J.* **141**, 976

Plavec, M.J.: 1982, in *Advances in Ultraviolet Astronomy: 4 years of* IUE *Research*, NASA C.P. 2238, p. 526

Note added in proof: New IUE observations, performed by S. Ferluga on August 8, 1983 in mid-totality phase, fully confirm Results from a) to e).

Paper III

SESSION 5: DISCUSSION (168)
"Effects of Variable Mass Loss on the Local Stellar Environment"
1983 Trieste Workshop - R.Stalio, R.Thomas Eds.: 1984, CLUET-Trieste Italy

- FERLUGA:

The case of Epsilon Aurigae
UV spectroscopy during the eclipse

I would like to report on the ultraviolet observations we recently made with IUE of ϵ Aur during the eclipse.

The spectrophotometric eclipsing binary ϵ Aur can be included among the restricted class of ζ Aur systems since it also contains a supergiant component, currently classified F0. However the case of ϵ Aur is very particular because the secondary component is a peculiar cool object -- appearing extended and obscured during the eclipses -- which may be composed by gas and/or dust. Its real physical nature is not yet well established.

Since the orbital period is very long (27.1 years), the eclipse, which is presently going on (from 1982 to 1984), is a rare occasion for studying the nature of this system. Recent UV observations by Boehm, Ferluga and Hack (Astron. Astrophys. 130, 419, 1984) seem to prove that the obscure secondary is embedding a hot object (presumably a B star). This is also found in the standard ζ Aur systems, but in ϵ Aur the geometry of the eclipse is somehow reversed: it is the secondary which eclipses the primary, and not vice-versa. In the ζ Aur systems it happens that normally the envelope of the primary supergiant eclipses the companion, so that one can see the lines of the envelope, superimposed over the spectrum of the secondary. In the case of ϵ Aur, on the contrary, one can see the the primary's envelope being eclipsed by the non-luminous extended companion.

We shall now discuss some preliminary data concerning the first UV observations of this phenomenon. The observations were made with IUE at eclipse phases corresponding to the end of the ingress (i), early totality (ii), and mid-totality (iii); by comparison a pre-eclipse spectrum (o) has also been studied. Only the region from 2400 to 3200 A can be studied at high resolution.

By comparing spectra taken at different phases, it clearly appears that, except for a minority of special features which we shall discuss later, almost all the lines show the "normal" phase-dependence presented in Figure 1. At ingress (i) there is a widening of the red side of the profiles. At early totality (ii) the effect is enhanced so that the lines appear deeper and red-shifted. At mid-totality (iii) the lines become deeper and larger but no more shift is present.

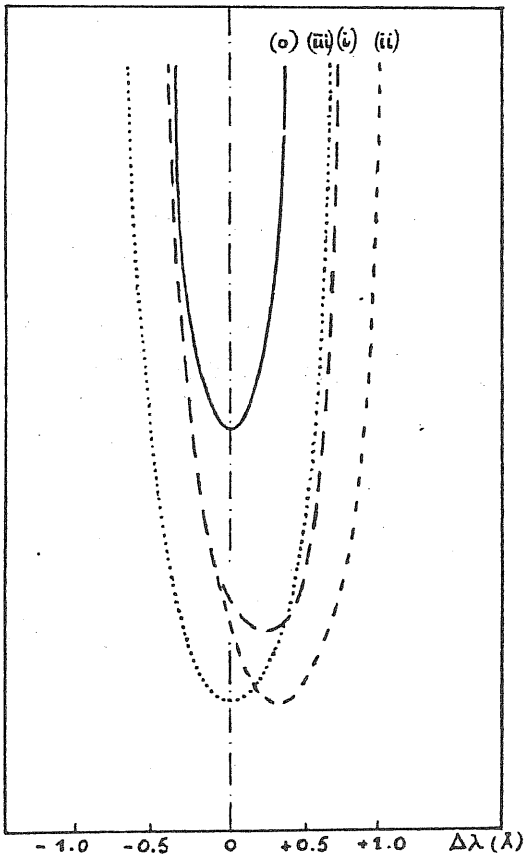

(o) Pre-eclipse, ———
(i) mid ingress, — — —
(ii) early totality, – – – – –
(iii) mid totality, ...

Figure 1: The "normal" phase-dependence of mid-UV lines (schematic).

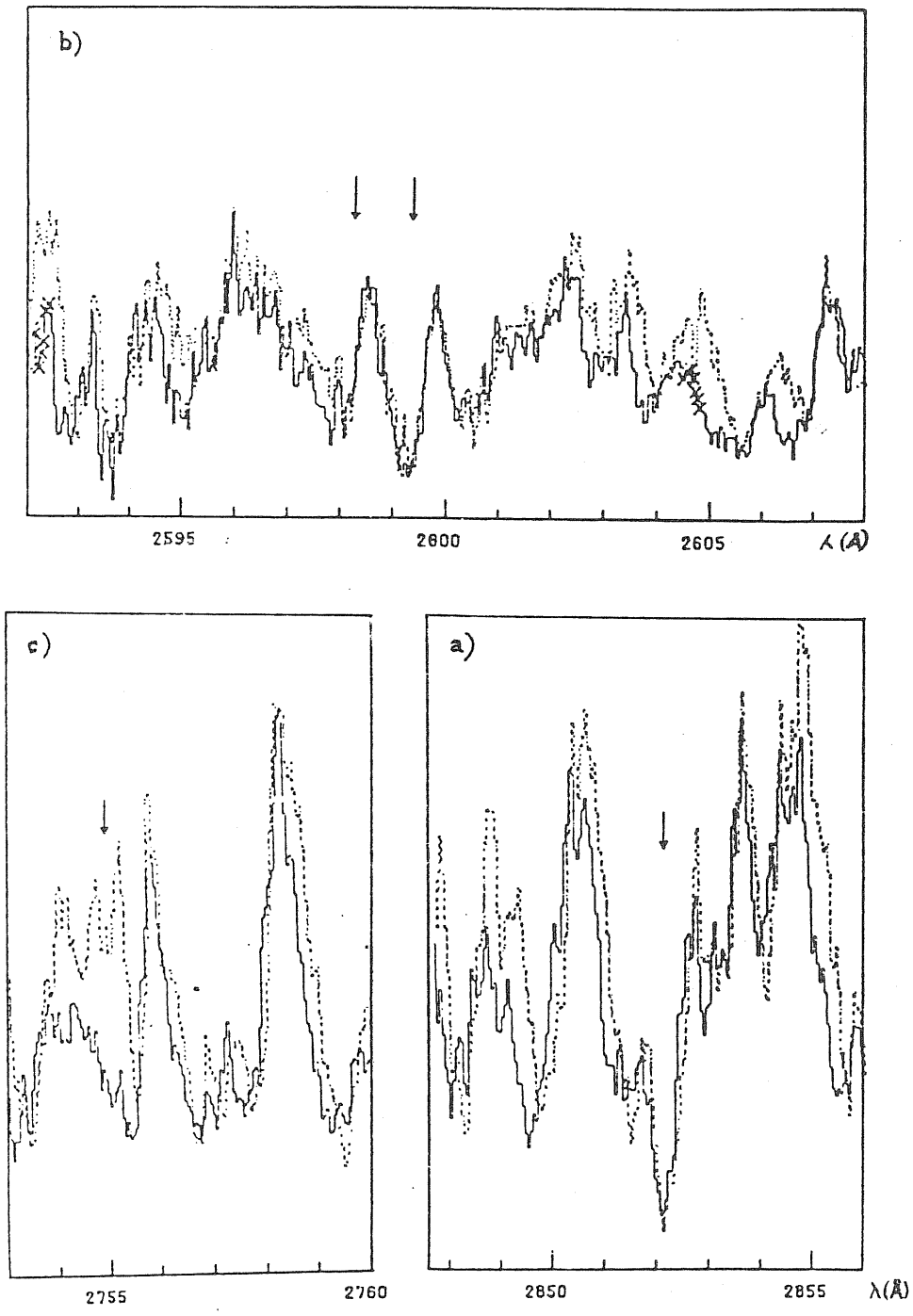

Fig 2. - "Special" UV lines during eclipse, in phases of end ingress (dotted line), and mid totality (solid line). Vertical scale is linear.

a) "Steady" line, with pure absorption: MgI λ 2852 resonance.
b) "Steady" lines, with emission: FeII λ 2598 and λ 2599 resonances.
c) "Shell absorptions", at λ 2755 Å.

As in the visible, this behaviour can be easily explained as an effect of the overcoming shell spectrum (Hack, Mem. S.A.It., 32, 351, 1961), produced by the interposition of the rotating eclipsing body, which passes in front of the primary. In the eclipsed spectrum there are some "special features" (Figure 2) which do not undergo this phenomenon. In particular there are: (a) Steady absorption lines, with no redshift effect during ingress: e.g. the Mg I resonance line at λ 2582. (b) Steady outcoming emissions, revealing themselves as independent emission components only when the overwhelming primary continuum is lowered by the eclipse: e.g. the Fe II (λ 2600) and Mg II (λ 2800) resonance lines. (c) Shell absorption lines, which appear particularly enhanced during totality: e.g. at λ 2755.

The explanation for the special behaviour of these features during the eclipse can be found, considering that the same features appear as "peculiarities " also over the uneclipsed spectra. In fact they do not fit the synthetic spectrum computed by Castelli et al. (Astron. Astrophys. Suppl. 50, 233, 1982); hence they are interpreted as to be formed inside an envelope surrounding the supergiant F star.

The different behaviours (a), (b) and (c) suggest the existence of different regions of line formation inside an extended envelope surrounding the primary and, probably, embedding the whole system. A detailed analysis of such phenomenon could then provide important information concerning the extension and physical conditions of the envelope around the F supergiant. This is an interesting point since the F supergiants are rather uncommon compared to the most usual K and M supergiants. It was suggested that the strange nature of the secondary in ϵ Aur could be simply related to the presence of a somehow peculiar primary.

- COHEN:

Which is the change in the magnitude of the system during totality?

- FERLUGA:

The depth of the eclipse corresponds to 0.8 mag; hence the light is reduced by about 50%. The minimum is flat, so that the eclipse is considered to be total. On the other hand, the spectrum of the primary remains visible, and this is a problem. A lot of models have been proposed to explain this apparent contradiction.

Paper IV

7th. European Regional Astronomy Meeting of IAU (Florence, 12-16 Dec. 1983) - Abstracts.

THE ECLIPSE OF EPSILON AURIGAE IN THE ULTRAVIOLET; LOW AND HIGH RESOLUTION SPECTROSCOPY

S. Ferluga, M. Hack
Trieste University, Trieste Astronomical Observatory

The eclipsing binary Epsilon Aur (FO Ia, +?) has a period of 27.1 years, and during 1983 is undergoing total eclipse. Past observations showed remarkable peculiarities (Gyldenkerne, 1970). The system seems to contain an extended non-luminous body,and various models have been proposed for this misterious secondary, e.g. by Hack (1961), Huang (1965), Handbury and Williams (1970).

We have used I.U.E. spectroscopic observations, at low and high resolution, to study respectively the continuum (a) and the lines (b), during the eclipse phases.

a). From low resolution spectra, taken in early phases of the eclipse, we obtained the following results (Boehm, Ferluga and Hack,1983), now fully confirmed by recent mid-totality observations.

A hot component, dominant in far UV, is associated with the extended body that eclipses the primary; far UV variability observed also out of eclipse, may originate from this component or from the extended object itself. Moreover the eclipsing body cannot be made of dust, and electron scattering is thus supposed to be responsible for the greyness of the eclipse. Finally the system is embedded in a large rarefied gaseous envelope.

b) . We are now using high resolution spectra, to study the properties of the envelope.

We find that lines can be classified as "normal" or "special", with respect to eclipse. In the first group we put the majority of lines, displaying a phase-dependent bahaviour; in the second group we collect a small number of lines, which appear to be eclipse-indipendent and often show emission components. This classification can be compared with the one given by Castelli et al. (1982), concerning lines which are "peculiar" out of eclipse, and seem to arise from an expanding circumstellar envelope; one then drives the following conclusion. The circumstellar envelope, outflowing from the primary, extends both internally and externally with respect to the orbit of the secondary.

References

Boehm, C., Ferluga, S. and Hack, M.: 1983, Astron. Astrophys., 130, 419.
Castelli, F., Hoekstra, R. and Kondo, Y.,: 1982, Astron. Astrophys. Suppl. Ser., 50, 233.
Hack, M.: 1961, Mem. Soc. Astron. Italiana, 32, no. 4.
Handbury, M.J. and Williams, I.P.: 1976, Astrophys. and Space Sci., 45, 439.
Huang, S.: 1965, Astrophys. J., 141, 976.

Paper V

OBSERVED PECULIARITIES DURING THE ECLIPSE OF EPSILON AURIGAE

Steno Ferluga

1. University of Trieste
2. S.I.S.S.A. Trieste, Italy

Margherita Hack

Astronomical Observatory of Trieste, Italy

ABSTRACT

Low and high resolution IUE spectra have been used, in order to study the totality phase of the eclipse of Epsilon Aurigae. In the far UV, the peculiar intrinsic variability, produced by a hot companion of the F star, is studied in function of wavelength and time. In the mid UV, the phase-dependence of lines is examined at high resolution, putting in evidence the existence of normal and peculiar features. Finally the unexpected mid-eclipse brightening, discovered photometrically in the visible, is detected also in the UV continuum.

Keywords: Peculiar binaries, Epsilon Aurigae, Ultraviolet Spectroscopy, Secondary Component, Shell Spectrum, Light Curve.

1. INTRODUCTION

The two-year-long eclipse of the peculiar binary Epsilon Aurigae (F0 Ia + ?) is now coming to its end, on May, 1984. It is then possible to give a first outlook at the complete evolution of the phenomenon; this eclipse is the first one to be studied in the UV, since the period is of 27.1 years. The peculiarities of the system are well known and different models have been proposed in order to explain the nature of the obscure secondary, which is responsible for the eclipse of the visible F star; e.g. see the papers quoted in Ref. 2,6.

The latest observations have shown an enhancement of both far-UV and far-IR excesses, during the eclipse (Ref. 2, 1). These new data support the picture of an eclipsing body, which may contain both a hot and a cool component: probably it could consist in a late-B star surrounded by an extended cloud of gas and dust. Shortward 170 nm the hot object, responsible for the UV excess, shows a strong variability, which appears to be eclipse-independent.

2. THE FAR-UV BEHAVIOUR

In order to study the variable UV excess, the method by Hack and Selvelli (Ref. 8, hereafter HS) is applied. The same theoretical flux distribution for the primary F star, and the same interstellar correction are assumed. Now, in addition, the depth of the F-star's eclipse at the various phases, obtained from FES counts, is taken into account. By these means, one can compute the expected flux distribution F_e from the primary at any time, and compare it with the observed continuum F_o received from the system at different epochs. The excess quantity

$$\eta = F_o / F_e - 1 \qquad (1)$$

is then regarded as the emissivity (in units of F_e) of the peculiar secondary component.

We have analized the contribution of the secondary component in function of wavelength and time, referring to a set of seven IUE low-resolution spectra. These spectra had been already considered in a previous paper by Boehm, Ferluga and Hack (Ref. 2, hereafter BFH), and they were labeled therein with numbers from (2) to (8).

For measuring F_o, the continuum was traced on BFH spectra, in the same way as it was originally done by HS in their first UV observation of Epsilon Aurigae (spectrum 0). The expected flux F_e was then computed on the basis of the quantities F_{pred}, F_{obs}, and F_{corr}, tabulated by HS. Out of eclipse one has, by definition of quantities in HS:

$$F_e = F_{pred} \cdot (F_{corr} / F_{obs})^{-1} \quad , \qquad (2)$$

while with an eclipse depth Δm it is obviously:

$$F_e = F_{pred} \cdot (F_{corr} / F_{obs})^{-1} \cdot 10^{-0.4\,\Delta m} \quad , \qquad (3)$$

where Δm is given by BFH.

The resulting excess η, given by Eq. (1), is tabulated in Table 1 for wavelengths shorter than 185 nm. It is evident that, towards the shortest wavelengths, the excess is raising over two orders of magnitude. On the contrary, longward 170 nm the excess is generally 0 (negative values are probably due to imperfections in continuum tracing and/or in compensating the interstellar absorption, and their amplitude can give an idea of the systematic errors related with this kind of determinations). At about 150 nm the secular variability has its maximum excursion, approaching a factor of 8.

Figure 1 shows the behaviour of the excess η in function of wavelength, shortward 165 nm, for selected spectra taken at different epochs before and during eclipse. Apparently , a rough parallelism

Table 1.

η	(0)	(2)	(3)	(4)	(5)	(6)	(7)	(8)
Date	'78	'81	'81	'82	'82	'82	'82	'83
λ (nm)	Apr 19	Aug 4	Aug 5	Mar 12	Mar 26	Sep 27	Nov 16	Mar 20
130	52	77	77	...	127	79	106	149
140	7.5	9.0	9.0	...	32	6.7	11	17
145	6.8	8.2	8.2	...	38	4.9	8.3	14
150	6.9	6.8	6.8	18	34	3.2	5.7	6.2
155	1.6	2.3	2.3	5.6	13	0.8	1.8	3.5
160	1.0	1.8	...	3.1	6.6	0.5	0.9	1.7
165	0.4	1.2	...	1.9	4.4	0.2	0.5	1.1
170	-.4	-.1	...	0.3	0.9	-.4	-.3	-.2
175	0.0	-.1	...	0.6	0.8	...	-.2	-.1
180	-.3	0.0	...	0.4	0.7	...	-.1	0.0
185	-.3	-.1	...	0.3	0.6	...	-.2	0.0

Table 2.

IUE	High Resolution Observations			
Sp.	Cam.	Image . Ap	Date	Observer
H1 *)	LWR	11247 . L	1981, Aug. 5	Stickland
H2	"	14645 . L	1982, Nov. 16	Molaro
H3	"	15522 . L	1983, Mar. 20	Morossi
H4 *)	"	15676 . L	1983, Apr. 8	Ake
H5 *)	"	15766 . L	1983, Apr. 18	Chapman
H6	"	16553 . L	1983, Aug. 8	Ferluga
H7	LWP	2763 . L	1984, Jan. 20	Boehm

*) Spectra released by VILSPA Data Bank

of curves can be noticed; if real this should mean that variability is not significantly depending on temperature. Hence, the phenomenon should rather be caused by inhomogeneities in the opacity of the cool and extended rotating body, in which the hot source is embedded (Ref. 1). Equivalently, the effective observable surface of the source could vary, by as much as a factor of 8.

Finally Figure 2 plots the secular variability of the excess at λ=145 nm, where the effect is particularly evident, and at λ = 165 nm where it is weaker. As one can see, an upper limit can be set on the timescale of these fluctuations, which appears not to exceed a few months. On the other hand, at short timescales, no variation was revealed over a one-day interval (1981, Aug.4-5).

3. THE MID-UV LINES

High resolution spectroscopic IUE observations have been used, in order to study the effects of the eclipse over the lines, in the mid UV. It was found by Ferluga and Hack (Ref. 5) that "normal" and "special" lines can be recognized with respect to the eclipse, since the first ones display a phase-dependent behaviour, while the others appear to be eclipse-independent. Studying in detail this phenomenology, a further characterization and classification of "normal" and "peculiar" features can now be performed; some simple physical interpretations come then strightforward.

3.1 "Normal" lines

Referring to Table 2, one can compare an uneclipsed spectrum (H1), with spectra taken at different phases of the eclipse (H2 at end ingress; H3 at early totality; H4,5,6 at mid totality; H7 at early egress). Since generally high-resolution spectra of Epsilon Aur. are underexposed at short wavelengths, we shall consider hereafter only the region from 240 nm to 320 nm. Examining the plots, as a first result one obtains that, except a few special lines examined later in 3.2, almost all the lines display a standard phase-dependent behaviour; this can be described as follows.

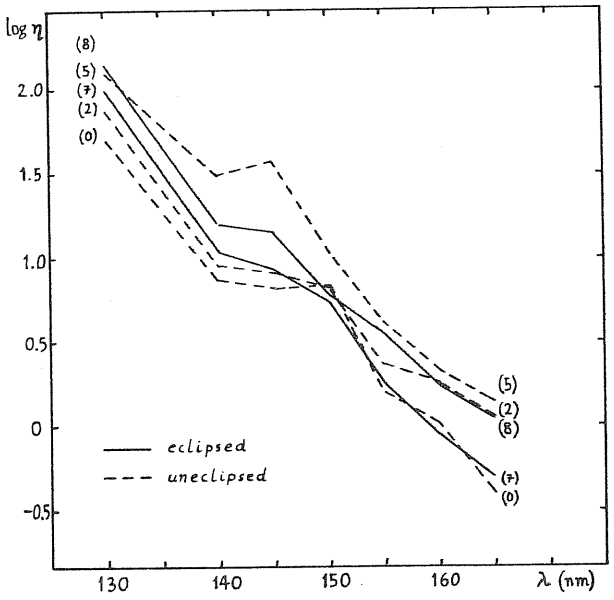

Figure 1. The variable UV excess, as a function of wavelength.

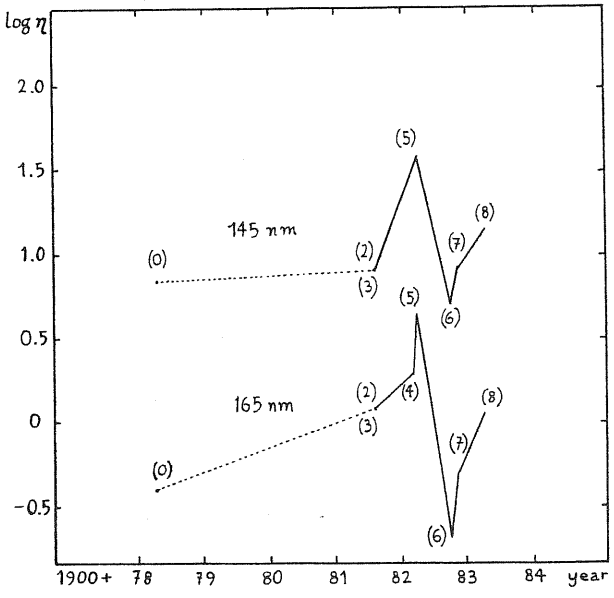

Figure 2. The variable UV excess, as a function of time.

(a) At ingress (H2), a widening of the profile on the red side appears, suggesting the presence of an additional unresolved absorption component, with a redshift corresponding to a velocity of about +30 km/sec.

(b) In early totality (H3) the effect is even more evident, presumably because of a corresponding enhancement of the red-shifted component. Although generally the two components are unresolved, giving the global appearence of a single larger and red-shifted line, there are also some cases in which a double-core structure can be directly observed.

(c) At mid-totality (H6), the lines remain deeper and larger with respect to out-of-eclipse ones, but no apparent redshift is present, as if the two absorption components were superimposed. Sometimes, a complex structure seems to be convoluted with the instrumental profile.

(d) At egress (H7) the widening of the profile appears at the violet side of the lines, and the situation is symmetrical to the one of case (a).

We must note that similar phenomena have already been recognized on the visible spectra, in occasion of the past eclipses, and have been interpreted as due to the "shell spectrum". It consists in the presence of a sharp absorption component (visible optical spectra) over F-star's lines; since this component is red-shifted during ingress and violet-shifted during egress, it must then be produced by a rotating eclipsing body, which is supposed to be a "shell" around the secondary (Ref. 7). This is then the first time, that it is possible to detect the shell spectrum in the UV; also if the resolution of IUE is not sufficient to show the shell component separately, its influence over the convoluted instrumental profile is evident.

3.2 "Special" lines

Some isolated lines in the mid-UV, such as resonance lines of MgI, MgII and FeII, do not partecipate to the general "oscillation" of profiles during the eclipse. Among these "special" lines there are some features, which moreover seem not to partecipate in the general lowering of the continuum, corresponding to the depth of the grey eclipse; as an effect, these features "come out" in the eclipsed spectra, appearing as emission components of P Cygni-like profiles. Therefore we can classify those lines, which display a special behaviour in eclipse, in the following way.

3.2.1 "Steady lines", with absorption profile. They are rare to be found; the best example is the strong MgI resonance line at 285.2 nm. Intermediate cases, displaying a more or less reduced oscillation during the eclipse, are common; and example can be MnII resonance lines at 257 and 259 nm.

3.2.2 "Steady lines", with outcoming emission. They can be represented by the striking case of MgII resonance doublet at 280 nm, where the existence of an eclipse-enhanced emission feature was already detected by Chapman et al. (Ref. 4). More generally, we find that the presence of an emission component is an extensive property of the stronger lines of FeII UV multiplets, especially (6), (62) and (63); the effect is more evident in the strongest lines, such as FeII resonance lines at 259.8 and 259.9 nm.

3.2.3 "Shell absorptions". Some absorption lines display occasional enhancements during totality, e.g. the features at 275.5 nm. Their identification, together with the complete classification of eclipse-dependent and independent features, is in progress.

3.3 Interpretation

In order to give an explanation to these observed phenomena, a key should be the following fundamental coincidence: all the lines, displaying the eclipse-independent behaviour described at points 3.2.1 and 3.2.2, were classified as "peculiar" out of eclipse, by Castelli et al. (Ref. 3). The reason was that the profile didn't fit the synthetic spectrum, because of variable blue shift or because a possible emission contribution, which were attributed to an F-star's expanding envelope.

On the other hand, there is also a group of lines classified "peculiar" out of eclipse, and hence "F-envelope lines", which in eclipse show the normal phase dependence described in 3.1 . This group represents about 50% of F-envelope lines; among them we find for instance TiII (5), CrII (5) (6), and MnII (5) UV multiplets.

Hence, the simplest interpretation that could be suggested is the following. F-envelope lines behave as "normal" (3.1) or "special" (3.2) with respect to the eclipse, correspondingly, if their intensity is "comparable" or "dominant" with respect to the shell spectrum. In case of a pure absorption profile, the normal phase-dependent F-envelope lines (3.1) seem to be probably chromospheric. On the contrary, the special steady behaviour (3.2.1) can be of interstellar origin (MgI resonance), or produced in an extended region surrounding the system. The existence of this region is proved by the presence of special lines, which do not partecipate to the general lowering of F-star's spectrum during the eclipse, and hence are revealed as outcoming emission features (3.2.2): beeing uneclipsed, these lines must be produced in a circumstellar envelope, which is external to the secondary's orbit around the primary. Finally the special absorption features, which appear during totality (3.2.3), must clearly be formed in a zone around the secondary.

Anyway to the test these indications, a detailed spectroscopical analysis is in progress, also on the basis of a large set of visible spectra that we have taken at the different phases of the eclipse at the Observatoire de Haute Provence.

4. THE MID-ECLIPSE BRIGHTENING

4.1 General

A rather complete light curve of the present eclipse is now available, from the latest UBV photometry report (Ref. 9). The most outstanding feature seems to be an apparent brightening of more than 0.2 mag, centered at mid totality, and having a duration of about 5 months. Small fluctuations, already observed in past eclipses, were generally interpreted as intrinsic cepheid-like activity of the F star (Ref. 6). Anyway, it was noticed that these fluctuations were larger in totality than out of eclipse, and hence a possible

relation with the eclipsing body was suspected. Now the strong intensity, and the exact mid-totality collocation of the present brightening, seem to favour the latter explanation ; for instance, the eclipsing body could display variable or differential transparency, e.g. as happens in the case of a ring-like structure, with a large opening in the center (Ref. 10). Unfortunately, the data coverage of the light curve at mid totality is very poor in the present eclipse, as well as in the past ones, because of seasonal observational constraints (proximity of the sun), and this could have caused the phenomenon not to be recognized during the past eclipses.

4.2 IUE Observations

In order to study the UV light curve during totality, a set of five recent IUE low-resolution spectra is now available, in addition to the BFH sample. These new spectra concern the central phase of the eclipse, and are listed in Table 3. Among them, the first three (9-11) are grouped at the beginning of the mid-totality brightening, the fourth (12) corresponds to its decreasing phase, and the last one (13) is taken just after the 3rd contact. Only large aperture images are considered.

Now, measuring the continuum at selected wavelenghts with the some procedure used by BFH, it is possible to extend their UV light curves at the whole totality phase. Then, by comparison with high-resolution spectra (H4-H7), which are contemporary to low-resolution ones (9,10,12,13), important complementary information can be derived about the beahviour of the lines. Clearly, this analysis is limited to the mid-UV spectral region (λ>200nm), since at short wavelength the phase-dependent behaviour is perturbed by the contribution of the variable far-UV source. In conclusion, one obtains the following results.

(a) The mid-eclipse brightening appears also in the UV, and it is even more pronounced towards the shorter wavelengths. This effect seems to follow the general trend, of the "quasi-greyness" of the eclipse; that is, one observes a slight deepening of the light-curve features, in the sense of decreasing λ. (for instance, the average depth of the eclipse in the near IR is 0.7 mag, while in the visible it becomes 0.8 mag and in the UV it ranges between 0.9 and 1.0 mag). In particular the eclipse depth, at 2nd and 3rd contact, seems to be enhanced towards the shorter wavelenghts.

(b) The mid-eclipse brightening depends only on the continuum which undergoes a general raising, while no significant variations of the lines occur during the phenomenon. So, also if one cannot exclude the hypothesis of intrinsic fluctuations of the F star, it seems that at mid totality the almost grey eclipsing body has apparently reduced its optical thickness and/or its projected area over the F star. Hence as a first approximation, the geometry of an eclipsing ring with a large central opening, seen obliquely (Ref. 10), seems to reproduce well the observed mid-eclipse effect.

TABLE 3.

IUE		Recent Low Resolution Observation		
Sp.	Cam.	Images	Date Observer	λ_{min} , λ_{max} (nm)
9 *)	SWP	19671		120 , 160
	SWP	19672	1983 Apr. 7	160 , 190
	LWR	15674	Ake	190 , 252
	LWR	15673		252 , 330
10 *)	SWP	19751	1983 Apr.18	150 , 190
	LWR	15767	Chapman	190 , 252
11 *)	SWP	19782		120 , 160
	SWP	19780	1983 Apr.21	160 , 190
	LWR	15790	Ake	190 , 252
	LWR	15788		252 , 330
12	SWP	20643		120 , 170
	SWP	20644	1983 Aug. 8	170 , 190
	LWR	16552	Ferluga	190 , 240
	LWR	16551		240 , 320
13	SWP	22055		120 , 168
	SWP	22054	1984 Jan.20	168 , 198
	LWP	2671	Boehm	234 , 264
	LWP	2672		264 , 330

*) Spectra released by VILSPA Data Bank.

5. REFERENCES

1. Backman D E, Becklin E E, Cruikshank D P, Joice R R, Simon T and Tokunaga A 1984, Astroph.J. in Press.

2. Boehm C, Ferluga S and Hack M 1984, Astron.Astroph. 130, 419.

3. Castelli F, Hoekstra R and Kondo J 1982, Astron.Astroph. Suppl. 50, 233.

4. Chapman R D, Kondo J and Stencel R E 1983, Astroph.J. Lett. 269, 17.

5. Ferluga S and Hack M 1983, Seventh European Reg. Meeting of IAU (Florence), abstracts p. 81.

6. Gyldenkerne K 1970, Vistas in Astronomy 12, 199.

7. Hack M 1959, Astroph.J. 129, 291.

8. Hack M and Selvelli P L 1979, Astron.Astroph. 75, 316.

9. Hopkins J L and Stencel R E 1984, Epsilon Aur Eclipse Campaign Newsletter no. 10, 2.

10. Wilson R E 1971, Astroph.J. 170, 529.

Astron. Astrophys. 144, 395–402 (1985)

ASTRONOMY AND ASTROPHYSICS

High-dispersion spectroscopy of the eclipse of Epsilon Aurigae at visible and ultraviolet wavelengths*

S. Ferluga[1,2] and M. Hack[2,3]

[1] Scuola Internazionale Superiore di Studi Avanzati (SISSA), Str. Costiera 11, I-34136 Trieste, Italy
[2] Università di Trieste, Istituto di Astronomia, Via Tiepolo 11, Succ. TS 5, I-34131 Trieste, Italy
[3] Osservatorio Astronomico di Trieste, Via Tiepolo 11, I-34131 Trieste, Italy

Received August 24, accepted October 5, 1984

Summary. Visual observations: We report some preliminary results of the study of three photographic spectrograms obtained during the ingress, totality and egress phases and compare them with one spectrogram taken before the start of the eclipse. We describe the characteristics of the "shell" spectrum which are similar to those observed during previous eclipses. They can be explained by a rarefied gaseous envelope associated with the secondary and rotating in the same direction as the orbital motion. The behaviour of Hα before and during eclipse is also described.

Ultraviolet observations: Comparing a set of high-resolution IUE spectra, taken at different epochs during the eclipse, we derive the following preliminary results. The pre-eclipse far-UV activity of March '82 is accompanied in the mid-UV by a general rising of the continuum. The depth of the eclipse deviates very slightly from greyness; discrepancies with the determinations of some other authors are discussed. Additional deepening during the eclipse is found over the absorption wings of the Mg II λ 2800 doublet. The mid-eclipse brightening seems to come from a rarefaction of the material, responsible for the continuous (grey) absorption factor. Finally, no evident UV counterpart is detected for the visual brightening around the 3rd contact, probably for instrumental reasons.

Key words: stars: binaries: spectroscopic – stars: binaries: peculiar – stars: individual: ε Aur – UV radiation

1. Introduction

A coordinated campaign of spectroscopic observations has been completed, at visible and UV wavelengths, covering all the phases of the 1982–84 eclipse of the peculiar binary ε Aur. In this system, the F0 Ia primary is obscured every 27.1 yr by a mysterious companion (Backman et al., 1984; Boehm et al., 1984, hereafter BFH).

At visible wavelengths, 13 runs of spectrographic observations were carried out at various epochs during the eclipse (Table 1), using the 193 cm and 152 cm Coudé telescopes of the "Observatoire de Haute Provence" (OHP) in France.

In the ultraviolet, using the IUE satellite in the high resolution mode, 4 observational shifts (giving spectra H2, H3, H6, and H7 listed in Table 2) were performed almost simultaneously with corresponding runs in the visible; moreover, data concerning 5 other shifts of IUE high-resolution observations, performed by different authors, have been obtained from VILSPA Data Bank (Madrid). Finally, at low resolution the complete set of IUE Spectra (1)...(13) listed by BFH and by Ferluga and Hack (1984, hereafter FH) has been used, in order to extend BFH's ultraviolet light-curves for selected wavelengths, throughout the eclipse until the egress.

Preliminary results concerning optical and ultraviolet data are given in the following sections.

2. Visible wavelengths

2.1. The "shell" spectrum

Here we report some preliminary results of the study of three photographic spectrograms of Epsilon Aurigae ($\lambda\lambda$ 3600 – 5000 Å) obtained during the ingress, totality and egress phases and we compare them with one spectrogram taken before the start of the eclipse. The spectrograms were taken at the Coudé spectrograph of the 152 cm telescope of the Haute Provence Observatory. The dispersion is 7.2 Å/mm and the spectral resolution is about 0.14 Å. Only the spectrogram taken during totality, on Aug. 7, 1983, has a lower dispersion, 12.4 Å/mm, because in that period of the year Epsilon Aurigae is observable just before dawn, and only short exposures can be made. The spectrograms were reduced with the Trieste Observatory digitized microdensitometer PDS, and $\log I - \lambda$ tracings were obtained at the ASTRONET pole using the ELSPEC 11 program prepared by Pasian et al. (1982). Table 3 gives the data relative to the four spectrograms.

As during the previous eclipses, we have observed the appearance of sharp absorption components on the red side of the strong low-excitation lines during the ingress phase, and on the violet side during the egress phase. This additional spectrum can be explained by a gaseous shell associated with the eclipsing body and rotating in the same direction as the orbital motion. It has about the same excitation temperature as the photosphere of the F0 Ia primary, but a much lower density and optical depth. This is indicated by the fact that the quantum number of the last resolved Balmer line is $n = 31$ in the photospheric spectrum and $n \sim 55$ in the shell spectrum, which, from the Inglis and Teller relation, give,

Send offprint requests to: S. Ferluga

* Based on observations at the Observatoire de Haute Provence (OHP) of CNRS, and on observations by the International Ultraviolet Explorer (IUE) collected at the Villafranca Satellite Tracking Station (VILSPA) of European Space Agency, or released by the VILSPA Data Bank. Data analysis was performed at the ASTRONET pole of Trieste, using the ELSPEC/11 procedure

(396)

Table 1. OHP spectrographic observations of ε AUR

DATES	OBSERVERS	BLUE SPECTRA (IIaO)	RED SPECTRA (IIIaF)	PHASE (b)
1981, Jan. 3- 5	Faraggiana	GC 1219,1220,1223, 1224,1226,1228	GC 1221,1222,1227	Pre-ecl.
1982, Jul. 31	Böhm Franco	GB 7313	-	Early ingress
1982, Sep. 21-30	Böhm Vladilo Ferluga	GB 7480 GC 1349,1350,1354, 1355,1357	GB 7459,7463,7471, 7474,7480	Ingress
1982, Nov. 19-21	Ferluga	GC 1358,1360,1362, 1363	GB 7512,7514 GC 1359	Late ingress (H2)
1983, Mar. 18-21	Ferluga	GB 7747,7749 GC 1410,1411,1416	GB 7748 GC 1409,1412,1415	Totality (H3)
1983, Aug. 2- 7	Böhm	GB 7972,7983	GB 7970,7984	Totality (H6)
1983, Sep. 26-27	Böhm	GB 8052	GB 8051	Totality
1983, Oct. 20-23	Böhm	GB 8084	GB 8085	Totality
1983, Dec. 21-23	Böhm	GB 8120,8122,8130 8136	GB 8121,8137	Late totality
1984, Jan. 24-29	Morossi Persic Ramella	GB 8177,8205 GC 1538	GB 8178,8181	Early egress (H7)
1984, Feb. 7-11	Persic (a)	W 7484,7485,7492 X 1218	W 7491 X 1219	Early egress
1984, Mar. 17-18	Persic	GB 8238,8239	-	Egress
1984, Mar. 29	Ferluga	GC 1563	GB 8253	Egress
1984, Jul. 9	Böhm Morossi	GB 8369	-	Post-ecl.

(a) Utilizing the 193 cm telescope, while all other observers used the 152 cm Coudé tel.

(b) In parenthesis: corresponding high-res. UV spectra, listed in Table 2.

respectively, $N = 1.2\,10^{12}$ and $N \sim 1.6\,10^{10}\,\mathrm{cm}^{-3}$; moreover the high-excitation lines and all the faint lines do not present the shell component (Fig. 1).

The spectrum during totality is very similar to that taken out of eclipse. The presence of the additional shell absorption is revealed by the slightly larger depth of the lines. The shell is very evident only in correspondence to the Balmer lines, which have very deep cores during totality (Fig. 2).

The difference in radial velocity between the photospheric lines at phase 0.91 and at phase 0.03 ranges from $+16$ to $+20\,\mathrm{km\,s}^{-1}$ and that between phase 0.91 and phase 0.003 it is about $+14\,\mathrm{km\,s}^{-1}$; this is in good agreement with the data obtained from the orbital radial-velocity curve (Kuiper et al., 1937; Struve et al., 1958).

The radial velocity of the shell lines, with respect to the primary, at ingress phase is about $+15\,\mathrm{km\,s}^{-1}$ and at egress phase

Table 2. IUE high resolution observations of ε AUR

DATE	OBSERVER	IMAGES	t_{exp}	PHASE	SPECTRUM
1981, Aug. 5	(a) Stickland	LWR 11247	-	Pre-eclipse	H1
1982, Mar. 12	(a) Chapman	SWP 16523	70m	Pre-eclipse	H1a
		LWR 12777	9m	"activity"	
1982, Mar. 26	(a) Stickland	SWP 16629	60m	Pre-eclipse	H1b
		LWR 12865	50m	"activity"	
		LWR 12866	8m		
1982, Nov. 16	Molaro	SWP 18751	55m	Late ingress	H2
		LWR 14645	15m		
		LWR 14646	50m		
1983, Mar. 20	Morossi	LWR 15522	60m	Totality	H3
1983, Apr. 8	(a) Ake	LWR 15675	55m	Totality	H4
		LWR 15676	15m	"brightening"	
1983, Apr. 18	(a) Chapman	SWP 19749	300m	Totality	H5
		LWR 15766	18m	"brightening"	
1983, Aug. 8	Ferluga	LWR 16553	15m	Totality	H6
1984, Jan. 20	Böhm	LWP 2763	12m	Early egress	H7

(a) Spectra released by VILSPA Data Bank

Table 3. Dates and phases for the visible spectrograms

PLATE No.	D A T E	JULIAN DAY	P H A S E	φ
GC 1224	Jan. 4, 1981	2444609.36	911 days before mid-eclipse	0.91
GC 1360	Nov.19, 1982	5293.54	227 days before mid-eclipse	0.98
GB 7983	Aug. 7, 1983	5554.52	34 days after mid-eclipse	0.003
GC 1563	Mar.29, 1984	5789.36	269 days after-mid-eclipse	0.03

about $-35\,\mathrm{km\,s^{-1}}$. The differences ΔRV between the radial velocities of the shell lines at ingress phase 0.98 and at egress phase 0.03 are given in Table 4.

The strongest lines in the spectrum – H and K of Ca II – have much lower ΔRV than the other lines. This may be due to the blending of shell, photospheric and circumstellar lines. In fact, the spectrum of Jan. 1981 shows that the H and K lines have a complex structure with a violet-shifted component at about $-30\,\mathrm{km\,s^{-1}}$, probably of circumstellar origin, which was observed also by Struve in 1950 (Struve, 1951) and by Adams in 1940. The Fe I, Fe II, and Hβ lines present a slightly lower ΔRV than the other lines. This effect may be real, but a physical interpretation will be attempted when the complete set of spectra has been completely analyzed.

A comparison of the central depths R of the shell lines at ingress and egress phases shows that the ratio R (egress)/R (ingress)

(398)

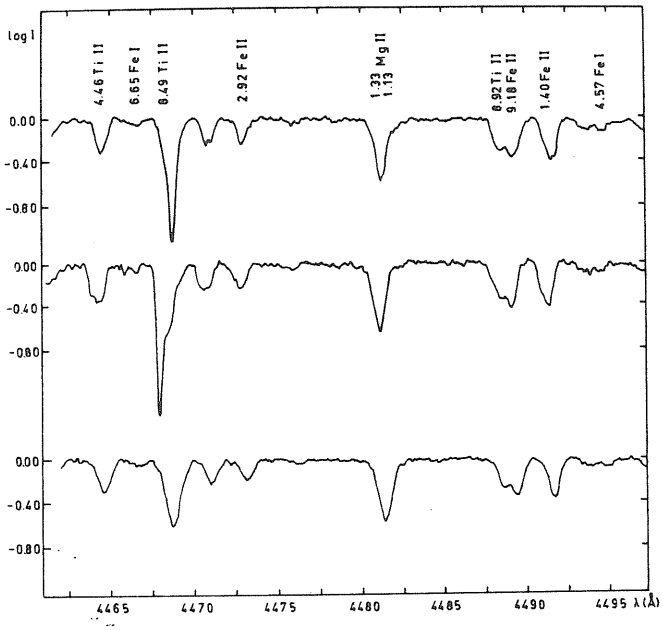

Fig. 1. The spectral region of Mg II λ 4481. Top: Nov. 19, 1982, 227 days before mid-eclipse. Middle: March 29, 1984, 269 days after mid-eclipse. Bottom: Jan. 4, 1981, out of eclipse. The two lines Ti II λ 4468.49 and Mg II λ 4481 have about the same intensity, in the spectrum taken out of eclipse. At the phases of ingress and egress only the line of Ti II, which has a low excitation potential of 1.13 eV, presents the shell component, while the line of Mg II (EP=8.83 eV) is a pure photospheric line

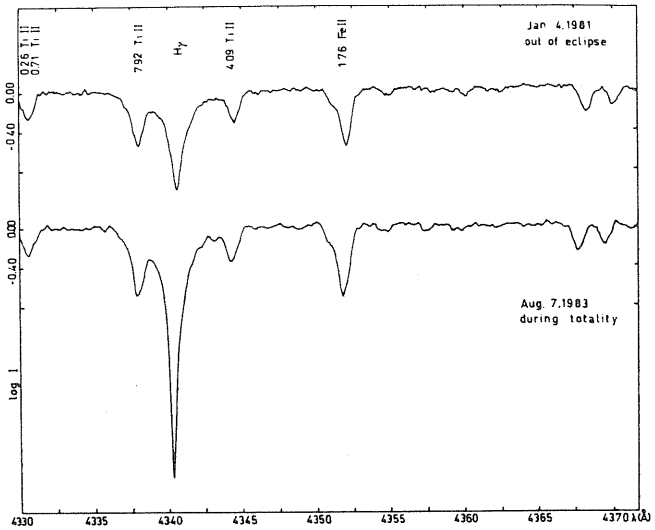

Fig. 2. One spectrum taken out eclipse (Jan. 4, 1981) is compared with one taken during totality (Aug. 7, 1983). The lines, which during the ingress and egress phases present a red-shifted and violet-shifted component respectively, during totality are deeper than out of eclipse. The shell component of Hγ is clearly visible, during totality

presents a rough dependence on the wavelength: at wavelengths shorter than about 4200 or 4300 Å the majority of the shell lines have about the same intensity at ingress and at egress, while at longer wavelengths the shell lines at egress are generally deeper than at ingress. The Balmer lines show a clear dependence on wavelength: Hβ is stronger at egress; Hγ, Hδ, H7 have about the same intensity at the two epochs; and the upper terms of the series are generally stronger at ingress phase.

An attempt to interpret this fact can be made when a more quantitative study, extended to all the spectrograms taken during the eclipse, has been completed. At present we suggest that a similar effect may be explained as follows; let us suppose that the shell is thicker at egress than at ingress; in addition to producing the spectral lines by absorbing the spectrum of the primary, it scatters the light of the blue companion more efficiently than at

Table 4. Differences Δ rv between the radial velocities of the shell lines at ingress and egress phases

LINES OF HYDROGEN	Δ RV (Km/s)	LINES OR IONS	NO. OF LINES USED IN THE AVERAGE	Δ RV (Km/s)
H β	49.4			
H γ	55.3	Mg I	2	54.75 ± 0.05
H δ	51.2	Ca I	1	53.2
H 7	56.7	Ca II H	1	26.4
H 8	61.7	Ca II K	1	22.8
H 9	58.7	Sc II	4	52.3 ± 0.2
H 10	59.2	Ti II	30	51.2 ± 0.6
H 11	47.7	Cr I	2	56.2 ± 3.3
H 12	64.0	Cr II	2	57.0 ± 0.5
H 13	56.2	Fe I	43	50.5 ± 0.7
H 14	60.4	Fe II	12	47.5 ± 1.4
H 15	64.7	Sr II	2	48.8 ± 1.0
H 18	52.8	Y II	1	58.7
H 38–H 43	49.0 ± 1.0			

ingress. This scattered light partially fills the shell lines, and because of the energy distribution of the light of the blue companion, the effect is stronger on the shorter wavelengths side.

The physical mechanism responsible for the scattering in the shell could be simply electron scattering, as discussed by BFH; however, infrared observations by Backman et al. (1984) indicate that also dust has to be present in the eclipsing body. This dust, which must be non-typical in size and/or in composition (no effect is observed at 2200 Å during the eclipse), could also produce the observed slight deepening of the eclipse towards the far-UV (if it is not caused by a blending of the shell lines as suggested in Sect. 3.3).

2.2. Variations of the Hα profile

The general behaviour of Hα, shown in Fig. 3, is very similar to that observed by Wright and Kushwaha (1957) during the short time-scale variability they also observed. Red and violet emission wings are always present out of eclipse, and have about the same intensity.

Table 5 gives the radial velocity of the various components of Hα at different epochs, the central depths of the absorption components and the intensity relative to the continuum of the emission wings. The exceptionally low intensity of the absorption can be explained by its being filled-in by the emission; this is confirmed by the fact that also Hβ, Hγ, Hδ are much fainter than is normally expected for an F0 Ia supergiant, while the Balmer lines with higher quantum numbers have normal intensity (Castelli, 1978). The variations of the emissions observed during eclipse can be easily explained by the absorbing effect of the shell components on the F0 Ia chromospheric Hα (see notes to Table 5).

3. Ultraviolet wavelengths

3.1. Out-of-eclipse activity

Comparing spectra H1a and H1b, taken at different epochs during the March '82 phase of far-UV activity, one does not find remarkable variations in the profile of the lines, longward of 1700 Å (unfortunately, at shorter wavelengths, high-res. spectra are underexposed). On the contrary, in the mid-UV, the overall

Table 5. Variations of the Hα profile

Days from mid-eclipse	Date	RV absorption components (a) km/s	Half-width (at ½ log I), km/s	Central depth (Absorption)	Emission intens. relative to cont. Red	Violet
- 277	Sep.30, 1982	+ 1.4 + 21.9	59	0.71	1.23	1.29
- 227	Nov.19, 1982	- 3.2 *+28.8*	69	0.65	1.10	1.17
- 108	Mar.18, 1983	-10.1 *+31.1*	91	0.82	-	1.26
+ 34	Aug. 7, 1983	-92.3 + 56.2 -83.2 *-30.6* + 88.2 -74.0	137	0.78	-	-
+ 85	Sep.27, 1983	-83.2 - 19.2 -60.3 *-42.1* + 12.8	100	0.86	-	-
+ 172	Dec.23, 1983	*-46.6*	73	0.90	1.41	-
+ 204	Jan.24, 1984	*-42.1*	73	0.81	1.45	-

(a) The values in italic refer to the strongest component.

Notes on Table 5

Sep. 30, 82: Ingress phase; the red-shifted shell lines are fainter than the photospheric lines. The red emission wing is fainter than the violet one because it is partially absorbed by the shell component.

Nov. 19, 82: Ingress phase; the red-shifted shell lines are deeper than the photospheric ones. The red emission wing is fainter than the violet one because it is partially absorbed by the shell component.

March 18, 83: Totality; the red emission wing is no longer observable. The stronger absorption component is the red-shifted shell line.

Aug. 7, 83: Totality; the line is very broad with several faint violet-shifted and red-shifted absorption components. No emissions are observable.

Sep. 27, 83: Totality; several violet-shifted and red-shifted absorption components; no emissions are observable.

Dec. 23, 83: Exit from totality; the absorption line is almost symmetrical. The presence of a violet-shifted shell component is suggested by the absence of the violet emission wing.

Jan. 24, 84: Egress phase; the profile is asymmetric, sharper on the violet side and there is no violet emission wing because of the presence of a violet-shifted shell component blended with the stellar line.

(400)

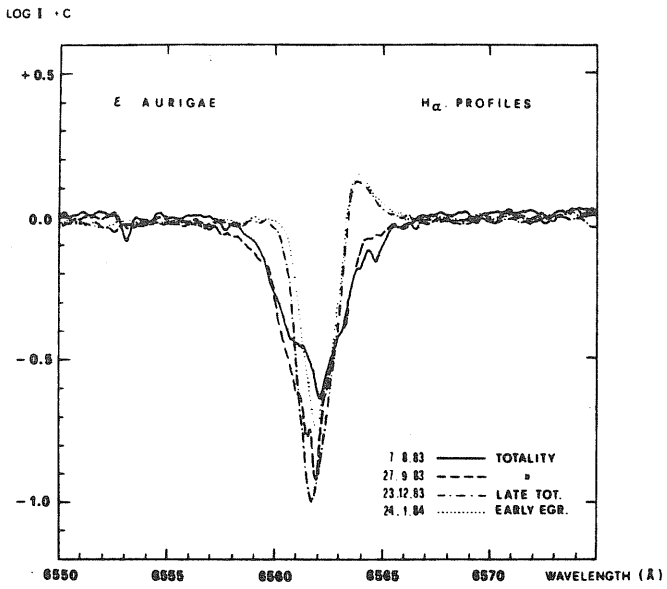

Fig. 3. Profiles of Hα during totality and early egress. Those before and during ingress were published by Boehm and Ferluga (1983)

intensity of the stellar continuum and lines seems to be affected by the superposition of an additional corresponding component, varying with time; this effect is slightly increasing towards the shorter wavelengths. It is then straightforward to relate this contribution to the activity of the additional far-UV source, which is supposed by BFH to the embedded inside the secondary body.

On the other hand, from a preliminary *UBV* photometry report (Hopkins and Stencel, 1984), in spite of poor data coverage, it seems that also the *V* brightness of the system was enhanced by about 0.1 – 0.2 mag on March '82, in coincidence with the far-UV activity. Moreover, the UV brightening and the *V* enhancement seem to be correlated also in intensity, simply by an extrapolation of the UV additional component, toward the longer wavelengths. If confirmed, this effect is puzzling since it suggests a contribution by the secondary to the variability of the system at visible wavelengths, while usually the intrinsic *V* fluctuations of ε Aur were interpreted as cepheid-like variations of the primary F0 supergiant (Gyldenkerne, 1970).

3.2. Depth of the eclipse

As happens in the visible, the observed mid-UV spectrum during the eclipse can be reproduced, assuming a general reduction of the primary's flux by an almost wavelength-independent factor (grey eclipse) and superimposing, over the strong low-excitation lines of the primary, a set of sharp absorption components (shell spectrum) convoluted with the IUE instrumental profile. However, the depth of the eclipse is not exactly constant along the mid-UV spectrum. Regions of greater deepening are found towards the shorter wavelengths, where the number of lines is particularly high; instead at longer wavelengths, where the continuum can be unambiguously recognized, no significant wavelength-dependence is found in the depth of the eclipse. These facts suggest a possible explanation: the deviation from greyness could come simply from the integrated contribution of the superimposed shell line-spectrum, which is richer in lines towards the shorter wavelengths.

Figure 4 shows that a significant depression is also present in a region about 40 Å wide, corresponding to the absorption wings of the strong Mg II λ2800 resonance doublet. This effect, if due to the presence of broad wings also in the shell spectrum, is surprising since all the other lines of the shell spectrum are sharp (see **Note added in proof**).

3.3. The question of non-greyness

Several authors (Chapman et al., 1983; Altner et al., 1984) found a considerable deepening of the eclipse towards the shorter wavelengths, and attributed it to the effect of dust, which is supposed to

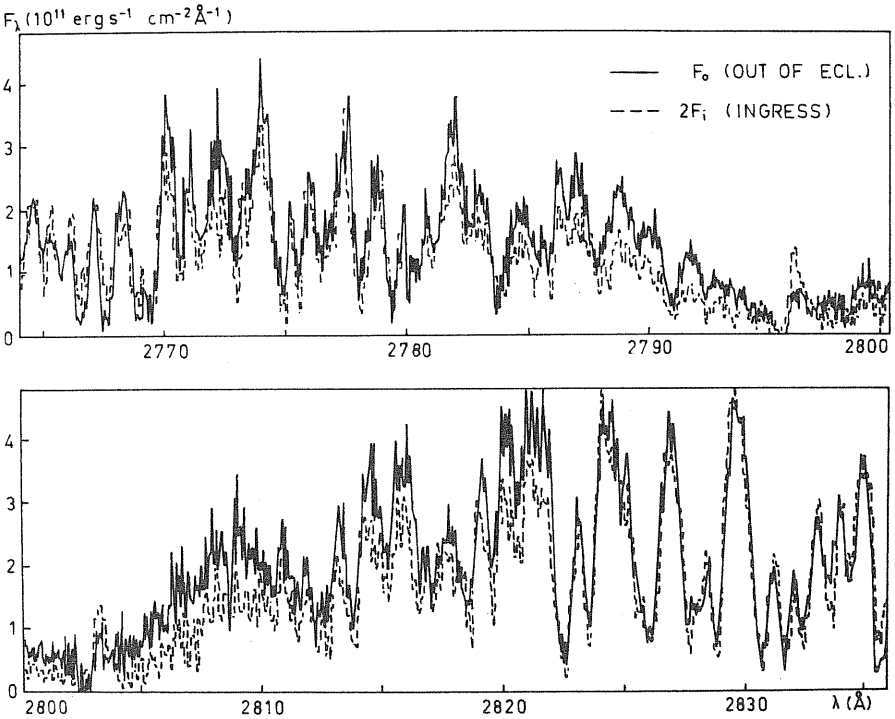

Fig. 4. Deepening of the Mg II λ2800 resonance doublet during the eclipse. In the figure we report the flux F_0 observed out of eclipse on March 12, 1982 (solid line), together with the flux F_i recorded at late ingress on November 16, 1982; in order to make comparison possible, the latter has been multiplied by a factor of 2 (dashed line). In this way, compensation for the depth of the eclipse is achieved; in fact, the tracings are superimposed in regions fairly distant from the feature of Mg II ($\lambda \lesssim 2780$ Å and $\lambda \gtrsim 2820$ Å). The systematic lowering of the eclipsed spectrum, along the wings of the doublet (2780 Å $\lesssim \lambda \lesssim$ 2820 Å), reveals either an additional broad absorption contribution of the eclipsing body, or an effect of "filling" by out-of-eclipse far-UV activity

be contained in the eclipsing body. On the contrary, only slight deviations from greyness are found at short wavelengths, comparing the low-resolution uneclipsed spectrum (2), taken on 4 Aug. 1981, with the eclipsed spectra (6)...(13). This discrepancy was already underlined by BFH, when discussing the results of Chapman et al.; let us now return to the topic.

Determination of the eclipse depth can differ substantially, since they depend on the choice of the out-of-eclipse reference spectrum; as was noticed by Altner et al., this is a delicate choice, because of the primary's cepheid-like variability. But still more critical is the problem of far-UV activity, coming from the hot source (probably embedded in the eclipsing body), and affecting in particular the region from 1300 Å to 1700 Å with a peak around 1500 Å. If the assumed out-of-eclipse reference spectrum were taken near the far-UV activity period of March 1982 (for example when the luminosity was enhanced by 1.5 mag at 1500 Å), then the depth of the eclipse at the various phases would appear systematically deeper in the far-UV (by 1.5 mag at 1500 Å), with respect to mid-UV. Such a deepening of the eclipse at short wavelengths is precisely the result obtained by Altner et al., assuming a reference spectrum taken on April 4, '82, right near the active period: the curves of eclipse depth vs. wavelengths, at the various phases, are exactly the mirror image of the out-of-eclipse activity vs. wavelength, reported by BFH in their Fig. 2. Hence, the disagreement concerning the non-greyness of the eclipse at short wavelengths can be easily explained by the far-UV variability; unfortunately it is still difficult to distinguish the pure effect of the eclipse from the superimposed contribution of intrinsic variability.

Probably all the determinations of the non-greyness of the eclipse, which are referred to uneclipsed spectra taken around March 1982 (near the highest peak of far-UV activity), are misleading. Instead measurements based, for example, on earlier out-of-eclipse observations, like spectrum (2) considered by BFH (when no particular far-UV activity was present), should be more reliable. In this case at short wavelengths the deviations from greyness, which we find, are much smaller or even absent, and they could be also produced by simple blending of the shell absorption lines.

Anyway, the problem remains open, since Altner et al. confirm that they still find that the eclipse was non-grey, after carefully re-examining the IUE archival data, using different pre-eclipse spectra for comparison. Such discrepancies between the current results and those by Altner et al. need then to be reconciled through further work.

3.4. *The mid-eclipse "hole"*

The question of the mid-eclipse brightening in the UV has been already discussed by FH, and independently by Altner et al. (1984). Let us now consider in more detail the pair of high-resolution spectra H4 and H5, taken at a time interval of 10 days during the increasing phase of the brightening. Since this interval is small with respect to the time-scale of the brightening, we are dealing with very small variations, but still appreciable ones, since they are systematic and correlated with those observed in the V band.

The most important conclusion that one can draw, from the inspection of the spectra, is that the profiles and the central intensities of the lines seem not to vary in the mid-UV, while on the contrary we observe a systematic brightening of the continuum only. This should mean that the mid-eclipse brightening is produced by a rarefaction of the material, (scattering electrons and/or dust), responsible for the continuous absorption during the eclipse, and located mainly in the inner regions of the eclipsing body.

3.5. *The behaviour at third contact*

Finally, we have to notice from Fig. 5 that the low-resolution spectrum (13), contemporary to H7, shows a deepening of the eclipse just after 3rd contact, towards the longer wavelengths (2500–3000 Å). Although it might be due in part to the deepening

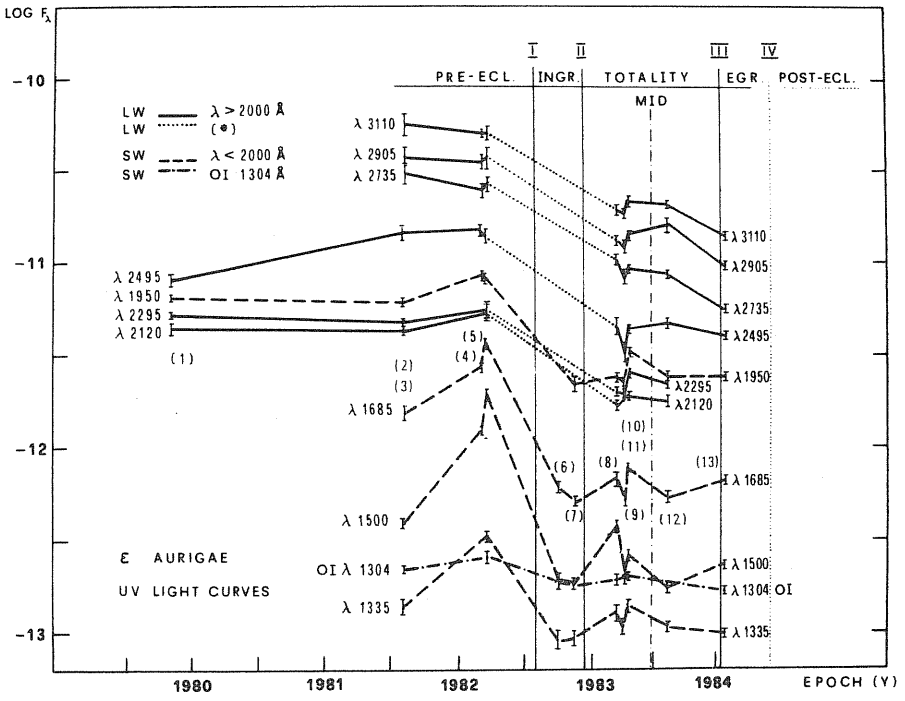

Fig. 5. Monochromatic UV light curves (prolonging those given by Boehm et al., 1984), based on IUE low-resolution data. Numbers in parenthesis indicate the low-resolution spectra, from which the experimental points are derived; fluxes F_λ are in erg s^{-1} cm^{-2} Å^{-1}. (*) Dotted lines: ingress data are now covered by Parthasarathy and Lambert (1983)

of shell absorption lines at egress (shown by H7), if confirmed this fact would be in contrast with the recent *UBV* photometry results of Ôki et al. (1984), who found, in the same period (J.D. 2245700–5740), a brightening of about 0.15 mag in the *U* band, decreasing towards the *B* and *V*. While this *UBV* brightening could be related with a corresponding activity shown by spectrum (13) in the far UV, there is no way to match the near-UV part of spectrum (13) with the *U* photometry. But since this is the only case in which the LWP camera of IUE was used in place of LWR, the most reasonable possibility is that the effect might be caused simply by a different calibration of LWP and LWR cameras of IUE.

4. Conclusions

Ultraviolet (IUE), visible and infrared observations reveal the complex structure of the eclipsing body. Ultraviolet observations of the eclipse indicate the presence of an excess of flux in the far UV; we suggest that it comes from a hot secondary star, which is in front during the eclipse and whose continuum dominates at $\lambda \lesssim 1500$ Å, as discussed by BFH[1].

The present visual observations together with those of the 1955–57 eclipse (Hack, 1959, 1961) indicate the presence of a gaseous shell excited and ionized by diluted radiation of the hot source; this shell is responsible for selectively absorbing the primary's light and producing the "shell" spectrum. The infrared observations (Backman et al., 1984), indicate the presence of a cool object ($T \simeq 500$ K) which is in front during the eclipse and which is responsible for the eclipse of the primary.

We may wonder how it is possible for the gaseous, partially ionized shell to coexist with the cool object. We think that the light of the hot secondary escaping from the poles is able to excite and ionize the thin gaseous shell which extends farther out of the orbital plane, while a cool disk or ring surrounding the secondary and eclipsing the primary lies in the vicinity of the orbital plane, and makes the secondary appear fainter than it really is.

1 Other possibilities can also be considered for the far-UV source; e.g. a hot spot on the primary (Parthasarathy and Lambert, 1983), or even a close binary embedded in the eclipsing body (Lissauer and Backman, 1985)

Acknowledgements. We wish to thank C. Boehm for performing PDS digitization and ELSPEC 11 procedure, and T. Valente for plotting the UV spectra at the Computing Center of the Trieste Astronomical Observatory. Moreover, we thank G. Buzan for drawing the figures and S. Giurco for typing the manuscript.

References

Adams: 1940, priv. comm. quoted by Struve, O.: 1951, *Astrophys. J.* **113**, 699
Altner, B.M., Chapman, R.D., Kondo, Y., Stencel, R.E.: 1984, Future of *UV* Astronomy based on 6 years of IUE research, Goddard S.F.C. Conf.; April '84 (in press) (Epsilon Aurigae Campaign Newsl. No. 11, p. 5)
Backman, D.E., Becklin, E.E., Cruikshank, D.B., Joice, R.R., Simon, T., Tokunaga, A.: 1984, *Astrophys. J.* **284**, 799
Boehm, C., Ferluga, S.: 1983, IBVS No. 2326
Boehm, C., Ferluga, S., Hack, M.: 1984, *Astron. Astrophys.* **130**, 419 (BFH)
Castelli, F., Hoekstra, R., Kondo, Y.: 1982, *Astron. Astrophys. Suppl. Ser.* **50**, 233
Chapman, R.D., Kondo, Y., Stencel, R.E.: 1983, *Astrophys. J. Letters* **269**, 17
Ferluga, S., Hack, M.: 1984, Proc. of the Fourth European IUE Conf.; Rome 15–18 May, p. 419 (FH)
Gyldenkerne, K.: 1970, *Vistas in Astronomy* **12**, 199
Hack, M.: 1959, *Astrophys. J.* **129**, 291
Hack, M.: 1961, *Mem. Soc. Astron. Ital.* **32**, 251
Hopkins, J.L., Stencel, R.E.: 1984; *Epsilon Aurigae Campaign Newsl.* No. 10, p. 2
Kemp, J., Henson, G., Kraus, D.: 1984, *Epsilon Aurigae Campaign Newsl.* No. 10, p. 8
Kuiper, G.P., Struve, O., Strömgren, B.: 1937, *Astrophys. J.* **86**, 570
Lissauer, J.J., Backman, D.E.: 1985, *Astrophys. J.* (in press)
Ôky, T., Sekita, I., Hirayama, K.: 1984, *Epsilon Aurigae Campaign Newsl.* No. 11, p. 17
Parthasarathy, M., Lambert, D.L.: 1983, *Publ. Astron. Soc. Pacific* **95**, 1012
Pasian, F., Rusconi, L., Sedmak, G.: 1982, Publ. OAT No. 806
Wright, K.O., Kushwaha, R.S.: 1957, Liège Colloq. No. 8, p. 421
Struve, O.: 1951, *Astrophys. J.* **113**, 699
Struve, O., Pillans, H., Zebergs, V.: 1958, *Astrophys. J.* **128**, 287

Note added in proof. Recent post-eclipse IUE data (LWP 4158 taken on Sep. 6, 1984) reveal that the effect on Mg II λ2800 Å, shown in Fig. 4, is probably due to an enhancement of the comparison flux F_0 caused by out-of-eclipse activity.

Paper VII

THE ECLIPSE OF EPSILON AURIGAE
VISIBLE SPECTROSCOPY AND ULTRAVIOLET ACTIVITY

S. Ferluga and M. Hack
Trieste University, Institute of Astronomy - Via Tiepolo 11, I34131 Trieste, Italy

We report the preliminary results of the study of several high-resolution spectrograms (λ3500 - λ7000 Å), obtained at the Haute Provence Observatory (OHP) in France, at different epochs before, during and after the eclipse. We also compare some of these spectrograms with corresponding IUE high-resolution observations, in order to study the effects of the intrinsic UV activity, towards the longer wavelengths.

1. The Visible Spectrum

As during the previous eclipses, we have observed the appearance of sharp absorption components on the red side of the strong low-excitation lines and of the Balmer lines during the ingress phase, and on the violet side during the egress phase (Ferluga and Hack, 1985: Paper I). This additional spectrum, which we call "shell spectrum", appears only during the eclipses and is very well observable during the partial phases of the eclipse. During totality it is observable as a strong deepening of the absorption cores of the strongest lines, especially the Balmer lines. The shell spectrum is explained by a gaseous envelope surrounding the eclipsing body and rotating in the same sense as the orbital motion. Since the shell spectrum appears before the beginning and disappears after the end of the photometric eclipse, the gaseous envelope must be more extended than the occulting body (a dusty disk, as suggested by the IR observations by Backman et al. 1984). The shell has about the same excitation temperature of the photosphere of the FOIa primary, but a much lower density. This is indicated by the fact that the quantum number of the last resolved Balmer line is n = 31 in the photospheric spectrum and n $\gtrsim$ 50 in the shell spectrum; moreover, the high excitation lines and all the faint lines do not present the shell component. (Fig.1)

The shell responsible for the additional spectrum has an absolute value of the rotational velocity lower before totality than after it (e.g., 277 days before mid eclipse the shell RV is +15 km/s and, 269 days after it, it is -35 km/s; 227 days before it, it is +17 km/s, and 221 days after it, it is -37 km/s). that is, the part of the shell which follows in the orbital motion rotates faster than the preceeding one. Moreover, both parts of the shell show a rotational velocity which increases from the outer part to the inner one, reaches a maximum and then decreases again (Fig. 2). The general behaviour and the values of the RV are the same as observed by Struve et al. (1958) during the 1955-57 eclipse.

At the epoch of the brightening on Jan. 1984 near the end of totality (Ôki et al., 1984) the shell has the maximum negative RV and also maximum intensity. Weak low-excitation lines which generally do not show the shell components show it in the spectrum (GB 8177) taken at the OHP on Jan 24, 1984 (*). This fact could indicate that in correspondence of a diminution of the density of the dusty disk we observe the absorption of the FO Ia

(*) Note. The same behaviour is shown in the UV by the spectrum LWP 2673, obtained with the IUE at high resolution on Jan 20, 1984.

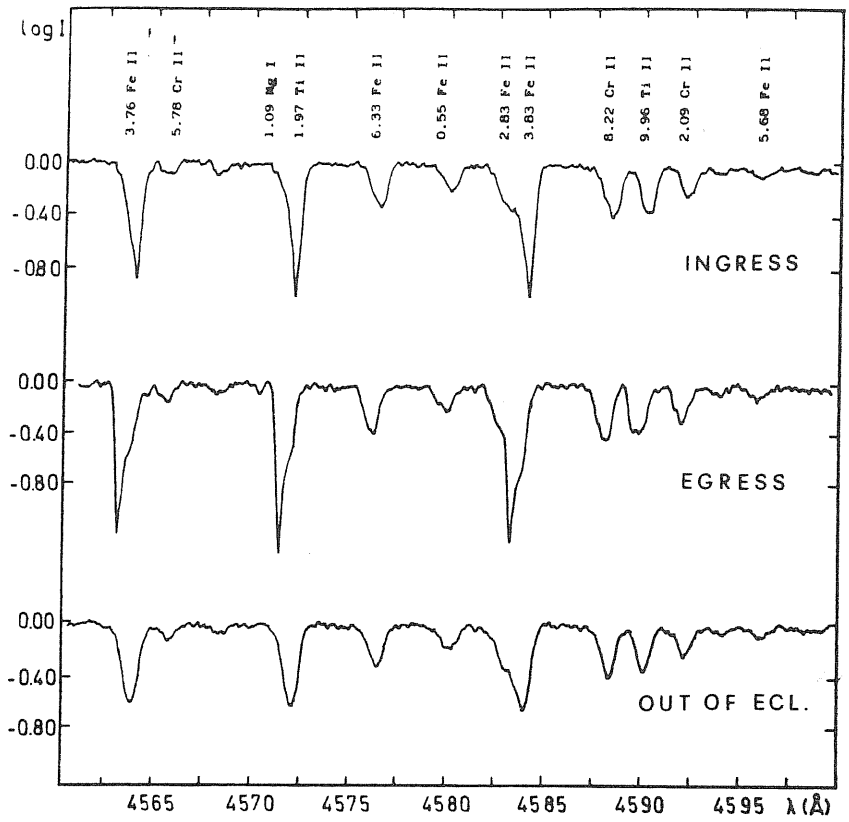

Fig. 1 - The shell spectrum. An additional component is superimposed over the stronger low-excitation lines. This component is red-shifted on ingress (Nov 19, 1982) and violet-shifted on egress (March 29, 1984). The spectrum taken out of eclipse (Jan 4, 1981) is reported for comparison.

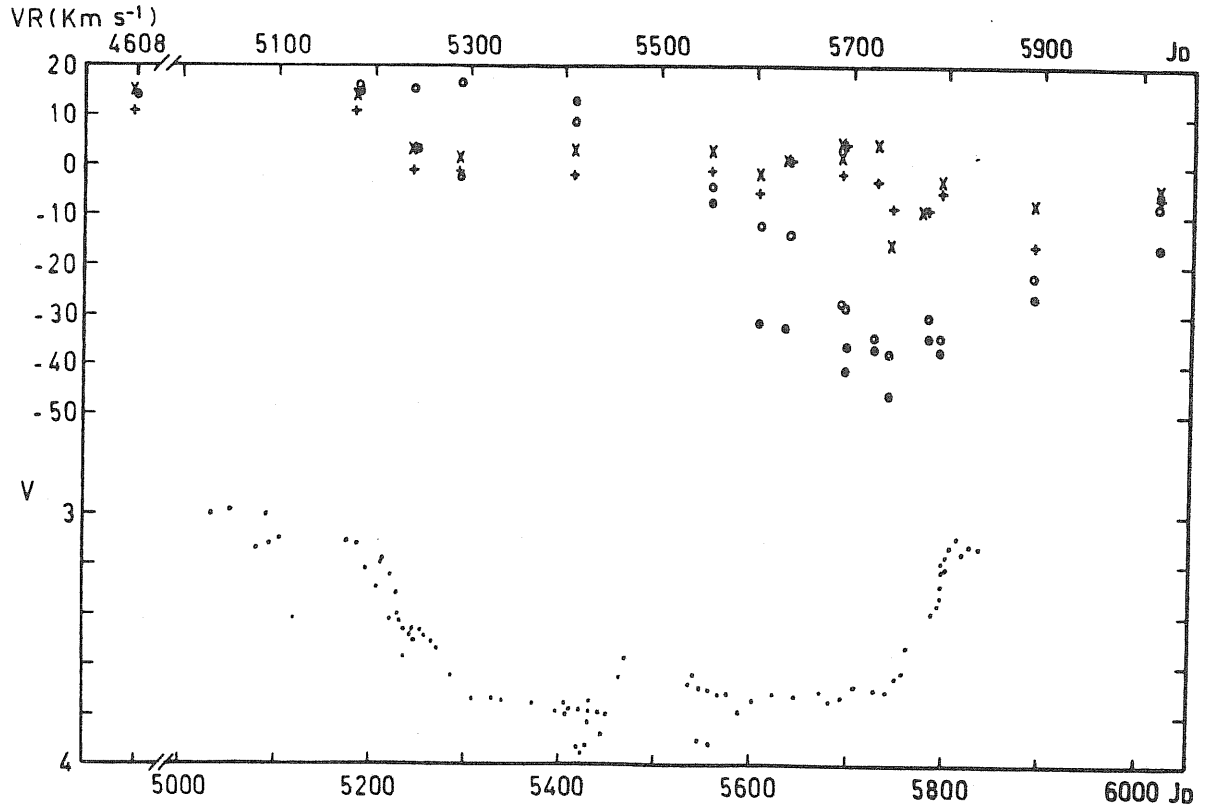

Fig. 2 - The radial velocity curve during the eclipse (together with the V light-curve reported at the bottom for comparison [ε Aur Newsl. 11, 32]). The shell components of Hα, Hβ, Hγ, (●), and of other lines (o), have radial velocities which are positive on ingress and negative on egress. At the same time the stellar line Mg II λ 4481 (+), and the other lines with dominant stellar component (x), show a remarkably slower variation, due to the orbital motion.

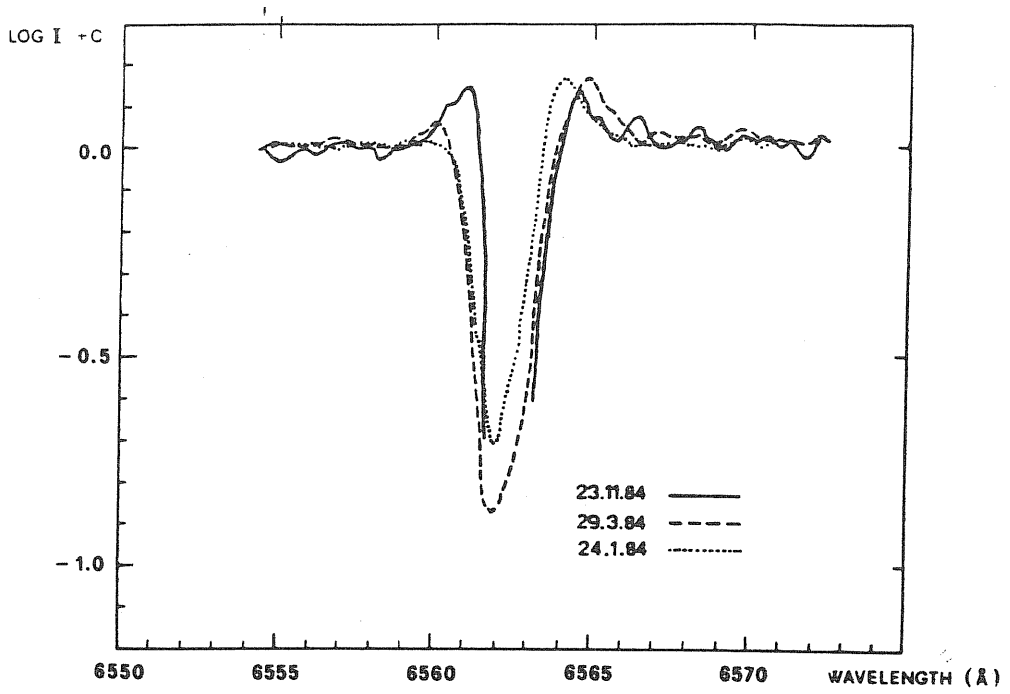

Fig. 3 - The behaviour of H_α at egress. A post-eclipse profile (solid line) is compared with the profiles at egress (dashed) and at early egress (dotted) . Profiles on totality are shown in paper I, while the profiles on ingress are given by Boehm,Ferluga,1984(IBVS 2326)

light from a part of the shell close to the orbital plane where the density and the rotational velocity are probably higher than above and below the plane.

The strongest lines in the photospheric spectrum, H and K of Ca II, during the partial phases of the eclipse appear to be predominantly due to the F0 Ia spectrum, while the contrary is true for the Balmer lines. Moreover, they have a complex structure also out of eclipse . In fact, the spectrum taken in Jan 1981 shows that the H and K lines have a violet-shifted component at about -30 km/s, probably of CS origin, which was observed also by Struve in 1950 (Struve 1951) and by Adams in 1940. The presence of a CS shell is confirmed by the UV emissions O I λ1302 and Mg II λ2800 which are not affected by the eclipse.

The general behaviour of H_α (Fig. 3) is very similar to that described by Wright and Kushwaha (1957) during the previous eclipse. The RV of the various absorption components, the half-width and intensity of absorptions and emissions are given in paper I.

During the UV phases of activity observed with IUE the lines of low excitation are weaker, while the lines of higher excitation are not weaker or are just slightly weakened. The weak lines which are all F0 Ia photospheric lines (i.e. without shell components) remain unchanged. This suggests (see the next section) that the UV activity of the companion increases the state of excitation of the shell. The same effect can be produced by the activity of a hot spot on the surface of the primary, hypothesized by Parthasarathy and Lambert in 1983 as an alternative explanation of the UV excess observed at λ shorter than about 1600 Å.

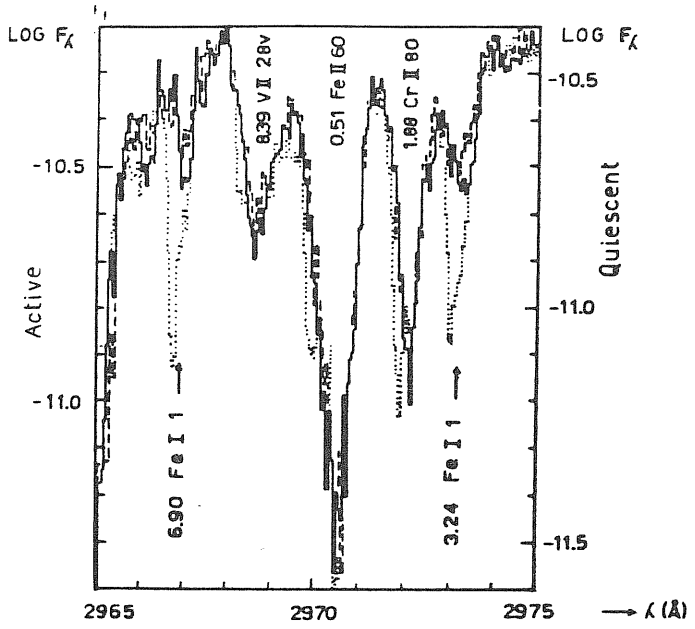

Fig. 4 - Line variations during UV activity. With respect to the quiescent phase on Sep 6, 1984 (·····), the profiles of Fe I UV 1 resonance lines are "filled" during activity on March 12, 1982 (———), and they are still more filled during the activity peak on March 26, 1982 (----). Note that the "filling" acts on the doppler-shifted part of the lines.

2. The "active spectrum"

As happens for the depth of the eclipse, also the determination of the shell spectrum, in principle, is affected by the problem of separating the effects of the eclipse from those related with the intrinsic far-UV activity. The influence of this activity, over the spectral lines of the system, can be studied in correspondence of the two active periods which have been observed in the UV since now: the first occurred before the eclipse, on March 1982, while the second occurred during totality, on March 1983. Since for the active period in totality it is difficult, if not impossible, to separate the effects of the eclipse and of the activity, here we shall discuss the pre-eclipse activity period in some detail.

The activity phase in 1982 was the strongest and reached its observed maximum, $\Delta m = 1.75$ mag at 1500 Å, on March 26 (Boehm, Ferluga, Hack, 1984); two weeks before, on March 12, the activity was weaker, $\Delta m = 1.25$ mag at 1500 Å. It is then particularly interesting to compare these two IUE high-resolution spectra, LWR 12777 and LWR 12866, taken in 1982 on March 12 and March 26 respectively (spectral range $\lambda\lambda$ 2600 ÷ 3100 Å); unfortunately, we do not have optical spectrograms at that epoch. Since both spectra are "active", there are no large variations in the line profiles (paper I); but a detailed inspection reveals that some groups of lines appear to change their relative intensities slightly.

In particular, we may notice that, in correspondence of a higher degree of activity, the stronger mid-UV lines of Fe I, such as $\lambda\lambda$ 2966.9 - 2973.1 Å resonances or the multiplet V9, seem to be partially "filled". The same thing happens to several low-excitation lines of Ti II, and in particular to the strong low-excitation lines of V II belonging to the multiplets UV 3-10-11-12 (EP $\lesssim$ 0.4 eV) and V 26-27-34-42. Also the absorption wings

of the Fe II λ 2599 Å resonance line, and particularly the large absorption wings of the Mg II λ 2800 Å resonance doublet, appear to be flattened by the effect of activity. The filling occurs generally on the *red side* of the lines, and on both wings of the Fe II and Mg II resonances; the effect is about 0.2 - 0.3 magnitudes, between March 12 and March 26, 1982. At the same time, the continuum is raised by about 0.1 mag, in the "window" around 3080 - 3087 Å.

Such effects are greatly enlarged, if we compare these *active* pre-eclipse spectra, with a *quiescent* post-eclipse spectrum: in our case let us consider LWP 4158, obtained with IUE at high resolution on September 6, 1984. After overcoming some calibration problems (the last spectrum was taken with a different IUE camera), there still remains a difference of about 0.5 mag, between the mid-UV continuum enhanced by activity (1982), and the quiescent one (1984); then, while the continuum is raised, the behaviour of the line-components of the mid-UV spectrum, with respect to activity, can be classified as follows.

(*i*) *Normal.* The majority of the lines apparently follow the variation of the continuum, increasing their central flux by ∼ 0.5 mag in activity, with no remarkable variation in the profile.

(*ii*) *Filled.* This is the case (Fig. 4) of the already-mentioned lines of Fe I, Ti II, V II, and wings of Fe II - Mg II resonance lines, which are filled in pre-eclipse activity by ∼ 1 mag. (*)

(*iii*) *Unchanged.* Activity does not affect remarkably the central flux of some high-excitation lines, such as Fe II multiplets UV 62 and higher (EP $\gtrsim$ 1 eV), or Cr II multiplets UV 5 and higher (EP $\gtrsim$ 1.5 eV); so these lines appear to be deepened, with respect to the enhanced continuum. This effect should be dominant in the far UV, producing the deepening of lines observed at low resolution. Moreover, these lines do not show any remarkable doppler shift depending on activity (or on eclipse phase).

(*iv*) *Circumstellar.* Also the circumstellar emission components of strong resonance lines, such as Fe II λ 2599 Å and Mg II λ 2800 Å, remain unchanged by activity, as well as O I λ 1302 Å (observed in the low-resolution mode).

These observed effects can be easily explained by the presence of an additional spectrum, produced by the source of far-UV variability, and superimposed over the spectrum of the system. This *active spectrum* should be very similar to that of the primary, in order to leave it practically identical; the only difference should be a slightly *higher temperature* (together with the absence of absorption wings in Fe II and Mg II resonance lines).

As a consequence, one would have (*ii*) fainter low-excitation lines, producing the observed filling (and the wings of Fe II and Mg II resonances would be filled as well); moreover, one would also have stronger high-excitation lines, adding no appreciable flux (*iii*) to the underlying stellar spectrum. Intermediate situations would generate case (*i*), while circumstellar emission

(*) Note. The behaviour of an even larger number of low-excitation lines, known to possess a violet-shifted shell component in the post-eclipse spectrum of Sept 1984, is apparently similar. The same behaviour is shown, symmetrically, in the pre-eclipse spectra of March 1982. Just because the shell absorption is weaker at ingress, on comparing a pre-eclipse spectrum with a post-eclipse one, these lines appear to be "filled" on the violet side before the eclipse: this effect has nothing to do with activity, and it should be distinguished from case (ii).

components (*iv*) would clearly remain unaffected. Finally, we note that in case (*ii*) the residual line is not red-shifted in pre-eclipse activity, since the "filling" acts on the *doppler-shifted* part of the line (Fig. 4); also in case (*iii*) there is no shift during activity. This should mean that the hot source is either on the primary, or at the center of the companion, but in any case not rotating with the shell.

3. Conclusions

From the results of the present and previous eclipses of Epsilon Aur it is evident that the spectroscopic and photometric observations are completely explained by the presence of the following bodies:

a) the F0 Ia primary, whose spectrum is always observable;

b) a cool body (T $\sim$ 500 K) which is responsible for the photometric eclipse of the primary (Bakman et al., 1984). This dusty disk or ring must be made of particles much larger than those present in the IS dust, because no additional reddening is observed at 2200 Å during the eclipse;

c) a gaseous envelope more extended than the dusty disk, which is responsible for the additional spectrum appearing during the eclipse;

d) an extended envelope surrounding the whole system, where the emissions of OI λ1302 and MgII λ 2800 are formed;

e) a faint hot body which is not eclipsed and whose radiation dominates at $\lambda \lesssim$ 1500 Å. In fact the depth of the eclipse tends to become zero at $\lambda \lesssim$1500 Å, thus indicating that the excess in the UV is real and not due simply to scattered light from longer wavelengths in the spectrum of the primary, or in other-words, it is not simply an instrumental effect. This hot body may be a star (as suggested by Hack and Selvelli, 1979) or a binary system (as suggested by Lissauer and Backman, 1984), whose radiation, escaping from the poles, excites and ionizes the gaseous envelope, producing the shell spectrum; or it may be a hot spot on that part of the surface of the primary which is not occulted by the dusty disk (as suggested by Parthasarathy and Lambert, 1983). The hot body (star, binary system or hot spot) is variable in light.

Acknowledgments

This work is based on observations made at the Haute Provence Obs. (France), and with the IUE satellite from VILSPA (Madrid). Data analysis was performed at the ASTRONET pole of Trieste, Italy.

References

Adams, W.S., 1940, priv. com. quoted by Struve, O.: 1951 Astroph. J. 113, 699.

Backman, D.E., Becklin, E.E., Cruikshank, D.B., Joice, R.R., Simon, T., Tokunaga, A.: 1984, Astroph. J. 284, 799.

Boehm, C., Ferluga, S., Hack, M.: 1984, Astron. Astroph. 130, 419: Paper I

Ferluga, S. and Hack, M.: 1985, Astron. Astroph. 144, 395

Hack, M. and Selvelli, P.L.: 1979, Astron. Astroph. 75, 316

Lissauer, J.J. and Backman, D.: 1985, Astroph. J. Lett. 286, L39

Ôki, T., Sekita, I., Hirayama, K.: 1984, ε Aur Campaign Newsl. no. 11, p. 17

Parthasarathy, M. and Lambert, D.L.: 1983, Publ. Astron. Soc. Pacific 95, 1012

Struve, O.: 1951, Astroph. J. 113, 699.

Struve, O., Pillans, H., Zebergs, V.: 1958, Astroph. J. 128, 287

Wright, K.A. and Kushwaha, R.S.: 1957, Liége Coll. N 8, p. 421.

Paper VIII

EXTRACTION OF THE SHELL SPECTRUM OF EPSILON AURIGAE (*)

Conrad Boehm

Trieste Observatory
Via G.B.Tiepolo, 11
I 34131 Trieste, Italy

Steno Ferluga

Trieste Univ.,Astronomy dept.
Via G.B.Tiepolo, 11
I 34131 Trieste, Italy

ABSTRACT. A sample of high-dispersion optical spectrograms of ε Aur,taken on different epochs before and during eclipse, has been processed by computer in order to extract the shell spectrum,produced by the eclipsing body. Using an uneclipsed spectrum as reference, the primary's dominant contribution was removed, and this makes it possible for the first time to study the secondary body spectrum separately at all eclipse phases. As the first striking result, one finds that the internal regions of the extended eclipsing body are hotter than the outer zones.

1. INTRODUCTION

During the two-year-long eclipse of ε Aur, an obscure object passes in front of the F0Ia primary star, reducing its optical luminosity to about one half. The eclipsing body was extensively studied during the last 1982-84 ecl. by different authors showing the presence of multiple components within an ellipsoidal rotating structure. A cool (500-1000K) and optically thick dusty disk, seen almost edge-on, is contained along the equatorial plane (Backman et al.,1984). A dwarf B star (Boehm,Ferluga and Hack,1984) or a close binary (Lissauer and Backman,1985) is probably embedded in the center. A rotating gaseous shell, having a temperature slightly lower than the primary star,surrounds the disk (Ferluga, Hack,1985: paper I).

This gaseous shell,during the eclipse,produces the well-known shell spectrum. It consists of a set of sharp additional absorption components, superimposed over the primary's spectral lines and drifting from the red side of the profile (at ingress) to the violet side (at egress), because of the shell rotation. These features were already studied during the egress phase of the previous 1955-57 eclipse, showing evidence of low density and diluted radiation (Hack,1959). During the last 1982-84 eclipse, we observed the shell features at all phases of the eclipse, analyzing a set of high-dispersion spectrograms (GC type, 7.2 Å/mm, or at least GB type, 12.4 Å/mm) taken at the Haute Provence Obs. (France) and listed in paper I.

At ingress and during totality the shell components of the metallic

(*) Based on observations at the Observatoire de Haute Provence (OHP), processed at the ASTRONET pole of Trieste with the ELSPEC/11 software.

J.-P. Swings (ed.), Highlights of Astronomy, 201–204.

lines are much fainter than at egress, and in the case of weak lines they can be revealed only as small perturbations of the stellar line profile. Around mid-eclipse, a considerable deepening of the Balmer series is observed, but the shell components are superimposed with no relative shift over the corresponding broad stellar lines, and cannot be analyzed separately. For these reasons, a complete study of the shell spectrum at all phases of the eclipse is not feasable simply by direct analysis of the observed spectrograms. The underlying contribution of the primary's spectral lines should be removed in advance. The removal procedure is described in section 2; finally the spectrum of the gaseous envelope, extracted in such a way, is discussed in section 3.

2. DATA PROCESSING

Reduction of the spectrograms was performed at the ASTRONET pole in Trieste, starting with the digitation at the PDS microdensitometer, and then following the standard ELSPEC/11 procedure (Pasian et al.,1982)which provides calibrated, heliocentric and normalized intensity tracings, and also allows mathematical treatment of the spectra. In order to minimize the noise,groups of spectra taken at the same phase,with only a few days' interval,were averaged together. Average spectra for a dozen different phases of the eclipse were then obtained, together with an almost noise-free reference spectrum, which is an average of 6 normalized spectra taken out of eclipse on January 1981. Doppler-shift correction was finally applied,reducing to zero the orbital velocity of the F star at all phases.

The shell spectrum is formed in the eclipsing body, by absorbing the radiation of the primary F star. Hence the local continuum,for a general shell line, is given by the profile of the corresponding line of the F star, on which the shell component is superimposed. So, if one divides an eclipsed spectrum containing the shell components,by a pure uneclipsed spectrum of the F star, one obtains a normalized spectrum of the eclipsing body. Such a method,taking the spectrum of the F star as the continuum for the shell lines, was already used in a single case for the extraction of the Hδ shell line during the previous 1955-57 eclipse (Hack,1959).

Taking the Jan.'81 uneclipsed spectrum as reference, we applied the extraction procedure to our sample of phase-averaged eclipsed spectra (after careful equalization of their zero-intensity levels). As a result, we could obtain the first individual spectra of the gaseous component of the eclipsing body, at all phases of the eclipse.

3. THE EXTRACTED SHELL SPECTRUM

A portion of the shell spectrum, extracted at different eclipse phases, is shown in Figure 1. All the properties of the shell lines, already detected by previous investigations, clearly appear at the first inspection of the shell spectra. One observes for example the sharpness of metallic lines, the prevalence of low-excitation features, the redward and blueward shift (depending on phase), and the deepening on egress. The dilution is evident, since the Fe I multiplet 152 is extremely weak, in particular at ingress. Undesired spurious effects,appearing in the extracted shell spectrum because of stellar variability, are generally

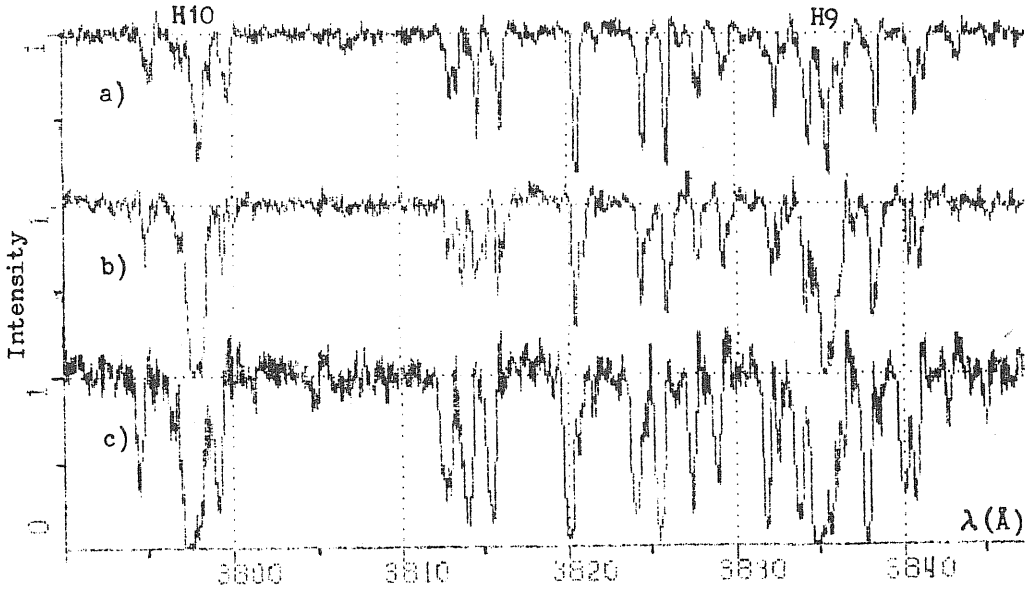

Fig.1. Extracted spectrum of the eclipsing companion of ε Aur. a) mid-ingress, Sep. 82; b) mid-totality, Aug. 83; c) early-egress, Mar. 84.

negligible: residual absorptions or over-compensations of stellar lines (pseudo-emissions) can appear during partial eclipse phases (because of shrinking line-profiles), or can affect the H and K lines of calcium which are intrinsically variable in the F star (Castelli, 1978).

Particularly interesting is the fact that a lot of new physical phenomena can be identified for the first time in the eclipsing body, by analyzing the extracted shell spectra. There is one striking difference between the shell spectra at mid-eclipse, and those in the partial phases: the Balmer series. It clearly dominates during the whole totality, showing broad lines with very steep profiles and no wings (width at half-depth corresponds to a velocity dispersion of ~90km/s); on the contrary at mid-ingress the Balmer series, for $n \geq 4$, is much sharper (corresponding to a velocity of ~30 km/s). Also the metallic lines are slightly broader in totality, than in the partial phases.

During the various phases of the eclipse, different parts of the eclipsing body pass in front of the F star; this means that the phase-dependence of the shell spectrum provides a natural "scanning" of the inner parts of the eclipsing body. The interpretation of the observed behaviour of the shell spectra during totality is then clear: the internal regions of the eclipsing body show evidence of low density, high rotational velocity, and a remarkably higher temperature, that is of the order of an A-type star (precision measurements are in progress). The hot source, causing the far-UV excess of ε Aur, should then be at the center of the shell.

ACKNOWLEDGEMENT: We are indebted with M. Hack for helpful discussion.

REFERENCES

Backman,D.E.,Becklin,E.E.,Kruikshank,D.B.,Joice,R.R.,Simon,T.,Tokunaga,A.: Astroph.J.284,799
Boehm,C., Ferluga,S. and Hack,M.: 1984, Astron. Astroph. 130, 419
Castelli,F.: 1978, Astron. Astroph. 69, 23
Lissauer,J.J. and Backman,:1984 ,Astroph. J. Lett. 286, L39
Ferluga,S and Hack,M.: 1985, Astron. Astroph. 144, 395
Hack,M.: 1959, Astroph. J. 129, 291
Pasian,F., Rusconi,L., Sedmack.G.: 1982, Publ. Oss. Astron. Trieste,No.806.

Paper IX

INFRARED MICHELSON INTERFEROMETRY OF ZETA AURIGAE TYPE SUPERGIANTS

G.Paolo Di Benedetto

Inst.Cosmic Phys.(IFCTR)
Via Bassini, 15
I 20133 Milano, Italy

Steno Ferluga

Trieste Univ.,Astronomy dept.
Via Tiepolo, 11
I 34131 Trieste, Italy

The system parameters of the ζAur-type binaries, all containing a cool supergiant and a hot dwarf,have been improved recently by IUE observations (N.P.Schroeder,1985;A.Ap.147,103). But the diameters of the supergiant components,determined with different indirect methods,are still discordant. We attempted to solve such discrepancies by measuring directly the angular sizes of these stars, expected to be of a few milli-arcseconds.

The measurements were performed by using a modern Michelson stellar interferometer (A.Labeyrie,1975;Ap.J.196,L71),operating at the CERGA Obs. in France. The fully developed instrument (Blazit,Bonneau,Josse,Koechlin, Labeyrie and Oneto,1977;Ap.J.217,L55),equipped with an infrared beam recombination table (Di Benedetto and Conti,1983;Ap.J.268,309), was used in collaboration with A.Blazit,D.Bonneau,R.Foy and Y.Rabbia of CERGA.

In the infrared,the contribution of the hot dwarf is almost negligible, and so we could observe the interferometric effects depending on the supergiant's finite angular size. The fringe visibility in the H and K atmospheric windows was measured with different baseline lengths,up to 55 m. Already from rough data,it appears that ζAur, 31 Cyg and 32 Cyg are all clearly resolved at 1.65 μm with the longest baselines (an example is given in Fig.1). This means that such measurements may provide angular diameters of these supergiants, with well established reliability (G.P. Di Benedetto,1985;A.Ap.148,169). Data analysis is in progress.

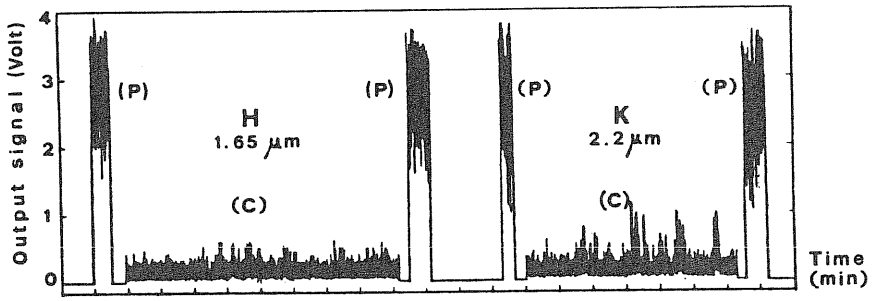

Fig.1. Total photometric energy (P) and coherent energy (C), recorded from 32 Cyg with 50m baselength, on 11/10/85. The spikes in (C) show the fringe signal detected in a scan of the coherence region (FWMH~10μm): the signal is lower in H than in K, while the mean photom. energy is almost the same in the two cases. This indicates that the source is clearly resolved in H, the point-source transfert function being about the same for H and K.

J.-P. Swings (ed.), Highlights of Astronomy, 215.

R E F E R E N C E S

General Bibliography of Epsilon Aurigae

(obtained from CDS, Strasbourg)

*Ident * EPS AUR

* -----HD 31964 ----------

Coord. 1950. = 04 58 22.530+43 45 05.36 Sp = A8Iab:
Coord. 2000. = 05 01 58.079+43 49 23.98 mb,p,mv = 3.53
Gal = 162.79 +01.18 V3
pm = +0.013 [9] / -0.015 [7] 2.99

HD 31964	GEN# +1.00031964J	SKY# 7879	SAO 39955
AG +43 552	UBV M 10528	GC 6123	N30 1068
PLX 1122	IRC +40..109	HR 1605	V* EPS AUR
* 7 AUR	* EPS AUR	ADS 3605A	EM* CDS 456
FK4 183	GCRV 2970	JP11 959	LS V +43 23
TD1 3824	ROT 705	SBC 200	UBV 4807
CSI +43 1166 1	LF 7 +43 70	BD +43 1166	

---

251 references from 1950 to Nov.1987 :

1950

SWINGS P. <Ann. Astrophys. 13,114> Le spectre de l'etoile supergeante 1 Pup de classe cA2ep.
KEENAN P.C., HYNEK J.A. <Astrophys. J. 111,1> Neutral Oxygen in stellar atmospheres.

1951

BIDELMAN W.P. <Astrophys. J. 113,304> Spectral classification of stars listed in Miss Payne's catalogue of C stars.
HUANG S-S. <Astrophys. J. 114,287> On the variation of turbulent velocities in stellar and solar atmospheres.
O'CONNELL D.J.K. <Mon. Not. R. Atron. Soc. 111,111> A new eclipsing binary of very long period.
FELLGETT P.B. <Mon. Not. R. Astron. Soc. 111,537> An exploration of infra-red stellar magnitudes using the photo-conductivity of lead sulfide.
STRUVE O. <Astron. J. 56,114> Recent progress in stellar spectroscopy.
STRUVE O. <Publ. Astron. Soc. Pac. 63,138> Notes on stellar spectra.
POVEDA A. <Publ. Astron. Soc. Pac. 63,254> Systematic displacements of absorption lines in eps Aur.

1952

BARBIER D. <Ann. Astrophys. 15,113> Sur la determination de la grandeur de la discontinuite de Balmer par les methodes de la photometrie a travers des filtres.
CHALONGE D., DIVAN L. <Ann. Astrophys. 15,201> Recherches sur les spectres continus stellaires .V. Etude du spectre continu de 150 etoiles entre 3150 et 4600 A.
McLAUGHLIN D.B. <Astrophys. J. 116,546> Radial velocities of 31 Cyg during atmospheric eclipse.

1953

KOPAL Z. <Astron. J. 58.219> The interpretation of eclipses of eps Aur.
STRUVE O. <Publ. Astron. Soc. Pac. 65,81> Notes on stellar spectra.
PECKER C. <Ann. Astrophys. 16,321> Contribution a l'etude de la zone convective des etoiles.
HACK M. <Ann. Astrophys. 16,417> Etude du spectre d'absorption de 243 etoiles de types spectraux compris entre O6 et F8 pour la recherche de criteres quantitatifs de classification spectrale bidimensionelle.
BREWER K.R.W. <Astrophys. J. 118,265> HD 50169, a spectrum variable with emission at H-alpha.
MILLER F.D. <Astrophys. J. 118,572> Note on spectra of cool stars in the 1 micron region.

1954

KRAFT R.P. <Astrophys. J. 120,391> The atmosphere of the I component of eps Aur.
GAPOSCHKIN S. <Publ. Astron. Soc. Pac. 66,112> Eps Aur.
PILLANS H.M. <Publ. Astron. Soc. Pac. 66,327> Interstellar lines of CH+ in the spectrum of eps Aur.

1955

HUANG S-S., STRUVE O. <Astrophys. J. 121,84> Study of Doppler velocities in stellar atmospheres: the spectrum of alf Cyg.
HERBIG G.H., SPALDING JR.J. <Astrophys. J. 121,118> Axial rotation and line broadening in stars of spectral types F0-K5.
SLETTEBAK A. <Astrophys. J. 121,653> The spectra and rotational velocities of the bright stars of Draper types A3-G0.
STRUVE O. <Publ. Astron. Soc. Pac. 67,135> An interesting group of pulsating stars.
PILLANS H.M. <Publ. Astron. Soc. Pac. 67,340> Peculiar features in the spectrum of eps Aur.

1956

STRUVE O. <Publ. Astron. Soc. Pac. 68,27> Eps Aur.
GAPOSCHKIN S. <Publ. Astron. Soc. Pac. 68,362> Note on Struve's paper on eps Aur.
GAPOSCHKIN S. <Astron. J. 61,177> The first two contacts of the eclipse of eps Aur in 1955.
HUANG S.S., STRUVE O. <Astron. J. 61,300> The radii and masses of eclipsing binary stars.
WOOD F.B. <Astron. J. 61,320> Reports of observatories.
DEUTSCH A.J. <Astrophys. J. 123,210> The circumstellar envelope of alf Her.
STEBBINS J., KRON G.E. <Astrophys. J. 123,440> 6-color photometry of stars .VIII. The colors of 409 stars of different spectral types.

1957

ABT H.A. <Astrophys. J. 126,138> The variability of supergiants.
STRUVE O., PILLANS H. <Publ. Astron. Soc. Pac. 69,169> The spectrum of eps Aur in October and November 1956.
HACK M. <Publ. Astron. Soc. Pac. 69,389> The spectrum of eps Aur in and before eclipse.
WRIGHT K.O., KUSHWAHA R.S. <Publ. Astron. Soc. Pac. 69,402> Observations of eps Aur.
PILLANS H., STRUVE O. <Astron. J. 62,145> The spectrum of eps Aur.
THIESSEN G. <Zeitschr. Astrophys. 43,233> Farbschwankungen des Systems eps Aur.

1958

WRIGHT K.O. <Astron. J. 63,312> Victoria spectrographic observations obtained at the 1955-57 eclips e of eps Aur.
WOOD F.B. <Astron. J. 63,504> Flower and Cook Observatory.
LINNELL A.P. <Astrophys. J. 127,211> Atmospheric eclipses .1.
STRUVE O., PILLANS H., ZEBERGS V. <Astrophys. J. 128,287> The radial velocity of eps Aur.
SAHADE J. <Publ. Astron. Soc. Pac. 70,316> Binaries having one component below the main sequence.
KRON G.E. <Publ. Astron. Soc. Pac. 70,561> Color excesses from six-color photometry of supergiant stars.

1959

HACK M. <Astrophys. J. 129,291> The spectrum of eps Aur.

1960

FREDRICK L.W. <Astron. J. 65,97> Observations of eps Aur.
KREIKEN E.A., SUER B. <Ann. Astrophys. 23,528> Note on the H-R diagram of binary stars.
GRIFFIN R.F., REDMAN R.O. <Mon. Not. R. Astron. Soc. 120,287> Photoeletric measurements of the 4200 CN band and the G-band in the G8-K5 spectra.
HACK M. <Mem. Soc. Astron. Ital. 31,195> Macro e microturbolenza nell'atmosfera di eps Aur.

1961

HACK M. <Mem. Soc. Astron. Ital. 32,351> A new explanation of the binary system eps Aur.

1962

BAIZE P. <J. Obs. 45,117> Catalogue d'etoiles doubles ayant une composante variable.

1963

BOULON J. <J. Obs. 46,225> Observations et donnees ayant servi a la determination de l'absorption dans les champs et les distances des etoiles.

1964

WILDEY R.L., MURRAY B.C. <Astrophys. J. 139,435> 10 microns photometry of 25 stars from B8 to M7.
KRAFT R.P. <Astrophys. J. 139,457> Binary stars among cataclysmic variables. III. 10 old Novae.
MITCHELL R.I. <Astrophys. J. 140,1607> Nine-colour photometry of eps Aur, 0.35 to 9.5 microns.

1965

CESTER B. <Zeitschr. Astrophys. 62,191> The empirical mass-luminosity relations for spectrophotometric binary systems.
WOOLF N.J. <Astrophys. J. 141,155> The problem of beta Lyr. II. The masses and the shapes.
LOW F.J., MITCHELL R.I. <Astrophys. J. 141,325> Optical-line profiles and radar observations in the corona.
HUANG S. <Astrophys. J. 141,976> An interpretation of eps Aur.
GEHRELS T., S.ILVESTER. <Astron. J. 70,579> Wavelength dependence of polarization. V. Position angles of interstellar polarization.
LOW F.J. <Astrophys. J. 141,327> New infrared photometry of eps Aur.

1966

COYNE G.V., GEHRELS T. <Astron. J. 71,355> Wavelength dependence of polarization. VIII. Interstellar polarization.
LILLER W. <Astrophys. J. 146,719> The central depth of the 6362 A auto-ionization feature of neutral Ca in stellar spectra.
MUSTEL E.R., BARANOVA L.I. <Sov. Astron. 10,388> An analysis of the chemical composition of Nova envelopes. III. Quantitative analysis of the atmosphere of Nova Her 1934 during decline.

1967

FEAST M.W. <Mon. Not. R. Astron. Soc. 135,287> The supergiant eclipsing system BL Tel.

1968

BATTEN A.H. <Astron. J. 73,551> Some interesting massive spectroscopic binary systems.
VAN DE KAMP P., LIPPINCOTT S.L. <Astron. J. 73,781> Summary of 133 parallaxes determined with the 24-inch refractor of the Sproul observatory.

1969

TRIMBLE V.L., THORNE.K.S. <Astrophys. J. 156,1013> Spectroscopic binaries and collapsed stars.
HOBBS L.M. <Astrophys. J. 157,135> Interferometric studies of interstellar sodium lines.
SERKOWSKI K., CHOJNACKI W. <Astron. Astrophys. 1,442> Polarimetric observations of magnetic stars with two-channel polarimeter.

1970

ABT H.A., BIDELMAN W. <Astrophys. J. 158,1091> Spectral classification of A-type spectroscopic binaries.
HUMPHREYS R.M. <Astron. J. 75,602> The space distribution and kinematics of supergiants.
BATTEN A.H. <Publ. Astron. Soc. Pac. 82,574> Observations of circumstellar matter in close binary systems.
HUANG S.S. <Astrophys. J. 161,1033> Light curve for eclipsing stars with scattering envelopes and its application to the V444 Cyg binary system.

1971

DOKUCHAEV V.P. <Sov. Astron. 15,573> Emission of magnetosonic waves by planets and binary stars revolving in circular orbits.
WILSON R.E. <Astrophys. J. 170,529> A model of epsilon Aur.
WALBORN N.R. <Publ. Astron. Soc. Pac. 83,813> Some spectroscopic observations of the early decline of Nova Ser 1970.
THACKERAY A.D. <Mon. Not. R. Astron. Soc. 154,103> A spectroscopic reconnaissance of a new bet Lyr system HD 72754.
HUTCHINGS J.B., WRIGHT K.O. <Mon. Not. R. Astron. Soc. 155,203> Rotationally extended stellar envelopes. III. The Be component of VV Cep.

1972

STUB H. <Astron. Astrophys. 20,161> Secondary fluctuations in the light curve eps Aur.
FERNIE J.D. <Astron. J. 77,150> Photometric data for 139 supergiants.
KOCH R.H. <Astron. J. 77,500> The complicated giant binary SX Cas.
DOKUCHAEV V.P. <Sov. Astron. 15,573> Emission of magnetosonic waves by planets and binary stars revolving in circular orbits.
STOTHERS R. <Publ. Astron. Soc. Pac. 84,373> A recalibration of the absolute magnitudes of supergiants.
SNOW T.P., WALLERSTEIN G. <Publ. Astron. Soc. Pac. 84,492> A search for diffuse interstellar features in stars with circumstellar dust shells.
OSMER D.S. <Astrophys. J. Suppl. Ser. 24,247> The atmospheres of the F-type supergiants 1. Calibration of the luminosity-sensitive OI lambda 7774 line.

1973

WILSON W.J., RIEGEL K.W. <Astron. Astrophys. 22,473> Research note-2 new main-line OH/IR stars.
NELSON M.R., GROTH E.J. <Astrophys. J. 181,157> Report on a search for new optical pulsars.
PEDOUSSAUT A., CARQUILLAT J.M. <Astron. Astrophys. Suppl. Ser. 10,105> Binaires spectroscopiques-12eme catalogue complementaire.
WOOLF N.J. <Astrophys. J. 185,229> Infrared emission from unusual binary stars.
ROSENDHAL J.D. <Astrophys. J. 186,909> A survey of H alf emission in early-type high-luminosity stars.

1974

HOBBS L.M. <Astrophys. J. 188,L67-L69> Interferometric scans of interstellar KI lines.
OCHSENBEIN F. <Astron. Astrophys. Suppl. Ser. 15,215-252> On the relationship between the apparent magnitudes given in several catalogues and the UBV system.
HUANG S.S. <Astrophys. J. 189,485-491> Interpretation of epsilon Aur.3. Study of the light curve based on disk models.
COYNE G.V., GEHRELS T., SERKOWSKI K. <Astron. J. 79,581-589> Wavelength dependence of polarization.26. The wavelength of maximum polarization as a characteristic parameter of interstellar grains.
WONG C.Y. <Astrophys. J. 190,675-694> Toroidal figures of equilibrium.
HOBBS L.M. <Astrophys. J. 191,381-393> A comparison of interstellar NaI,CaII, and KI absorption.
HOBBS L.M. <Astrophys. J. 191,395-399> Statistical properties of interstellar clouds.
SORVARI J. <Astron. J. 79,1416-1423> Photometry of the near-infrared OI feature in A- and F-type stars.

1975

SERKOWSKI K., MATHENSON D.S., FORD V.L. <Astrophys. J. 196,261-290> Wavelength dependence of interstellar polarisation and ratio of total to selective extinction.
SADEH N.D., FROHLICH A. <Astron. Astrophys. 42,247-250> A search for optical pulsations from single line spectroscopic binaries.
HUANG SU-SHU <Astrophys. J. 195,127-135> Interpretation of BM Ori.
HILDITCH R.W., HILL G. <Mem. R. Astron. Soc. 79,101-129> Stromgren four-colour observations of northern hemisphere binary systems.
HILL G., HILDITCH R.W., YOUNGER F., FISHER W.A. <Mem. R. Astron. Soc. 79,131-144> MK classifications of some northern hemisphere binary systems.
WU C.C. <Astrophys. Space Sci. 36,407-426> The origin of the emission lines shown by RW Tau and other binary systems.
LEQUEUX J. <Astron. Astrophys. 39,257-261> On the interstellar abundance of sodium and potassium .

1976

ZIRIN H. <Astrophys. J. 208,414-425> Further observations of the lambda 10830 He line in stars and their significance as a measure of stellar activity.
BELL R.A., GUSTAFSSON B., NORDH H.L., OLOFSSON S.G. <Astron. Astrophys. 46,391-396> The luminosity dependence of the 1.65 micron flux from K and early M stars. Observations and interpretation.
COWLEY A.P. <Publ. Astron. Soc. Pac. 88,95-110> Spectral classification of the bright F stars.
MCALISTER H.A. <Publ. Astron. Soc. Pac. 88,317-322> Spectroscopic binaries as a source for astrometric and speckle interferometric studies.
HANDBURY M.J., WILLIAMS I.P. <Astrophys. Space Sci. 45,439-446> The peculiar binary system eps Aur.
CASTELLI F. <IAU Inform. Bull. Var. Stars 1165,1-4> Fast variations of eps Aur.

1977

WOODSWORTH A.W., HUGHES V.A. <Astron. Astrophys. 58,105-111> Observations of radio stars at 10.6 GHz.
HECK A., ALBERT A., DEFAYS D., MERSCH G. <Astron. Astrophys. 61,563-566> Detection of errors in spectral classification by cluster analysis.
LUTZ T.E., LUTZ J.H. <Astron. J. 82,431-434> Spectral classification and UBV photometry of bright visual double stars.
BLACKWELL D.E., SHALLIS M.J. <Mon. Not. R. Astron. Soc. 180,177-191> Stellar angular diameters from infrared photometry. Application to Arcturus and other stars with effective temperatures.
CASTELLI F. <Astrophys. Space Sci. 49,179-197> The spectrum of eps Aur outside eclipse.
HANDBURY M.J., WILLIAMS I.P. <Obs. 97,73-76> Is eps Aur a semi-detached system with an accretion disk ?
SHEVCHENKO V.S., ZAKIROV M.M. <Perem. Zvezdy 20,361-368> A preliminary study of the spectrum of BM Ori.

1978

VANDEN BOUT P.A., SNELL R.L., VOGT S.S., TULL R.G. <Astrophys. J. 221,598-600> Observations of interstellar lithium toward zet Per and eps Aur.
BURKI G. <Astron. Astrophys. 65,357-362> The semi-period-luminosity-colour relation for supergiant stars.
CASTELLI F. <Astron. Astrophys. 69,23-33> Fine analysis of the F component of the eps Aur system.
VAN DE KAMP P. <Astron. J. 83,975-977> Astrometric study of the eclipsing binary eps Aur from plates taken with the Sproul 61 cm refractor.
MCALISTER H.A. <Publ. Astron. Soc. Pac. 90,288-296> Binary stars unresolved by speckle interferometry.
AYDIN C., HACK M., YILMAZ N. <Astrophys. Space Sci. 53,345-370> Spectroscopic study of the eclipsing binary V367 Cyg.
VAN DE KAMP P. <Sky Telesc. 56,397> The distances of VV Cep and eps Aur.
HACK M., SELVELLI P.L. <Nature 276,376-378> IUE observations of the eclipsing binary eps Aur.
JOHNSON H.L. <Rev. Mex. Astron. 4,3-201> An atlas of stellar spectra. II.
HACK M., SELVELLI P.L. <IAU Inf. Bull. Var. Stars 1439,1> The far ultraviolet spectrum of the binary system eps Aur.

1979

KONDO Y., DE JAGER C., HOEKSTRA R., VAN DER HUCHT K.A., KAMPERMAN T.M., LAMERS H.J.G.L.M., MODISETTE J.L., MORGAN T.H. <Astrophys. J. 230,526-533> Balloon-borne ultraviolet stellar spectrograph.I. Instrumentation and observation.
STENCEL R.E., KONDO Y., BERNAT A.P., MCCLUSKEY G.E. <Astrophys. J. 233,621-632> IUE observations of 32 Cyg: the effects of the B star within the upper chromosphere of a late-type supergiant.
HACK M., SELVELLI P. <Astron. Astrophys. 75,316-321> The ultraviolet spectrum of the eclipsing binary eps Aur.
MENDOZA E.E., JOHNSON H.L. <Publ. Astron. Soc. Pac. 91,465-470> Equivalent widths and narrow-band photometry of three stellar lines.
STARIKOVA G.A. <Soviet Astron. Lett. 5,188-192> Absolute magnitudes and masses for three types of variable stars .

1980

PARSONS S.B. <Astrophys. J. 239,555-564> Ultraviolet spectroscopy of F and G supergiants with IUE .I. First results on Cepheid variables .
MEADE M.R., CODE A.D. <Astrophys. J. Suppl. Ser. 42,283-331> Ultraviolet photometry from the orbiting astronomical observatory. XXXVIII. A second atlas of ultraviolet stellar spectra .
CODE A.D., HOLM A.V., BOTTEMILLER R.L. <Astrophys. J. Suppl. Ser. 43,501-545> Ultraviolet photometry from the orbiting astronomical observatory .XXXIV. Filter photometry of 531 stars of diverse types .
CANAVAGGIA R. <Astron. Astrophys. 83,105-113> Dual aspect of the wavelength-dependent fluctuations of eps Aur .
HECK A., MERSCH G. <Astron. Astrophys. 83,287-296> Prediction of spectral classification from photometric observations-application to the uvby bet photometry and the MK spectral classification .I. .Prediction assuming a luminosity class.
MERSCH G., HECK A. <Astron. Astrophys. 85,93-100> Prediction of spectral classification from photometric observations - application to the uvby beta photometry and the MK spectral classification .II. General case.
MAEDER A. <Astron. Astrophys. 90,311-317> Supergiant variability : amplitudes and pulsation constants in relationn with mass loss and convection.
GILRA D.P., WESSELIUS P.R., KAMESWARA RAO N. <Second European IUE Conference. Proceedings of an International Conference held at Tubingen, Germany, 26-28 March 1980. Ed. B.Battrick, J.Mort. ESA SP-157.227-228> Observations of late-type stars with 'hot' companions.
PLAVEC M.J. <The Universe at ultraviolet wavelengths. The first two years of IUE. Proceedings of a symposium held at NASA Goddard Space Flight Center, Greenbelt, Maryland, May 7-9, 1980. Ed. R.D. Chapman . NASA CP-2171.397-413> The impact of IUE on binary star studies.

1981

HALLIWELL M. <Astrophys. J., Suppl. Ser. 47,243-278> Preliminary orbital parallax catalog.
VAN HOUTEN C.J. <Astron. Astrophys. 97,46-55> Gas streaming in semi-detached binary systems.
PROUST D., OCHSENBEIN F., PETTERSEN B.R. <Astron. Astrophys. Suppl. Ser. 44,179-187> A catalogue of variable-visual binary stars .
GRUBER R., KOO D., MIDDLEDITCH J. <Publ. Astron. Soc. Pac. 93,777-782> Speed of light outside the solar system : a new test using visual binary stars.
MENDOZA V.E.E. <Rev. Mex. Astron. 6,137-143> Fourier transform spectroscopy of six stars.
BUSCOMBE W. <Bull. Inf. Centre Donnees Stellaires 21,26-34> Refined data for parallax stars.

1982

ZIRIN H. <Astrophys. J. 260,655-669> Lambda 10830 He I observations of 455 stars.
MEISEL D.D., SAUNDERS B.A., FRANK Z.A., PACKARD M.P. <Astrophys. J. 263,759-776> The helium 10830 angstrom line in early-type stars : an atlas of Fabry-Perot scans.
CASTELLI F., HOEKSTRA R., KONDO Y. <Astron. Astrophys., Suppl. Ser. 50,233-245> The mid-ultraviolet spectrum of eps Aur.
KOORNNEEF J., MEADE M.R., WESSELIUS P.R., CODE A.D., VAN DUINEN R.J. <Astron. Astrophys., Suppl. Ser. 47,341-418> Picture gallery : a structured presentation of DAO-2 photometric data supported by OAO-2 spectrophotometric data and UBV, and TD1 observations.
VANSINA F., DE GREVE J.P. <Astrophys. Space Sci. 87,377-401> Close binary systems before and after mass transfer.
REDDY F.J. <Sky Telesc. 63,460-465> The mystery of eps Aur.
HOFFLEIT D. <Bull. Inf. Centre Donnees Stellaires 23,53-58> Variable stars in the General Catalogue of trigonometric parallaxes.
GILRA D.P. <Third European IUE Conference. Proceedings of the Third International Ultraviolet Explorer Conference, Madrid, Spain, 10-13 May 1982. Ed. Rolfe E., Heck A., Battrick B. ESA SP-176. p.139-141> Fe II absorption lines in the IUE high-resolution spectra of F supergiants and shell stars.
MCCLUSKEY G.E. <Advances in ultraviolet astronomy: Four years of IUE Research. Proceedings of a symposium held at NASA Goddard Space Flight Center, Greenbelt, Maryland, March 30 - April 1,1982. Ed. Y.Kondo, J.M.Mead, R.D.Chapman. NASA CP-2238. 102-113> IUE spectroscopic investigation of interacting binary systems.
STENCEL R.E., CHAPMAN R.D., KONDO Y., WING R.F. <Advances in ultraviolet astronomy: Four years of IUE Research. Proceedings of a symposium held at NASA Goddard Space Flight Center, Greenbelt, Maryland, March 30 - April 1,1982. Ed. Y.Kondo, J.M.Mead, R.D.Chapman. NASA CP-2238.497-500> UV observations of the 1981 eclipse of 32 Cygni.
CHAPMAN R.D., KONDO Y., STENCEL R.E. <Advances in ultraviolet astronomy: Four years of IUE Research. Proceedings of a symposium held at NASA Goddard Space Flight Center, Greenbelt, Maryland, March 30 - April 1,1982. Ed. Y.Kondo, J.M.Mead, R.D.Chapman. NASA CP-2238.505-508> Pre-eclipse ultraviolet spectra of epsilon Aurigae.
PLAVEC M.J. <Advances in ultraviolet astronomy: Four years of IUE Research. Proceedings of a symposium held at NASA Goddard Space Flight Center, Greenbelt, Maryland, March 30 - April 1,1982. Ed. Y.Kondo, J.M. Mead, R.D.Chapman. NASA CP-2238.526-529> A progress report on the W Serpentis binaries, with a few words on eps Aurigae.

1983

PARSONS S.B. <Astrophys. J., Suppl. Ser. 53, 553-572 Erratum vol. 54, 372-374> Ultraviolet and optical studies of binaries with luminous cool primaries and hot companions. III. Reticon radial velocities.
BURKI G., MAYOR M. <Astron. Astrophys. 124,256-266> Nineteen new spectroscopic binaries and the rate of binary stars among F-M supergiants.

BACKMAN D., SIMON T. <Publ. Astron. Soc. Pac. 95, 586> FTS observations of the eclipse of epsilon Aurigae at 2.2 and 4-microns.
PARTHASARATHY M., LAMBERT D.L. <Publ. Astron. Soc. Pac. 95,1012-1018> Epsilon Aurigae in eclipse. I. Ultraviolet spectroscopy during ingress and totality.
PaperI BOEHM C., FERLUGA S. <IAU Inform. Bull. Var. Stars 2326, 1-4> H Alpha observations of epsilon Aurigae.
JAPOA (Japan Amateur Photoelectric Observers Association). <IAU Inform. Bull. Var. Stars 2371, 1-3> Photoelectric observations of epsilon Aurigae during the ingress.
NHA I.S., LEE S.J. <IAU Inform. Bull. Var. Stars 2405> Flare activity of epsilon Aurigae.
MENDOZA E.E.V. <IAU Inform. Bull. Var. Stars 2444, 1-2> Epsilon Aurigae.
BURNASHEV V.I. <Izv. Krym. Astrofiz. Obs. 66, 162-182> Spectrophotometric analysis of some unresolved double stars.
HENSON G.D., KEMP J.C., KRAUS D.J. <Bull. American Astron. Soc. 15-665> Variable polarization in the eclipse of Epsilon Aurigae.
LOCKWOOD G.W., LUTZ B.L., THOMPSON D.T., SOWELL J.R. <Bull. American Astron. Soc. 15, 925> Absolute spectrophotometry of epsilon Aurigae.
BACKMAN D.E., BECKLIN E.E., CRUIKSHANK D.P., JOYCE R.R., TOKUNAGA A.T. <Bull. American Astron. Soc. 15, 925> Infrared observations of the eclipse of epsilon Aurigae.
HENSON G., KEMP J., KRAUS D. <I.A.U. CIRC. 3759> Epsilon AURIGAE.
HENSON G., KEMP J., KRAUS D. <I.A.U. CIRC. 3759> Epsilon Aurigae.
AKE T.B., SIMON T. <I.A.U. CIRC. 3763> Epsilon AURIGAE
PARTHASARATHY M., LAMBERT D.L. <I.A.U. Circ. 3766> Epsilon Aurigae.
PARTHASARATHY M., LAMBERT D.L. <Circ. Bureau Central Telegrammes 3848> Epsilon Aurigae.
PARTHASARATHY M., LAMBERT D.L. <Circ. Bureau Central Telegrammes 3857> Epsilon Aurigae.

1984

PaperII BOEHM C., FERLUGA S., HACK M. <Astron. Astrophys. 130, 419-423> The eclipse of epsilon Aurigae in the ultraviolet.
DE JAGER C. <Astron. Astrophys. 138, 246-252> The stability limit of hypergiant photospheres.
HARTKOPF W.I., MCALISTER H.A. <Publ. Astron. Soc. Pac. 96, 105-116> Binary stars unresolved by speckle interferometry.III.
SAITO M., KAWABATA S., SAIJO ., SATO H. <Astrophys. Space Sci. 99, 269-272> A spectroscopic study of epsilon Aurigae.
BHATT H.C., CHANDRASEKHAR T., ASHOK N.M., DESAI J.N. <Astrophys. Space Sci. 104, 293-296> Near-infrared observations of the peculiar binary system epsilon Aurigae.
BACKMAN D.E., BECKLIN E.E., CRUIKSHANK D.P., JOYCE R.R., SIMON T., TOKUNAGA A. <Astrophys. J. 284, 799-805> Infrared observations of the eclipse of epsilon Aurigae : direct measurement of the 500 K secondary at 5, 10 and 20 microns.
HOBBS L.M. <Astrophys. J. 286, 252-254> The abundance of interstellar lithium.
LISSAUER J.J., BACKMAN D.E. <Astrophys. J. 286, L39-L41> The epsilon Aurigae secondary : a binary embedded within a disk?
MAKARENKO E.N. <Astron. Tsirk. 1340, 7-8> Information on the photoelectric observations of variable stars deposited at Odessa Astronomical Observatory.

MAYER P. <Observatory 104, 77-80> Secular brightening of supergiants.
TOSIO OKI, IKUO SEKIYA, KATSUNORI HIRAMAYA. <IAU Inform. Bull. Var. Stars 2496> An UV active phenomenon of epsilon Aurigae.
BHATT H.C., ASHOK N.M., CHANDRASEKHAR T. <IAU Inform. Bull. Var. Stars 2509> Epsilon Aurigae: BVRIJHK photometry.
BOYD L.J., GENET R.M., HALL D.S. <IAU Inform. Bull. Var. Stars 2511> Automatic photoelectric telescope : fourth 1983 observations.
BOEHM C., CESTER B. <IAU Inform. Bull. Var. Stars 2512> Infrared observations of epsilon Aurigae.
WALLERSTEIN G. <IAU Inform. Bull. Var. Stars No 2534> High dispersion observations of epsilon Aur from sept. 1982 to march 1983.
BOYD L.J., GENET R.M., HALL D.S. <IAU Inform. Bull. Var. Stars 2561, 1-3.> Automatic photoelectric telescope: first quarter 1984 observations.
BOYD L.J., GENET R.M., HALL D.S. <IAU Inform. Bull. Var. Stars 2562> A photometric anomaly around third contact in epsilon Aurigae.
TAN H.S. <Acta Astron. Sinica 25,264-271> Short time-scale variations of epsilon Aurigae in the H-alpha region.
HUISONG T. <Acta Astrophys. Sinica 4, 264-271> Short time-scale variations of Epsilon Aurigae in the H-alpha region.
KEMP J., HENSON G., KRAUS D. <Circ. Bureau Central Telegrammes No 3931 + Erratum 3940> Epsilon Aurigae.
HACK M. <Scientific American 251, 4, 92-99> Epsilon Aurigae.
HENSON G.D., KEMP J.C., KRAUS D.J. <Bull. American Astron. Soc. 16, 1013> Polarimetry of epsilon Aurigae : 1982-1984 eclipse.
CHENG A.Y.S., WOOLF N.J. <Bull. American Astron. Soc. 16, 1013> Modelling epsilon Aurigae without solid particles.
AKE T.B., SIMON T. <Future of Ultraviolet Astronomy based on six years of IUE Research. Ed. by J.M. Mead,R.D. Chapman and Y. Kondo. NASA Goddard Space Flight Center Greenbelt, Maryland April 3-5,1984. NASA CP 2349. pp 361-364> Eclipse observations of epsilon Aurigae.
ALTNER B.M., CHAPMAN R.D., KONDO Y., STENCEL R.E. <Future of Ultraviolet Astronomy based on six years of IUE Research. Ed. by J.M. Mead,R.D. Chapman and Y. Kondo. NASA Goddard Space Flight Center Greenbelt, Maryland April 3-5,1984. NASA CP 2349. pp 365-368> UV observations of epsilon Aurigae during ingress and totality.

1985

EGGLETON P.P., PRINGLE J.E. <Astrophys. J. 288, 275-276> Possible evolution of a triple system into epsilon Aurigae.
PaperVI FERLUGA S., HACK M. <Astron. Astrophys. 144, 395-402> High-dispersion spectroscopy of the eclipse of epsilon Aurigae at visible and ultraviolet wavelengths.
ARELLANO FERRO A. <Mon. Not. R. Astron. Soc. 216, 571-587> Periodicity and pulsational mode of five bright yellow supergiants.
BACKMAN D.E., SIMON TH., HINKLE K. <Publ. Astron. Soc. Pac. 97, 1163-1171> Emission in the hydrogen-brackett lines of epsilon Aurigae during eclipse.
GOLAY M., CRAMER N., HUGUENIN D., NICOLET B., BLECHA A. <Astrophys. Space Sci. 109, 191-212> An UV survey of the galactic plane.
CHAPMAN R.D. <Astrophys. Space Sci. 110, 177-182> Epsilon Aurigae.
BACKMAN D.E., GILLETT F.C. <Astrophys. J. 299,L99-L102> Epsilon Aurigae during eclipse : IRAS observations of the cool secondary component.

MACROBERT A. <Sky Telesc. 70, 527-529> The puzzle of epsilon Aurigae.
STICKLAND D.J. <Observatory 105, 90-93> IRAS observations of epsilon Aurigae during the 1983 eclipse.
BOHME D. <Mitt. Veraenderliche Sterne 10, 119> Photoelektische Beobachtung des Bedekungsminiums von epsilon Aurigae (1982 bis 84).!
BRETSCHNEIDER H., BOHME D., ENSKONATUS P., KOHLER M., RATZ M., RATZ K., SCHMIDT J.B., YVTHOMISCH P., ZISCHE E. <Mitt. Veraenderliche Sterne 10, 136-137> Visuelle Beobachtung des Bedeckungsminimums von epsilon Aurigae.
ARELLANO FERRO A. <Rev. Mex. Astron. 11, 113-120> H-alpha profile variations in va riable luminous yellow supergiants.
FLIN P., WINIARSKI M., ZOLA S. <2678> Photoelectric photometry of epsilon Aurigae.
BOYD L.J., GENET R.M., HALL D.S. <IAU Inform. Bull. Var. Stars 2680> Automatic photoelectric telescope: second and third quarter 1984 observations.
SCHMIDTKE P.C., HOPKINS J.L., INGVARSSON S.I., STENCEL R.E. <IAU Inform. Bull. Var. Stars 2748> Contact times for the 1982-4 eclipse of epsilon Aurigae.
LIU X.-F., PENG S.-G., CA G.-W., LI X.-Y. <Acta Astron. Sinica 26, 144-151> A new exploration of epsilon Aurigae during ingress and totality of the 1982-1984 eclipse.
TAN H.S. <Acta Astron. Sinica 26, 226-234> The rotation of all primaries and five secondaries in twenty binary systems.
TAN HUISONG <Acta Astrophys. Sinica 5, 180-187> The H-alpha variations of epsilon Aurigae from total eclipse to 4th contact.
TIMM K.-P. <Sterne und Weltraum 24, 153> Beobachtungen an epsilon Aurigae.
HOPKINS J.L., STENCEL R.E. <Bull. Amer. Astron. Soc. 16, 910> Epsilon Aurigae 1982-1984 eclipse campaign report.

1986

KEMP J.C., HENSON G.D., KRAUS D.J., BEARDSLEY I.S., CARROLL L.C., AKE T.B., SIMON T., COLLINS G.W. <Astrophys. J. 300, L11-L14> Epsilon Aurigae : polarization, light curves, and geometry of the 1982-1984 eclipse.
VAN HAMME W., WILSON R.E. <Astrophys. J. 306, L33-L36> The restricted four-body problem and epsilon Aurigae.
HABETS G.M.H.J. <Astron. Astrophys. 165, 95-109> The evolution of a single and a binary helium star of 2.5 solar mass up to neon ignition.
LAMBERT D.L., SAWYER S.R. <Publ. Astron. Soc. Pac. 98, 389-402> Epsilon Aurigae in eclipse II. Optical absorption lines from the secondary.
SCHAEFFER B.E. <Publ. Astron. Soc. Pac. 98, 556-560> IRAS observations of binaries with compact objects.
SASSELOV D.D. <Publ. Astron. Soc. Pac. 98, 561-571> Normal supergiants and their imitations. I. Sodium as a mass indicator ?
BARSONY M., LUTZ B.L., MOULD J.R. <Publ. Astron. Soc. Pac. 98, 637-646> High-resolution spectroscopy of the unique eclipsing binary system : epsilon Aurigae.
TAKEUTI M. <Astrophys. Space Sci. 120, 1-7> A low-mass model of epsilon Aurigae.
TAKEUTI M. <Astrophys. Space Sci. 121, 127-135> An accretion disc surrounding a component of epsilon Aurigae.

SAITO M., KITAMURA M. <Astrophys. Space Sci. 122, 387-393> Possible shrinking of the primary component of epsilon Aurigae.
PARTHASARATHY M., FRUEH M.L. <Astrophys. Space Sci. 123, 31-48> Epsilon Aurigae in eclipse : the light and colour variations.
WHITE R.E. <Astrophys. J. 307, 777-786> Interstellar lithium : differential depletion in diffuse clouds.
ISLES J.E. <J. Br. Astron. Soc. 96, 148-151> The 1982-84 eclipse of epsilon Aurigae.
MORRISON N.D., GREGORY S. <Mercury 15, 177-180> The puzzle of epsilon Aurigae : results from the recent eclipse.
HOPKINS J.L., STENCEL R.E. <Astronomy 14, 2, 6> Epsilon Aurigae.
MUSTEL E.R., ANTIPOVA L.I. <Nauchn. Inf. 60, 131-137> On the abundances in novae envelopes.

1987

HINKLE K.H., SIMON T. <Astrophys. J. 315, 296-304> Two micron CO absorption lines in the spectrum of epsilon Aurigae during eclipse.
KUMAR S. <Mon. Not. R. Astron. Soc. 225, 823-835> Twisted accretion discs - III. Application to epsilon Aurigae.
THOMPSON D.T., LUTZ B.L., LOCKWOOD G.W., SOWELL J.R. <Astrophys. J. 321, 450-458> Spectrophotometry of epsilon Aurigae.
KALER J.B. <Sky Telesc. 73, 491-494> White Sirian stars : class A.
KALER J.B. <Sky Telesc. 74, 147-150> The B stars : beacons of the skies.
HARMANEC P. <Bull. Astron. Inst. Czech. 38, 52-58> Non-canonical insights into the evolution of stars. 2. Are variable supergiants indeed pulsating ?
SAITO M., KAWABATA S., SAIJO K. <Publ. Astron. Soc. Jap. 39, 135-161> Epsilon Aurigae : rotation curve of the secondary disk and masses of the components.
FUMIO SATO., AKIHIRO NISHIMURA. <IAU Inform. Bull. Var. Stars 3041> UBV photometry of epsilon Aurigae outside eclipse.
KRAUS D.J., KEMP J.C., HENSON G.D., DUNAWAY M.H., HOPKINS J.L., SCHMIDTKE P.C. <Bull. American Astron. Soc. 19, 752> Epsilon Aurigae : pulsations and the post-eclipse (1984-1987) polarization and light curves.
SAHADE J. <Comments on Astrophysics 12, 13-16> A working hypothesis to try to make sense out of the peculiar interacting binaries.

Missing from the list ; Congress Reports:

paperIII, 1984:STALIO,ed.(Effects of Variable Mass Loss on the local Stellar Environment) Session 5- FERLUGA: Epsilon Aurigae; Cluet Press, Trieste; p.168.
paper V, 1984:ESA SP-218 Proc. 4th Europ. IUE Conf.- FERLUGA & HACK (Observed Pecluliarities during the eclipse of Epsilon Aurigae), p.419.
paperVII, 1985:STENCEL,ed.(1982-1984 Eclipse of Epsilon Aurigae): 16 papers by different Authors - NASA Conf.Publ.2384;124pages
paperVIII, 1986:SWINGS,ed. (Joint Discussion on Long-period Eclipsing Binaries): 6 papers by different Authors about Epsilon Aurigae - IAU, Highlights of Astronomy, 7 , pp. 143-206.
1982-1985:HOPKINS & STENCEL, eds. (Epsilon Aurigae Campaign Newsletters),observ.bulletin; 13 numbers.

MASTER THESIS : 1984 - S. FERLUGA: "The 1982-1984 Eclipse of the Peculiar Binary Star Epsilon Aurigae", SISSA/ISAS Trieste, 130 pages.

ACKNOWLEDGEMENTS

The writer is grateful to Conrad Boehm for valuable collaboration during this five-year long research. He also thanks Mrs. Patrizia Ferluga for preparing the figures of this book.